Novel roles of smallGTPase Rac1 in invasive collective cell migration within tissues

Sijia Zhou

Université Fédérale
Toulouse Midi-Pyrénées

THÈSE

En vue de l'obtention du
DOCTORAT DE L'UNIVERSITÉ DE TOULOUSE

Délivré par l'Université Toulouse 3 - Paul Sabatier

Présentée et soutenue par

SIJIA ZHOU

Le 10 mars 2023

Nouveaux rôles de smallGTPase Rac1 dans la migration cellulaire collective invasive dans les tissus

---

Ecole doctorale : **BSB - Biologie, Santé, Biotechnologies**

Spécialité : **BIOLOGIE CELLULAIRE**

Unité de recherche :
MCD - Molecular, Cellular and Developmental Biology Unit

Thèse dirigée par
Xiaobo WANG

Jury
M.David CRIBBS, Président
M. Nicolas DAVID, Rapporteur
Mme Angela GIANGRANDE, Rapporteure
M. Olivier DESTAING, Examinateur
M. Xiaobo WANG, Directeur de thèse

ACKNOWLEDGEMENTS

My PhD studies in France, which have lasted three and a half years, are drawing to a close. These past few years at Toulouse have undoubtedly shaped me into the kind of graduate I set out to become.

My time in Toulouse equipped me not just with a solid technical and scientific foundation but also with the practical expertise that I'll need to overcome a wide range of challenges. First and foremost, I would like to thank my supervisor, Dr. Xiaobo Wang. With his unwavering support throughout the years, I was able to make tremendous strides in my studies. I'd also like to thank my labmates, especially Karine Belguise, Jiaying Liu, Hao Li, Bing Liu, Aurelien Guillou, Kelvin Mouysset, and Amandine Nicolas.

I'm grateful to the China Scholarship Council (CSC) for funding the first three years of my PhD program and La Ligue contre le Cancer for funding the extra six months.

Thanks to my mother Xiuping Liu and my father Wenlin Zhou, my cute boyfriend, soul mate, Jesse van de Linde, my best homie Yingqi Liu, and my close friends, I have received endless encouragement and love from them.

Lastly, I want to thank my thesis jury members from the bottom of my heart. Your suggestions have been very helpful and will guide me as I continue to explore the world of science.

Sijia Zhou

December 2022 in Toulouse

APPENDIX

Proposed publications

[1] **Zhou S,** Li P, Liu J, Liao J, Li H, Chen L, Li Z, Guo Q, Belguise K, Yi B and Wang X. Two Rac1 pools integrate the direction and coordination of collective cell migration. Nat Commun (2022) 13(1):6014.

[2] **Zhou S**, Liu J, Grammont M, Mangeat T, Balor S, Li H, Xue S, Wang X. Tissue physical property governing collective cell migration. Manuscript in preparation.

[3] Liu C*, **Zhou S***, Chen L, Liu J, McDonald J, Cadamuro V, Dupré L, Chen J, Belguise K, Yi B and Wang X. Pulsatile actomyosin networks orchestrate collective cell migration in tissues. Manuscript in preparation. (*Joint First author)

Oral presentations

[1] The 2nd cell la vie! September 21st -23rd 2022; Paris, France.

[2] The 3rd meeting of the French Optogenetics club. June 23rd -24th 2022; Toulouse, France

[3] Drosophila Development and Genetics in Toulouse: 35 years and beyond. September 30 and October 1st 2021; Toulouse, France

ABSTRACT

Collective cell migration plays important roles in development and cancer biology. By using *Drosophila* border cell migration as an *in vivo* model, and applying *Drosophila* genetics, live imaging, and optogenetics, I unraveled two novel important roles of small GTPase Rac1 in controlling both migrating cell collective guidance and environment cell physical properties, two critical aspects in collective cell migration within tissues. Firstly, I revealed that two Rac1 pools govern border cell protrusions and supracellular cables, two important structures responsible for direction and coordination; and a balance between these two Rac1 pools ensures the realization of collective guidance for migration efficiency. Secondly, I identified another new function of Rac1 in environment substrate cells, which controls tension force to cooperate with substrate cell pressure for the establishment of various travel paths, thus governing collective cell migration behaviours.

RÉSUMÉ

La migration cellulaire collective joue un rôle important dans le développement et la biologie du cancer. En utilisant la migration des cellules de bordure de la drosophile comme modèle in vivo et en appliquant la génétique de la drosophile, l'imagerie en direct et l'optogénétique, j'ai découvert deux nouveaux rôles importants de la petite GTPase Rac1 dans le contrôle du guidage collectif des cellules migrantes et des propriétés physiques des cellules substrat de l'environnements, deux aspects critiques de la migration cellulaire collective dans les tissus. Tout d'abord J'ai découvert que deux pools fonctionnels de Rac1 sont répartis au niveau de deux structures cellulaires importantes pour la migration collective, que sont les protrusions et les câbles des cellules migrantes ; l'intégration de ces deux pools de Rac1 est importante pour le guidage collectif des cellules migrantes et ainsi pour l'efficacité de leur migration collective.. Deuxièmement, J'ai montré que Rac1 contrôlait la tension corticale des cellules substrats de l'environnement, et cette tension coopère avec la pression à l'intérieur de ces cellules afin de modifier la voie de passage des cellules migrantes, contrôlant ainsi l'efficacité de leur migration à travers les tissus.

CONTENTS

ABBREVIATIONS

ACHR: Acetylcholine receptor

ARP2/3: Actin-related protein-2/3

BMP: Bone morphogenetic protein

BNL: Branchless

BTL: Breathless

CA: Constitutively active

CIB1: Cryptochrome interacting basic helix-loop-helix 1

CRY2: Crytochrome 2

DDRs: Discoidin domain receptors

DN: Dominantly negative

DPP: Decapentaplegic

ECM: Extracellular matrix

ECR: Ecdysone receptor

EGF: Epidermal growth factor

ELMO: Engulfment and cell motility

ERK: Extracellular signal-regulated kinase

FGF: Fibroblast growth factor

FRET: Fluorescence resonance energy transfer

GAPs: GTPase activating proteins

GEFs: Guanosine nucleotide exchange factors

HNT: Hindsight

HPF: Hours after fertilization

JNK: Jun N-terminal kinase

LARIAT: Light activated reversible inhibition by assembled trap

LINC: Linker of nucleoskeleton and cytoskeleton

LOV: Light-oxygen-voltage domains

MAPK: Mitogen-activated protein kinase

MBC: Myoblast city

MDCK: Madin-darby canine kidney

MELC: Myosin essential light chains

MHC: Myosin heavy chains

MRLC: Myosin regulatory light chains

NMs: Neuromasts

NMII : Non-muscle myosin II

PA : Photoactivatable

PCB: Phycocyanobilin

PDGF: Platelet-derived growth factor

PHYB: Phytochrom B

PLLP: Posterior lateral line primordium

PP1: Protein phosphatase 1

PTPs: Protein tyrosine phosphatases

PVR: PDGF-and VEGF-related receptor

ROCK: Rho-associated coiled-coil kinase

RREB1: RAS responsive element binding protein 1

ROS: Reactive oxygen species

RTK: Receptor tyrosine kinases

SDF: Stromal cell-derived factor-1

TAI: Taiman

TSL: Torso-like

UPD: Unpaired

USP: Ultra spiracle

VEGF: Vascular endothelial growth factor

WAVE: WASP family verprolin homology domain-containing protein

WT: Wildtype

FIGURE LISTS

INTRODUCTION

RESULTS

Chapter *I*

INTRODUCTION

Chapter *I: General cell migration*

I.1. History of cell migration

Cell migration is known as the movement of cells that occurs in response to the reception of a migration signal or the detection of a specific signal gradient. It is a spatiotemporal process that switches between extending pseudopodia at the cell's head, forming new adhesions, and contraction at the cell's tail (Kirfel et al., 2004; Ridley et al., 2003). This is a normal kind of cellular mobility and a fundamental aspect of cellular life. It is also an essential physiological activity for the growth and development of organisms (Friedl and Gilmour, 2009; Schumacher, 2019; Tahara et al., 2016).

Cell migration was firstly discovered in the 17th century by Antonie Van Leeuwenhoek using his own handmade microscope. His letter to the Royal Society described the movement of bacteria and opened the first page of scientists' study on cell migration. For more than 300 years, attempts have been made to understand the details of cell migration (Fuchs, 1984). The cytoskeleton, a key material for cell migration, was not discovered until the 20th century. In 1939, Albert Sandergui discovered actin and myosin, which are part of the cytoskeleton. However, sample preparation for electron microscope required cryo-fixation at 0 to 4 °C, so the cytoskeleton will depolymerize in this case. But after the 1960s, people began to gradually discover the cytoskeleton using the method of glutaraldehyde fixation at room temperature. Scientists have found that the cytoskeleton plays a role in carrying and supporting cells in the process of cell migration (Haston, 1987; Seetharaman and Etienne-Manneville, 2020; Warchol et al., 1975). In the late 20th and early 21st centuries, scientists made great progress in the understanding of complex mechanisms controlling

cell migration and cell-matrix adhesion, asymmetric polarization, and intracellular stratification movement (Amelio et al., 2012; Bixby and Jhabvala, 1990; Katoh, 2005). However, the whole process is still not fully understood, and many substances in the intermediate processes are not clear.

I.2. Importance of cell migration

Compared with the movement mode and morphology, cell migration is a directional movement through the deformation of the cell body, which is different from the movement of cells through flagella and cilia, or the position change of cells with the blood flow, and the speed of cell migration is much slower than them. Although it is slow, cell migration is important for numerous cellular functions, including foraging, wound repair, and immunological responses (Freitas et al., 2021; Liu et al., 2021; Nikolopoulou et al., 2017). For example, during the gastrulation stage of embryo development, a large number of cells from different germ layers move as thin sheets within the embryo (McMahon et al., 2008). This leads to early morphogenesis and helps to form tissues and organs. Another example is wound healing or skin renewal, which is also highly dependent on cell migration. When a wound occurs, cells in the dermis start to multiply and move toward the wound, and then they close the wound (Nanba et al., 2021). In immune surveillance and immune responses, the lymphatic network helps immune cells move (Hwang et al., 2007).

However, as a crucial process, cell migration can also contribute to disease, especially the spread of cancer cells (Friedl and Gilmour, 2009; Zanotelli et al., 2021). During malignant cancer progression, aggressive cancer cells can cross the basement membrane, penetrate the connective tissue and matrix microenvironments, and pass barriers (Fig.1). These behaviors all require the interaction between malignant cancer cells and their surrounding environment (Chang and

Chaudhuri, 2019). Therefore, studies of cell migration mechanisms can help us find better ways to reduce the spread of highly malignant cancer cells, to improve wound healing, or to promote tissue regeneration and transplantation.

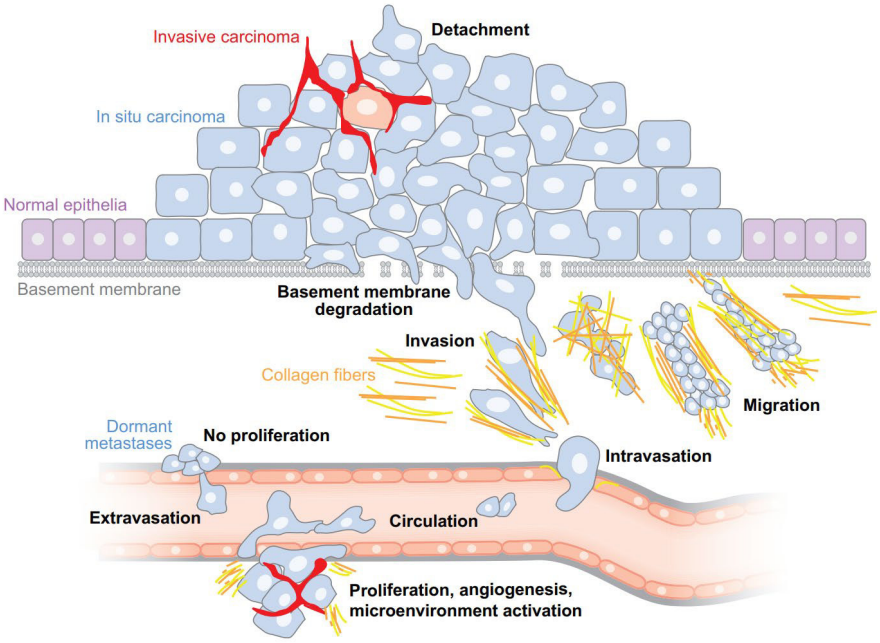

Figure 1. Penetration of the basement membrane by tumor cells and invasion of the surrounding tissues.

Adapted from (Marina Bacac and Ivan Stamenkovic, 2008)

I.3. Different types of cell migration

I.3.1 Single cell migration

Cell migration is divided into single cell migration and collective cell migration. Single cell migration presents a complex set of cellular behaviours including sensing, polarization, cytoskeletal rearrangement, adhesion changes and morphological changes (Mak et al., 2016; Stock and Pauli, 2021). As individual cells migrate, all these behaviours are under continuous and precise

regulation and feedback control to maintain directional cell motility. The fundamentals of single cell movements have been extensively studied in cells such as fibroblasts or keratocytes.

Two major modes of single cell migration have been described: mesenchymal and amoeboid (Fig2. B). The mesenchymal mode is slow, and it is based on large lamellipodial protrusions caused by actin polymerization and dependent on extracellular matrix (ECM) adhesion as well as matrix degradation; differently, the amoeboid mode is much faster and is based on membrane bleb, and it squeezes through pores in the matrix primarily by cortical actomyosin contractility (Yamada and Sixt, 2019). Depending on the surrounding environment, these two states may switch. Therefore, through this switch, cancer cells may modify their migration patterns, which may aid in tumour progression (Wolf et al., 2003).

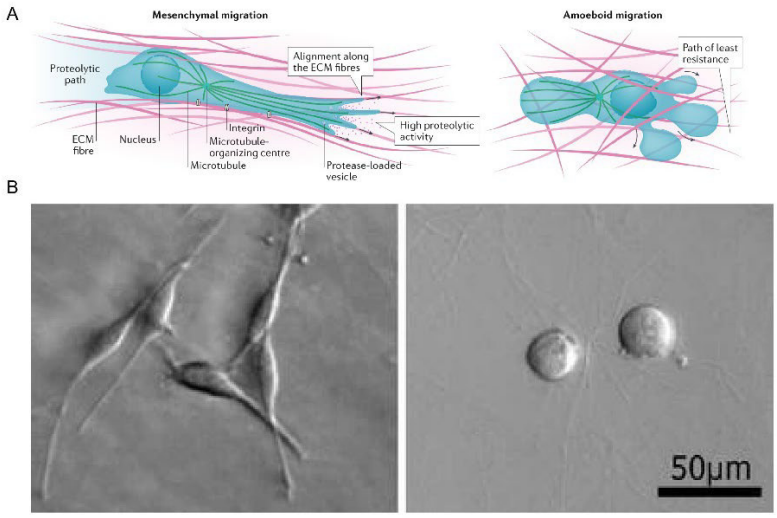

Figure 2. Two main modes of single cell migration.

(A) The mesenchymal cell aligns along tension lines of anterior-aligned ECM fibre, and the amoeboid cell moves by protruding through ECM pores.

(B) Mesenchymal K4 sarcoma cell line (left) and amoeboid A3 sarcoma cell line (right)

Adapted from (Kenneth M. Yamada and Michael Sixt, 2019, K. Paňková et al., 2010)

I.3.1.1 Fibroblasts

Fibroblasts are derived from the mesoderm and are usually found in connective tissue. They make collagen, glycosaminoglycans, and important glycoproteins such as fibronectin in the ECM (Samlaska and Winfield, 1994). *In vitro*, these cells have been widely studied due to their ease of culture and simplicity. In cell culture, fibroblasts move slowly, at an average of less than 1 μm per minute, and in different directions (Abercrombie et al., 1970). They have been found to have different shapes, such as spread or spindle-shaped, which are specified by several extending processes (Puck et al., 1957) (Fig. 3A). The textbook model of classical motility stages has been drawn from fibroblast movement. It divided the motility cycle into four stages: protrusion of cells, sticking to the leading edge, generation of contractile forces between the leading and trailing edges, and ultimately release of the trailing adhesion (Chen, 1979). Over the last century, great efforts have been devoted to elucidating the process of cell migration exemplified by fibroblasts over the past hundred years (Pollard and Borisy, 2003; Waldeland et al., 2020).

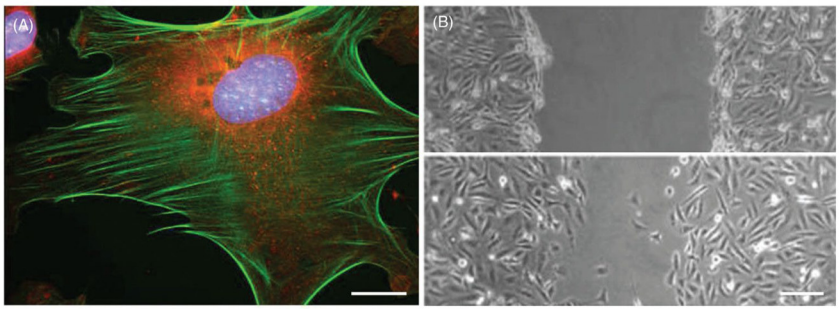

Figure 3. Fibroblasts shape and migration.

(A) A C3H10T1/2 fibroblast labeled with DAPI (blue) for DNA, MitoTracker (red) for mitochondria, and Alexa Fluor phalloidin (94) for F-actin.

(B) Fibroblasts moving into wound.

Adapted from (Xavier Trepat et al., 2012)

Fibroblasts are very important in wound healing. After injury (both *in vivo* and *in vitro*), fibroblasts move to the wound, where they generate and deposit ECM (Martin, 1997; Schreier et al., 1993). Interestingly, compared to individual fibroblasts in cell culture, fibroblasts often migrate at different rates and morphologies. Quiescent fibroblasts have smaller lamellipodia and have multiple stress fibers; in contrast, fibroblasts migrating into the wound always have large lamellipodia protruding into the wound and have fewer stress fibers. Many growth factors, such as epidermal growth factor (EGF) (Ware et al., 1998) and platelet-derived growth factor (PDGF) (Suetsugu et al., 2003), are known to act as mitogens or chemokines for fibroblasts in wounds. Notably, growth factor stimulation can enhance the migration speed of individual fibroblasts by a factor of 3, as well as increase changes in the direction of cell migration.

I.3.1.2 Dictyostelium

The typical model for amoeboid migration is Dictyostelium. Discoideum is a tiny (10-20 μm in diameter) mobile soil amoeba that has long been used as a model organism to investigate the actomyosin cytoskeleton and chemotactic migration (Neuhaus et al., 2002) (Fig. 4). During its movement, a single amoeba cell must extend a rapid protrusion at the front and retract at the rear part. Due to the gradient simulation of chemoattractants, this requires different controls at the leading and trailing edges simultaneously. These two distinct cellular behaviors are the result of a spatiotemporal sensing system. First, protrusions in the correct upward gradient direction are activated, so the cell turns to chemoattractants (Langridge and Kay, 2006). Second, randomly oriented (incorrect) protrusions are suppressed (Wessels et al., 2007). By that way, amoebae moving in the correct direction will continue to do so, while those that are wrong will be more

likely to change to a new randomly chosen direction. These behaviours are more common in steady, shallow gradients, but in steep gradients, the inhibition of erroneous turns and the activation of correct turns are so precise that the amoebae hardly make random turns.

It is well known that actomyosin contraction mediated by myosin II at the cell rear can provide the main force for amoeboid migration (Lämmermann and Sixt, 2009). By applying reverse genetics, mutants lacking conventional myosin II still migrate slowly and have low chemotaxis (Wang et al., 2011). This indicates that other actin motor proteins also play a role in amoeboid migration. In addition to mchA, which encodes the conventional myosin II heavy chain gene, 12 genes encoding unconventional myosin have been identified in Dictyostelium (Titus et al., 1994). Some of these unusual myosins participate in overlapping, redundant functions in motility, help to suppress lateral random protrusion, and promote actin polymerization at the front of the cell. But even in triple mutants lacking three different unconventional myosins, chemotaxis and motility are reduced, but not eliminated (Jung et al., 1996). One of the persistent conundrums in chemotaxis research is that knocking out so many related genes can only reduce, but not eliminate, chemotaxis. There is a consensus that this is because multiple pathways are involved, and thus chemotactic orientation can only be completely prevented by eliminating all pathways. Recent studies have shown that the chemotaxis of *Dictyostelium* involves up to four key signaling pathways, including PI3 kinase, phospholipase A2, the noncatalytic domains of soluble guanylate cyclase in the front of the cell, and the cGMP at rear of the cell (van Haastert et al., 2007; Veltman and Van Haastert, 2006).

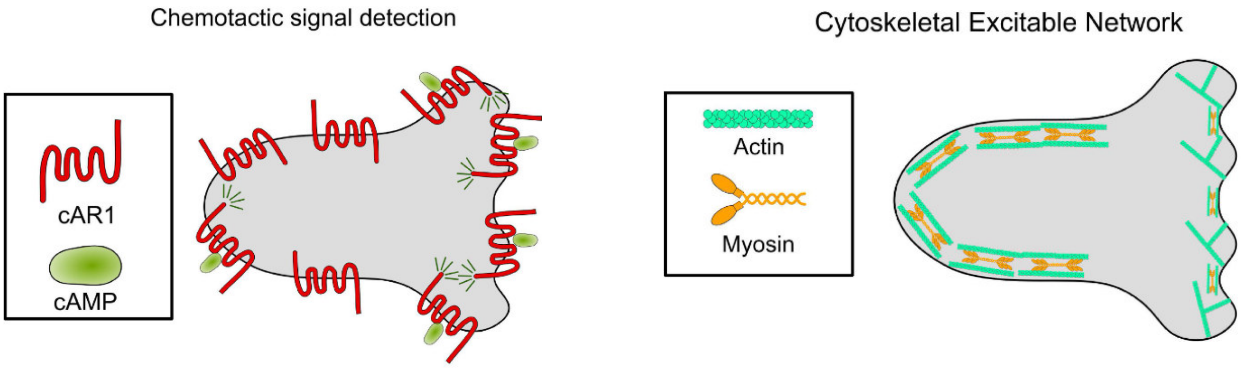

Figure 4. Diagrams of the chemotaxis network and actomyosin network in *Dictyostelium*.

Adapted from (Jonathan Kuhn et al., 2021)

I.3.2 Collective cell migration

Collective cell migration is the movement of several cells as a tightly or loosely connected group in a coherent and coordinated way. It is the most common form of migration during development, wound healing, and tissue regeneration (Bianco et al., 2007b; Ewald et al., 2008; Xiao et al., 2019). Furthermore, it is increasingly recognized as a widespread mode of migration during metastasis in epithelial cancers (Friedl and Wolf, 2003; Wolf et al., 2007). Collectively migrating cells protrude, polarize, shrink, and attach to the surrounding matrix through the same process as individually migrating cells (Fig. 5). However, their capacity to chemically and physically link with each other provides an additional migration mechanism for cells to migrate in groups. Little is known about how groups of cells move together compared to about how individual cells move, but new techniques in genomics, proteomics, imaging, and biomechanics are making rapid progress in this field (Aman and Piotrowski, 2008; Chen et al., 2021; Czerniak et al., 2016; Lecaudey et al., 2008).

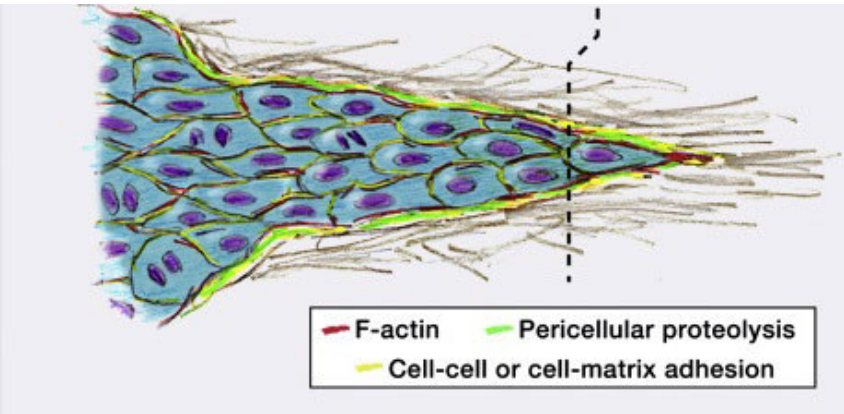

Figure 5. Diagram of collective cell migration

Adapted from (Peter Friedl and Stephanie Alexander, 2011)

From early embryogenesis, the development of an organism is driven by the movement of cell populations. Given the difficulty in studying the cell movement of higher animals, collective cell migration is often studied in relatively simple models, such as *Drosophila*, C. elegans, or zebrafish. These model systems offer structural simplicity and genetic accessibility, allowing direct visualization of motor groups expressing selectively fluorescently tagged proteins. Classic models of collective migrations include: (a) *Drosophila* dorsal closure; (b) development of the lateral line system in zebrafish; (c) tracheal branching morphogenesis in *Drosophila*; (d) *Drosophila* border cell migration. Studies of these models show that the motion of cell groups depends not only on the movement of individual cells, but also on the supracellular network and the interaction with the surrounding environment.

While collective cell migration is critical for development, it also contributes to diseases such as cancer (Janiszewska et al., 2020; Park et al., 2016). The conventional view of cancer metastasis is based on the idea that single cells migrate and colonize healthy tissue to form secondary tumors.

However, increasing evidence suggests that tumor spread is not only driven by single cells but also by cohesive cell populations (Majidpoor and Mortezaee, 2021; van de Merbel et al., 2018). This notion is supported by the observation that clusters of metastatic cells are often present in the blood and lymphatic vasculature of cancer patients. Furthermore, histopathological sections of breast, colon, ovarian, lung, and other differentiated carcinomas show clusters, chains, and sheets in the stromal regions surrounding the primary tumor (Choi et al., 2016; Ghosh et al., 2021; Mei et al., 2021; Richardson et al., 2018). Therefore, a clear understanding of the mechanisms underlying collective cell migration is very helpful in reducing the spread of highly malignant cancer cells.

Here, I will describe the first three models of collective cell migration, while leaving border cell migration (related to main topic of my PhD projects) in an independent section.

I.3.2.1 Dorsal closure in *Drosophila*

Morphogenesis is one of the main topics of developmental biology, and it involves the formation of cells, tissues, organs, and organismal forms. Dorsal closure is the last major morphogenetic process in *Drosophila* embryogenesis, and it is a fundamental model system for cell sheet morphogenesis in chordates (Heisenberg, 2009). During the onset of dorsal closure, the embryos have an uneven rectangular shape. The germ band includes the ventral, lateral, and dorsal epithelia. The dorsal opening of the epithelium is filled by a thin layer of squamous cells called amniotic serosa. When these cells enter the advancing epidermal cell layer, it contracts to provide the closing force and then undergo apoptosis. Furthermore, protruding actomyosin-rich purse strings or cables at the leading edges of the two lateral epidermal cell sheets facilitate closure (Fig. 6). Taken together, the applied forces drive the circumference of the outer epidermis to extend dorsally until the two flanking cell layers meet in the absence of cell proliferation and convergent extension. The

next step is to zip up the canthi, which makes first a patched epithelium and then a smooth epithelium (Kiehart et al., 2017).

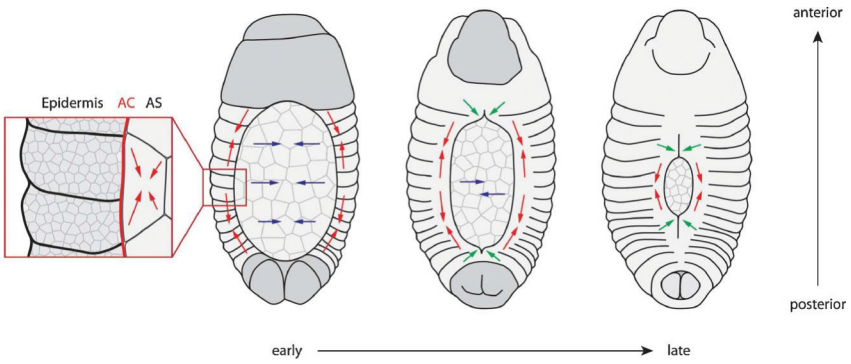

Figure 6. Diagrams of dorsal closure in Drosophila embryos.

Adapted from (Carl-Philipp Heisenberg, 2009)

Complex signaling mechanisms regulating dorsal closure include the Rho superfamily small GTPases, non-receptor tyrosine kinases, the Wg/Wnt system, the Notch pathway, the Jun N-terminal kinase (JNK) pathway, the bone morphogenetic protein/ decapentaplegic (BMP/DPP) pathway, and the insect steroid hormone Ecdysone. During dorsal closure, the JNK pathway controls actin cytoskeleton polymerization which activates the protrusion of lateral epithelial leading cells; the canonical Wnt pathway, signaling through beta-catenin (Armadillo in *Drosophila*), controls epidermal cell polarization; and the Rho family is a key signaling pathway to regulate actomyosin contractility and actin network, which are required for the generation of intrinsic tension required for the purse string segments, junctional belts and medioapical arrays in amnioserosa cells (Mishra et al. 2021; Harden 2002; Tafesh-Edwards and Eleftherianos 2020).

I.3.2.2 Posterior lateral line primordium (pLLP) migration in zebrafish

The lateral line in fish and amphibians is a mechanosensory system. It can detect changes in water flow and is necessary for feeding and swimming (Montgomery et al., 2000). Due to its proximity to the skin surface, this is a readily tractable system to explore the process of collective cell migration. The posterior lateral line primordium (pLLP) in zebrafish consists of approximately 100 cells that travel down the flanks of the embryo throughout development. At about 22 hours after fertilization (hpf), the distant part of the pLLP begins to move along one side of the body, while the part including the sensory neurons stays behind. Migration along the body is directed to the tail and will reach 48 hpf. During the pLLP migration, some clusters of around 20–30 cells at the tail edge will differentiate into mechanosensory neuromasts (NMs). pLLP migration is complete when the terminal cluster (i.e., a group of two or three NMs in a faraway area) is put down (Chitnis et al., 2012; Nogare et al., 2017).

pLLP applies Cxcl12a as a chemotactic cue. Cxcl12a-deleted mutants cause a failure in pLLP migration, and ectopic expression of cxcl12a can redirect pLLP migration toward an incorrect Cxcl12a source. Because Cxcl12a does not have a gradient along the trunk, pLLP generates an intrinsic gradient by expressing two chemokine receptors, Cxcr4b in the leading region and Cxcr7 in the rear area. Inhibiting either Cxcr4b or Cxcr7 results in a failure of migration, indicating the importance of both receptors. By using live imaging, the chemokine-receptor internalization of Cxcl12a and Cxcr7 is observed. As a result, an internal gradient of Cxcl12a is formed, with a high level in the leading region and a low level in the rear area (Fig. 7). It has been suggested that the expression of cxcr7 is downstream of two active signaling pathways in pLLP: Wnt (leading area) and Fibroblast growth factor (Fgf) (rear area) signaling (Perlin and Talbot, 2007). However, the expression of chemokine receptors did not reflect the Wnt and Fgf signaling domains, indicating

that regulation is indirect. More testing is needed to understand how chemokine receptor expression is controlled during pLLP migration.

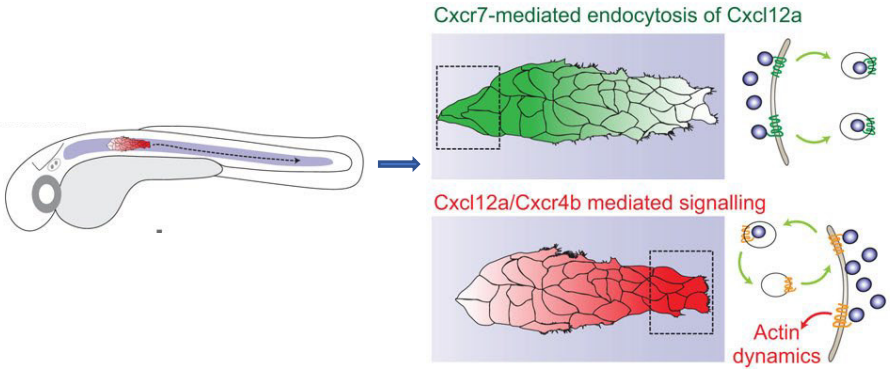

Figure 7. Model of pLLP migration in zebrafish. The internal gradient of Cxcl12a (purple) caused by Cxcr4b (orange) and Cxcr7 (green).

Adapted from (Germán Reig et al., 2014)

I.3.2.3 Tracheal branching morphogenesis in Drosophila

The insect tracheal system is a network of epithelial tubules that act as respiratory organs, providing oxygen to numerous target organs. In the absence of cell division, tracheal branching occurs in *Drosophila* through collective movement and cell intercalation. Clusters of tracheal cells separate from epidermal cells and invaginate to form a sac-like tracheal structure (Ghabrial et al., 2003). They respond to the ligand branchless (Bnl) secreted in adjacent tissues through the receptor breathless (Btl), migrate towards the source of Fgf and remain attachment to their tracheal adjacencies. The tip cells at the end of the branches consistently have the most Btl signaling. They produce large protrusions and lead the group to migrate, while the rest are seen as followers making only small, faint protrusions (Lee et al., 1996) (Fig.7a).

In this scenario, the leader cell setup is strongly stereotyped, and requires Delta-Notch-dependent lateral inhibition. Btl-positive cells may produce Delta, which activates Notch in neighbouring cells. Furthermore, Btl+ cells can migrate to the tip location to restore branching morphogenesis in a Btl mutant, indicating the importance of Btl signaling in tip cells (Fig.7b). Laser ablation of tip cells results in damage to stalk cell intercalation, indicating that tensile forces derived from tip cell migration control intercalation. With the movement of tip cells, stalk cells form passive intercalation, thus contributing to the elongation of the branches (Affolter et al., 2009). The mechanism of this collective cell migration differs from the zebrafish lateral line, in which entire populations of cells migrate.

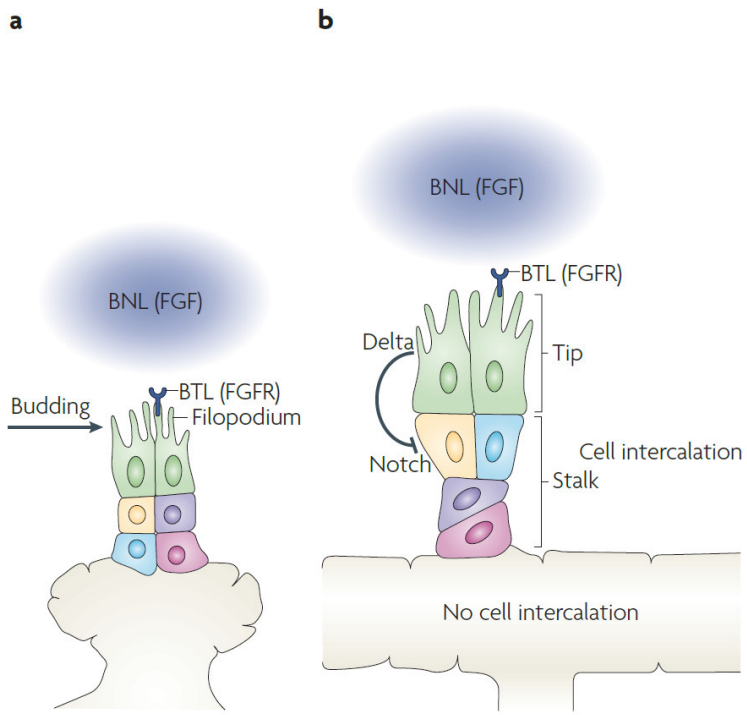

Figure 8. Diagrams of *Drosophila* Tracheal branching. Branchless, a fibroblast growth factor, leads Drosophila melanogaster's tracheal branching hierarchy.

a. Bnl gradients drive tracheal cell motility closer to the source. Tracheal cells reacting to Bnl (green) via the Breathless Fgf receptor (FGFR) grow many filopodia and travel along the BNL gradient, forming bud-like structures.

b. The tracheal bud quickly forms a tip and stalk. Delta–Notch signaling controls this identification determination. The stalk elongates as tip cells move away from the starting structure. And the stalk cells intercalate (note the relative locations of the yellow, purple, blue, and pink cells throughout a–b) to release tensile force from stalk elongation.

Adapted from (Markus Affolter et al., 2009)

Chapter ***II:*** *Border cell migration*

II.1. Fundamentals of border cell migration

The female fruit flies, Drosophila melanogaster, have a pair of ovaries, either of which contain 15-20 strings of egg chambers (named as ovarioles). The egg chambers are progressing through 14 developmental stages. Each egg chamber contains 16 interconnected germ cells, including one oocyte and 15 supporting cells that are called nurse cells, surrounded by a monolayer of somatic epithelial follicle cells (Spradling and Bate, 1993). Germ cells come from the 4 cycles of incomplete mitosis during the beginning stages of oogenesis, whereas follicle cells keep dividing until around 850 during the end of stage 6 (Edgar and Orr-Weaver, 2001). Each egg chamber keeps a pair of special follicle cells called polar cells that are located at both anterior and posterior end of tissue (Ruohola et al., 1991). These two polar cells secrete a cytokine called Unpaired that can activate JAK-STAT signaling in their neighbouring follicle cells (Silver and Montell, 2001). During early stage 9, along with the high level of JAK-STAT signaling, the nearby 4-8 follicle

cells are recruited by the polar cells, and then surround these two central polar cells to form a migratory border cell cluster (Montell et al., 1992; Starz-Gaiano et al., 2008) (Fig.9). Notably, only the surrounding border cells exhibit migrating ability, while the motility of two center polar cells is undetectable (Montell et al., 2012). Among this migratory group, 1-2 of the border cells extend lamellipodial protrusions at the leading edge to invade in between the front nurse cells. Then, the whole cluster detaches from the external epithelial monolayer, and migrates in the center between the nurse cells, and finally arrives at the anterior dorsal side of oocyte at stage 10 (Montell, 2003; Rørth, 2002).

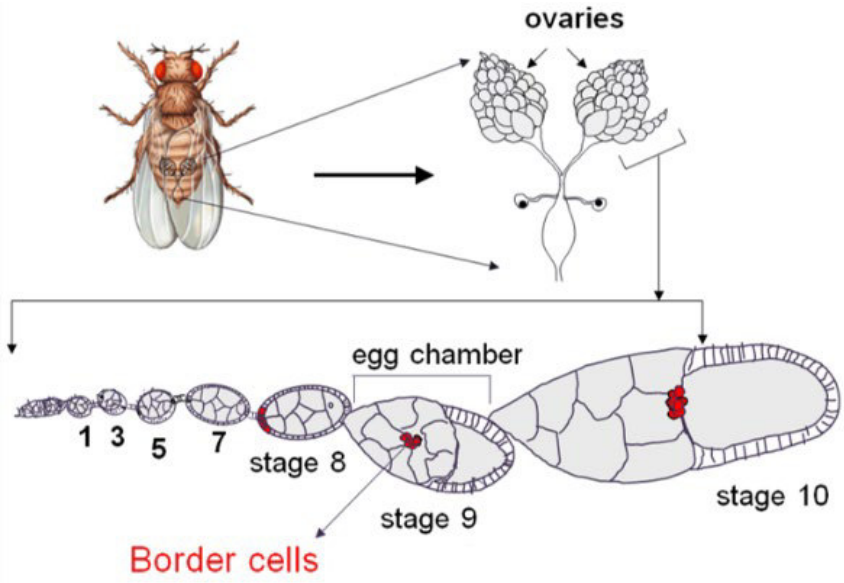

Figure 9. Diagram of Female fruit fly ovarian dissection and an expanded single ovariole with border cell migration within tissue.

Adapted from (Mohit Prasad et al.,2011)

During this process, border cells migrate about 150-200 μm within 3-6 h, exhibiting a big variation (Prasad and Montell, 2007). Apart from the differences in individual migration speed, one border cell cluster also presents different speeds along the way to the oocyte, excited and faster at the beginning, while tired and slower near the end (Bianco et al., 2007b; Prasad et al., 2007). Thanks to the live imaging, more detailed dynamics of border cell migration have been unrevealed (Prasad et al., 2011; Tekotte et al., 2007). The protrusions of border cells are preferably in the front, and can be retracted in a short time if they are not stably attached to the nurse cells. The cluster migrates in a crawling way with big protrusions, or moves forward in a rotating manner without big protrusions. The leading cells are changeable during moving while the polar cells remain at the center of the cluster (Prasad and Montell, 2007). Although polar cells are non-motile, they can still roll and spin together with outer border cells. During the past 15 years, the combination of live imaging with genetics, drug treatments or optogenetics allows us to explore the mechanisms of border cell migration from a higher and broader perspective (Montell et al., 2012).

II.2. Importance of border cell migration

Border cell migration plays a key role in eggshell production. After border cells reach the oocyte, they will bind tightly with some centripetal cells, creating the micropyle, a structure that serve as the channel for sperm to go through the eggshell (King, 1970; Montell et al., 1992). Since border cells are the first follicle cells to arrive at the location of micropyle and secrete a specific signal that help build the micropyle, it is widely believed that they initiate the micropyle generation (Montell et al., 2012). Moreover, border cells have been reported to synthesize and model the vitelline and chorion components of micropyle structure (Montell et al., 1992). Therefore, the failure of border cell migration causes infertility in Drosophila females. In addition, border cells

also express the patterning gene torso-like (tsl), which encodes a secreted protein that promotes the construction of the specialized head and tail regions of the embryo (Furriols et al., 2007).

One the other hand, the transition from static epithelial cells to invasive migratory cells is not only found in border cell migration, but also observed in embryonic development and tumour metastasis. This allows border cell migration to be a simple in vivo model for studying invasive collective cell migration within tissues, with advantages such as economic benefits, rapid development, ease of manipulation, and genetic traceability. Four major signal pathways have been identified by traditional genetic studies to regulate different aspects of border cell migration: the highly localized cytokine signal that activates JAK/STAT pathway (Silver and Montell, 2001), the global steroid-hormone pathway (Riddiford, 1993.), cell-cell contact dependent Notch pathway (Wang et al., 2007), and Receptor tyrosine kinases (RTK) pathway (Jékely et al., 2005). The JAK/STAT pathway is activated in border cells by a ligand called Unpaired (Upd) which is secreted from two polar cells. It is an essential signal for both the conversion of stationary epithelial cells to migratory cells and the maintenance of this migratory ability (Denef and Schüpbach, 2003; McGregor et al., 2002). Both subunits of Ecdysone receptor (EcR) and Ultra spiracle (Usp), and its coactivator Taiman (Tai) are required for border cell migration probably through the regulation of cell adhesion dynamics (Bai et al., 2000; Yao et al., 1993). Notch activation is required for the detachment of the cluster from the anterior pole. The RTK pathway is activated by Drosophila EGF and PVF ligands secreted from oocyte. EGF and PVF receptors (EGFR and PVR) function redundantly to provide guidance cue for the directional migration (Bianco et al., 2007b). The polarized localization of RTKs in border cells depends on the Rab11 mediated recycling of endocyted receptors (Assaker et al., 2010). In addition to these 4 major signals, the cell-cell

connection is also controlled by JNK signaling which may function through the regulation of integrin mediated adhesion (Llense and Martin-Blanco, 2008).

II.3. Cell-cell interactions within border cell cluster

II.3.1 Adhesions within border cell cluster

DE-cadherin adhesion complexes, composed of DE-cadherin, Armadillo also known as β-catenin and α-catenin, form the adherent junctions between border cells and central polar cells, as well as between adjacent border cells in border cell clusters. A low level of DE-cadherin is even found at the border cell-nurse cell interface, which has been proved to be necessary for border cell migration because the lack of DE-cadherin in nurse cells causes the failure of border cell migration (Niewiadomska et al., 1999). In addition, overexpression of DE-cadherin to excessively high levels in border cells also results in defective border cell motility (Schober et al., 2005). Taken together, a certain range of DE-cadherin expressions is required to balance the cohesion and traction of border cells, which thus guarantees normal migrating behaviours.

The regulation of DE-cadherin is very complex. Many mutations in important signals such as Stat, slbo, tai, yan, hnt and msn can influence the level and/or localization of DE-cadherin in border cells, thereby regulating border cell motility (Bai et al., 2000; Borghese et al., 2006; Cobreros-Reguera et al., 2010; Melani et al., 2008; Schober et al., 2005). For border cell detachment, post-transcriptional regulation is involved in the destruction of DE-cadherin to dissociate the physical association between border cells and epithelial monolayer (De Graeve et al., 2012). Perturbation of DE-cadherin levels in border cells also disturbs the dynamics of leader border cell protrusions extending in between nurse cells, indicating that DE-cadherin plays a critical role in border cell

adhesion on nurse cells (Pacquelet and Rørth, 2005). Recently, DE-cadherin has been found to help guide border cell migration, by controlling the polarity of each individual border cell (Veeman and McDonald, 2016) (Fig.10).

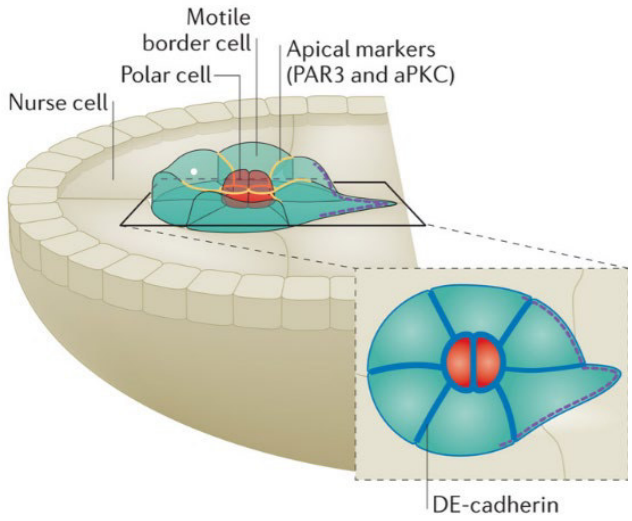

Figure 10. The inside–outside polarity of border cell group. Red indicates center non-motile polar cells. Drosophila melanogaster cadherin (DE-cadherin; blue) levels are high at border cell–border cell and border cell–polar cell interfaces and decreased at border cell–nurse cell interfaces. The apical–basal axis is perpendicular to the page, and the leading edge (purple dots) is to the right.

Adapted from (Denise J Montell et al., 2012)

II.3.2 Cohesions between border cell cluster

Although DE-cadherin adhesion complexes are regarded as the adherent junctions at cell-cell contacts both between polar cells and border cells or adjacent border cells, downregulation of DE-cadherin in border cells does not result in a dissociation of the border cell cluster (Niewiadomska et al., 1999). This suggests that in addition to DE-cadherin, some other signals would help maintain the cluster cohesion. Inhibition of JNK signalling results in cluster dissociation and long extension,

with a modest effect on border cell migration. Because the lack of JNK in border cells leads to mis-localization of the β-integrin from border cell-cell contacts to the protrusion tip, indicating that β-integrin could be an important factor in maintaining the integrity of the border cell cluster (Llense and Martin-Blanco, 2008).

Consistently, the reduction of the JNK pathway can be achieved by the overexpression of the transcription factor Hindsight (HNT), which also leads to the dissociation of the border cell cluster (Melani et al., 2008). Overexpression of HNT strongly delays the border cell movement, compared with the weak effect by inhibiting the JNK-pathway, likely due to the HNT-mediated control on STAT and SLBO (downstream of JAK/STAT pathway). On the other hand, the hnt mutant cells increase cell-cell adhesion and decrease the migrating ability of the border cell cluster, which is highly consistent with the role of a homologue human protein called RAS responsive element binding protein 1 (RREB1), thus indicating that the function of the HNT is highly conserved. Moreover, downregulation of the RHO-family GTPase Cdc42 or the apical polarity determinants PAR3 or PAR6, can also result in cluster separation (Pinheiro and Montell, 2004).

II.4. Actin cytoskeleton and the regulation of border cell migration

II.4.1 Actin cytoskeleton

During cell migration, the actin cytoskeleton plays a key role in protrusions, retraction, and adhesion formation (Insall and Machesky, 2009). Monomers of globular actin (G-actin) are continuously polymerized, first forming an actin nucleus and then a helical structure. And when the elongating is finished, the polymers assemble in a double helix, resulting in the formation of filamentous actin (F-actin). The polarized F-actin has two different ends, one called the plus end

promoting the polymerization and the other called the minus end functioning as depolymerization (Fig.11). The actin cytoskeleton polymerization at the leading edge provides the main force driving protrusions, thereby contributing to directed cell migration (Pantaloni et al., 2001).

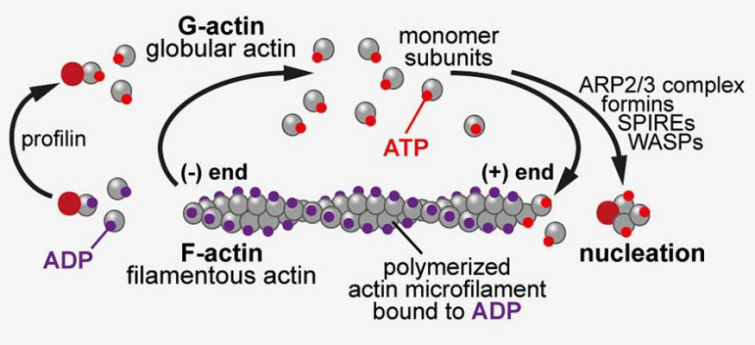

Figure 11. The actin filament dynamics.

Adapted from (Claire E. L. Smith et al., 2020)

Actin controls protrusions by assembling on the cortex just under the plasma membrane. There are two basic protrusion shapes, such as branched filaments forming lamellipodia or bundled/parallel filaments forming filopodia (Insall and Machesky, 2009). The lamellipodial protrusions are assembled from the Scar/Wave and Arp2/3 complexes, whereas filopodia protrusions are formed in two ways: either from branched networks by actin bundling proteins such as fascin, or from unbranched actin filaments by the formin family of proteins. Receptors on the plasma membrane can activate the Rho-family small GTPases, such as Rho, Rac, and Cdc42, and these smallGTPases can trigger the nucleation of new actin filaments through distinct downstream pathways, resulting in linear or branched filament arrays (Burridge and Wennerberg, 2004; Heasman and Ridley, 2008; Raftopoulou and Hall, 2004). The discovery of these pathways has revealed a better understanding of how cells move. Hundreds of actin binding proteins are also involved in modifying the structure of filaments and regulating their rotation and dynamics.

II.4.2 Myosin

Myosins are actin-dependent molecular motor proteins that have contractile ability and play a crucial role in various cellular processes. Myosins can hydrolyze ATP into mechanical energy thereby driving contractile force (Sellers, 1999). Although there are more than 10 classes of myosins, most of them belong to class II (myosin II), which drive the major contractile force in skeletal, cardiac, smooth muscle and non-muscle eukaryotic cells (Clark et al., 2007; Krendel and Mooseker, 2005). My PhD project focused on non-muscle myosin II (NMII), which plays a key role in border cell migration.

NMII consists of three pairs of peptides: two 230 kDa heavy chains (MHC), two 20 kDa regulatory light chains (MRLC) and two 17 kDa essential light chains (MELC). There are three subtypes (A, B and C) of NMIIHC in mammals but only one NMIIHC gene called zipper in Drosophila (Mansfield et al., 1996). Phosphorylation of MRLC regulates the motor domain activity and MELC works as the link between MHC and MRLC. After the MRLC is phosphorylated, the conformation of NMII is transformed, and the two globular heads of NMII can do a crosslinking with F-actin through the actin-binding domains. During this process, NMII pulls on F-actin thereby inducing its sliding, which contributes to actin filament dynamics (Fig.12). And a new cycle occurs when the ATP hydrolysis dissociates the NMII and F-actin from the actin-binding domains and restore NMII to its original conformation (Vicente-Manzanares et al., 2009).

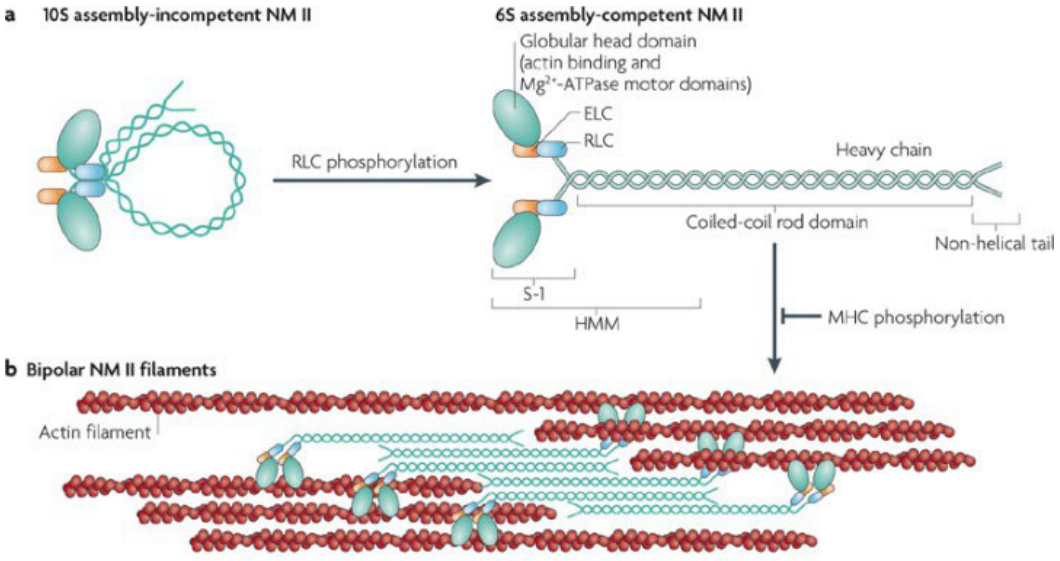

Figure 12. Non-muscle myosin II structure and the interactions between non-muscle myosin II and F-actin filaments.

a. Non-muscle myosin II structure and phosphorylation change from compact to stretch state.

b. Non-muscle myosin II bind to actin and form cytoskeleton structures.

Adapted from (Vicente-Manzanares et al., 2009)

II.4.3. RHO-family GTPases

F-actin dynamics, often with myosin contractility, are always the main power of cell movement *in vivo* and *in vitro*. Some small GTPases of the Rho-family, including Rac, RhoA and Cdc42, play a key role in the control of actin organization and dynamics as well as myosin activity (Haga and Ridley, 2016; Spiering and Hodgson, 2011). In cultured cells, Rac1 and Cdc42 function in controlling the extension of lamellipodia and filopodia, respectively, while RhoA controls the actomyosin stress fibers (Nobes and Hall, 1999) (Fig.13). The activities of these 3 small GTPases depend on their GTP or GFP loaded form. The Guanosine nucleotide exchange factors (GEFs)

catalyze the nucleotide exchange from GDP to GTP to induce the active form of these small GTPases (called GTP bound form). Oppositely, the GTPase activating proteins (GAPs), as a negative regulator, inactivate the GTPases by converting the GTPase-GTP form to the GTPase-GDP form (Narumiya, 1996).

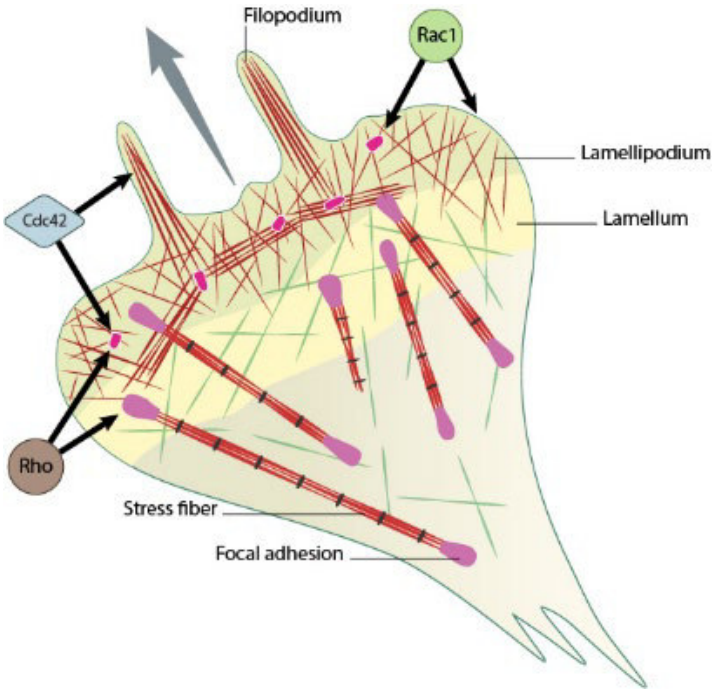

Figure 13. Rho family GTPases Rac1, Cdc42and Rho control cell migration at distinct locations (arrows). Rac1 mainly governs lamellipodium actin assembly. Cdc42 regulates filopodia and Rho controls stress fiber production and contractile activity.

II.4.3.1. Rac1

Rac in vivo functions was firstly demonstrated in *Drosophila* studies, including axon outgrowth, F-actin accumulation, and cell protrusion and migration (Harden et al., 1995; Luo et al., 1994; Murphy and Montell, 1996). Then, Rac activity has been found in almost all types of cell migration, either collective or individual, in normal or tumour cells. RacGEFs are also conserved, with 3

RacGEFS found in *Drosophila*: Vav guanine nucleotide exchange factor (Vav) (Malartre et al., 2010), and a heterodimer of Myoblast city (Mbc) and Engulfment and cell motility (ELMO) (Bianco et al., 2007b).

Three Rac genes are expressed in *Drosophila*: Rac1, Rac2 and Mtl (Hakeda-Suzuki et al., 2002). When comparing mutants blocking different Rac genes, only the inhibition of Rac1 is sufficient to prevent border cell migration. Many Rac1 effector proteins that bind Rac1-GTP have been discovered, including PAKs (p21-Activated Kinases), MRCK/CDC42BPA (CDC42 binding protein kinase Alpha DMPK-like), POR1 (Partner of Rac1) and POSH (Plenty of SH3s) (Kimura et al., 2006). During border cell migration, Rac1 binds the WASP family verprolin homology domain-containing protein (WAVE) complex to activate WAVE, which activates the ARP2/3 Actin-related protein-2/3 (ARP2/3) thus promoting the actin polymerization for the emergence of the lamellipodia protrusions (Miki et al., 1998).

Therefore, most *Drosophila* studies, including my PhD project, focused on Rac1 gene. When border cells specifically overexpress a dominant negative form of Rac1 (Rac1N17), most of them lose the ability to detach and move. Interestingly, overexpression of a constitutive active form of Rac1 (Rac1V12) also severely blocks this process, with 90% of border cell groups failing to detach (Geisbrecht and Montell, 2004). These two phenotypes derived from Rac1 activation and inhibition implicate the importance of Rac1 spatiotemporal activity on border cell migration.

To test this hypothesis, my PhD advisor, Dr. Xiaobo Wang, established a Rac1 Fluorescence resonance energy transfer (FRET) biosensor probe to monitor the activity of Rac1 in border cells during his postdoc training in Denise Montell's lab, and he revealed a Rac1 gradient, a high level at the front region to a low level at the rear region, in migrating border cell cluster. At the same time, he also introduced, the first time, an optogenetic tool called photoactivatable Rac (PA-Rac)

into *Drosophila* in vivo system, which enables Rac1 to be activated or inhibited in migrating border cells by blue light illumination. His optogenetic experiments confirmed that the small GTPase Rac1 is responsible for actin polymerization and protrusion dynamics during border cell migration. Consistently, local activation of Rac1 induces membrane ruffling and controls the direction of border cell migration. Unexpectedly, he found that local activation or inhibition of Rac1 activity in one border cell can strongly affect the migration and protrusion behaviours of neighboring border cells as well as distant border cells (Wang et al., 2010). This is the first report of cell-to-cell communication occurring during collective cell migration, which has led to many studies on how collective cells communicate with each other to achieve integrated migration behaviours. These studies hint at the potential importance of the membrane or cytoskeletal tension for intercellular communication. My PhD studies have focused on some controversial aspects of Rac1 activity and its role in border cell migration.

II.4.3.2. Cdc42

Similar to Rac1, Cdc42 also controls the actin polymerization, but the difference is that this process is critical for the extension of filopodia, but not lamellipodia. Activation of Cdc42 via conformational changes in p21-activated kinases PAK1 and PAK2 triggers actin polymerization to regulate cell adhesion, migration, and invasion (Rane and Minden, 2014). The role of Cdc42 has been wildly reported in cancer cells but very little in border cells (Arias-Romero and Chernoff, 2013; Murphy et al., 2021; Qadir et al., 2015). That could be due to the mild phenotype because overexpression of a dominant negative form of Cdc42 in border cells only causes 25% of the clusters to fail to reach the oocyte. In contrast, more than 40% border cell clusters appear to spread with several ectopic long protrusions by inhibiting Cdc42 activity, which is like the effect of

inhibiting JNK activity in border cells (Llense and Martin-Blanco, 2008). Consistently, Cdc42 has been found to positively regulate JNK by its reporter assay. Through the JNK pathway, Cdc42 thus controls the polarity protein (PAR-3), border cell adhesion protein DE-cadherin, substrate adhesion molecule β-integrin - and motor protein (myosin VI) in border cells, Particularly, inhibition of Cdc42 mis-localizes DE-cadherin from cell-cell contacts and also results in the accumulation of β-integrin and myosin VI at the tips of ectopic protrusions (Llense and Martin-Blanco, 2008). However, the mechanism of this small Rho GTPase and its effect on actin cytoskeleton is not as clear as Rac1. My PhD studies also explored the unknown function of Cdc42 in border cell migration. To this end, I introduced our recently established optogenetic tool called photoactivatable Cdc42 (PA-cdc42), which allowed to elucidate the spatiotemporal role of Cdc42 in migrating border cells.

II.4.3.3. Rho1

Rho1, the Drosophila homologue of the human RhoA protein, is essential for actomyosin stress fibre dynamics (Lu and Settleman, 1999). Rho1 regulates actomyosin force through the downstream Rho-associated coiled-coil kinase (ROCK) and NMII (Julian and Olson, 2014). In *Drosophila*, there is only one ROCK homologue, encoded by the rock gene. Similar to Cdc42, the role of Rho and its downstream effectors (ROCK, NMII) has not been clearly understood due to the mild phenotype of inhibiting Rho1 activity on border cell migration.

Nonetheless, expression of the dominant-negative form of Rho (RhoN19) in border cells still alters their morphology. As Rho1 is important during retraction, border cell clusters elongate along the anterior-posterior axis with the absence of Rho1 activity. In addition, with the inhibition of Rho1 activity, border cell group shows a strong migration delay. In fact, many groups exhibit the reduced

migration ability and thus fail to reach the oocyte. On the contrary, border cell clusters expressing a constitutive active form of Rho (RhoV14) are compact and round, and their protrusions are strongly reduced in both size and number, compared with wild type clusters. About 50% of these clusters show delays in their migration process (Bastock and Strutt, 2007). The individual border cells within these Rho1 active clusters trend to be dissociated from each other, and thus some inhibitory factors such as Protein tyrosine phosphatases (PTPs) need to be present in border cells to repress Rho1 downstream factors for the integrity of border cell clusters. Protein phosphatase 1 (PP1) has been shown to regulate the cadherin-catenin complex proteins at cell-cell junctions within the cluster and to limit actomyosin contractility to the cluster's edge (McDonald and Tomoyasu, 2020). Moreover, Rho1 activity can activate the planar polarity pathway Frizzled/Strabismus, thus keeping the border cell migration efficiency (Bastock and Strutt, 2007). Taken together, all results indicate that Rho1 also plays crucial role in border cell migration.

The relevance of myosin II for border cell migration was firstly reported by Edwards et al. in 1996. Myosin II accumulates at the leading and trailing edges of clusters to facilitate the movement of border cell clusters. The myosin II mutation prevents migration, and practically almost all border cell mutants in Sqh (Spaghetti squash, Drosophila homologue of MRLC) do not detach. The expression of a null allele of sqh, a dominant negative form of zip (Drosophila MHC homologue), RNAi against sqh or zip, a robust mutant allele of ROCK, or RNAi against ROCK in border cells inhibits the migration of border cell clusters. Cells harboring the null allele of Sqh, or the dominant negative version of Zip protrude further than wild type cells (Fulga and Rørth, 2002). McDonald's lab showed that ROCK and myosin II are also important for detachment (Majumder et al., 2012). Par-1, which phosphorylates and inactivates myosin II, regulates myosin II activity and localization during border cell detachment. Her lab also discovered a role for myosin II activity in

border cell migration. Myosin II maintains the form and organization of border cell clusters. Interestingly, her lab reported that nurse cells may be able to push border cells, and they proposed a model in which myosin II is increased near the cluster perimeter to preserve the cluster shape. This model has been used to explain how manipulation of nurse cell tension by RhoGEF2 overexpression in nurse cells limits border cell migration (Aranjuez et al., 2016). However, the pushing effect of actomyosin network proposed in this model is somehow contradictory to the common contractile property of actomyosin network. In addition, little is known about the influence of the environment on migrating border cells, while it may be critical for efficient migration.

Although actomyosin pulses have been well studied in epithelial cell contractility during tissue morphogenesis (He et al., 2010; Mason et al., 2013b; Qin et al., 2017), little is known about how this biochemical oscillator functions in border cells. Actomyosin pulses have been reported in a couple of recent studies, and these pulsed networks often present some flow patterns in migrating border cells. Currently, these actomyosin pulsed flows have been observed in either the base of leader protrusions of border cell clusters or supracellular cables around the cluster (from our unpublished data). However, how these pulsed flows are initiated and then governed, and how they play roles in border cell migration are still largely unknown.

Chapter ***III:*** *Environmental guidance*

III.1. Physical guidance by extracellular matrix

Collective cell migration is an important process by which groups of cells connected by cell–cell junctions move together. As previously mentioned, collective cell movement promotes ductal,

glandular, vascular development as well as epithelial homeostasis and regeneration (Montell, 2008). In addition, reactivated in mature tissue during tumorigenesis, coordinated motions lead to cancer invasion and metastasis (Sahai and Marshall, 2003; Wolf et al., 2003). By linking the actin cytoskeleton across numerous cell bodies, intercellular junctions ensure supracellular adhesion, polarization, and mechanical coupling, which are important for sensing and integrating external guiding cues and sharing signal processing and force transmission throughout the migrating collective group (Trepat and Fredberg, 2011). Moreover, cell–cell interactions govern collective behaviors beyond movement, including 'purse-string' contraction, epithelial gap closing, and tissue folding (Anon et al., 2012).

Physical guidance through different stiffnesses, dimensions and geometries of the environment, as well as chemical guidance, are well-understood ways for directing the migration of individual cells (Ridley et al., 2003). These guiding mechanisms could theoretically also be used for collective cell migration. However, collective cell movement involves intercellular connections and guidance signals to lead and maintain the migration of cohesive cell group, in contrast to single-cell migration, which results from the processing of extracellular input within the body of a single cell (Rørth, 2011). This includes external mechanical, chemical, and/or electrical inputs to direct collective cell migration. In the following sections, we will learn about the extracellular properties that control the polarity and guidance of collective cell migration.

III.1.1. Confinement

In physiological settings, the ECM or other cells in the vicinity usually prevents cells from moving. In general, environmental confinement may restrict the lateral extension of membrane protrusions and allow cells to stay in touch with their environment in the absence of cell adhesions. Recent

achievements in microfabrication methods have made it possible to alter cell confinement independently of ECM chemistry and stiffness. This allows us to understand that many characteristics of cell migration may be altered by the degree and type of confinement.

Cell movement on a two-dimensional (2D) surface is usually controlled by branched arrays of actin polymerization that propel the cell membrane forward in lamellipodia (Svitkina and Borisy, 1999). One possible reason is the inhibition of the antagonistic link between contractility and adhesion under restraint (Hung et al., 2013). Actomyosin contractions are restricted because the large contractile forces on a 2D surface might cause cell adhesions to break apart (Lauffenburger and Horwitz, 1996). In restricted situations, there is less demand for cell-matrix adhesion molecules, which is commensurate with the reduced importance of adhesion (Lämmermann et al., 2008). These results demonstrate that variations in confinement affect cell motility.

Although it is known that confinement affects cell migration, previous studies have not provided any mechanism. In constrained situations, cell adhesions change greatly: the large focal adhesions that most cells have as they move over 2D surfaces become a lot smaller (Fraley et al., 2010; Kubow and Horwitz, 2011). Because of the well-known role of focal adhesions as centers of cellular signaling, these structural changes may be a way to alter cellular phenotypes (Huveneers and Danen, 2009). In this idea, a flat, unrestricted surface would make it easier for cell adhesions and ARP2/3 activity to work together in a positive way, leading to cell movement driven by lamellipodia. If the confinement prevents a lamellipodium from forming in a certain way, other adhesion structures may form. Indeed, the distribution of adhesion complex components changes as cells move through narrow channels instead of dense 3D collagen matrices. Intriguingly, cells confined in one dimension may have shapes that look like cells that are confined in higher dimensions (Doyle et al., 2009). This supports the idea that the changes in cell adhesion found in

cells that cannot move much in 3D environments may be due to the fact that lamellipodium development is slowed down. As confinement increases, cells become more difficult to deform enough to pass through the environment. Compared with other cell organelles, the nucleus is the biggest obstacle to cell compression because of its size, stiffness, and how it moves (Harada et al., 2014; Wolf et al., 2013).

III.1.2. Stiffness

The physical deformability of the environment varies by orders of magnitude in different tissues. Therefore, rigidity is another key factor to consider for cell migration. Numerous cells can detect the stiffness of ECM through a mechanism called mechanotransduction. If a cell has multiple attachment points on a rigid substrate, the force exerted by actomyosin cables (also known as stress fibers) on these attachments may cause either the generation of tension within the cell or the movement of the cell if some adhesions detach or slide (resulting in asymmetrical tension). Consequently, the coordination of actomyosin on matrix adhesions serves as a mechanosensing unit (Schwarz and Gardel, 2012; Trichet et al., 2012). Forces generated by stress fibers on integrin-mediated adhesions may alter the shape of adhesion complex components. For example, the application of force to the adhesion complex adaptor protein CRK-associated substrate (CAS; also known as BCAR1) exposes phosphorylation sites for SRC-family kinases, which may bind signaling proteins and hence trigger downstream signaling of Rac1 and RAP1A activity (Huveneers and Danen, 2009; Sawada et al., 2006). A positive feedback loop involving Rho guanine nucleotide exchange factor 1 (ARHGEF1) and ARHGEF12 leads to RhoA activation and enhanced actomyosin force generation (Guilluy et al., 2011). This mechanosensing process will eventually result in actomyosin contractility producing higher forces on increasingly stiffer

substrates. It means that the forces generated by the cells will match the amount of force required to change the shape of the ECM.

Cells are able to sense both the global and local stiffness of their substrates, and they need mechanosensing equipment of varying sizes in order to detect differences in the substrate rigidity at subcellular sites. In recent studies, 1 μm mechanosensing modules have been described (Ghassemi et al., 2012). These complexes have a similar composition to that of large stress fiber–focal adhesion complexes in terms of their molecular components. Actin, myosin, and paxillin are the three proteins that make up these structures, and they likely use the same actomyosin force principle as cell–ECM attachment sites. Actin polymerization and the dynamic behavior of integrin bonds might be the means by which focal adhesions detect stiffness (Elosegui-Artola et al., 2014; Plotnikov et al., 2012). These modules could polarize the cytoskeleton and aid in controlling cell movement in specific directions.

In addition, stiffness perception may occur more directly in the nucleus. The nuclear envelope is directly connected to the actin cytoskeleton through the linker of nucleoskeleton and cytoskeleton (LINC) complex and Nesprin-containing complexes (Mellad et al., 2011). These complexes are able to transmit stress from the actin network in the cytoplasm to the nuclear envelope. They may also alter the function of nuclear proteins. LaminA deficiency reduces the activation of transcriptional responses mediated by YAP, TAZ, and MKL (Ho et al., 2013; Swift et al., 2013). Therefore, the nuclear lamina can be regarded as a third mechanosensory system that detects both confinement and rigidity.

III.1.3. Surface topology

In 1D surface, cells must align their adhesion sites to be as thin as the ligand, resulting in chain-like movement along this single cue (Doyle et al., 2012; Doyle et al., 2009). And in 2D surface, moving cell sheets have lateral twists and occasional lateral rotations. The 2D surfaces, such as the plane of a cell culture dish *in vitro* or the basement membrane of blood vessels *in vivo*, can provide the topographically unrestricted distribution of adhesion sites underneath the cell group, thus allowing 2D haptokinesis as a multicellular sheet to occur (Kim et al., 2013; Yevick et al., 2015). In 3D environment, cell groups migrate in the correct direction by using 3D topographic information, while avoiding other directions (Fig.14). Moreover, sheet-like 2D interfaces between muscle fibers or larger nerves and ECM fibril networks or neuronal filaments constitute aligned 3D tissue (Gritsenko et al., 2012; Weigelin et al., 2012). As a result, adhesion processes determine the directionality of haptokinesis in 1D, 2D, and 2.5D. In 3D haptokinesis, multilateral extracellular structures determine the path of least resistance (Ilina et al., 2011).

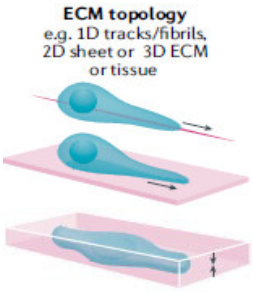

Figure 14. Cell migration in 1D, 2D and 3D environment.

Adapted from (Kenneth M. Yamada and Michael Sixt, 2019)

During migration, cells encounter two distinct types of surfaces: continuous surfaces, with negligible gaps compared to the size of the cell (e.g., basement membranes), and discontinuous

environments, with ECM fibers or solid surfaces more than a few hundred nanometers apart (e.g., isotropic collagen gels) (Mason et al., 2013a; Rowe and Weiss, 2008). Positive feedback from cell adhesions to the actin polymerization machinery enables plasma membrane protrusion in situations in which the contact area between the cell and the substrate is extensive and unbroken (similar to migration under unrestricted conditions) (Small et al., 2002). This feedback is interrupted by discontinuous environments; hence, protrusion strategies that are not amplified by adhesion signals may provide superior results (Tozluoğlu et al., 2013). Since it is not connected to the ECM, the front of the cell is unable to generate traction forces in discontinuous situations. Even in the case where the protrusion at the front of the cell is in contact with very small patches of ECM, these contacts may not cause the focal adhesions to develop into larger adhesions that are capable of generating considerable traction forces. Therefore, movement in a discontinuous environment may require traction in the cell body and a protruding mechanism that does not need the establishment of focal adhesions. It's possible that hydrostatic pressure from the cell body may push membrane forward. The water pressure inside of cells that move in 3D is the reason what causes membrane blebs (Hung et al., 2013; Petrie et al., 2012; Petrie et al., 2014).

Other topological characteristics may interfere with lamellipodia formation, matrix adhesions, and downstream signaling. Complex geometries, such as steps and corners *in vitro* and matrix fibre crosslinking *in vivo*, may restrict planar actin polymerization, like confinement. Surface topology influences cell migration by preventing the formation of cellular structures. The surface topology may be sensed directly by cells and the surfaces that a cell encounter has an impact on its plasma membrane (Czeisler et al., 2016). BAR proteins with intrinsic curvature can detect changes in curvature by attaching to charged lipid head groups. Protein binding to membranes with various curvatures may be altered by BAR protein curvature (Daub and Merks, 2013). F-actin is recruited

by these membrane-bound proteins. It is established using matrices with 'bumps', in which convex parts of the inner plasma membrane attract NBAR proteins to recruit myosin (Galic et al., 2012). This approach can help cells pass through constrictions by locally increasing their substrate forces.

III.1.4. Adhesion to the substrate

Forces from the cytoskeleton require cell adhesion to be translated into motion. Different types of adhesion molecules have significant effects on how cells react to stresses and exert forces on their surroundings. Integrin cell adhesion receptors can bind to a variety of surfaces through which cells pass, such as collagen, laminins, and fibronectin (major ECM components). In addition, some substances on the surface of other cells activate integrins, enabling migratory cells to use other cells as substrates (Campbell and Humphries, 2011). Integrin adhesions play a key role in cell migration. The force on integrins fortifies them, which enables cells to alter their adherence depending on the substrate and the forces exerted on the cells (Boettiger, 2012). This property is critical for sensing matrix stiffness and responding to shear stress. Cells can change the substrate affinity of integrins by binding talin and kindlin to their intracellular tails (Fig.15). The function of talin is regulated by the adaptor protein RAP1GTP-interacting adaptor molecule (RIAM; also known as APBB1IP) (Lee et al., 2009). RAIAM is regulated by RAP1 and the enabled/vasodilator-stimulated phosphoprotein (ENA/VASP) F-actin modulator (Lafuente et al., 2004). In fact, tuning the force of integrin-mediated adhesions has been shown in leukocytes. RAP1 may be activated in circulating leukocytes that interact with blood vessel endothelial cells in inflammatory tissues (Hogg et al., 2011). This results in the activation of integrin, enabling leukocytes to adhere to endothelial cells and enter inflammatory tissue. When leukocytes make contact with endothelial cells, the high shear pressure created by the bloodstream can cause them to move. Shear stress thus

improves the adherence of leukocyte integrins to their ligands and accelerates intracellular signaling.

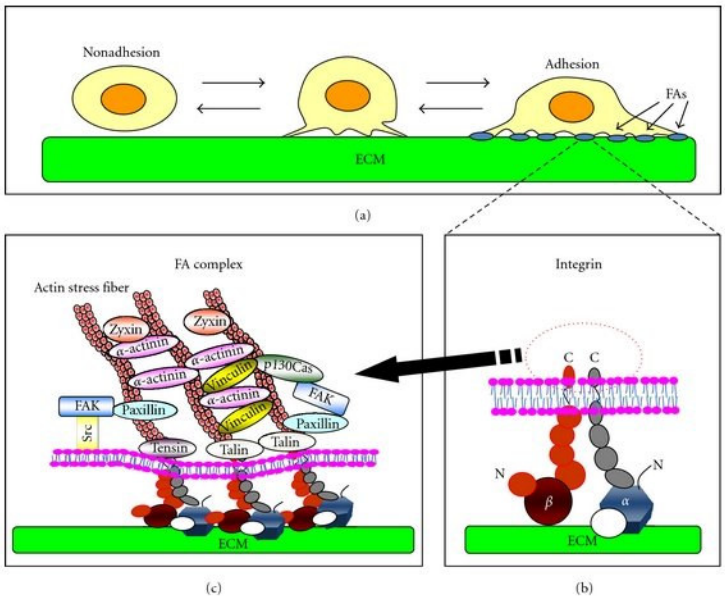

Figure 15. Integrin-mediated ECM-cell adhesion.

a. Integrins attach suspended cells to ECM. Some developing adhesion connections become focal adhesions (FAs).

b. Integrins are heterodimers comprising α- and β-chains.

Adapted from (Makoto Nagano et al., 2012)

Integrin-mediated adhesions are favorable but not required for cell migration. Leukocytes can still move across the 3D collagen matrix and interstitial collagen in the absence of integrins. How do leukocytes gain traction in this situation? They may use discoidin domain receptors (DDRs) to bind collagen. However, DDR1 ablation does not result in leukocyte migratory defect (Gross et al., 2004). Nonspecific, weak electrostatic interactions between glycosylated cell surface

molecules and ECM components may be exploited by leukocytes (Moon et al., 2005). These interactions might cause friction and transmit cellular forces to the ECM. According to computational modeling, some ECM groups do not require adhesion forces. Traction is generated by the interdigitation of cell components into the ECM space. The cell cortex and cytoplasm have the ability to resist deformation and transmit force. Interactions between cells and the external substrate cause friction, generate traction, and facilitate movement.

In some cases, addhesion signaling may be redundant (Tozluoğlu et al., 2013). It is likely that cells frequently acquire contradictory biochemical and biophysical direction signals; for instance, a soluble chemokine gradient may not correspond to the predominant orientation of ECM fiber alignment (Petrie et al., 2012). If adhesions are predominant, haptotaxis is likely to occur. If chemotaxis is more significant, adhesion receptor signaling might hinder matrix-directed migration. In this case, low integrin signaling may be advantageous (Lämmermann et al., 2008). Moreover, leukocytes do not require integrins to follow chemokine gradients in certain periods.

III.2. Chemical guidance through chemotaxis

Chemotaxis refers to the movement of cells in response to soluble chemical signals. These signals have the power to draw or repel cells. Most studies have been focused on chemoattraction, which involves soluble chemical cues such as chemokines, cytokines, pH shifts, and reactive oxygen species (ROS) (Majumdar et al., 2014). This leads to gradual but temporary molecular gradients due to fluid drift and convection. Chemotactic chemicals bind and activate receptors, resulting in local downstream signaling and cytoskeletal extension. The cells then polarize and migrate toward the region with the highest concentration of chemoattractants (Insall, 2010). For collective cell migration, leading cell rows have more signaling pathways that are activated in response to a

chemoattractant gradient than other cell rows. This thus strengthens supracellular polarity and stabilizes cell polarity and intercellular adhesion (Theveneau et al., 2010; Wan et al., 2013).

Collective chemotaxis is a developmental guiding mechanism as well as an experimental tool for directing collective cell migration (Shamloo, 2014). Chemotaxis is mediated by diffusive substances secreted by neighboring cells, but it may also be created or maintained by the cells themselves (Bagorda and Parent, 2008). Cell collectives can generate a self-generated chemokine gradient by: (a) releasing a migration-enhancing factor near the front, which feeds back on leader cells (Kriebel et al., 2008); (b) releasing chemokine-degrading enzymes that diffuse along the cell group and gradually clear chemokines along the length axis (Garcia et al., 2009); and/or (c) expressing migration-inducing receptors in leader cells (Cai and Montell, 2014). This self-generated chemotactic gradient generates supracellular polarity, which is required for lateral line migration in zebrafish (Donà et al., 2013). Furthermore, a surprising variety of chemokines and signaling molecules are involved in collective chemotaxis, which occurs across many cell bodies (Carmona-Fontaine et al., 2011; Malet-Engra et al., 2015).

III.3. Electrical guidance

Electrotaxis, also known as galvanotaxis, is the movement of cells in a certain direction with respect to a direct-current electric field, with an orientation toward the cathode or anode (Cortese et al., 2014; Feng et al., 2017; Liu and Song, 2014). Electric fields have the potential to activate Ca2+ or Na+ ion channels. Because of this, ions are allowed to enter the cell, activate ion transports such as Na/K-ATPase and sodium-hydrogen exchanger 3 (NHE3), and polarize the cytoskeleton (Zhao, 2009). Furthermore, electric fields activate the PI3K/Akt and MAPK/ (extracellular signal-regulated kinase) ERK signaling to affect the migration-inducing cell surface receptors such as

EGF receptor (EGFR), acetylcholine receptor (AchR) and integrins (Liu and Song, 2014; Zhao et al., 2006). During electrotaxis, leader and follower cells in epithelial sheets are able to generate traction forces parallel to the electric field. In addition, these cells can adaptively reposition when the polarity of the field changes (Cohen et al., 2014).

Electrotaxis stimulates the migration of numerous cell types, such as fibroblasts, epithelial and endothelial cells, neurons, immune cells, and cancer cells (Cortese et al., 2014). Group electrotaxis promotes tissue repair and wound closure. Disruption of the epithelial cell sheet induces an endogenous gradient of weak current that promotes migration into open areas beyond closure. In addition to migrating epithelial cells, endothelial and neuronal cells are also essential to ensure complete tissue regeneration (Zhao, 2009; Zhao et al., 2006). This tissue-intrinsic response can be successfully exploited and enhanced by applying external electrical stimulation, thereby accelerating the healing process (Li et al., 2020; Torkaman, 2014).

III.4. Environmental guidance for border cell migration

The migration of collective cell groups throughout development and tumor metastasis remains unclear. *Drosophila* border cell migration serves as a powerful model for controlling collective cell migration and guidance *in vivo*, providing insight into this process. Chemoattractants that activate receptor tyrosine kinases (RTKs) are secreted by the oocyte. PDGF-and VEGF-related receptors (PVR) are activated by platelet-derived growth factor/vascular endothelial growth factor (PDGF/VEGF)-related factor 1 (PVF1) (Duchek et al., 2001b). *Drosophila* EGFR is activated by the ligands Spitz (Spi), Keren (Krn), and Gurken (Grk) (Duchek and Rørth, 2001). Lack of expression or activity of both RTKs prevents border cells from reaching oocyte (Duchek et al., 2001b). It has been reported that border cells move in two distinct stages. Genetic analysis and live

imaging demonstrated that, firstly, highly polarized cells migrate posteriorly quickly, and secondly, during half of migration, border cells move slowly as a cluster and cells rotate within the clusters. During the first phase of migration, polarized cell behavior is essential, while collective behavior prevails later. In both stages, PVR and EGFR, are active, but employ different effector pathways. The Mbc (also known as DOCK18) and ELMO (also known as Ced-12) pathways are necessary for the first phase, in which guidance is dependent on subcellular localization of leader intracellular signaling. During the second phase, mitogen-activated protein kinase (MAPK) and phospholipase C are employed redundantly, and the cluster utilizes differences in signaling levels between cells to direct migration. Thus, chemotaxis-induced multicellular information processing is employed to direct the collective activity of a border cell cluster (Bianco et al., 2007).

To address the environmental posterior and medial guidance for border cell migration, Montell's group examined and adjusted chemical, adhesive, and topographical signals in the nurse cell environment to elucidate their respective contributions to the selection of a single migratory route among numerous (Dai et al., 2020). Typically, RTK signaling draws border cells posteriorly in the direction of maximal ligand concentration. Before this study, their previous work showed that E-cadherin amplifies modest changes in chemoattractant concentration between the front and rear of the cluster, thereby facilitating strong posterior migration (Cai et al., 2014). However, nurse cell E-cadherin generates traction, but differential adhesion does not medially steer the cells. Surprisingly, they found that at junctures where numerous nurse cells meet, the cell membranes do not close due to their geometry, allowing small spaces for protrusion growth between nurse cells. This geometry aids in center routing. The more cells that form junctures near the center of the egg chamber, the less energy it takes for border cells to migrate through this intercellular space. In conclusion, they thus proposed a model that the integration of chemoattractants and

multicellular junctures governs the posterior and central direction of border cell migration (Dai et al., 2020) (Fig.16).

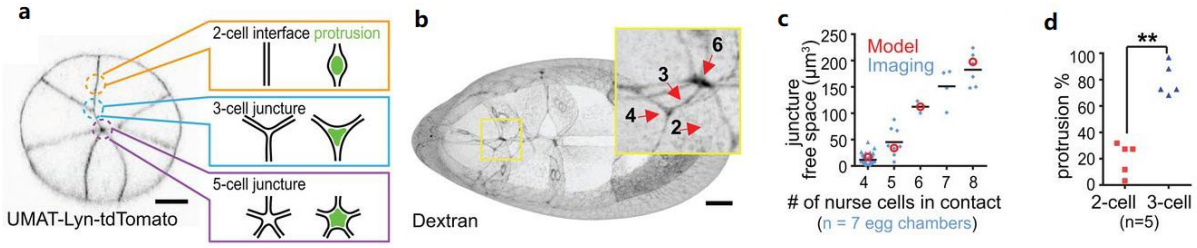

Figure 16. Relationship between nurse cell junctions and protrusions.

a. Schematic of protrusion into junctions of nurse cells.

b. Extracellular spaces in WT.

c. Extracellular juncture volume. 3D model (red) and experimental data (blue).

d. Percentage of protrusions reaching two- or three-cell junctures.

Adapted from (Wei Dai et al., 2020)

Chapter *IV: Optogenetics tools*

IV.1. History of optogenetics

As an emerging biological technology, optogenetics is less than 50 years, and it consists of genetic and optical technologies that induce or inhibit the activity of proteins in live tissues. Light is utilized to spatiotemporally manipulate protein activity of interest using optogenetics. The rise of optogenetics with great spatiotemporal resolution started in 2005, when a single component optogenetic instrument was first used in neuroscience (Boyden et al., 2005). Following its success in neuroscience, optogenetics is now being applied to a wide range of other biological concerns.

The conventional approach for controlling the activation or inhibition of a protein is using genetic tools. However, this technique has a long-term impact and may be lethal (Liu et al., 2008). Chemical inhibitors are another common method for examining signaling networks, but their disadvantages include side effects on biological processes and low resolution. It seems that there is one strategy that can circumvent all these limitations with its capacity for quick reaction and great spatiotemporal precision, and that is optogenetics, which is an excellent choice for such protein regulation.

Francis Crick first proposed the idea of optogenetics in 1979, when he proposed manipulating only one cell in the brain without affecting others. Crick hypothesized that light may have useful qualities in the absence of electrodes and medications, but at the time, neuroscientists lacked a method for targeting particular cells to trigger a response to illumination (Deisseroth, 2011). Around the same time, scientists studying microbes discovered proteins that can respond to light and control the transport of ions across membranes. For instance, bacteriorhodopsin may function as an ion pump that is rapidly triggered by photons of visible light (Oesterhelt and Stoeckenius, 1971). Halorhodopsin was discovered by Matsuno-Yagi and Mukohata in 1977 (Matsuno-Yagi and Mukohata, 1977), while channelrhodopsin was discovered by Hegemann, Nagel, and his colleagues in 2002 (Nagel et al., 2002). Initially, however, it was thought that this method was unlikely to affect cell activity. Nonetheless, in 2005, it was reported that neurons become exactly light-responsive by introducing a microbial opsin gene without additional parts, substances, or components nent optogenetic instrument was first used in neuroscience (Boyden et al., 2005). In 2010, bacteriorhodopsin, channelrhodopsin, and halorhodopsin all demonstrated the ability to activate or inactivate neurons in response to various hues of light. Recently, optogenetic approaches have revealed the significance of specific cell types and projections in normal and

disease-related physiology and behavior, from fundamental homeostasis to sophisticated cognitive processes. They are utilized in driving specifical cells to active or inhibit the most fundamental of organismal functions, including hunger, thirst, energy balance, respiration, alertness, sleep, and circadian rhythm. Optogenetics has also been used to study the transmission of primary sensory information to the brain, including olfactory, auditory, visual, and tactile.

IV.2. Various optogenetic tools

Optogenetics relies on spatiotemporal control to prevent the long-term effects of genetic alteration. And it is characterized by the insertion of light-activated channels and enzymes. Due to the efficient use of light in neuroscience, more and more proteins and cellular activities have been found to be controlled by light. Well-defined light-sensitive domains for optogenetic regulation of biochemical signals include cryptochrome proteins, phytochrome proteins, light-oxygen-voltage domains (LOV) and fluorescent protein Dronpa. A comprehensive introduction of these several photoreceptor subdomains is shown below.

Crytochrome 2 protein

Crytochrome 2 (CRY2) protein isolated from Arabidopsis thaliana can be activated by blue light (excitation wavelength around 405–488 nm). When this occurs, CRY2 is able to homo-oligomerize and recruit its binding partner, Cryptochrome interacting basic helix-loop-helix 1 (CIB1) (Mas et al., 2000). Within minutes, CRY2 can transition back to its original condition during the dark phase. The ubiquitously produced endogenous across species flavin serves as the chromophore for CRY2 in this system.

Phytochrome B protein

Phytochrom B (PHYB) can be triggered by red light (maximal excitation wavelength at 650 nm) and deactivated by far-red light (700 nm) (maximal excitation wavelength at 750 nm). Initially, the chromophore-free apo-PHYB protein is not light sensitive, but upon binding to the chromophore Phycocyanobilin (PCB), it becomes light sensitive. PCB exits in photosynthetic organisms, and through autocatalysis, it can maintain the function of PHYB (Gambetta and Lagarias, 2001; Müller et al., 2013). The conformation of PHYB-PCB molecule can be altered by red light excitation, and the compound then attaches to the Phytochrom interacting factor (PIF) protein (Ni et al., 1999). In response to far-red stimulation, the association process is reversible.

The LOV domains

The LOV domains found in a variety of species are sensitive to blue light with the excitation wavelength range of 440–473 nm, and they utilise flavin, an endogenous compound that is ubiquitously produced, as a chromophore. It is known that LOV domains undergo the light-induced conformational change that abolishes auto-inhibition and allows activation (Wu et al., 2009). In the absence of blue light irradiation, the LOV domain conformation rapidly resets to its original state.

Dronpa protein

Dronpa is a monomeric fluorescent protein that is sensitive to light with maximal excitation wavelength at 390 nm. This monomer can be dimerized by light treatment. In this way, Dronpa can limit the activity of target protein through its own C-terminal aggregation. On the other hand, Dronpa can be converted back to a monomer by light with maximal excitation wavelength at 490 nm (Zhou et al., 2012).

IV.3. Strategies to manipulate signals with optogenetic tools

Using a variety of light-sensitive proteins and controllers, optogenetics allows for the manipulation of intracellular signals in five distinct ways (Tischer and Weiner, 2014) (Fig.17).

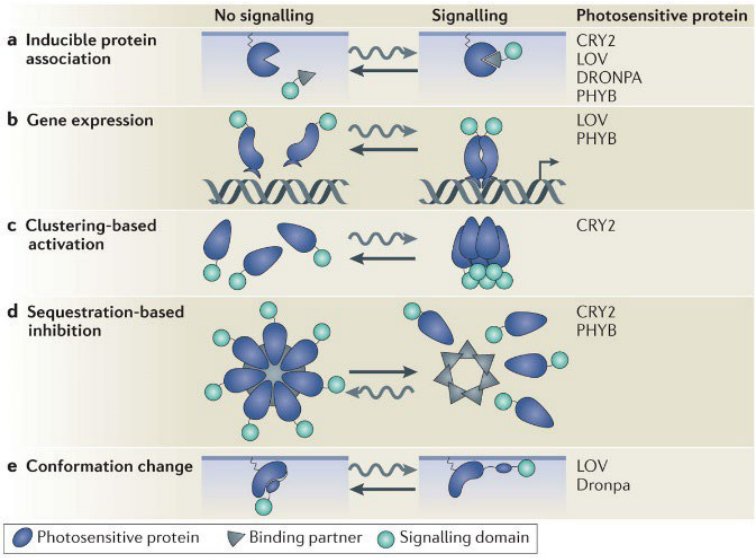

Figure 17. Different optogenetics signaling techniques.

Adapted from (Doug Tischer and Orion D. Weiner, 2014)

The first technique is to control the target by protein association. Light can stimulate the interaction of the two proteins and subsequently modulate intracellular signaling, since the light-sensitive protein and the effector heterodimerize upon exposure to light. This heterodimerization leads to the recruitment or repulsion of proteins, either activating or inhibiting intracellular signals, respectively. These light-inducible proteins are mainly composed of the CRY2–CIBN, PHYB–PIF, and LOV domains.

The second approach is to regulate gene expression through heterodimerization of PHYB–PIF (Shimizu-Sato et al., 2002) or LOV-domains (Lungu et al., 2012; Motta-Mena et al., 2014) to

control the target protein. By targeting a transcriptional activator to a gene's promoter, this activation mechanism can control gene transcription.

Clustering-based activation is the third one. Activation of a signaling cascade begins with the oligomerization of signaling proteins in response to light. This form of activation usually requires significant quantities of signaling proteins in the local area. Crytochrome-based regulation of β-catenin and Rho in charge of transcription and cytoskeletal rearrangements, respectively, is an illustration of this activation (Bugaj et al., 2013).

Inhibition based on sequestration is the fourth method. A cluster trap is employed to remove proteins from their operational location (Yang et al., 2013). For instance, the light activated reversible inhibition by assembled trap (LARIAT) system relies on the heterodimerization of CIB1 and CRY2. It consists of a multimeric protein (MP) that is attached to CIB1 and CRY2. The MP domain is a component of calmodulin-dependent protein kinase II that self-assembles into an oligomer composed of 12 identical subunits (Rosenberg et al., 2005). Upon blue light treatment, CRY2 proteins oligomerize (Bugaj et al., 2013) and attach to CIB1, and then the cross-linked MPs form into clusters. This method has been used to stop multiple regulators of the actin cytoskeleton and as a general way to control GFP-tagged proteins with a GFP-nanobody (Lee et al., 2014).

The last and most used one in my PhD project is conformational changes within a processed protein. This method has been applied to the LOV domains to control Rac, Cdc42, and formin in the regulation of cell movements (Rao et al., 2013), and used with Dronpa to control Cdc42 and proteinase K. It shares the principle of converting an autoinhibited signaling protein into an active state by light treatment, and it is highly efficient and reversible (Zhou et al., 2012). However, since it relies so much on the conformational match between the light-sensitive domain and the target

protein, fewer tools have successfully been developed with this technique than with other techniques.

IV.4. Optogenetics in collective migration

As mentioned earlier, my PhD advisor revealed, for the first time in Drosophila in vivo model, the possibility of using optogenetics to modify morphogenesis of multicellular animals, thereby confirming the ability of optogenetics to control single cell activity *in vivo.* He introduced and successfully applied PA-Rac1, aiming to control the Rac1 activity in cells by light, to study the spatiotemporal role of Rac1 in regulating border cell motility. PA-Rac1 is a fusion protein composed of Rac1 and the AsLOV2 domain, which is the light-sensitive domain to block Rac1 from interacting with its downstream effectors in the dark state by sterically inhibiting the effector-binding site. Light exposure generates a conformational transition that releases Rac1 from its inhibitory state (photo-uncaging) to activatable state (Fig.18). PA-Rac1 facilitates the polarized remodeling of the cytoskeleton with complete temporal control and subcellular accuracy. Photoactivating Rac1 in a single cell during border cell migration is sufficient to control the movement of all cells as a group. This suggests that cells find their direction based on the relative levels of Rac1 activity in each cell (Wang et al., 2010). However, as the technique has progressed over 10 years, we finally revealed that there are actually 2 Rac1 pools integrated together that govern the direction and the coordination of the border cell migration (See result-I in my PhD thesis).

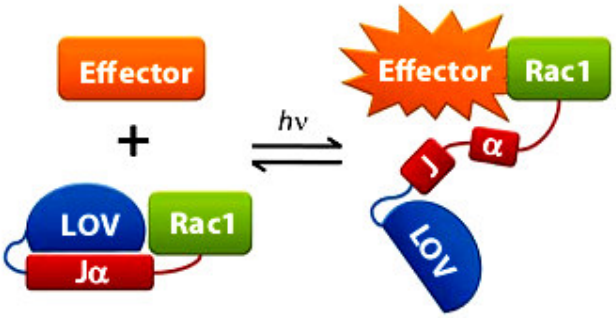

Figure 18. Illustration of PA-Rac1. The PA-Rac1 is based on the conformation change of LOV domain.

Adapted from (Yi I. Wu et al., 2009)

Optogenetics has also been used to study how cells move in the embryos of zebrafish (Simmich et al., 2012). During embryonic development, cells receive signaling inputs to gain migratory competence (permissive signaling) and to guide their movements along specific routes (instructive signaling). For example, non-canonical Wnt signaling is required for coordinated cell migration during metazoan development. To better understand better how non-canonical Wnt signaling affects directed cell migration during zebrafish gastrulation, Čapek and co-workers engineered a light-sensitive version of the non-canonical Wnt receptor Frizzled 7 (Fz7) by substituting the intracellular domains of the photoreceptor rhodopsin with the corresponding domains of Fz7 (Fig.19). Using this new tool, they demonstrated that uniform photoactivation rescues mesenchymal cell migration during gastrulation of otherwise Fz7 mutant zebrafish embryos (Čapek et al., 2019). This result argues that, in addition to its instructive role in controlling cell polarization in epithelial tissues, non-canonical Wnt signaling acts permissively in directing zebrafish mesenchymal migration, without the requirement of localized subcellular activation of Fz7 signaling.

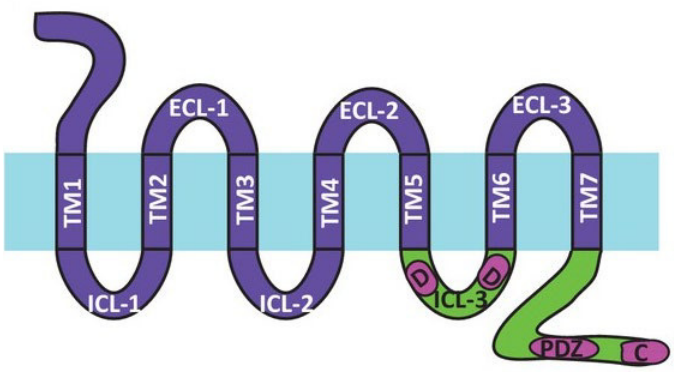

Figure 19. Diagram of the Opto-Fz7 receptor. Light blue bar represents plasma membrane with extracellular and intracellular space above and below. Rhodopsin is purple, Fz7 is green. Transmembrane domains 1–7; extracellular loops 1–3, intracellular loops 1–3. Fz7 domains have two Dsh-binding sites in ICL3 (D1, D2), a PDZ domain-binding site (PDZ) at the C-terminus, and four amino acids (ETTV) at the end.

Adapted from (Daniel Čapek et al., 2019)

Furthermore, Roberto Mayor's group studied the role of neural crest migration in *Xenopus* and Zebrafish using an optogenetic system. They applied optoGEF-contract or optoGEF-relax to either increase or decrease contractility and myosin phosphorylation by blue light, thereby regulating the contractility of the actomyosin supracellular cable in the phototreated region. First, they discovered the chemokine stromal cell-derived factor-1 (SDF1) gradient that resulted in an asymmetric actomyosin contraction that was stronger in the rear than in the front. Then, to see how this rear contractility affects chemotaxis, they used optogenetics to block either the rear or front contractility, and the results demonstrated that the former might reduce chemotaxis. Moreover, photoactivation of front contractility is harmful to neural crest migration. They also found that, in

the absence of SDF1, photoactivation of the rear contractility or photoinhibition of the front contractility could restore directional cell movement. In addition, the same effects occurred both *in vitro* and *in vivo*. Taken together, they showed that collective chemotaxis happens in neural crest cells via rear-wheel drive (Shellard et al., 2018) (Fig. 20).

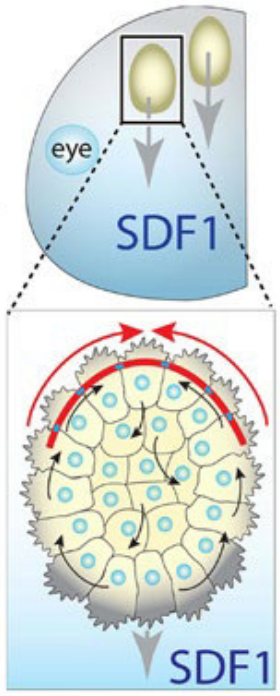

Figure 20. Diagram of actomyosin contractility at the rear (red arrows) drives collective cell chemotaxis. SDF1 stabilizes the protrusions at the front (darker gray).

Adapted from (Adam Shellard et al., 2019)

RESULTS

Chapter ***I:*** *Two Rac1 pools integrate the direction and coordination of collective cell migration*

I.1. Introduction

Collective cell migration plays fundamental roles in tissue morphogenesis, wound healing, cancer invasion and metastasis (Friedl and Gilmour, 2009; Rorth, 2009). Collective guidance is the most important characteristic by which collective cell migration differs from individual cell movement (Haeger et al., 2015; Rorth, 2011). Under chemotaxis, leader cells among a migrating group usually form major protrusions to guide global migration direction, and protrusive forces provide the traction cue for this leading guidance (Khalil and Friedl, 2010; Mayor and Etienne-Manneville, 2016). Differently, intercellular communication coordinates individual cell behaviours within the group to guarantee migration in a highly cooperative manner (Etienne-Manneville, 2014; Mayor and Etienne-Manneville, 2016), with tensile forces maintaining either group integrity or force balance between cells (Bazellieres et al., 2015; Cai et al., 2014; Hidalgo-Carcedo et al., 2011; Llense and Martin-Blanco, 2008; Peglion et al., 2014; Reffay et al., 2014; Tambe et al., 2011; Theveneau et al., 2010; Trepat and Fredberg, 2011). Direction and coordination of collective cells, controlled by the protrusive vs. tensile forces, thus need to be well integrated to ensure collective guidance (Haeger et al., 2015; Rorth, 2011).

Drosophila border cell migration is a powerful *in vivo* system for studying collective cell migration within a tissue (Bai et al., 2000; Cai et al., 2014; Duchek and Rorth, 2001; Duchek et al., 2001a; Fulga and Rorth, 2002; Geisbrecht and Montell, 2004; Montell et al., 2012; Pinheiro and Montell, 2004; Silver and Montell, 2001; Wang et al., 2006). Previous studies established the importance of Rac1 in collective guidance of the border cell movement (Cai et al., 2014; Ramel et al., 2013;

Wang et al., 2010). This collective chemotaxis is guided by two chemokine receptors (Duchek and Rorth, 2001; Duchek et al., 2001a): the PVR and the EGFR. EGFR and PVR are believed to establish a gradient of relative Rac1 activity within a border cell group for collective guidance (Cai et al., 2014; Prasad and Montell, 2007; Ramel et al., 2013; Wang et al., 2010). Currently, a molecular mechano-transduction pathway has been reported to coordinate polarized Rac1 activation and lamellipodium formation at the multicellular length scale in 2D epithelial cell monolayers (Das et al., 2015; Farooqui and Fenteany, 2005). Whether border cells, as a 3D cluster of epithelial cells, use a similar mechano-transduction pathway or another mechanism to achieve integration between direction and coordination is unclear, mainly due to two reasons. Firstly, all current knowledge about Rac1 activity in border cells is based on the analyses of a Rac1 FRET biosensor (Cai et al., 2014; Fernandez-Espartero et al., 2013; Ramel et al., 2013; Wang et al., 2018; Wang et al., 2010) which lacks membrane-anchored CAAX motif, missing subcellular Rac1 activity resolution. Secondly, dynamic behaviour of F-actin, the direct outcome downstream of Rac1 activity, is largely missing in those Rac1-related studies (Cai et al., 2014; Ramel et al., 2013; Wang et al., 2010).

To assess how Rac1 activity gradient governs collective guidance, we applied another Rac1 probe, PAK3RBD-GFP (Abreu-Blanco et al., 2014; Sun et al., 2017), feasible to monitor subcellular Rac1 activity, as well as different methods to determine F-actin signals and actin flows in different subcellular regions. Surprisingly, we revealed two Rac1 functional pools which cooperate to guide and coordinate border cell migration.

I.2. Results

I.2.1 F-actin signals and Rac1 activity vary between protrusions and cables in border cells

To understand how Rac1 activity gradient integrates leading guidance and intercellular communication during border cell migration, we first needed to clearly map subcellular F-actin networks responsible for either protrusive or contractile properties. F-actin networks in border cells have been shown at two peripheral regions including protrusions and cables, and one inner region at border cell-to-cell contacts (Wang et al., 2020; Wang et al., 2018). Yet, a systematic characterization of spatiotemporal subcellular F-actin signals has never been explored. Here, we developed a semi-automatic method to analyse 3D images of border cells expressing LifeAct-GFP in order to quantify subcellular F-actin signals distributed at protrusions, cables and contacts (Supplementary Fig. 1a and Methods). By using this method, we also obtained other important factors such as protrusion number, supracellular cable continuity and border cell area (protrusion area vs. total area), to better clarify border cell protrusive vs. contractile structures.

A previous study has indicated that protrusions and cables, two peripheral regions, account for border cell morphology, which might correlate with migratory behaviours (Wang et al., 2020). We thus defined the border cell groups into three categories (Fig. 1a), based on their morphologies that can be reflected as the percentage of protrusion area (Fig. 1b) and supracellular cable continuity (Fig. 1c): 1) “tight group” presented less than 10% of protrusion area, lacking any large protrusion while showing globally continued supracellular cables (cable discontinuity ≤ 8%); 2) “loose group” presented more than 25% of protrusion area, displaying multiple large protrusions (at least 2) but discontinued cable structures (cable discontinuity ≥ 25%); 3) “balanced group” presented 10-25% of protrusion area, demonstrating 1-2 large protrusions with discontinued cables while showing continued cables in other border cells (8% < cable discontinuity < 25%). And we found that tight

or loose border cell groups showed slow migration speed, while balanced border cell groups exhibited fast migration speed thus implicating efficient migration ability (Fig. 1d). During migration, these three groups randomly occurred and often switched from one to the other. Among these three categories, F-actin levels in inner contacts appeared to be constant (Fig. 1e). But F-actin levels at protrusions and cables varied over a large range (Fig. 1e), indicating that subcellular F-actin signals might switch between these peripheral regions. Too low or too high ratios of F-actin cable/periphery signals (Fig. 1f) correlated with loose or tight groups respectively, presenting multiple vs. little protrusions (Supplementary Fig. 1b), loose vs. tight cell area (Supplementary Fig. 1c), and broken vs. maintained cable continuity (Fig. 1c). Differently, balanced groups showed intermediate levels in these factors (Fig. 1c, f and Supplementary Fig. 1b, c). Total peripheral F-actin levels did not show major differences among the front, middle or rear cells within these three groups (Supplementary Fig. 1d). However, in balanced groups, leader cells demonstrated higher F-actin signals at protrusions but lower signals at cables, compared with the middle and rear cells (Fig. 1g). Taken together, our results demonstrate that border cell groups present different protrusion F-actin vs. cable F-actin signals, which correlates with different morphologies and migrating abilities.

Next, we applied a recently reported Particle Image Velocimetry (PIV) method (Yolland et al., 2019) to determine F-actin dynamics in peripheral regions. We detected actin flows at both cables and protrusions. Protrusions displayed mainly retrograde actin flows together with some anterograde actin flows, while cables mostly showed centripetal actin flows (Fig. 1i). Strong actin flows were observed at cables or protrusions in tight or loose groups respectively, while detected at both regions in balanced groups (Fig. 1j). Actin flows seemed to support dynamic accumulation of Myosin-II (viewed using the mCherry-tagged Sqh, the *Drosophila* homologue of the non-

muscle myosin II regulatory light chain (Majumder et al., 2012; Martin et al., 2009)) at mainly cables but also cable-protrusion boundaries (Supplementary Fig. 1e). Myosin-II accumulation at cables showed a high to low level from tight to loose groups (Supplementary Fig. 1f). Strikingly, negative divergence reflecting actin network sinks (Yolland et al., 2019), but not flow speed, significantly correlated with Myosin-II cable accumulation (Supplementary Fig. 1g, h). It thus indicates that actin flows from different directions converge and collide at either cables or protrusion-cable boundaries, resulting in a sharp transition of PIV strength and the formation of network sinks with different F-actin polarities to load Myosin-II signals (Coravos and Martin, 2016; Reymann et al., 2012).

To determine whether Rac1 activity might correlate with subcellular F-actin signals, we applied a reported Rac1 probe, PAK3RBD-GFP (Abreu-Blanco et al., 2014; Sun et al., 2017), to monitor and quantify subcellular Rac1 activity. Firstly, we confirmed, by the *in vitro* binding assay, that GST-PAK3RBD-GFP strongly interacts with GTP-loaded His-dRac1, but not with GDP-loaded His-dRac1 (Supplementary Fig. 2), thus demonstrating the specificity of this reporter for the active form of *Drosophila* Rac1. In migrating border cells, PAK3RBD-GFP intensity was prominently distributed in both inner and peripheral regions, and was highly consistent with subcellular F-actin signals (Fig. 2a). Since this reporter might also monitor Cdc42 activity, we compared the effect of Rac1 or Cdc42 activity inhibition on this reporter. Inhibition of Rac1 activity by expressing its dominant negative (DN) form significantly suppressed PAK3RBD-GFP intensity at both protrusions and cables; oppositely, inhibition of Cdc42 activity strongly reduced reporter intensity at inner contacts (Supplementary Fig. 3a, b). Here, Rac1-DN form might impede the protein function of other *Drosophila* Rac genes, as well as affect any GEFs that could act on both Rac1 and Cdc42. To exclude these potential issues, firstly we compared the protein expression of 3

Drosophila Rac genes in migrating border cell groups. Strong Rac1 protein was prominently distributed at both cables and protrusions of migrating cells; differently, Rac2 protein was highly enriched in two central polar cells but little in border cells, and Rac3 protein was undetectable in both border cells and polar cells (Supplementary Fig. 3c). Furthermore, we compared the effect of either RNAi or loss-of-function (LOF) mutant of different Rac proteins or Cdc42 on PAK3RBD-GFP intensity. Expression of Rac1 RNAi or Cdc42 RNAi strongly reduced either protein in border cell groups (Supplementary Fig. 3f, g); and either inhibition led to the effect on PAK3RBD-GFP intensity in border cells, which is similar to that observed from the respective DN form (Compare Supplementary Fig. 3d, e with Supplementary Fig. 3a, b)**.** But Rac2 LOF mutant and Rac3 RNAi expression had no effect on PAK3RBD-GFP intensity in border cells, resembling wildtype (WT) border cells (Supplementary Fig. 3d, e). These confirmation experiments thus excluded potential off-target issues. Altogether, these results suggest that Rac1 activity is mainly located in peripheral regions, while absent from inner contacts which are highly enriched with Cdc42 activity. Importantly, our results reveal for the first time an unknown subcellular Rac1 pool at cables, in addition to the expected localization at protrusions.

PAK3RBD-GFP intensity was constant in inner contacts, while varied in peripheral regions: either dominant at protrusions or cables in loose or tight groups respectively, while detected at both peripheral regions in balanced groups (Fig. 2b). These distinct distribution patterns in different border cell groups indicate that two Rac1 functional pools might control F-actin signals at protrusions and cables. In addition, total peripheral PAK3RBD-GFP intensity did not show any difference from front-to-rear positions within all three groups (Fig. 2c), thus contradicting the previous “Rac1 activity gradient” model. In balanced groups, compared with the middle and rear cells, leader cells presented higher PAK3RBD-GFP intensity at protrusions but lower intensity at

cables, which was similar to the polarized distribution of peripheral F-actin signals (Compare Fig. 2d with Fig. 1g). Based on these results, we thus propose a "two Rac1 pools" model to replace the previous "Rac1 activity gradient" model (Fig. 2e).

I.2.2 Two Rac1 pools control F-actin signal exchange between two peripheral regions

This model thus implicates some unknown roles for Rac1 in border cells. Here, we took advantage of our established optogenetic tool for Rac1, called photoactivatable-Rac (abbreviated as PA-Rac) (Wang et al., 2010; Wu et al., 2009; Wu et al., 2011), to explore these roles. To this end, we generated transgenic flies expressing untagged PA-Rac (either active or DN forms, PA-RacQ61L or PA-RacT17N, respectively) under the control of the *slbo*-Gal4/UAS system, and photo-activated PA-Rac in different subcellular regions to test the effect on F-actin signals monitored by LifeAct-RFP (see Methods).

First, we assessed the effects of local Rac1 inhibition. Border cell inner contacts have been implicated in controlling intercellular communication via E-cadherin adherens junctions (Cai et al., 2014). Focal Rac1 inhibition at these contacts had no effect on border cells (Supplementary Fig. 4a, b, 5a-c), thus excluding a role for Rac1 in this region. Then, we tested the photo-inhibitory effect at cables or protrusions, either of which are highly enriched with Rac1 activity. Strikingly, focal Rac1 inhibition at leader cell cables resulted in two dramatic changes: 1) at the intracellular level, the photo-treated cell gradually lost cable F-actin signals while achieving protrusion F-actin signals, and correspondingly leading protrusions strongly grew along with cable reduction; 2) at the supracellular level, other cells also lost their cable F-actin signals as well as cable continuity, while they strongly acquired protrusion F-actin signals to form multiple protrusions, finally switching to a loose group (Fig. 3a-d, Supplementary Fig. 5d-f). As a negative control, focal photo-

treatment of a light insensitive control at leader cell cables had no effect (Supplementary Fig. 4a, b, 5d-f). Next, at the intracellular and supracellular levels, the phenotypes caused by focal Rac1 inhibition on leading protrusions were completely opposite to that induced by Rac1 photo-inhibition at leader cables: protrusions completely disappeared, while supracellular cables were gradually strengthened, forming a tight group (Fig. 3a-c, e, Supplementary Fig. 5g-i).

Second, we characterized the effects of local Rac1 activation. Focal Rac1 activation at either cables or protrusions of a leader cell phenocopied those observed from focal Rac1 inhibition at leading protrusions or cables, respectively (Fig. 3a-e and Supplementary Fig. 5d-i). Compared with no effect from the photo-treated light insensitive control (Supplementary Fig. 5o), focal Rac1 modifications at leader protrusions or cables gradually slowed down border cell migration speed (Fig. 3g), consistent with a gradual switch from balanced to loose or tight group. Furthermore, focal Rac1 modifications at cables or protrusions didn't change F-actin signals at inner contacts (Fig. 3f and Supplementary Fig. 5m, n), while strongly exchanging F-actin signals between cables and protrusions (Fig. 3d, e). Hence, this explains our observed constant levels of F-actin signals and Rac1 activity in total peripheral regions, while indicating that Rac1 activity might often switch between cables and protrusions.

Third, we determined the effect of PA-Rac in rear cells. Focal Rac1 modifications at rear cell cables led to similar phenotypes to those from Rac1 photo-manipulations at leader cell cables (Supplementary Fig. 4a, b, 5j-l). Thus, this confirms that PA-Rac induced effects also occur in other positioned cells.

Altogether, our optogenetic results support two main conclusions:1) two Rac1 pools govern the exchange of intracellular F-actin signals between protrusions and cables, creating intracellular antagonism in an individual border cell; 2) via supracellular cables, these two Rac1 pools

orchestrate F-actin signals at the multicellular levels, participating in the coordination of intercellular communication and leading guidance. Therefore, here our conclusions highlight the importance of a Rac1 activity exchange between two functional pools in border cells.

I.2.3 Rac1 and Rho1 signals synergistically support mechanical coupling at supracellular cables

Our next question was how these two Rac1 pools govern either cables or protrusions. Firstly, we wondered whether cable Rac1 activity might provide F-actin networks to load Myosin-II, thus participating in the control of actomyosin mechanical properties supporting intercellular communication. Here, we monitored and quantified the Sqh dynamics as an indirect reading-out of actomyosin mechanical properties as used in most studies (Martin et al., 2009; Rauzi et al., 2010), together with actin flow analysis, in our optogenetic studies (see Methods).

After focal Rac1 activation at cables in a border cell, the occurrence of cable actin flows gradually increased along with flow disappearance at protrusions; pulsed Sqh accumulation at cables was correspondingly enhanced in both photo-treated and other cells, with signals reaching maximal values (Fig. 4a-d). Oppositely, after focal Rac1 inhibition, actin flow occurrence and Sqh accumulation at cables were reduced to minimal values in all cells (Fig. 4e-h). Here, we detected a synchronized pattern of Sqh accumulation at photo-treated vs. other cells, disproving local mechanical transfer between border cells (Wang et al., 2020). On the contrary, it suggests that supracellular cables, functioning as a whole unit, might immediately respond to local changes in cable Rac1 activity and F-actin networks from one cell, promptly transferring actomyosin mechanical properties among all cells, therefore achieving mechanical coupling in entire group.

Within this mechanical coupling, the high-to-low cable actomyosin levels reflect the equilibrium status of border cell mechanical properties for intercellular communication.

Considering the role of Rho1 signalling at supracellular cables (Wang et al., 2020), we then asked whether cable Rac1 activity might be linked with Rho1 signalling. Genetic activation of Rho1 or downstream Rock in border cells strongly enhanced PAK3RBD-GFP intensity at cables, while reducing reporter intensity at protrusions (Fig. 5a, b and Supplementary Fig. 6a, b). Conversely, genetic inhibition of Rho1 to Myosin-II in border cells, or chemical inhibition of Rock activity by Y27632 treatment oppositely changed reporter intensity in border cells (Fig. 5a, b and Supplementary Fig. 6a-d). Considering the fast effect from chemical inhibition, we determined whether Rho1 signalling might spatiotemporally govern cable Rac1 activity. Here, we applied two optogenetic tools, called Opto-RhoGEF2 and Opto-Rho1DN (Eritano et al., 2020; Izquierdo et al., 2018), to photo-activate or -inhibit Rho1 in border cells. To confirm the specificity of these two optogenetic tools, we analysed their effect on Sqh accumulation at leader cables, and we detected rapid enrichment or reduction of Sqh signals at leader cables by Opto-RhoGEF2 or Opto-Rho1DN, respectively (Supplementary Fig. 6e-h). Focal Rho1 activation at leader cables quickly enhanced PAK3RBD-GFP intensity within these regions, while reducing reporter intensity at leading protrusions, within 3 to 5 minutes; conversely, focal Rho1 inhibition within the same regions oppositely modified reporter intensity in border cells (Fig. 5c, d and Supplementary Fig. 6i, j). When Rock activity was chemically inhibited, PAK3RBD-GFP intensity enhancement at cables by focal Rho1 activation got blocked (Compare Fig. 5e, f with Fig. 5c, d). These results thus support that Rho1 signalling spatiotemporally governs cable Rac1 activity while limiting Rac1 activity switch to protrusions.

Based on this spatiotemporal control, next we wondered whether mechanical coupling between cells might guide cable Rac1-dependent actomyosin mechanical property changes from one border cell to the other border cells, possibly forming a positive feedback loop. Indeed, focal Rac1 activation at cables of one cell gradually enriched PAK3RBD-GFP intensity at supracellular cables, while decreasing reporter intensity at protrusions; conversely, focal Rac1 inhibition modified reporter intensity in an opposite manner (Fig. 5g, h and Supplementary Fig. 6k, l). However, Rho1 genetic inhibition or ROCK chemical inhibition completely blocked the spatiotemporal influence by focal Rac1 stimulation (Fig. 5i-l, compared with Fig. 5g, h). Thus, these results strongly support our hypothesized positive feedback loop. And this feedback loop explains the absence of intercellular communication with Rho1 signalling inhibition (Fig. 5i-l).

The role of supracellular cables in controlling intercellular communication seems to contradict our previous model in which intercellular communication is mediated through E-cadherin adhesions between border cells (Cai et al., 2014). Thus, we re-evaluated the effect of inhibiting E-cadherin adhesions by expressing E-cadherin RNAi in one random border cell or in a whole group. WT border cell groups typically exhibited actomyosin pulsed movement at the periphery supracellular cables (Supplementary Fig. 7a); in a random border cell expressing E-cadherin RNAi, actomyosin pulsed signals entered the border cell-cell contacts, or they moved along the plane other than the one of supracellular cables (Supplementary 7b, c). These abnormal actomyosin movements thus indicate that the cable in this E-cadherin inhibiting cell is dissociated from supracellular cables that connect other border cells. Consistent with the damage in supracellular cables linking the whole group, focal Rac1 activation at a border cell cable within the E-cadherin RNAi expressing group had no effect on other border cells (Supplementary Fig. 7d, e). These results further support the importance of mechanical coupling via supracellular cables in intercellular communication.

I.2.4 Rac1 cooperates with Cdc42 to control protrusions and their coordination with cables

Next, we asked how Rac1 governs protrusions and coordinates the signal exchange between protrusions and cables. Different from dramatic control of F-actin levels at protrusions, focal Rac1 activation or inhibition at protrusion tips within a few minutes didn't affect the speed and direction ratio of protrusion actin flows, compared with the photo-treated control cells (Fig. 6a-c). This thus excludes a role for Rac1 on protrusion actin flows.

We suspected that another Rho-family small GTPase might play the control. Considering the role of Cdc42 on retrograde flows, we next determined the effect of Cdc42 photo-manipulations, by using a PA-Cdc42Q61L or PA-Cdc42T17N, on protrusion actin flows. Focal Cdc42 activation or inhibition at protrusion tips quickly enhanced or reduced the speed as well as the direction ratio of protrusion actin flows (Fig. 6a-c), confirming a critical role of Cdc42 on this control. Concurrent modifications of Cdc42 and Rac1 activities at protrusion tips further strengthened our conclusion (Supplementary Fig. 8a-c). Therefore, it seems that Cdc42 governs actin flows while Rac1 controls global F-actin levels at protrusions, functioning like the faucet switch vs. volume control of a water tank.

Retrograde and anterograde actin flows usually started near protrusion tips, while covering the main or tip regions of protrusions, respectively (Fig. 6a). Retrograde actin flows often converged with and then separated from cable actin flows at protrusion-cable boundaries, thus suggesting that F-actin signals at protrusions and cables might often communicate and exchange with each other possibly through fusion and fission of actin flows. Considering the critical role of Cdc42 on protrusion actin flows, we wondered whether Cdc42 might govern this signal communication and exchange. To test this hypothesis, firstly we determined the effect of PA-Cdc42 on actin flow divergence at protrusions, since collision between these two actin flows led to the sharp transition

of PIV strength reflected by negative divergence (Fig. 6a). Cdc42 focal activation or inhibition at protrusion tips strongly increased or reduced, respectively, negative divergence near protrusion-cable boundaries (Fig. 6d). Secondly, we characterized whether intracellular and intercellular effects induced by PA-Rac are dependent on Cdc42 activity, considering that these effects were initiated by actin flow communication at protrusion-cable boundaries. Concurrent focal inhibition of Cdc42 completely blocked the effects induced by Rac1 focal activation or inhibition at leading protrusions (compare Supplementary Fig. 8d-g with Fig. 3a, e). Taken together, these results support Cdc42 as the key factor controlling communication and exchange of actin flows and F-actin signals between protrusions and cables.

So, what is the function for communication and exchange of actin flows and F-actin signals between protrusions and cables in border cell migration? We hypothesized that this signal communication and exchange might coordinate protrusive and contractile properties thereby controlling border cell migration efficiency. By analysing migration speed, we found that focal Cdc42 inhibition, with or without concurrent Rac1 modification, at leading protrusion tips significantly blocked the migratory ability (Fig. 6e, g and Supplementary Fig. 8h). In addition, focal Cdc42 activation concurrent with Rac1 inhibition quickly resulted in the disappearance of leading protrusions and thus the loss of migration ability (Supplementary Fig. 8h). Oppositely, focal Cdc42 activation, alone or concurrent with Rac1 activation, at leading protrusions led to even faster migration speed than that observed in balanced groups (Fig. 6f, g and Supplementary Fig. 8h). Altogether, these results support that actin signal communication and exchange between protrusions and cables are critical for border cell migration efficiency. These results also indicate that active Cdc42, alone or together with active Rac1, at protrusions can balance F-actin signals

between leading protrusions and supracellular cables, thereby achieving the highest migration efficiency.

I.2.5 Chemoattractant receptors differentially govern two Rac1 pools

According to our model, balanced Rac1 activity and F-actin signals between leading protrusions and supracellular cables enable border cells to achieve perfect integration between leading guidance and intercellular communication. It thus contradicts the previous "Rac1 activity gradient" model governed by chemokine receptors (Cai et al., 2014; Wang et al., 2010), while supporting some other previous findings about the different roles of PVR or EGFR signalling on border cell migration (Bianco et al., 2007a; Poukkula et al., 2011a).

To determine the precise roles of EGFR or PVR signalling, we characterized the effects of EGFR or PVR inhibition on Rac1 activity and F-actin signals in border cells. With the inhibition of PVR signalling by PVR-DN overexpression in border cells, PAK3RBD-GFP intensity was strongly enriched at cables, while reduced at protrusions (Fig. 7a, b); meanwhile, this reporter was more diffusive within protrusions (Supplementary Fig. 9a). Consistently, this inhibition significantly enhanced supracellular cables while blocking protrusion formation (Fig. 7a). Actin flows at cables got enhanced (Supplementary Fig. 9g), while protrusion actin flows presented reduced speed and disturbed direction (Fig. 7c-f). Particularly, both anterograde and retrograde actin flows never started near protrusion tips but often from protrusion inner regions (Fig. 7d). All these phenotypes thus indicate that PVR signalling can govern correct Rac1 activity distribution at or near protrusion tips to start actin polymerization, therefore guiding the correct initiation of protrusion actin flows.

Differently, inhibition of EGFR signalling by expressing EGFR-DN in border cells significantly interfered with cable Rac1 activity, and PAK3RBD-GFP reporter was often trapped in cytosolic regions near cables thus disrupting its continuity at cables (Supplementary Fig. 9a); conversely, this inhibition globally enhanced protrusion Rac1 activity (Fig. 7b). Consistently, this inhibition led to a significant spatial limitation in the occurrence of cable actin flows (Supplementary Fig. 9g), while not affecting protrusion actin flows (Fig. 7c-f). Moreover, due to this limited occurrence of actin flows at cables, supracellular cables were significantly disturbed while protrusion formation was increased (Fig. 7a). EGFR-DN expressing border cell groups migrated much slower than balanced border cell groups (migrating speed of EGFR-DN vs. balanced groups: 0.324+/-0.194 vs. 0.64+/-0.364 μm/min), while presenting migrating speed and protrusion numbers somehow similar to loose border cell groups (migrating speed of EGFR-DN vs. loose group: 0.324+/-0.194 vs. 0.23+/-0.102 μm/min; protrusion number of EGFR-DN vs. loose group: 2.7+/-0.988 vs. 3.5+/-1.075). Altogether, these results thus implicate that EGFR signalling can govern correct Rac1 activity distribution at cables, thus maintaining cable actin flows and network continuity.

With concurrent inhibition of PVR and EGFR signalling in border cells, PAK3RBD-GFP intensity was strongly reduced at cables, appearing in a discontinuous manner (Supplementary Fig. 9b, c); even with strong loss of PAK3RBD-GFP intensity at protrusion tips, total reporter activity from multiple protrusions was similar to that of WT border cell groups (Supplementary Fig. 9b, c). These results confirm concurrent disturbance of Rac1 activity at protrusions and cables when both receptors are inhibited in border cells. Consistent with mis-localized Rac1 activity in both regions, we detected reduced speed and disturbed direction of actin flows at protrusions, and spatially limited actin flows at supracellular cables (Supplementary Fig. 9d-g). Moreover, simultaneously

disturbed actin flows at protrusions and cables seemed to result in the formation of multiple large protrusions and exacerbate the discontinuous supracellular cables. These results further support the main conclusion that chemokine receptors guide correct localization of Rac1 activity at protrusions and cables.

Based on this conclusion, we then asked whether focal Rac1 activation at either protrusions or cables might rescue the defect in either region mediated by the inhibition of PVR or EGFR signalling. Compared with the light insensitive control, focal Rac1 activation at the randomly formed protrusion tip of the PVR-inhibiting groups gradually enhanced protrusion growth in both photo-treated and other cells, while significantly reducing supracellular cables, finally resulting in a phenotype close to balanced WT group (Fig. 7g, h). Oppositely, focal Rac1 activation at cables within a border cell of EGFR-inhibiting groups recovered supracellular cables, while strongly repressing protrusions in all cells, finally resembling tight WT group (Fig. 7i, j). For concurrent inhibition of PVR and EGFR signalling, focal Rac1 activation at cables in one of these border cells gradually recovered supracellular cables along with almost complete protrusion loss, finally similar to the PVR-inhibiting groups (Supplementary Fig. 9h, i); while focal Rac1 activation at protrusions in one of these border cells moderately reduced the size and number of protrusions, and partially recovered the disconnected supracellular cables, finally resembling the EGFR-inhibiting groups (Supplementary Fig. 9j, k). Thus, these focal Rac1 recovery results support that inhibition of guidance receptor signalling mislocates Rac1 activity in border cells.

Our following questions include how guidance receptors PVR and EGFR govern Rac1 activity at protrusions and cables, respectively, and how Rac1 downstream signals govern border cell protrusions. A previous study reported that PVR and EGFR use different effector pathways in controlling border cell migration (Bianco et al., 2007a), thus indicating them as the potential

upstream control of Rac1 activity. The myoblast city (Mbc, also known as DOCK180) and engulfment and cell motility (ELMO, also known as Ced-12) pathway is required for the early phase when leader protrusions dominate border cell migration, while mitogen-activated protein kinase (MAPK) and phospholipase Cgamma are used redundantly during later phase when leading protrusions are not prominent (Bianco et al., 2007a). Thus, we asked whether these reported effector pathways might act downstream of guidance receptors to control Rac1 activity at protrusions or cables. Inhibition of Mbc and ELMO by their RNAi expression in border cells strongly reduced protrusion PAK3RBD-GFP intensity, while enhancing cable PAK3RBD-GFP intensity (Supplementary Fig. 10a, b); consistently, either inhibition significantly enhanced supracellular cables while blocking protrusion formation, resembling the PVR-DN expressing border cell groups (Supplementary Fig. 10c, e). Differently, inhibition of rapidly accelerated fibrosarcoma (Raf) kinase, the intermediator between EGFR and MAPK, strongly reduced cable PAK3RBD-GFP intensity, while enhancing protrusion PAK3RBD-GFP intensity (Supplementary Fig. 10a, b); consistently, this inhibition strongly disturbed supracellular cables while promoting protrusion formation, phenocopying EGFR-DN overexpression in border cells (Supplementary Fig. 10d, f). Taken together, these results thus implicate Mbc and ELMO as the PVR downstream effectors in controlling Rac1 activity at protrusions, while indicating Raf as the EGFR downstream effector in controlling Rac1 activity at cables.

Finally, we characterized the roles of Wave and PAK signals, two important Rac1 downstream effectors, in controlling border cell protrusions. Inhibition of Scar and Abi (two critical components in WAVE complex) as well as their downstream factor Arp3, by expressing their respective RNAi, in border cells strongly blocked protrusion formation (Supplementary Fig. 10g, h); consistently, we detected prominent distribution of Abi-GFP signals near the protrusion tips

(Supplementary Fig. 10i). Both results support the importance of WAVE complex in controlling protrusion formation. Differently, inhibition of PAK1 and PAK3 by expressing their RNAi in border cells increased protrusion number, while these protrusions appeared to be relatively stiff compared with more dynamic protrusions from WT border cells (Supplementary Fig. 10g, h). Altogether, our results support different roles of Wave and PAK signals in border cell protrusions.

I.3. Conclusions

Studies over the past 10 years established the "Rac1 activity gradient" model, in which chemokine receptors PVR and EGFR govern the formation of relative Rac1 activity in border cell migration to ensure collective guidance for migration efficiency16,27 (Fig. 8a). However, this model cannot explain the failure of detecting either polarized peripheral F-actin distribution in border cell groups or F-actin signal switch between the PA-Rac photo-modified cells and other cells. Surprisingly, we identified two Rac1 functional pools at border cell supracellular cables and protrusions (Fig. 8b). Tensile Rac1 activity forms a positive feedback loop with Rho1−Myosin-II signalling to govern the integrity of supracellular cables and maintain mechanical force coupling between border cells for intercellular communication (Fig. 8c). Differently, protrusive Rac1 activity synergizes with Cdc42 signalling to control actin signals at protrusions for dynamic protrusion growth and signal exchange between protrusions and cables, thus achieving leading guidance and its integration with intercellular communication (Fig. 8d). Based on the previous "Rac1 activity gradient" model, chemokine receptors have been thought to govern yet unknown factors which repress the protrusive property of follower border cells. However, we found that chemokine receptors EGFR and PVR differentially guide correct localization of Rac1 activity and thus actin flows at either cables or protrusions (Fig. 8e, f). Therefore, our studies support the "two Rac1 pools" model to explain an unidentified mechanistic control of collective guidance.

I.4. Figures

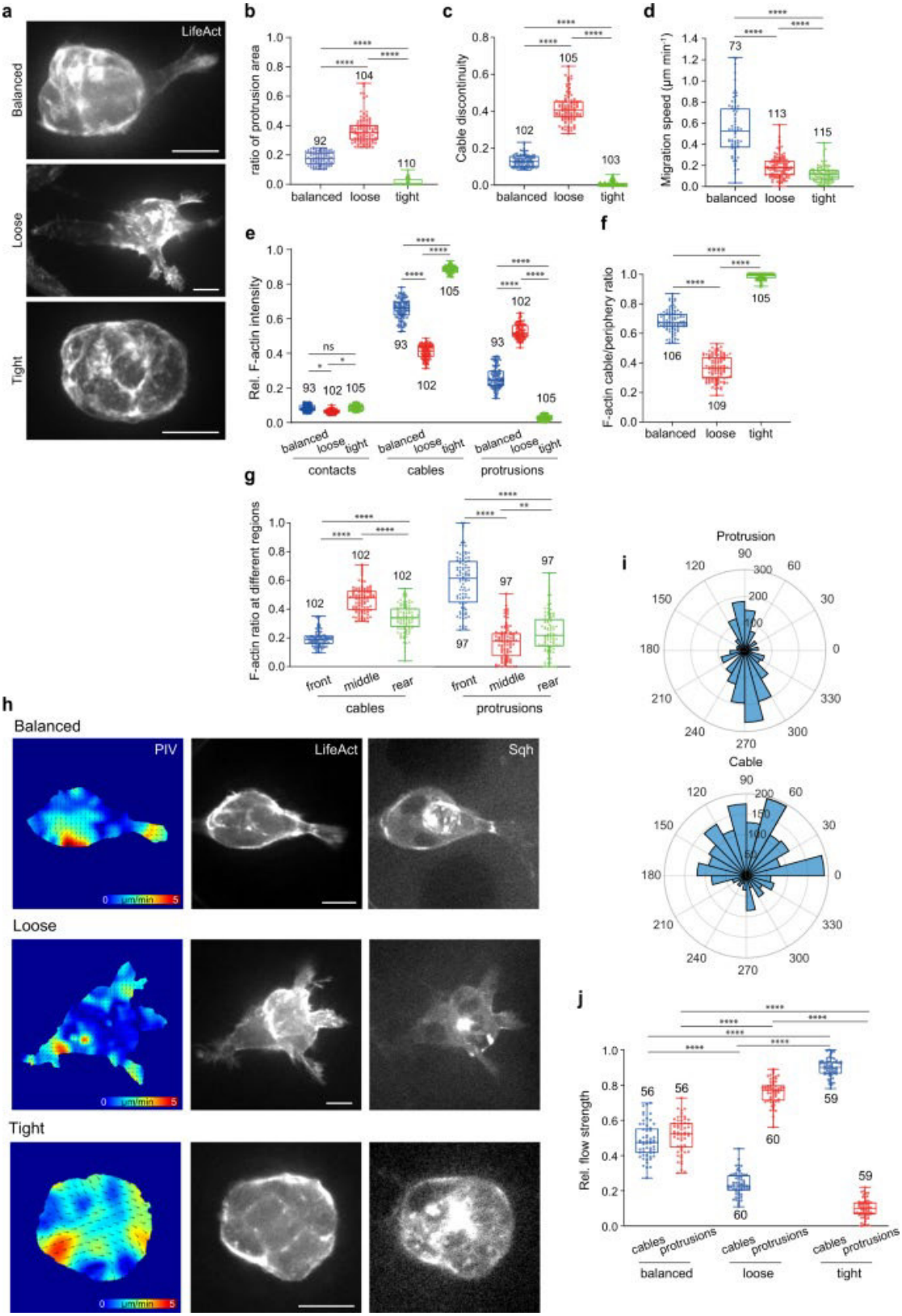
a
LifeAct
Balanced
Loose
Tight
b
ratio of protrusion area
balanced loose tight
c
Cable discontinuity
d
Migration speed (µm min⁻¹)
e
Rel. F-actin intensity
contacts
cables
protrusions
f
F-actin cable/periphery ratio
g
F-actin ratio at different regions
front middle rear
cables
protrusions
h
Balanced
PIV
LifeAct
Sqh
Loose
Tight
i
Protrusion
Cable
j
Rel. flow strength
cables protrusions
balanced
loose
tight

Figure 1. F-actin signals and actin flows vary between protrusions and cables in migrating border cell groups.

a Representative image of balanced, loose or tight border cell groups expressing LifeAct-GFP to monitor subcellular F-actin signals at either inner (border cell-to-cell contacts) or peripheral (cables or protrusions) regions. **b** Quantification of the ratio of protrusion area (protrusion area/total area ratio) in balanced, loose or tight border cell groups. **c** Quantification of cable discontinuity in balanced, loose or tight border cell groups. **d** Quantification of mean migration speed (μm per minute) in balanced, loose or tight border cell groups. **e** The quantification of relative F-actin intensity located at contacts, cables or protrusions in balanced, loose or tight border cell groups. **f** Quantification of the ratio between cable F-actin signals and total peripheral F-actin signals in balanced, loose or tight border cell groups. **g** Ratio quantification of cable F-actin signals or protrusion F-actin signals distributed at the front, middle or rear cells in balanced border cell groups. **h** Particle Image Velocimetry (PIV) analysis of actin flows in balanced, loose or tight border cell groups expressing LifeAct-GFP and Sqh-mCherry for F-actin and Myosin-II signals. PIV analysis performed on the LifeAct-GFP signals to highlight the direction and magnitude of actin flows. **i** Angle quantification of actin flows occurring at cables or protrusions in border cell groups, respectively. Number at perimeter showing the angle degree, while number at radius showing the occurrence amount of actin flow. For the direction of actin flows occurring at protrusions, 90 degree and 270 degree marking anterograde flows and retrograde flows, respectively. **j** Quantification of relative number of actin flows occurring at cables and protrusions in balanced, loose or tight border cell groups. Scale bars are 10 μm in (**a**) and (**h**). Boxplot shows medians, 25th and 75th percentiles as box limits, minimum and maximum values as whiskers; each datapoint is displayed as a dot (from n biologically independent samples for each border cell group), in (**b**–**g**) and (**j**). *P* values by two-sided Mann–Whitney test have been listed in Supplementary Note 1 at the end of all figures.

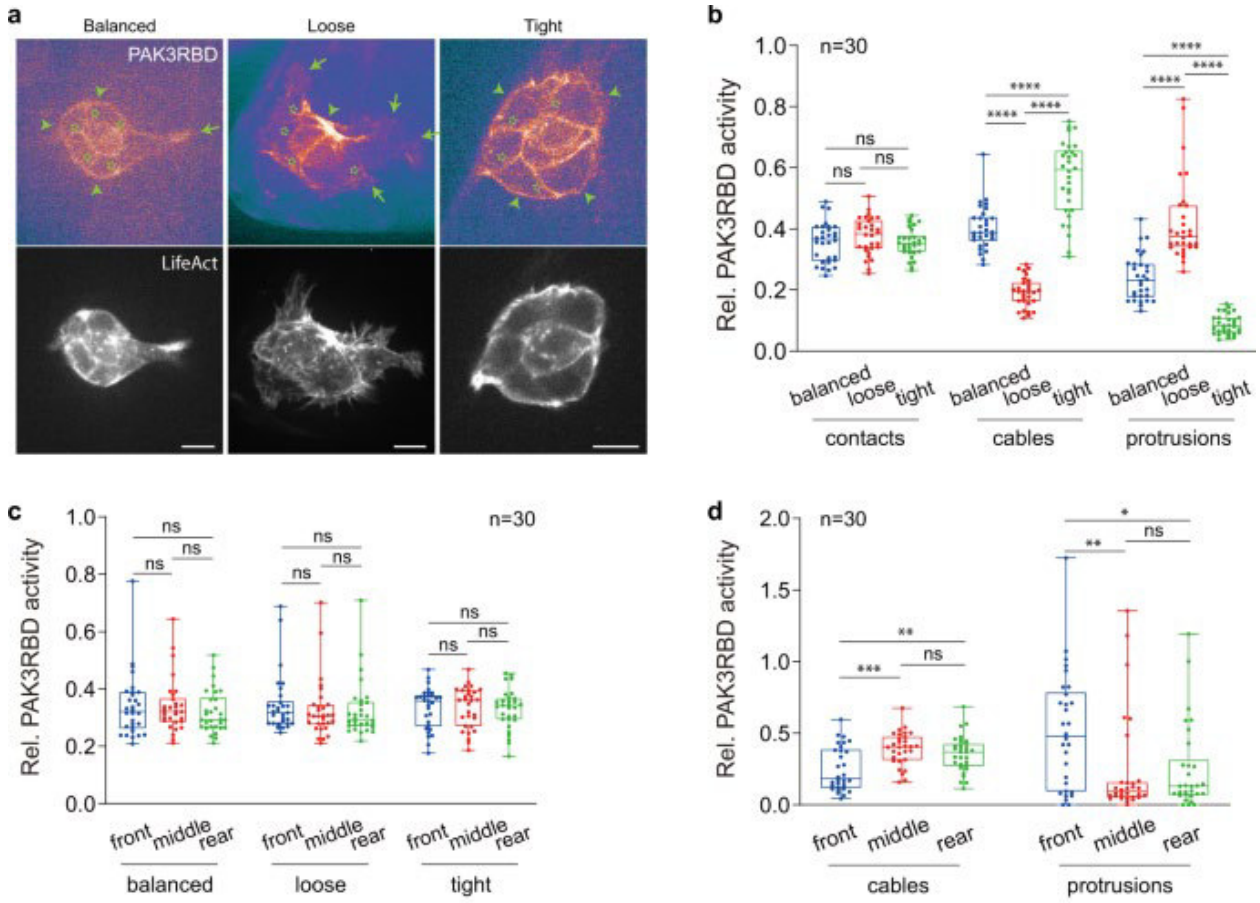
a
Balanced
Loose
Tight
PAK3RBD
LifeAct
b
n=30
Rel. PAK3RBD activity
balanced
loose
tight
contacts
cables
protrusions
c
n=30
Rel. PAK3RBD activity
front
middle
rear
balanced
loose
tight
d
n=30
Rel. PAK3RBD activity
front
middle
rear
cables
protrusions
e
"Two Rac1 pools" model
"Rac1 activity gradient" model
F-actin
Rac1

Figure 2. Rac1 activities vary between protrusions and cables in migrating border cell groups.

a Representative PAK3RBD-GFP and F-actin images in balanced, loose or tight border cell groups expressing LifeAct-RFP to discriminate and label different regions enriched with subcellular F-actin signals. Green arrows marking protrusions, green arrowheads marking cables, while green stars marking border cell-to-cell contacts. **b** Quantification of relative PAK3RBD-GFP intensity located at contacts, cables or protrusions in balanced, loose or tight border cell groups. **c** Quantification of relative intensity of total peripheral PAK3RBD-GFP signals distributed at the front, middle or rear cells in balanced, loose or tight border cell groups. **d** Quantification of relative cable PAK3RBD-GFP intensity or relative protrusion PAK3RBD-GFP intensity distributed at the front, middle or rear cells in balanced border cell groups. **e** Representative cartoon to summarize the "two Rac1 pools" model (left panel), compared with the "Rac1 activity gradient" model (right panel). Scale bars are 10 μm in (**a**). Boxplot shows medians, 25th and 75th percentiles as box limits, minimum and maximum values as whiskers; each datapoint is displayed as a dot (from n biologically independent samples for each border cell group), in (**b–d**). *P* values by two-sided Mann–Whitney test have been listed in Supplementary Note 1.

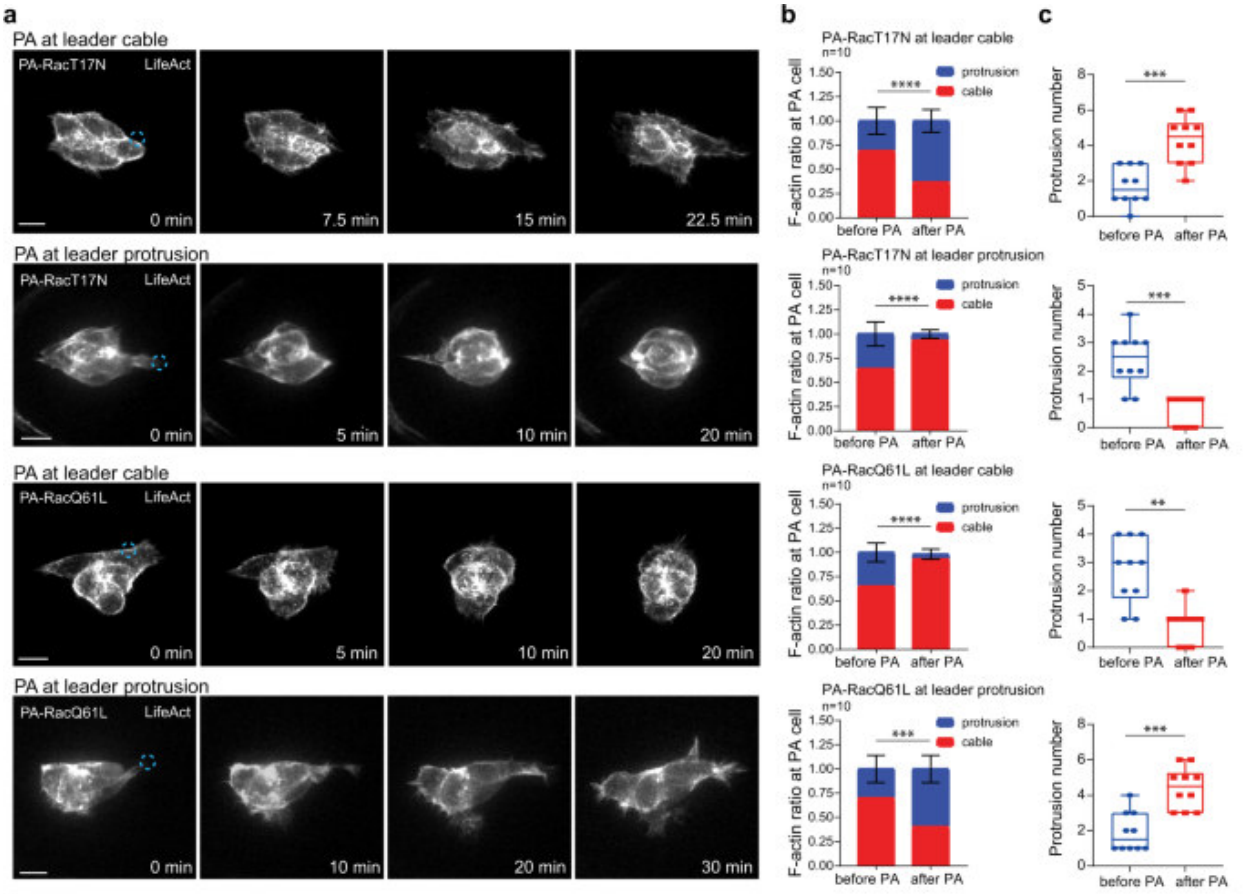
a
PA at leader cable
PA-RacT17N
LifeAct
0 min
7.5 min
15 min
22.5 min
PA at leader protrusion
PA-RacT17N
LifeAct
0 min
5 min
10 min
20 min
PA at leader cable
PA-RacQ61L
LifeAct
0 min
5 min
10 min
20 min
PA at leader protrusion
PA-RacQ61L
LifeAct
0 min
10 min
20 min
30 min
b
PA-RacT17N at leader cable
PA-RacT17N at leader protrusion
PA-RacQ61L at leader cable
PA-RacQ61L at leader protrusion
n=10
protrusion
cable
****
***
**
F-actin ratio at PA cell
before PA
after PA
c
Protrusion number
before PA
after PA

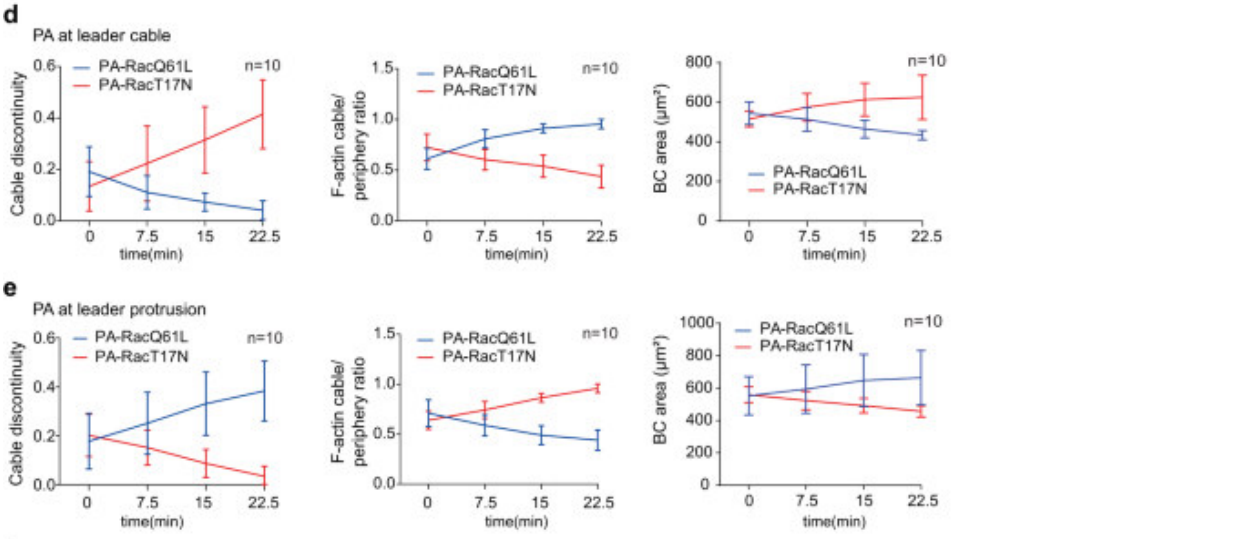
d
PA at leader cable
e
PA at leader protrusion
PA-RacQ61L
PA-RacT17N
n=10
Cable discontinuity
F-actin cable/ periphery ratio
BC area (μm²)
time(min)

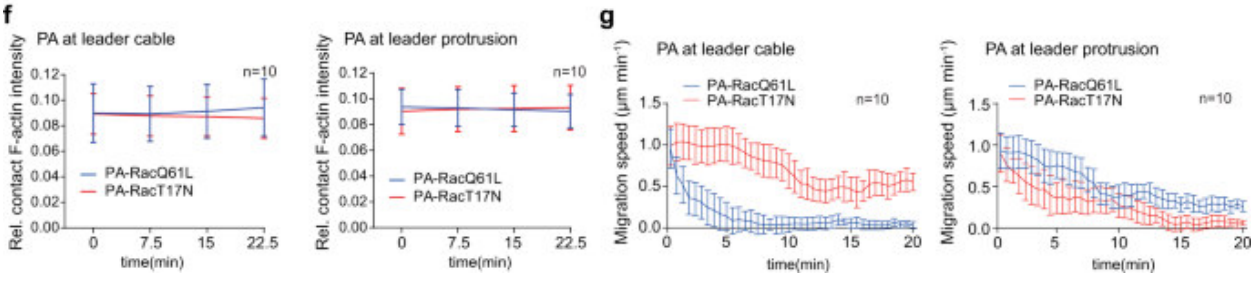
f
PA at leader cable
PA at leader protrusion
Rel. contact F-actin intensity
PA-RacQ61L
PA-RacT17N
n=10
time(min)
g
PA at leader cable
PA at leader protrusion
Migration speed (μm min⁻¹)
PA-RacQ61L
PA-RacT17N
n=10
time(min)

Figure 3. Focal Rac1 modifications by optogenetics unravel intracellular and intercellular changes of F-actin signals by two Rac1 pools in peripheral regions.

a Representative time-lapse F-actin images of border cell groups expressing either PA-RacT17N or PA-RacQ61L, together with LifeAct-RFP to monitor subcellular F-actin signals, before and after photo-activation of PA-Rac at cables or protrusions of one leader border cell. Dotted blue circle labelling the PA regions with blue light illumination, either at cables or protrusions in leader border cells. PA means photo-activation. Ratio quantifications of cable F-actin intensity and protrusion F-actin intensity in the photo-treated leader border cells (**b**), and quantifications of protrusion number (**c**), before and after 18–25−minute photo-activation of either PA-RacT17N or PA-RacQ61L at cables or protrusions in leader border cells. Time-lapse quantifications of cable discontinuity (left panels in **d**, **e**), the ratio between cable F-actin signals and total peripheral F-actin signals (middle panels in **d**, **e**), and total cell area (right panels in **d**, **e**) in the indicated border cell groups, before and after photo-activation of PA-Rac at leader cell cables (**d**) and at leader protrusions (**e**). **f** Time-lapse quantifications of relative F-actin intensity located at the border cell-to-cell contacts in the indicated border cell groups, before and after photo-activation of PA-Rac at leader border cell cables (left panel) or protrusions (right panel). **g** Time-lapse quantifications of mean migration speed (μm per minute) in the indicated border cell groups, before and after photo-activation of PA-Rac at leader border cell cables (left penal) or protrusions (right panel). Scale bars are 10 μm in (**a**). Data are presented as mean values ± SD in (**b**), (**d–g**) (from n biologically independent samples for each border cell group). Boxplot shows medians, 25th and 75th percentiles as box limits, minimum and maximum values as whiskers; each datapoint is displayed as a dot (from n biologically independent samples for each border cell group) in (**c**). *P* values by two-sided Mann–Whitney test have been listed in Supplementary Note 1.

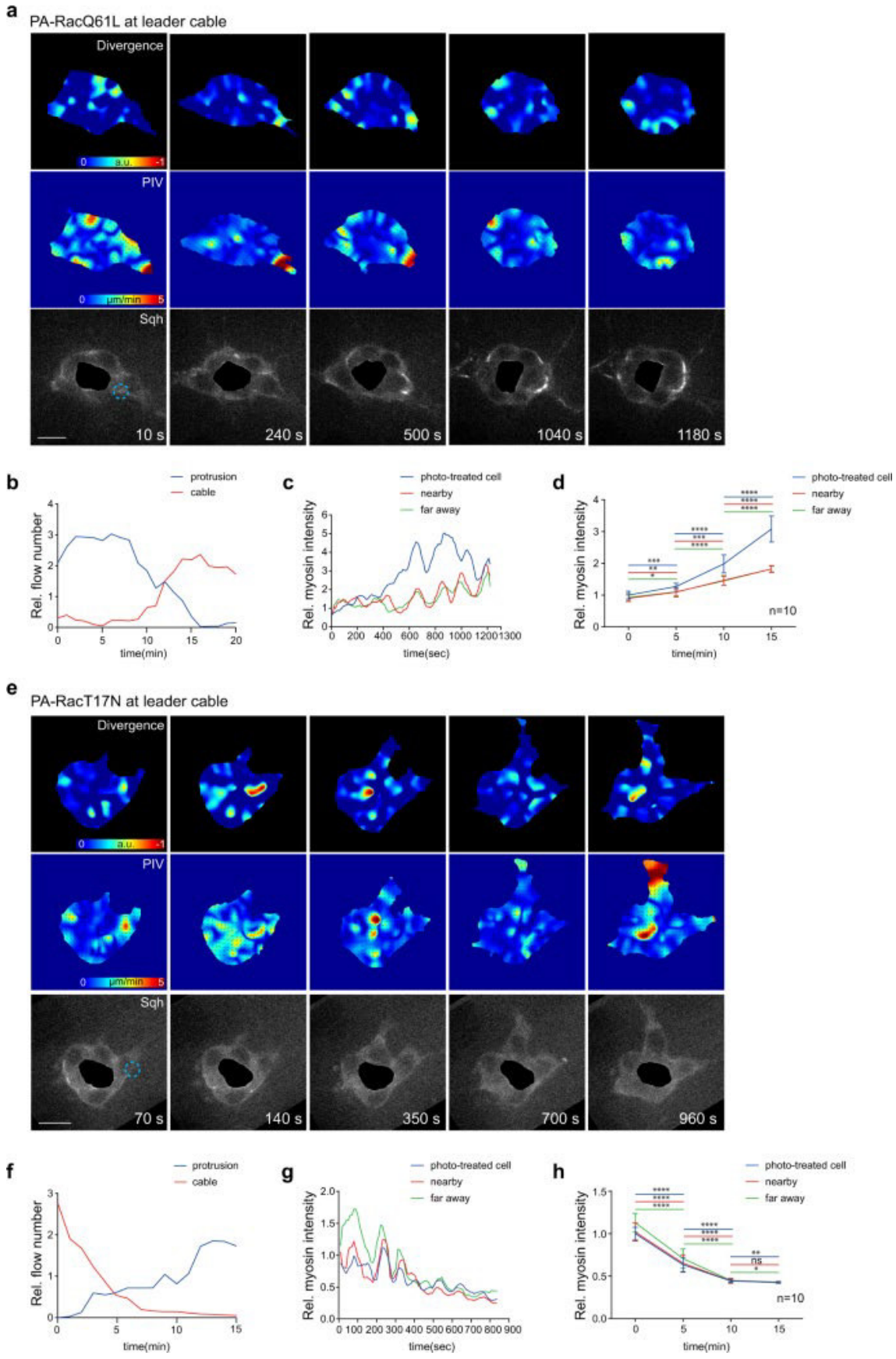
a
PA-RacQ61L at leader cable
Divergence
PIV
Sqh
10 s
240 s
500 s
1040 s
1180 s
b
protrusion
cable
Rel. flow number
time(min)
c
photo-treated cell
nearby
far away
Rel. myosin intensity
time(sec)
d
photo-treated cell
nearby
far away
Rel. myosin intensity
n=10
time(min)
e
PA-RacT17N at leader cable
Divergence
PIV
Sqh
70 s
140 s
350 s
700 s
960 s
f
protrusion
cable
Rel. flow number
time(min)
g
photo-treated cell
nearby
far away
Rel. myosin intensity
time(sec)
h
photo-treated cell
nearby
far away
Rel. myosin intensity
n=10
time(min)

Figure 4. Focal modifications of cable Rac1 activity control pulsed Myosin-II signal accumulation at supracellular cables.

Time-lapse PIV and divergence analyses of actin flows in one representative border cell group expressing either PA-RacQ61L (**a**) or PA-RacT17N (**e**), and LifeAct-GFP and Sqh-mCherry for F-actin and Myosin-II signals, after photo-activation of PA-Rac at cables of one border cell. a.u. means arbitrary unit for divergence level. Dotted blue circle marking the PA regions with blue light illumination. PA means photo-activation. Time-lapse quantifications of relative area of actin flows occurring per minute at cables or protrusions of one representative border cell group expressing either PA-RacQ61L (**b**) or PA-RacT17N (**f**), after photo-activation of PA-Rac at cables of one border cell. Strong actin flows have been counted for the quantification. Time-lapse quantifications of relative Myosin-II intensity accumulated at cables of three border cell types (photo-treated cells, cells in contact with the photo-treated cells, or cells far away from the photo-treated cells) in one representative border cell group expressing PA-RacQ61L (**c**) or PA-RacT17N (**g**), after photo-activation of PA-Rac at cables of one border cell. Time-lapse quantifications of relative Myosin-II intensity accumulated at cables of three border cell types in n border cell groups expressing PA-RacQ61L (**d**) or PA-RacT17N (**h**), after photo-activation of PA-Rac at cables of one border cell. Scale bars are 10 μm in (**a**) and (**e**). Data are presented as mean values ± SD in (**d**) and (**h**) (from n biologically independent samples for each border cell group). *P* values by two-sided Mann–Whitney test have been listed in Supplementary Note 1.

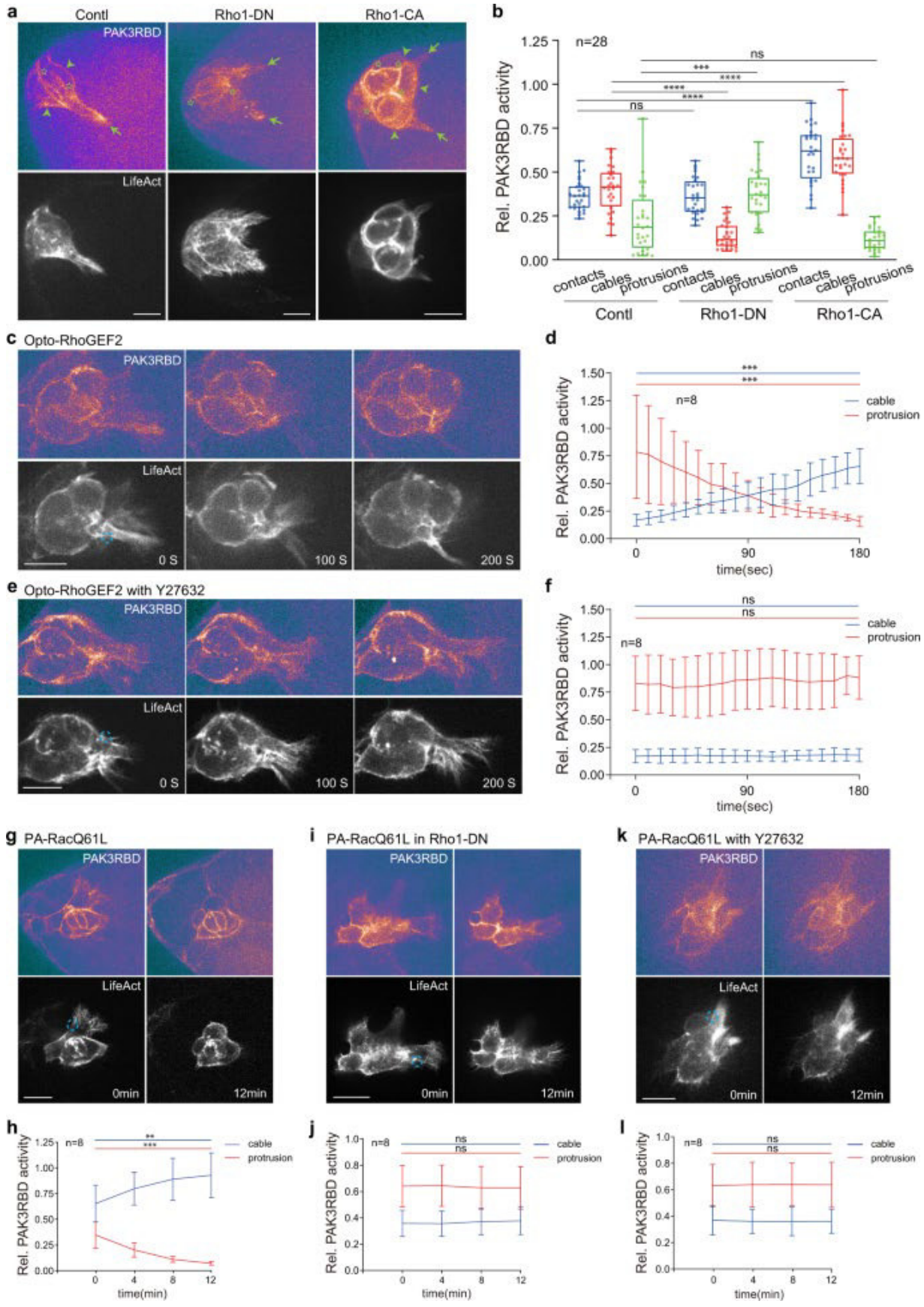
a
Contl
Rho1-DN
Rho1-CA
PAK3RBD
LifeAct
b
n=28
Rel. PAK3RBD activity
contacts
cables
protrusions
Contl
Rho1-DN
Rho1-CA
c Opto-RhoGEF2
0 S
100 S
200 S
d
n=8
cable
protrusion
time(sec)
e Opto-RhoGEF2 with Y27632
f
g PA-RacQ61L
0min
12min
i PA-RacQ61L in Rho1-DN
k PA-RacQ61L with Y27632
h
j
l
time(min)

Figure 5. Rho1 signalling governs cable Rac1 activity to support supracellular cables.

a Representative PAK3RBD-GFP and F-actin images in border cell groups expressing Rho1DN, Rho1CA or control, together with LifeAct-RFP to discriminate and label different regions enriched with subcellular F-actin signals. Green arrows marking protrusions, green arrowheads marking cables, while green stars marking border cell-cell contacts. **b** Quantification of relative PAK3RBD-GFP intensity located at contacts, cables or protrusions in the indicated border cell groups. Representative time-lapse PAK3RBD-GFP and F-actin images in border cell groups expressing Opto-RhoGEF2 and LifeAct-RFP, without (**c**) or with Y27632 treatment (**e**), before and after blue light illumination at the cable regions near leading protrusions. Dotted blue circle labelling the PA regions with blue light illumination. PA means photo-activation. Time-lapse quantifications of relative PAK3RBD-GFP intensity located at cables or protrusions in the photo-treated cells, without (**d**) or with Y27632 treatment (**f**), before and after photo-activation of Opto-RhoGEF2 (in **c** and **e**). Representative PAK3RBD-GFP and F-actin images in border cell groups expressing PA-RacQ61L and LifeAct-RFP (**g**), PA-RacQ61L and LifeAct-RFP as well as Rho1 DN (**i**), or PA-RacQ61L and LifeAct-RFP together with Y27632 treatment (**k**), before and after photo-activation of PA-Rac at cables of one border cell. Time-lapse quantifications of relative PAK3RBD-GFP intensity located at cables or protrusions in the border cell groups expressing PA-RacQ61L and LifeAct-RFP (**h**), PA-RacQ61L and LifeAct-RFP as well as Rho1 DN (**j**), or PA-RacQ61L and LifeAct-RFP together with Y27632 treatment (**l**), before and after photo-activation of PA-Rac. Scale bars are 10 μm in (**a**), (**c**), (**e**), (**g**), (**i**) and (**k**). Boxplot shows medians, 25th and 75th percentiles as box limits, minimum and maximum values as whiskers; each datapoint is displayed as a dot (from n biologically independent samples for each border cell group), in (**b**). Data are presented as mean values ± SD in (**d**), (**f**), (**h**), (**j**) and (**l**) (from n biologically independent samples for each border cell group). *P* values by two-sided Mann–Whitney test have been listed in Supplementary Note 1.

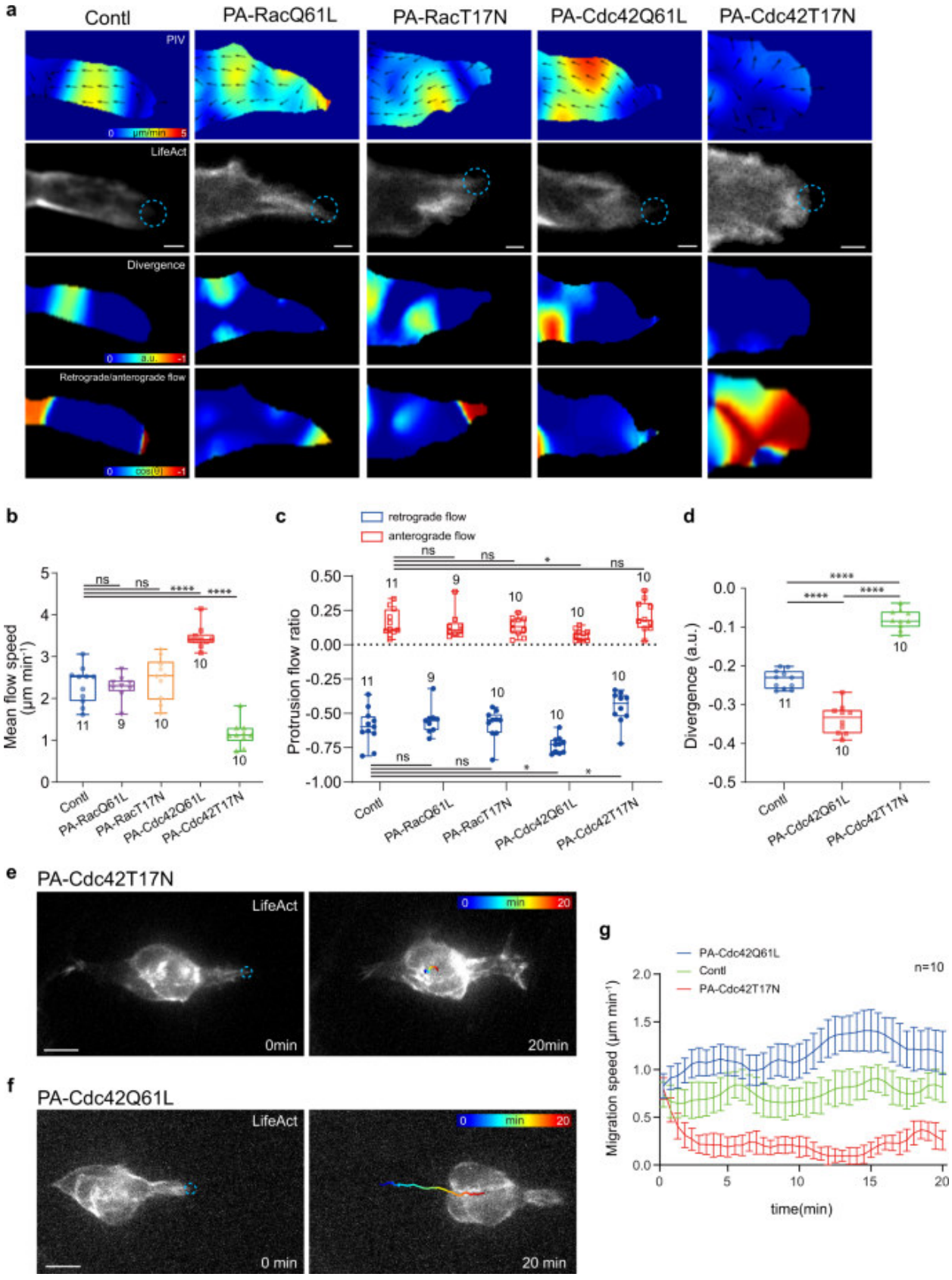
a
Contl
PA-RacQ61L
PA-RacT17N
PA-Cdc42Q61L
PA-Cdc42T17N
PIV
LifeAct
Divergence
Retrograde/anterograde flow
b
Mean flow speed (μm min-1)
c
retrograde flow
anterograde flow
Protrusion flow ratio
d
Divergence (a.u.)
e
PA-Cdc42T17N
LifeAct
0min
20min
f
PA-Cdc42Q61L
LifeAct
0 min
20 min
g
PA-Cdc42Q61L
Contl
PA-Cdc42T17N
n=10
Migration speed (μm min-1)
time(min)

Figure 6. Cdc42 governs actin flows at protrusions and border cell migration efficiency.

a Representative PIV, divergence and retrograde/anterograde direction analyses of actin flows at leading protrusions in the border cell groups expressing PA-RacQ61L, PA-RacT17N, PA-Cdc42Q61L, PA-Cdc42T17N or control (yw as WT), together with LifeAct-GFP for F-actin signals. Dotted blue circle labelling the PA regions with blue light illumination. PA means photo-activation. a.u. means arbitrary unit for divergence level. **b** Quantification of mean flow speed (μm per minute) at leading protrusions in the indicated border cell groups. **c** Quantification of the occurrence ratio of retrograde and anterograde actin flows at leading protrusions in the indicated border cell groups. **d** Quantification of divergence of actin flows at leading protrusions in the indicated border cell groups. Representative time-lapse images of border cell groups expressing PA-Cdc42T17N (**e**) or PA-Cdc42Q61L (**f**), together with LifeAct-RFP to monitor subcellular F-actin signals, before and after photo-activation of PA-Cdc42 at leader border cell protrusions. Dotted blue circle labelling the PA regions with blue light illumination. PA means photo-activation. RGB colours marking the trajectory of border cell migration. **g** Time-lapse quantifications of mean migration speed (μm per minute) in the border cell groups expressing either PA-Cdc42T17N or PA-Cdc42Q61L, after photo-activation of PA-Cdc42 at leader border cell protrusions, compared with photo-treated WT border cell groups. Scale bars are 2 μm in (**a**), and 10 μm in (**e**) and (**f**). Boxplot shows medians, 25th and 75th percentiles as box limits, minimum and maximum values as whiskers; each datapoint is displayed as a dot (from n biologically independent samples for each border cell group) in (**b–d**). Data are presented as mean values ± SD in (**g**) (from n biologically independent samples for each border cell group). *P* values by two-sided Mann–Whitney test have been listed in Supplementary Note 1.

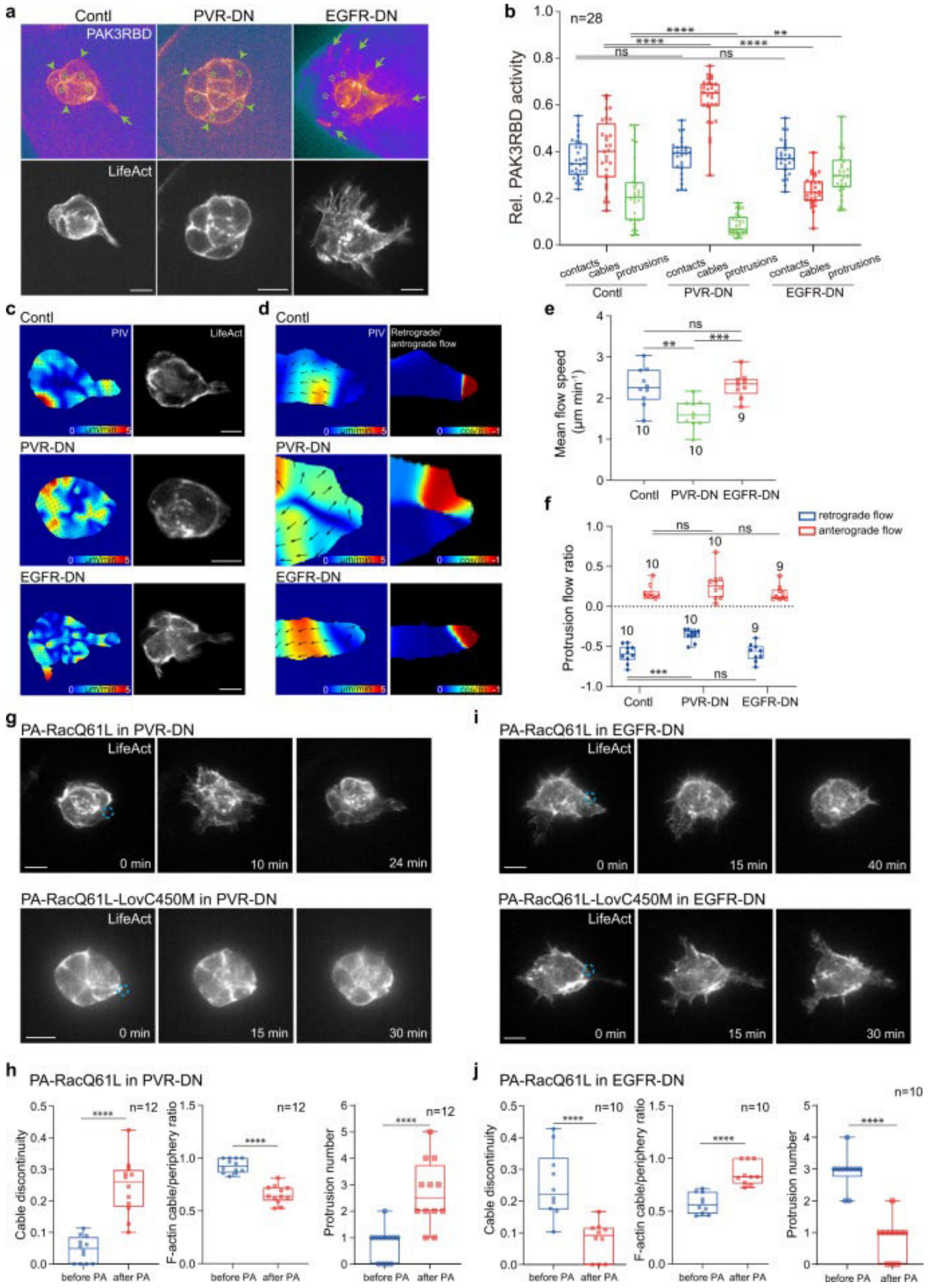
a
Contl
PVR-DN
EGFR-DN
PAK3RBD
LifeAct
b
n=28
Rel. PAK3RBD activity
contacts
cables
protrusions
Contl
PVR-DN
EGFR-DN
c
Contl
PIV
LifeAct
PVR-DN
EGFR-DN
d
Contl
PIV
Retrograde/
antrograde flow
PVR-DN
EGFR-DN
e
Mean flow speed
(µm min-1)
Contl
PVR-DN
EGFR-DN
f
retrograde flow
anterograde flow
Protrusion flow ratio
Contl
PVR-DN
EGFR-DN
g
PA-RacQ61L in PVR-DN
LifeAct
0 min
10 min
24 min
PA-RacQ61L-LovC450M in PVR-DN
LifeAct
0 min
15 min
30 min
i
PA-RacQ61L in EGFR-DN
LifeAct
0 min
15 min
40 min
PA-RacQ61L-LovC450M in EGFR-DN
LifeAct
0 min
15 min
30 min
h
PA-RacQ61L in PVR-DN
Cable discontinuity
F-actin cable/periphery ratio
Protrusion number
before PA
after PA
j
PA-RacQ61L in EGFR-DN
Cable discontinuity
F-actin cable/periphery ratio
Protrusion number
before PA
after PA

Figure 7. PVR and EGFR differently guide Rac1 activity and actin flows at protrusions and cables of migrating border cells.

a Representative PAK3RBD-GFP and F-actin images in border cell groups expressing PVR-DN, EGFR-DN or control, together with LifeAct-RFP to monitor subcellular F-actin signals. Green arrows marking protrusions, green arrowheads marking cables, while green stars marking border cell-cell contacts. **b** Quantification of relative PAK3RBD-GFP intensity located at contacts, cables or protrusions in the indicated border cell groups. Representative PIV analyses of actin flows in the whole groups (**c**), PIV and retrograde/anterograde direction analyses of actin flows at leading protrusions in the border cell groups (**d**) expressing PVR-DN, EGFR-DN or control, together with LifeAct-GFP for F-actin signals. Quantification of mean flow speed (μm per minute) at protrusions (**e**) and occurrence ratio of protrusion retrograde and anterograde actin flows (**f**) in the indicated border cell groups. Representative time-lapse F-actin images of border cell groups expressing PA-RacQ61L and PVR-DN (upper in **g**), or PA-RacQ61L-LovC450M and PVR-DN (lower in **g**), or PA-RacQ61L and EGFR-DN (upper in **i**), or PA-RacQ61L-LovC450M and EGFR-DN (lower in **i**), together with LifeAct-RFP to monitor subcellular F-actin signals, before and after photo-activation of PA-RacQ61L at one border cell. Dotted blue circle labelling the PA regions with blue light illumination. PA means photo-activation. Quantifications of cable discontinuity, the ratio between cable F-actin signals and total peripheral F-actin signals, and protrusion number in the border cell groups expressing PA-RacQ61L and PVR-DN (**h**) or PA-RacQ61L and EGFR-DN (**j**), before and after 20–30−minute photo-activation at one border cell. Scale bars are 10 μm in (**a**, **c**, **g** and **i**). Boxplot shows medians, 25th and 75th percentiles as box limits, minimum and maximum values as whiskers; each datapoint is displayed as a dot (from n biologically independent samples for each border cell group), in (**b**, **e**, **f**, **h** and **j**) (from n biologically independent samples for each border cell group). *P* values by two-sided Mann–Whitney test have been listed in Supplementary Note 1.

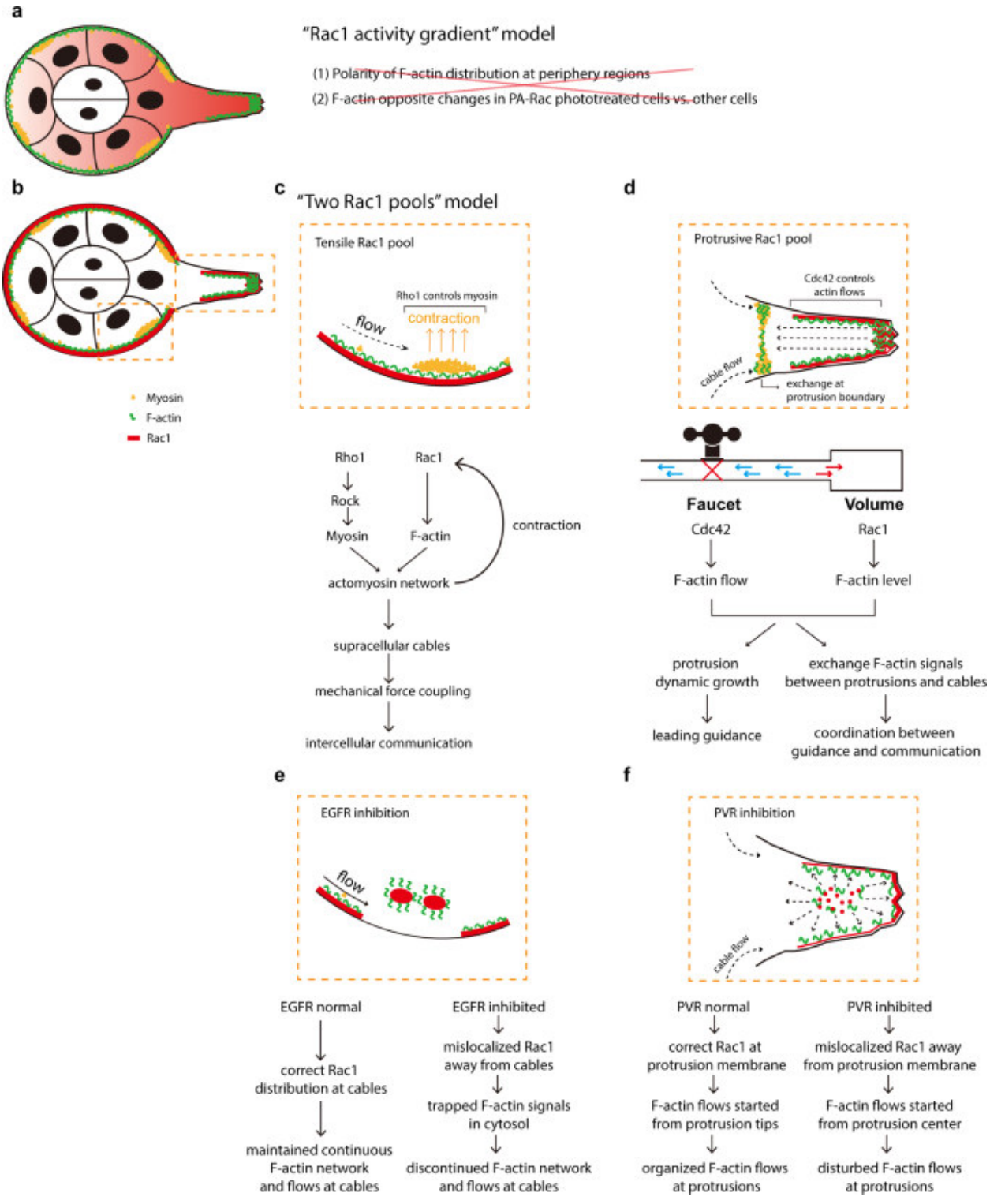
a
"Rac1 activity gradient" model
(1) Polarity of F-actin distribution at periphery regions
(2) F-actin opposite changes in PA-Rac phototreated cells vs. other cells
b
Myosin
F-actin
Rac1
c
"Two Rac1 pools" model
Tensile Rac1 pool
Rho1 controls myosin
contraction
flow
Rho1
Rac1
Rock
Myosin
F-actin
contraction
actomyosin network
supracellular cables
mechanical force coupling
intercellular communication
d
Protrusive Rac1 pool
Cdc42 controls actin flows
cable flow
exchange at protrusion boundary
Faucet
Volume
Cdc42
Rac1
F-actin flow
F-actin level
protrusion dynamic growth
exchange F-actin signals between protrusions and cables
leading guidance
coordination between guidance and communication
e
EGFR inhibition
flow
EGFR normal
correct Rac1 distribution at cables
maintained continuous F-actin network and flows at cables
EGFR inhibited
mislocalized Rac1 away from cables
trapped F-actin signals in cytosol
discontinued F-actin network and flows at cables
f
PVR inhibition
cable flow
PVR normal
correct Rac1 at protrusion membrane
F-actin flows started from protrusion tips
organized F-actin flows at protrusions
PVR inhibited
mislocalized Rac1 away from protrusion membrane
F-actin flows started from protrusion center
disturbed F-actin flows at protrusions

Figure 8. Comparison between "Rac1 activity gradient" model and "two Rac1 pools" model.

a Representative cartoon to summarize the "Rac1 activity gradient" model governed by chemokine receptors EGFR and PVR in migrating border cell groups. However, this model cannot explain the failure of detecting either polarized F-actin distribution in peripheral regions of border cell groups or F-actin signal switch between the PA-Rac photo-treated border cells and other border cells. **b** Representative cartoon to summarize the "two Rac1 pools" model supported by this study. **c** Tensile Rac1 pool at cables form a positive feedback loop with Rho1−Myosin-II signalling to support supracellular cables and mechanical force coupling between cells, thus controlling intercellular communication. **d** Protrusive Rac1 pool synergizes with Cdc42 to control F-actin intensity level or actin flows at protrusions, functioning like either volume control or faucet switch of a water tank, thus governing both dynamic protrusion growth for leading guidance and F-actin signal exchange between protrusions and cables for the coordination between leading guidance and intercellular communication. **e**, **f** Different from "Rac1 activity gradient" model, EGFR and PVR guide correct activity localization of tensile and protrusive Rac1 pools at cables and protrusions respectively: the inhibition of EGFR or PVR signalling results in the mis-localization of Rac1 activity from cables or protrusion tips, thus causing the disturbed actin flows at either region to affect the WT border cell migration behaviours.

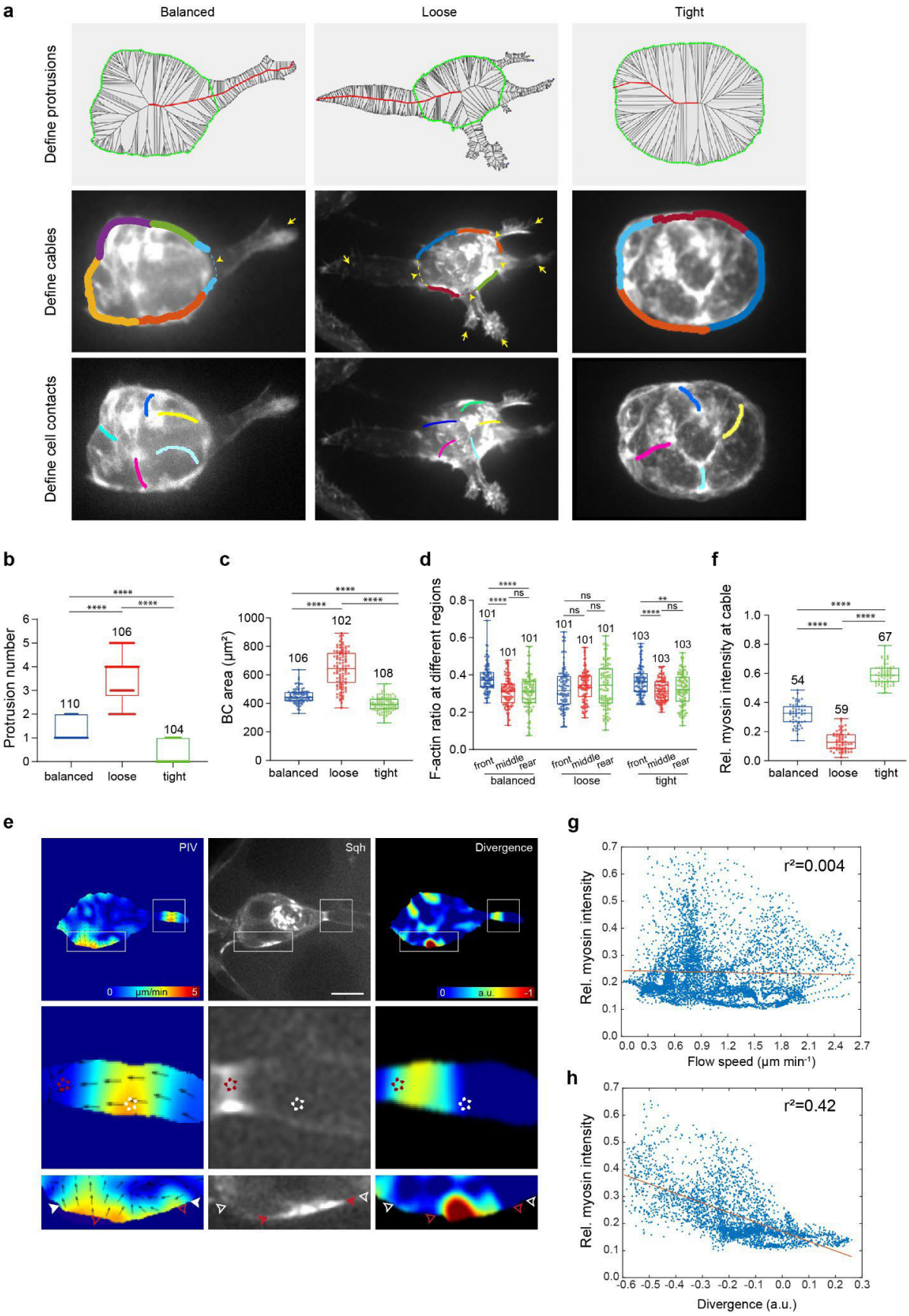
a
Balanced
Loose
Tight
Define protrusions
Define cables
Define cell contacts
b
Protrusion number
110
106
104
balanced
loose
tight
c
BC area (µm²)
106
102
108
balanced
loose
tight
d
F-actin ratio at different regions
front
middle
rear
balanced
loose
tight
f
Rel. myosin intensity at cable
54
59
67
balanced
loose
tight
e
PIV
Sqh
Divergence
0 µm/min 5
0 a.u. 1
g
Rel. myosin intensity
r²=0.004
Flow speed (µm min⁻¹)
h
Rel. myosin intensity
r²=0.42
Divergence (a.u.)

Supplementary Figure 1. Analyses of subcellular F-actin signals and actin flows in migrating border cell groups.

a. Definition of protrusions, cables and the cell-to-cell contacts in representative balanced, loose or tight border cell groups expressing LifeAct-GFP. Different colors marking either cables in one border cells or cell-cell contacts between two border cells. Yellow arrows marking protrusions, yellow arrowheads marking broken cables. **b, c.** Quantifications of protrusion number (**b**) and border cell area (**c**) in the indicated border cell groups. **d.** Ratio quantification of total peripheral F-actin signals distributed at the front, middle or rear cells in the indicated border cell groups. **e.** Representative PIV and divergence analyses of actin flows in balanced border cell group expressing LifeAct-GFP and Sqh-mCherry for F-actin and Myosin-II signals. PIV analysis performed on the LifeAct-GFP signals to highlight the direction and magnitude of actin flows. Divergence calculated from the actin flowfield to highlight the region where actin flows from different directions converge and thus Myosin-II signals accumulate at cables or protrusion-cable boundaries. a.u. means arbitrary unit for divergence level. White arrowheads (cables) or stars (protrusions) marking high PIV regions, while red arrowheads (cables) or stars (protrusions) marking negative divergence regions. **f.** Quantification of relative Myosin-II signals accumulated at cables in the indicated border cell groups. **g, h.** Scatter plot comparing a random sample of points in the actin flowfield for relative actin flow speed and relative Myosin-II intensity (**g**), or for divergence and relative Myosin-II intensity (**h**). Note the positive relationship between negative divergence and relative Myosin-II intensity (n = 6156 random points, 9 biologically independent samples); but no significant relationship between actin flow speed and relative Myosin-II intensity (n = 5876 random points, 9 biologically independent samples). Scale bars are 10 μm in **e**. Boxplot shows medians, 25th and 75th percentiles as box limits, minimum and maximum values as whiskers; each datapoint is displayed as a dot (from n biologically independent samples for each border cell group), in **b, c, d** and **f**. P values by two-sided Mann–Whitney test have been listed in Supplementary Note 1.

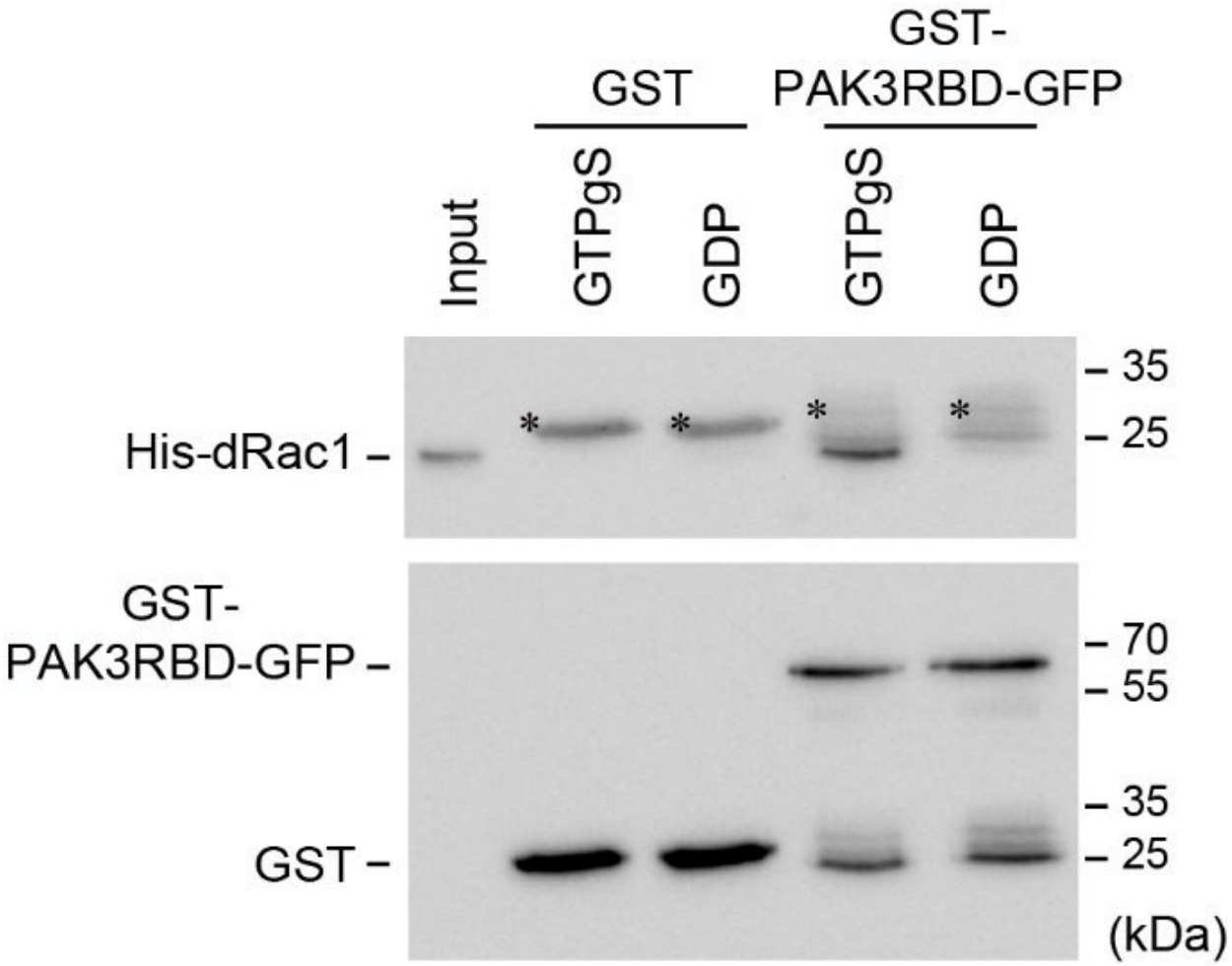
GST
GST-
PAK3RBD-GFP
Input
GTPgS
GDP
GTPgS
GDP
His-dRac1
GST-
PAK3RBD-GFP
GST
35
25
70
55
35
25
(kDa)

Supplementary Figure 2. Control experiments for the binding specificity of GTP-loaded dRac1 to PAK3RBD-GFP.

GTPγS- or GDP-loaded His-dRac1 was incubated with GST or GST-PAK3RBD-GFP recombinant proteins purified from *E. coli*. Input and pull-down samples were analysed by immunoblotting with antibodies against His (top panel) or GST (bottom panel). Asterisk marks non-specific signals. The results have been successfully repeated from the at least 3 independent experiments.

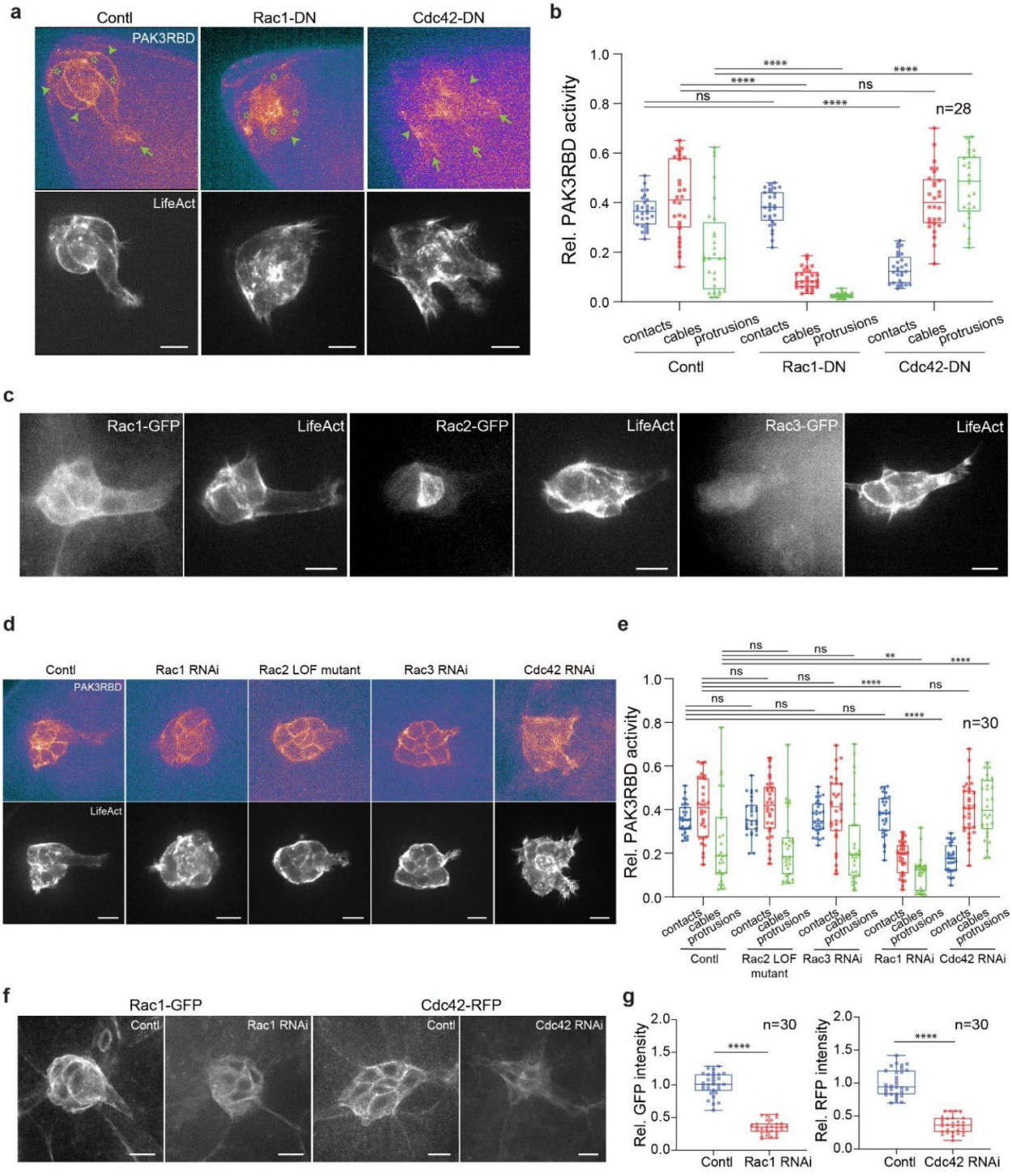
a
Contl
Rac1-DN
Cdc42-DN
PAK3RBD
LifeAct
b
Rel. PAK3RBD activity
n=28
ns
****
contacts
cables
protrusions
Contl
Rac1-DN
Cdc42-DN
c
Rac1-GFP
LifeAct
Rac2-GFP
Rac3-GFP
d
Contl
Rac1 RNAi
Rac2 LOF mutant
Rac3 RNAi
Cdc42 RNAi
e
n=30
Rac2 LOF mutant
f
Rac1-GFP
Cdc42-RFP
g
Rel. GFP intensity
Rel. RFP intensity
n=30

Supplementary Figure 3. Control experiments for subcellular Rac1 activity in border cells.

a. Representative PAK3RBD-GFP and F-actin images in border cell groups expressing Rac1DN, Cdc42DN and control (yw; named as WT), together with LifeAct-RFP to discriminate and label different regions enriched with subcellular F-actin. Since the expression of Rac1DN and Cdc42DN in border cells led to the defect in border cell detachment, we chose all these three border cell groups during detachment for the comparison. Green arrows marking protrusions, green arrowheads marking cables, while green stars marking border cell-cell contacts. **b.** Quantification of relative PAK3RBD-GFP intensity located at contacts, cables or protrusions in the indicated border cell groups. **c.** Representative GFP and F-actin images in border cell groups expressing Rac1-GFP, Rac2-GFP and Rac3-GFP (endogenous patterns), together with LifeAct-RFP to monitor subcellular F-actin signals. Rac1-GFP vs. Rac2-GFP in border cells (but not two internal polar cells): 1+/-0.168 vs. 0.24+/-0.096, and Rac1-GFP vs. Rac3-GFP in border cells: 1+/-0.168 vs. 0.17+/-0.071, from n=35 independent samples. **d.** Representative PAK3RBD-GFP and F-actin images in border cell groups expressing Rac1 RNAi, Rac3 RNAi or Cdc42 RNAi, or with Rac2 LOF mutant, together with LifeAct-RFP to discriminate different regions enriched with subcellular F-actin. **e.** Quantification of relative PAK3RBD-GFP intensity located at contacts, cables or protrusions in the indicated border cell groups. **f.** Representative GFP and RFP images in border cell groups expressing Rac1-GFP (and Rac1 RNAi or control), or Cdc42-RFP (and Cdc42 RNAi or control), from fixed imaging. **g.** Quantification of relative GFP/RFP intensity in total border cell groups in the indicated border cell groups. Scale bars are 10 μm in **a, c, d, f**. Boxplot shows medians, 25th and 75th percentiles as box limits, minimum and maximum values as whiskers; each datapoint is displayed as a dot (from n biologically independent samples for each border cell group), in **b, e, g**. P values by two-sided Mann–Whitney test have been listed in Supplementary Note 1.

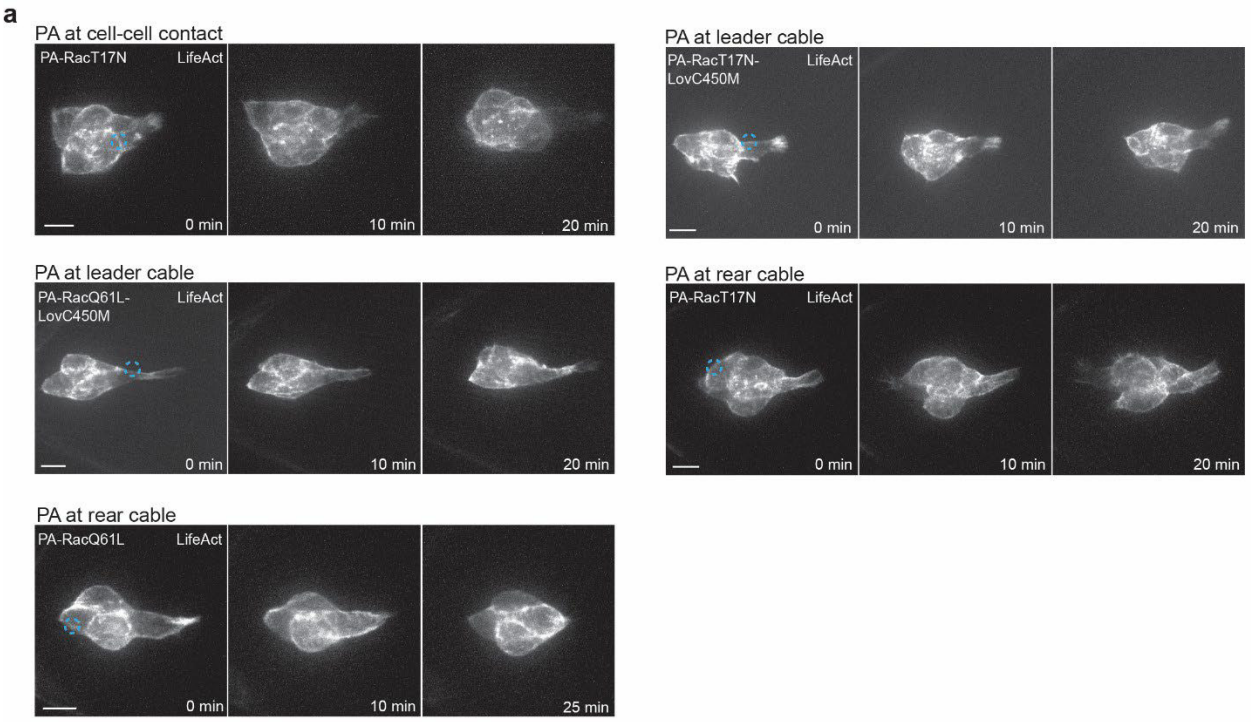
a
PA at cell-cell contact
PA-RacT17N
LifeAct
0 min
10 min
20 min
PA at leader cable
PA-RacT17N-LovC450M
LifeAct
0 min
10 min
20 min
PA at leader cable
PA-RacQ61L-LovC450M
LifeAct
0 min
10 min
20 min
PA at rear cable
PA-RacT17N
LifeAct
0 min
10 min
20 min
PA at rear cable
PA-RacQ61L
LifeAct
0 min
10 min
25 min

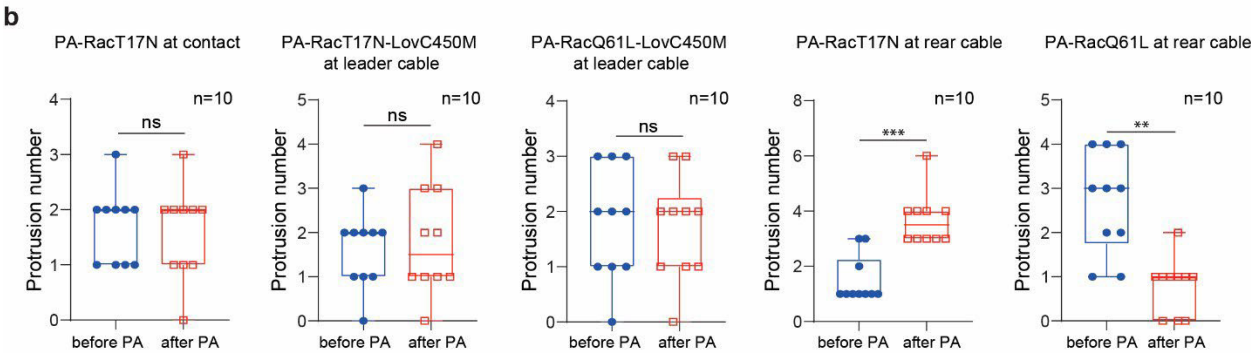
b
PA-RacT17N at contact
PA-RacT17N-LovC450M at leader cable
PA-RacQ61L-LovC450M at leader cable
PA-RacT17N at rear cable
PA-RacQ61L at rear cable
Protrusion number
n=10
ns
***
**
before PA
after PA

Supplementary Figure 4. Control experiments for PA-Rac effects.

a. Representative time-lapse images of border cell groups expressing the indicated PA-Rac forms, together with LifeAct-RFP to monitor subcellular F-actin signals. Dotted blue circle labelling the PA regions with blue light illumination, either at cables in leader or rear border cells, or at border cell-to-cell contacts. PA means photo-activation. **b**. Quantification of protrusion number before and after 18-25 minute photo-activation of the indicated PA-Rac forms at cables or border cell-to-cell contacts. Scale bars are 10 μm in **a**. Boxplot shows medians, 25th and 75th percentiles as box limits, minimum and maximum values as whiskers; each datapoint is displayed as a dot (from n biologically independent samples for each border cell group) in **b**. P values by two-sided Mann–Whitney test have been listed in Supplementary Note 1.

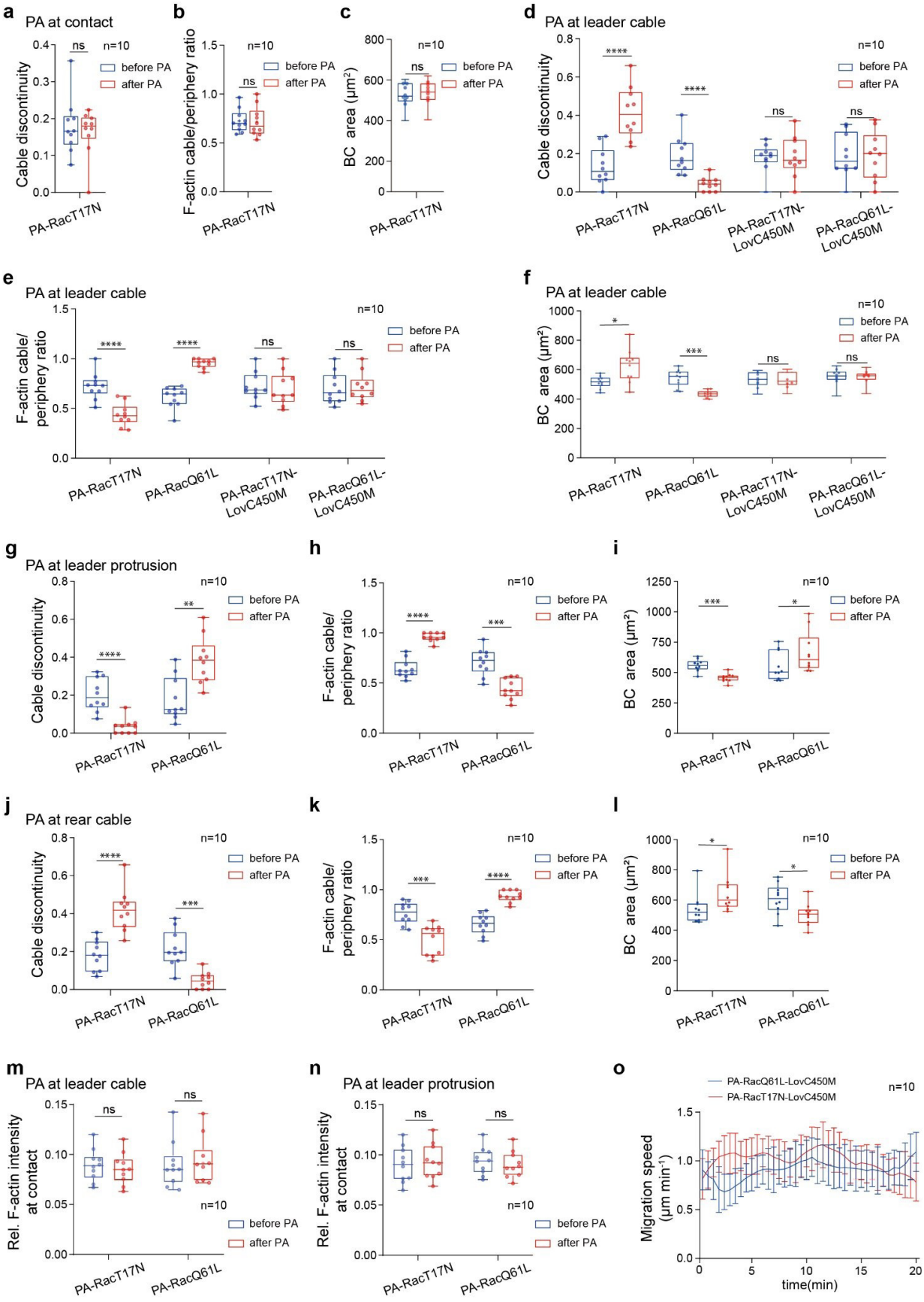
a
PA at contact
Cable discontinuity
ns
n=10
before PA
after PA
PA-RacT17N
b
F-actin cable/periphery ratio
c
BC area (μm²)
d
PA at leader cable
****
PA-RacQ61L
PA-RacT17N-LovC450M
PA-RacQ61L-LovC450M
e
F-actin cable/ periphery ratio
f
BC area (μm²)
g
PA at leader protrusion
h
i
j
PA at rear cable
k
l
m
Rel. F-actin intensity at contact
n
o
PA-RacQ61L-LovC450M
PA-RacT17N-LovC450M
Migration speed (μm min⁻¹)
time(min)

Supplementary Figure 5. Quantifications of the PA-Rac effect.

a-c, d-f, g-i, j-l. Quantifications of cable discontinuity (**a, d, g, j**), the ratio between cable F-actin signals and total peripheral F-actin signals (**b, e, h, k**), and total cell area (**c, f, i, l**) in the indicated border cell groups, before and after 18-25□minute photo-activation at the indicated regions. **m, n.** Quantifications of relative F-actin intensity located at the border cell-to-cell contacts in the border cell groups expressing either PA-RacT17N or PA-RacQ61L, before and after 18-25□minute photo-activation of PA-Rac at leader border cell cables (**m**) or protrusions (**n**). o. Time-lapse quantifications of mean migration speed (μm per minute) in the border cell groups expressing either PA-RacQ61L-LovC450M or PA-RacT17-LovC450M, before and after focal illumination of PA-Rac-LovC450M at leader border cell cables. Boxplot shows medians, 25th and 75th percentiles as box limits, minimum and maximum values as whiskers; each datapoint is displayed as a dot (from n biologically independent samples for each border cell group), in **a-n**. Data are presented as mean values +/− SD in **o** (from n biologically independent samples for each border cell group). P values by two-sided Mann–Whitney test have been listed in Supplementary Note 1.

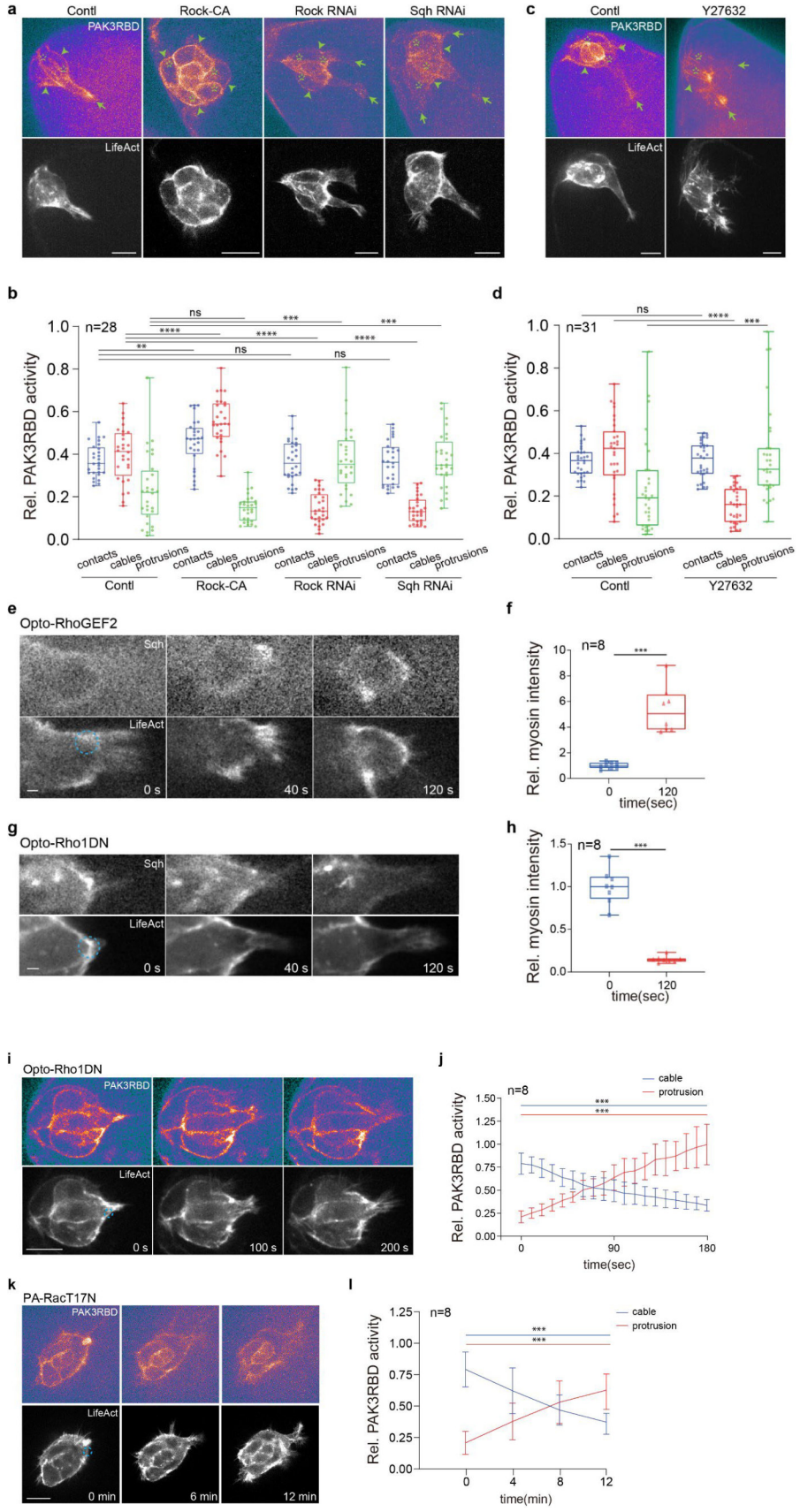
a
Contl
Rock-CA
Rock RNAi
Sqh RNAi
PAK3RBD
LifeAct
c
Contl
Y27632
b
n=28
Rel. PAK3RBD activity
contacts
cables
protrusions
Contl
Rock-CA
Rock RNAi
Sqh RNAi
d
n=31
Y27632
e
Opto-RhoGEF2
Sqh
0 s
40 s
120 s
f
n=8
Rel. myosin intensity
time(sec)
g
Opto-Rho1DN
h
i
Opto-Rho1DN
100 s
200 s
j
cable
protrusion
Rel. PAK3RBD activity
k
PA-RacT17N
0 min
6 min
12 min
l
time(min)

Supplementary Figure 6. Rho1 signalling governs cable Rac1 activity to support supracellular cables.

a, c. Representative PAK3RBD-GFP and F-actin images in border cell groups with the expression of Rock-CA, Rock RNAi, Myosin-II RNAi or control (**a**), and with the treatment of Y27632 or DMSO control (**c**), together with LifeAct-RFP for different subcellular F-actin signals. Green arrows marking protrusions, green arrowheads marking cables, while green stars marking border cell-cell contacts. **b, d.** Quantification of relative PAK3RBD-GFP intensity located at contacts, cables or protrusions in border cell groups with the indicated genetic backgrounds (**b**) and treatment (**d**). **e, g.** Representative time-lapse Sqh-GFP and F-actin images in border cell groups expressing Opto-RhoGEF2 and LifeAct-RFP (**e**) and Opto-Rho1DN and LifeAct-RFP (**g**), before and after blue light illumination at the cable regions near border cell leading protrusions. Dotted blue circle labelling the PA regions with blue light illumination. PA means photo-activation. **f, h.** Quantification of relative Myosin-II intensity before and after 120-second photo-activation of Opto-RhoGEF2 (**f**) and Opto-Rho1DN (**h**) at the cable regions near leading protrusions. **i, k.** Representative time-lapse PAK3RBD-GFP and F-actin images in border cell groups expressing Opto-Rho1DN and LifeAct-RFP (**i**) and PA-RacT17N and LifeAct-RFP (**k**), before and after blue light illumination at the cable regions of one border cell. **j, l.** Time-lapse quantification of relative PAK3RBD-GFP intensity located at cables or protrusions in one cell with Opto-Rho1DN photo-treatment (**j**) and in the whole groups with PA-RacT17N photo-treatment at one border cell cable (**l**), before and after photo-activation. Scale bars are 10 μm in **a, c, i** and **k**, 2 μm in **e** and **g**. Boxplot shows medians, 25th and 75th percentiles as box limits, minimum and maximum values as whiskers; each datapoint is displayed as a dot (from n biologically independent samples for each border cell group), in **b, d, f and h.** Data are presented as mean values +/− SD in **j** and **l** (from n biologically independent samples for each border cell group). P values by two-sided Mann–Whitney test have been listed in Supplementary Note 1.

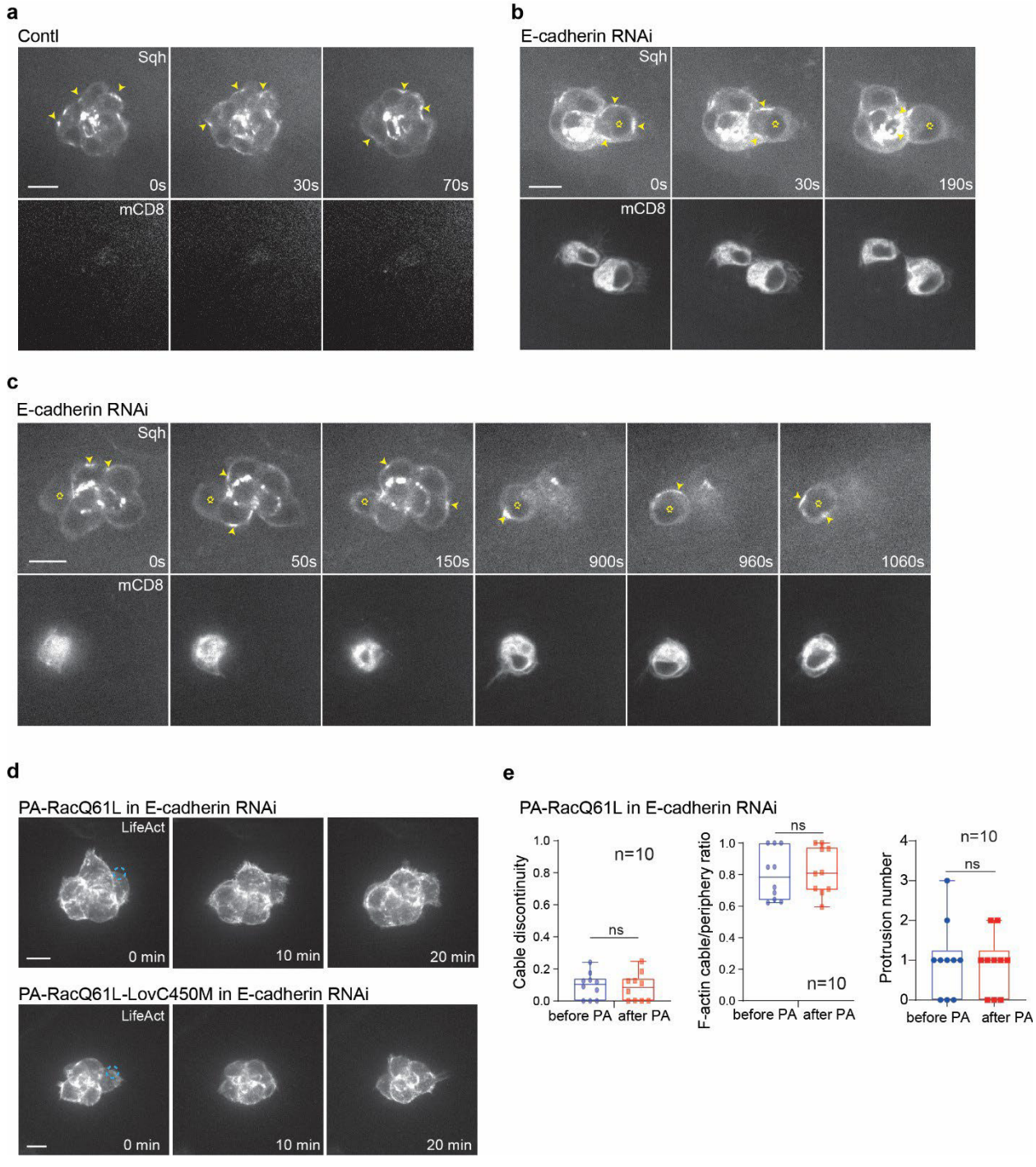
a
Contl
Sqh
0s
30s
70s
mCD8
b
E-cadherin RNAi
Sqh
0s
30s
190s
mCD8
c
E-cadherin RNAi
Sqh
0s
50s
150s
900s
960s
1060s
mCD8
d
PA-RacQ61L in E-cadherin RNAi
LifeAct
0 min
10 min
20 min
PA-RacQ61L-LovC450M in E-cadherin RNAi
LifeAct
0 min
10 min
20 min
e
PA-RacQ61L in E-cadherin RNAi
Cable discontinuity
n=10
ns
before PA
after PA
F-actin cable/periphery ratio
ns
n=10
before PA
after PA
Protrusion number
n=10
ns
before PA
after PA

Supplementary Figure 7. Confirmation for the role of E-cadherin on controlling pulsed Myosin-II signal transmission at supracellular cables.

a. Time-lapse images of Myosin-II flows in one representative WT border cell group expressing Sqh-GFP but not mCD8-RFP signals. Yellow arrowheads marking Myosin-II pulsed flows. **b.** Time-lapse images of Myosin-II flows in one representative Sqh-GFP expressing border cell group, in which 1-2 border cell clone(s) express E-cadherin RNAi (*ShgRNAi*) together with mCD8-RFP as the clone marker. Yellow arrowheads marking Myosin-II pulsed flows, while yellow stars marking the clonal cell. **c.** Time-lapse images of Myosin-II flows in one representative Sqh-GFP expressing border cell group, in which 1-2 border cell clone(s) express E-cadherin RNAi (*ShgRNAi*) together with mCD8-RFP as the clone marker. Yellow arrowheads marking Myosin-II pulsed flows, while yellow stars marking the clonal cell. The plane of time-lapse images between 900 seconds and 1060 seconds is 5 μm higher than the one between 0 seconds and 150 seconds. The results (**a-c**) have been successfully repeated from the at least 4 independent experiments. **d.** Representative time-lapse F-actin images of border cell groups expressing PA-RacQ61L and E-cadherin RNAi (upper), or PA-RacQ61L-LovC450M and E-cadherin RNAi (lower), together with LifeAct-RFP to monitor subcellular F-actin signals, before and after photo-activation of PA-RacQ61L at one border cell. Dotted blue circle labelling the PA regions with blue light illumination. PA means photo-activation. **e.** Quantifications of cable discontinuity, the ratio between cable F-actin signals and total peripheral F-actin signals, and protrusion number in the border cell groups expressing PA-RacQ61L and E-cadherin RNAi, before and after 20 minute photo-activation at one border cell. Scale bars are 10 μm in **a-d**. Boxplot shows medians, 25th and 75th percentiles as box limits, minimum and maximum values as whiskers; each datapoint is displayed as a dot (from n biologically independent samples for each border cell group) in **e.** P values by two-sided Mann–Whitney test have been listed in Supplementary Note 1.

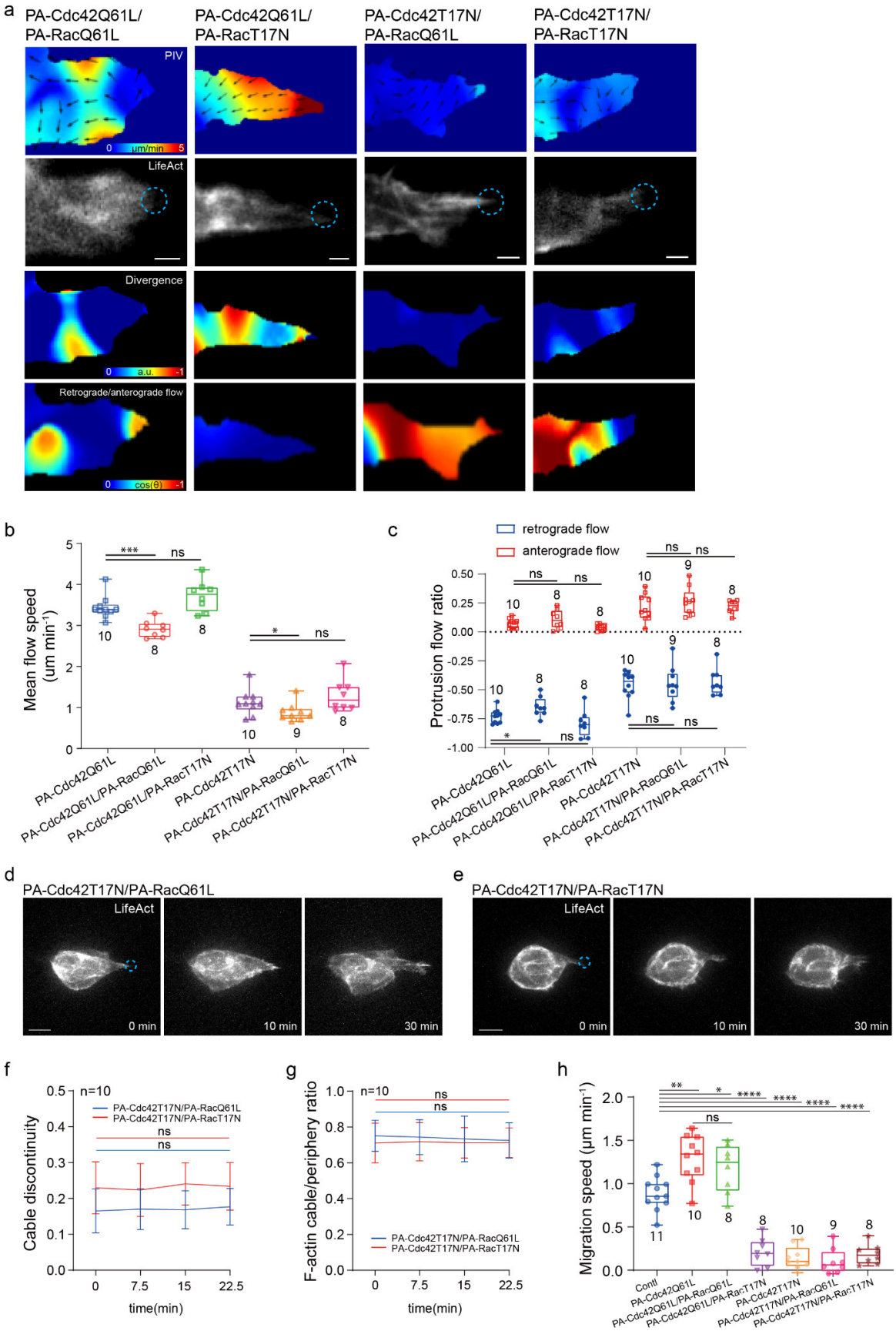
a
PA-Cdc42Q61L/ PA-RacQ61L
PA-Cdc42Q61L/ PA-RacT17N
PA-Cdc42T17N/ PA-RacQ61L
PA-Cdc42T17N/ PA-RacT17N
PIV
0 μm/min 5
LifeAct
Divergence
0 a.u. -1
Retrograde/anterograde flow
0 cos(θ) -1
b
Mean flow speed (um min-1)
***
ns
*
ns
10
8
8
10
9
8
PA-Cdc42Q61L
PA-Cdc42Q61L/PA-RacQ61L
PA-Cdc42Q61L/PA-RacT17N
PA-Cdc42T17N
PA-Cdc42T17N/PA-RacQ61L
PA-Cdc42T17N/PA-RacT17N
c
retrograde flow
anterograde flow
Protrusion flow ratio
ns
ns
ns
ns
*
ns
ns
ns
d
PA-Cdc42T17N/PA-RacQ61L
LifeAct
0 min
10 min
30 min
e
PA-Cdc42T17N/PA-RacT17N
LifeAct
0 min
10 min
30 min
f
Cable discontinuity
n=10
PA-Cdc42T17N/PA-RacQ61L
PA-Cdc42T17N/PA-RacT17N
ns
ns
time(min)
g
F-actin cable/periphery ratio
n=10
ns
ns
PA-Cdc42T17N/PA-RacQ61L
PA-Cdc42T17N/PA-RacT17N
time(min)
h
Migration speed (μm min-1)
**
*
****
****
****
****
ns
11
10
8
8
10
9
8
Contl
PA-Cdc42Q61L
PA-Cdc42Q61L/PA-RacQ61L
PA-Cdc42Q61L/PA-RacT17N
PA-Cdc42T17N
PA-Cdc42T17N/PA-RacQ61L
PA-Cdc42T17N/PA-RacT17N

Supplementary Figure 8. Confirmation for the role of Cdc42 on governing actin flows at protrusions and F-actin signal exchange between protrusion and cables for efficient border cell migration.

a. Representative PIV, divergence and retrograde/anterograde direction analyses of actin flows at leading protrusions in the border cell groups expressing PA-Cdc42Q61L/PA-RacQ61L, PA-Cdc42Q61L/PA-RacT17N, PA-Cdc42T17N/PA-RacQ61L or PA-Cdc42T17N/PA-RacT17N, together with LifeAct-GFP for F-actin signals. a.u. means arbitrary unit for divergence level. Dotted blue circle labelling the PA regions with blue light illumination. PA means photo-activation. **b.** Quantification of mean flow speed (μm per minute) at leading protrusions in the indicated border cell groups. **c.** Quantification of the occurrence ratio of retrograde and anterograde actin flows at leading protrusions in the indicated border cell groups. **d, e.** Representative time-lapse images of border cell groups expressing PA-RacQ61L/PA-Cdc42T17N (**d**) or PA-RacT17N/PA-Cdc42T17N (**e**), together with LifeAct-RFP to monitor subcellular F-actin signals. Dotted blue circle labelling the PA regions with blue light illumination. PA means photo-activation. **f, g.** Time-lapse quantifications of cable discontinuity (**f**) and the ratio between cable F-actin signals and total peripheral F-actin signals (**g**) in the indicated border cell groups, before and after photo-activation of the indicated PA-Rac and PA-Cdc42 at leader border cell protrusions. **h.** Quantification of mean migration speed (μm per minute) in the indicated border cell groups, after photo-activation of the PA-Cdc42 or/and PA-Rac at leader border cell protrusions, compared with the photo-treated WT border cell groups. Scale bars are 2 μm in **a**, and 10 μm in **d** and **e**. Boxplot shows medians, 25th and 75th percentiles as box limits, minimum and maximum values as whiskers; each datapoint is displayed as a dot (from n biologically independent samples for each border cell group), in **b, c** and **h.** Data are presented as mean values +/− SD in **f** and **g** (from n biologically independent samples for each border cell group). P values by two-sided Mann–Whitney test have been listed in Supplementary Note 1.

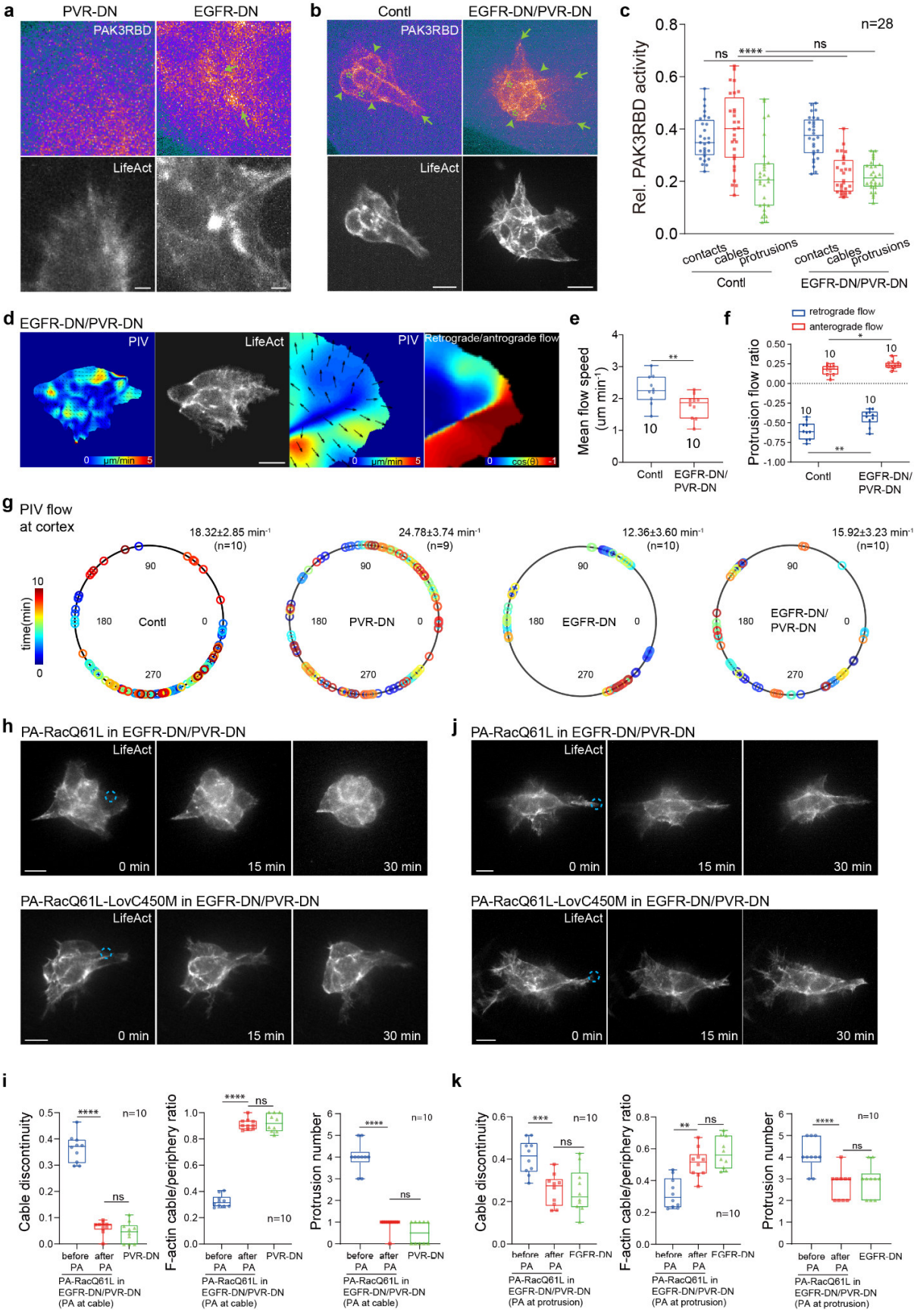
a
PVR-DN
EGFR-DN
PAK3RBD
LifeAct
b
Contl
EGFR-DN/PVR-DN
PAK3RBD
LifeAct
c
n=28
Rel. PAK3RBD activity
ns
****
ns
contacts
cables
protrusions
contacts
cables
protrusions
Contl
EGFR-DN/PVR-DN
d
EGFR-DN/PVR-DN
PIV
LifeAct
PIV
Retrograde/antrograde flow
μm/min
cos(θ)
e
Mean flow speed (um min-1)
Contl
EGFR-DN/ PVR-DN
f
retrograde flow
anterograde flow
Protrusion flow ratio
Contl
EGFR-DN/ PVR-DN
g
PIV flow at cortex
time(min)
18.32±2.85 min-1 (n=10)
24.78±3.74 min-1 (n=9)
12.36±3.60 min-1 (n=10)
15.92±3.23 min-1 (n=10)
Contl
PVR-DN
EGFR-DN
EGFR-DN/ PVR-DN
h
PA-RacQ61L in EGFR-DN/PVR-DN
LifeAct
0 min
15 min
30 min
PA-RacQ61L-LovC450M in EGFR-DN/PVR-DN
j
PA-RacQ61L in EGFR-DN/PVR-DN
PA-RacQ61L-LovC450M in EGFR-DN/PVR-DN
i
Cable discontinuity
F-actin cable/periphery ratio
Protrusion number
before PA
after PA
PVR-DN
PA-RacQ61L in EGFR-DN/PVR-DN (PA at cable)
k
Cable discontinuity
F-actin cable/periphery ratio
Protrusion number
EGFR-DN
PA-RacQ61L in EGFR-DN/PVR-DN (PA at protrusion)

Supplementary Figure 9. PVR and EGFR guide Rac1 activity and actin flows at protrusions and cables of migrating border cells.

a. Representative PAK3RBD-GFP and F-actin images in the indicated groups for signal mis-localization. **b.** Representative PAK3RBD-GFP and F-actin images in the indicated groups. Green arrows marking protrusions, green arrowheads marking cables, while green stars marking border cell-cell contacts. **c.** Quantification of relative PAK3RBD-GFP intensity located at contacts, cables or protrusions in the indicated groups. **d.** Representative PIV analyses of actin flows in the whole group and at protrusions, and retrograde/anterograde direction analysis of actin flows at protrusions in the indicated group. **e, f, g.** Quantification of mean flow speed (μm per minute) at protrusions (**e**), the occurrence ratio of protrusion retrograde and anterograde actin flows (**f**) and actin flows occurring at cables (**g**) in the indicated border cell groups. In **g**, RGB colour marking the time window; number at perimeter showing the angle degree where actin flows occur during the indicated time window. Number above the circle showing the occurrence number of actin flows at cable with mean values +/− SD. **h, j.** Representative time-lapse F-actin images of the indicated groups, before and after photo-activation of PA-RacQ61L at cables (**h**) or protrusions (**j**) of one border cell. Dotted blue circle labelling the PA regions with blue light illumination. PA means photo-activation. **i, k.** Quantifications of cable discontinuity, the ratio between cable F-actin signals and total peripheral F-actin signals, and total cell area in the groups expressing PA-RacQ61L, PVR-DN and EGFR-DN, before and after 20-30□minute photo-activation at cables (**i**) or protrusions (**k**) of one border cell. Scale bars are 1 μm in **a**, and 10 μm in **b, d, h** and **j**. Boxplot shows medians, 25th and 75th percentiles as box limits, minimum and maximum values as whiskers; each datapoint is displayed as a dot (from n biologically independent samples for each border cell group), in **c, e, f, i** and **k**. P values by two-sided Mann–Whitney test have been listed in Supplementary Note 1.

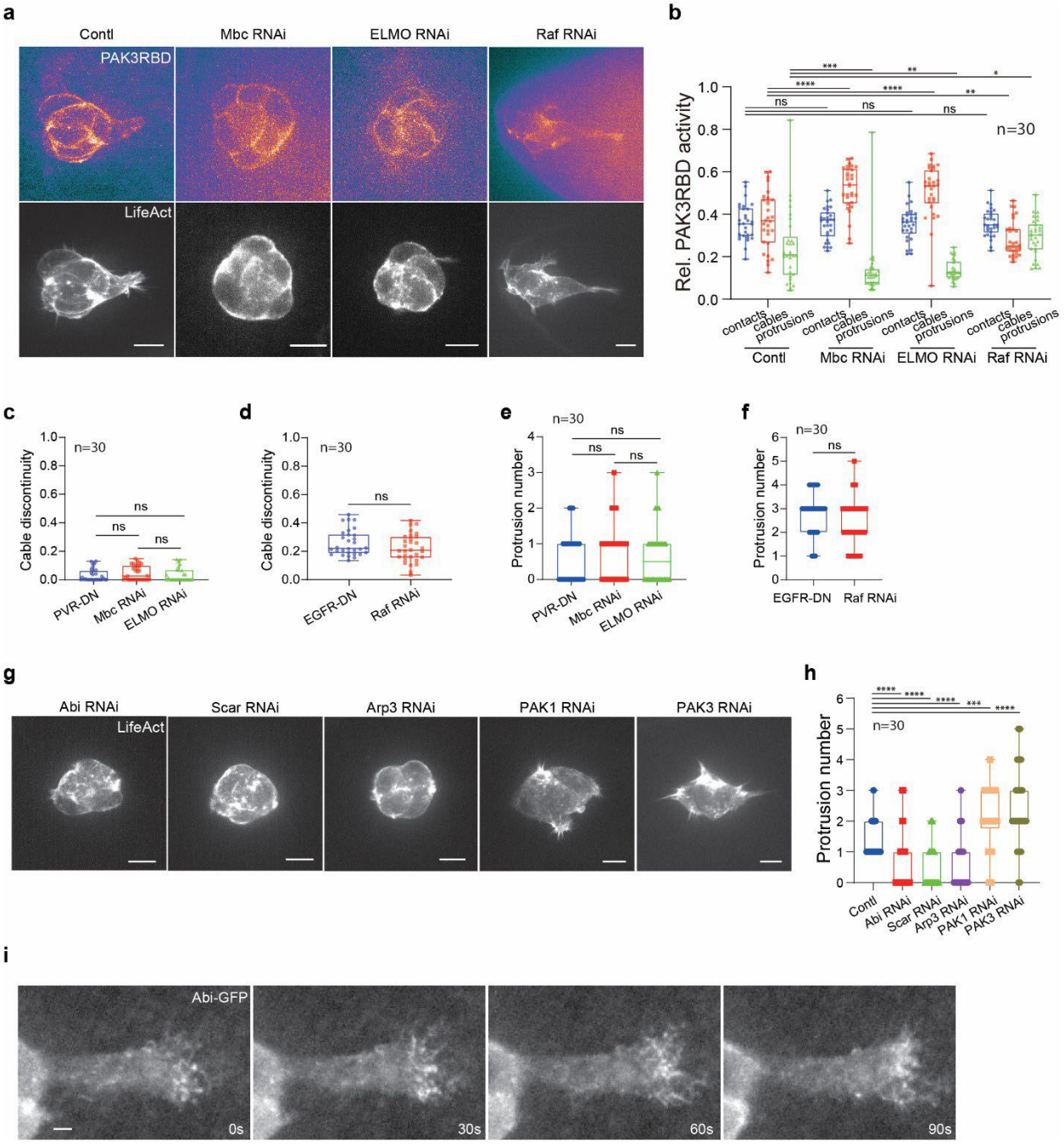
a
Contl
Mbc RNAi
ELMO RNAi
Raf RNAi
PAK3RBD
LifeAct
b
Rel. PAK3RBD activity
n=30
contacts
cables
protrusions
Contl
Mbc RNAi
ELMO RNAi
Raf RNAi
c
Cable discontinuity
n=30
PVR-DN
Mbc RNAi
ELMO RNAi
d
Cable discontinuity
n=30
EGFR-DN
Raf RNAi
e
Protrusion number
n=30
PVR-DN
Mbc RNAi
ELMO RNAi
f
Protrusion number
n=30
EGFR-DN
Raf RNAi
g
Abi RNAi
Scar RNAi
Arp3 RNAi
PAK1 RNAi
PAK3 RNAi
LifeAct
h
Protrusion number
n=30
Contl
Abi RNAi
Scar RNAi
Arp3 RNAi
PAK1 RNAi
PAK3 RNAi
i
Abi-GFP
0s
30s
60s
90s

Supplementary Figure 10. Characterization of the intermediators between guidance receptors and Rac1, and of the effectors downstream of Rac1 in controlling border cell protrusions.

a. Representative PAK3RBD-GFP and F-actin images in border cell groups expressing Mbc RNAi, ELMO RNAi, Raf RNAi or control, together with LifeAct-RFP to discriminate and label different regions enriched with subcellular F-actin signals. **b.** Quantification of relative PAK3RBD-GFP intensity located at contacts, cables or protrusions in the indicated border cell groups. **c, d.** Quantification of cable discontinuity in border cell groups expressing PVR-DN, Mbc RNAi or ELMO RNAi (**c**), EGFR-DN or Raf RNAi (**d**). **e, f.** Quantification of protrusion number in border cell groups expressing PVR-DN, Mbc RNAi or ELMO RNAi (**e**), EGFR-DN or Raf RNAi (**f**). **g.** Representative F-actin images of border cell groups expressing Abi RNAi, Scar RNAi, Arp3 RNAi, PAK1 RNAi or PAK3 RNAi, together with LifeAct-RFP to monitor subcellular F-actin signals. **h.** Quantification of protrusion number in border cell groups expressing Abi RNAi, Scar RNAi, Arp3 RNAi, PAK1 RNAi or PAK3 RNAi**. i.** Representative time-lapse images of border cell groups expressing Abi-GFP, driven by *Slbo-Gal4/UAS* genetic tool. The results of these time-lapse images for Abi-GFP distribution pattern at protrusion tips have been successfully repeated from the at least 3 independent experiments. Scale bars are 2 μm in **i**, and 10 μm in **a** and **g**. Boxplot shows medians, 25th and 75th percentiles as box limits, minimum and maximum values as whiskers; each datapoint is displayed as a dot (from n biologically independent samples for each border cell group), in **b-f, h**. P values by two-sided Mann–Whitney test have been listed in Supplementary Note 1.

Figures P value

Figure 1. b			
balanced *vs.* loose	<0.0001		
loose *vs.* tight	<0.0001		
balanced *vs.* tight	<0.0001		
Figure 1. c			
balanced *vs.* loose	<0.0001		
loose *vs.* tight	<0.0001		
balanced *vs.* tight	<0.0001		
Figure 1. d			
balanced *vs.* loose	<0.0001		
loose *vs.* tight	<0.0001		
balanced *vs.* tight	<0.0001		
Figure 1. e	contacts	cables	protrusions
balanced *vs.* loose	0.04	<0.0001	<0.0001
loose *vs.* tight	0.0476	<0.0001	<0.0001
balanced *vs.* tight	0.9487	<0.0001	<0.0001
Figure 1. f			
balanced *vs.* loose	<0.0001		
loose *vs.* tight	<0.0001		
balanced *vs.* tight	<0.0001		
Figure 1. g	cables	protrusions	
front *vs.* middle	<0.0001	<0.0001	
front *vs.* rear	<0.0001	<0.0001	
middle *vs.* rear	<0.0001	0.0012	
Figure 1. j	cables	protrusions	
balanced *vs.* loose	<0.0001	<0.0001	
loose *vs.* tight	<0.0001	<0.0001	
balanced *vs.* tight	<0.0001	<0.0001	

Figure 2. b	contacts	cables	protrusions
balanced *vs.* loose	0.2359	<0.0001	<0.0001
loose *vs.* tight	0.1462	<0.0001	<0.0001
balanced *vs.* tight	0.8545	<0.0001	<0.0001
Figure 2. c	balanced	loose	tight
front *vs.* middle	0.8545	0.3504	0.8545
front *vs.* rear	0.665	0.2301	0.4581
middle *vs.* rear	0.3354	0.7973	0.8545
Figure 2. d	cables	protrusions	
front *vs.* middle	0.0003	0.0063	
front *vs.* rear	0.0084	0.0105	
middle *vs.* rear	0.1973	0.4986	

Figure 3. b	PA-RacT17N (PA at leader cell cables)	PA-RacT17N (PA at leader cell protrusions)	PA-RacQ61L (PA at leader cell cables)	PA-RacQ61L (PA at leader cell protrusions)
before PA *vs.* after PA	<0.0001	<0.0001	<0.0001	0.0005
Figure 3. b'	PA-RacT17N (PA at leader cell cables)	PA-RacT17N (PA at leader cell protrusions)	PA-RacQ61L (PA at leader cell cables)	PA-RacQ61L (PA at leader cell protrusions)
before PA *vs.* after PA	0.0005	0.0003	0.0084	0.0005

Figure 4. d	photo treated cell	nearby	far away
0 min *vs.* 5 min	0.0001	0.0029	0.0115
5 min *vs.* 10 min	<0.0001	0.0001	<0.0001
10 min *vs.* 15 min	<0.0001	<0.0001	<0.0001
Figure 4. h	photo treated cell	nearby	far away
0 min *vs.* 5 min	<0.0001	<0.0001	<0.0001
5 min *vs.* 10 min	<0.0001	<0.0001	<0.0001
10 min *vs.* 15 min	0.0029	0.1431	0.0232

Figure 5. b	contacts	cables	protrusions
Contl *vs.* Rho1DN	0.8137	< 0.0001	0.0002
Contl *vs.* Rho1CA	< 0.0001	< 0.0001	0.0602
Figure 5. d	cables	protrusions	
0 sec *vs.* 180 sec	0.0002	0.0002	
Figure 5. f	cables	protrusions	
0 sec *vs.* 180 sec	>0.9999	0.7209	
Figure 5. h	cables	protrusions	
0 min *vs.* 12 min	0.003	0.0002	
Figure 5. J	cables	protrusions	
0 min *vs.* 12 min	0.6454	0.8785	
Figure 5. l	cables	protrusions	
0 min *vs.* 12 min	0.9591	0.7984	

Figure 6. b		
Contl *vs.* PA-RacQ61L	0.7103	
Contl *vs.* PA-RacT17N	0.3494	
Contl *vs.* PA-Cdc42Q79L	<0.0001	
Contl *vs.* PA-Cdc42T17N	<0.0001	
Figure 6. c	retrograde flow	anterograde flow
Contl *vs.* PA-RacQ61L	0.4119	0.5516
Contl *vs.* PA-RacT17N	0.5573	0.6539
Contl *vs.* PA-Cdc42Q79L	0.0197	0.0127
Contl *vs.* PA-Cdc42T17N	0.0159	0.0430
Figure 6. d		
Contl *vs.* PA-Cdc42Q79L	<0.0001	
Contl *vs.* PA-Cdc42T17N	<0.0001	
PA-Cdc42Q79L *vs.* PA-Cdc42T17N	<0.0001	

Figure 7. b	contacts	cables	protrusions
Contl *vs.* PVR-DN	0.4689	< 0.0001	< 0.0001
Contl *vs.* EGFR-DN	0.5310	< 0.0001	0.0026
Figure 7. d			
Contl *vs.* PVR-DN	0.0029		
Contl *vs.* EGFR-DN	0.9048		
PVR-DN *vs.* EGFR-DN	0.0001		
Figure 7. e	retrograde flow	anterograde flow	
Contl *vs.* PVR-DN	0.0001	0.0115	
Contl *vs.* EGFR-DN	0.8421	0.4967	
Figure 7. g	cable discontinuity	F-actin cable/periphery ratio	protrusion number
before PA *vs.* after PA	<0.0001	<0.0001	<0.0001
Figure 7. i	cable discontinuity	F-actin cable/periphery ratio	protrusion number
before PA *vs.* after PA	<0.0001	<0.0001	<0.0001

Supplementary Figures P value

Supplementary Figure 1. b			
balanced *vs.* loose	<0.0001		
loose *vs.* tight	<0.0001		
balanced *vs.* tight	<0.0001		
Supplementary Figure 1. c			
balanced *vs.* loose	<0.0001		
loose *vs.* tight	<0.0001		
balanced *vs.* tight	<0.0001		
Supplementary Figure 1. d	balanced	loose	tight
front *vs.* middle	<0.0001	0.2301	<0.0001
front *vs.* rear	<0.0001	0.2589	0.005
middle *vs.* rear	0.2301	0.909	0.4133
Supplementary Figure 1. f			
balanced *vs.* loose	<0.0001		
loose *vs.* tight	<0.0001		
balanced *vs.* tight	<0.0001		

Supplementary Figure 3. b	contacts	cables	protrusions
Contl *vs.* Rac1DN	0.3489	<0.0001	< 0.0001
Contl *vs.* Cdc42DN	<0.0001	0.9109	< 0.0001
Supplementary Figure 3. e	contacts	cables	protrusions
Contl vs.Rac2 LOF	0.6228	0.786	0.9007
Contl vs. Rac3 RNAi	0.7635	0.9824	0.9007
Contl vs. Rac RNAi	0.4147	< 0.0001	0.0015
Contl vs. Cdc42 RNAi	< 0.0001	0.9124	< 0.0001
Supplementary Figure 3. g			
Contl vs.Rac1 RNAi	< 0.0001		
Contl vs. Cdc42 RNAi	< 0.0001		

Supplementary Figure 4. b	PA-RacT17N (PA at border cell-to-cell contacts)	PA-RacT17N-LovC450M (PA at leader cell cables)	PA-RacQ61L-LovC450M (PA at leader cell cables)	PA-RacT17N (PA at rear cell cables)	PA-RacQ61L (PA at rear cell cables)
before PA *vs.* after PA	0.9727	0.9099	0.9105	0.0002	0.001

Supplementary Figure 5. a	cable discontinuity	F-actin cable/periphery ratio	BC area	
before PA *vs.* after PA	0.8126	0.6987	0.7959	
Supplementary Figure 5. b	PA-RacT17N	PA-RacQ61L	PA-RacT17N-LovC450M	PA-RacQ61L-LovC450M
before PA *vs.* after PA (cable discontinuity)	<0.0001	<0.0001	0.8973	0.7959
before PA *vs.* after PA (F-actin cable/periphery ratio)	<0.0001	<0.0001	0.4665	0.7004
before PA *vs.* after PA (BC area)	0.0147	0.0001	0.9118	0.2301
Supplementary Figure 5. c	PA-RacT17N	PA-RacQ61L		
before PA *vs.* after PA (cable discontinuity)	<0.0001	0.0021		
before PA *vs.* after PA (F-actin cable/periphery ratio)	<0.0001	0.0004		
before PA *vs.* after PA (BC area)	0.0002	0.0232		
Supplementary Figure 5. d	PA-RacT17N	PA-RacQ61L		
before PA *vs.* after PA	<0.0001	0.0001		

(cable discontinuity) before PA *vs.* after PA		
(F-actin cable/periphery ratio) before PA *vs.* after PA	0.0001	<0.0001
(BC area)	0.0185	0.0232
Supplementary Figure 5. e	PA-RacT17N	PA-RacQ61L
before PA *vs.* after PA (leader cables)	0.6305	0.469
before PA *vs.* after PA (leader protrusions)	0.6305	0.5417

Supplementary Figure 6. b	contacts	cables	protrusions
Contl *vs.* ROCK-CA	0.0017	<0.0001	0.0809
Contl *vs.*ROCK RNAi	0.7421	<0.0001	0.0005
Contl *vs.* Sqh RNAi	0.646	<0.0001	0.0003
Supplementary Figure 6. d	contacts	cables	protrusions
Contl *vs.* Y27632	0.7421	< 0.0001	0.0005
Supplementary Figure 6. f			
0 s vs. 120 s	0.002		
Supplementary Figure 6. h			
0 s vs. 120 s	0.002		
Supplementary Figure 6 j	cables	protrusions	
0 sec *vs.* 180 sec	0.0002	0.0002	
Supplementary Figure 6. l	cables	protrusions	
0 min *vs.* 12 min	0.0002	0.0006	

Supplementary Figure 7. e	cable discontinuity	F-actin cable/periphery ratio	protrusion number
before PA *vs.* after PA	0.7109	0.25	>0.9999

Supplementary Figure 8. b		
PA-Cdc42Q79L *vs.* PA-Cdc42Q79L/PA-RacQ61L	0.0002	
PA-Cdc42Q79L *vs.* PA-Cdc42Q79L/PA-RacT17N	0.1457	
PA-Cdc42T17N *vs.* PA-Cdc42T17N/PA-RacQ61L	0.0435	
PA-Cdc42T17N *vs.* PA-Cdc42T17N/PA-RacT17N	0.6965	
Supplementary Figure 8. c	retrograde flow	anterograde flow
PA-Cdc42Q79L *vs.* PA-Cdc42Q79L/PA-RacQ61L	0.0266	0.0434
PA-Cdc42Q79L *vs.* PA-Cdc42Q79L/PA-RacT17N	0.1011	0.122
PA-Cdc42T17N *vs.* PA-Cdc42T17N/PA-RacQ61L	0.9682	0.4002
PA-Cdc42T17N *vs.* PA-Cdc42T17N/PA-RacT17N	0.9654	0.8968
Supplementary Figure 8. f	PA-Cdc42T17N/PA-RacQ61L	PA-Cdc42T17N/PA-RacT17N
0 min *vs.* 22.5 min	0.7959	0.9116
Supplementary Figure 8. g	PA-Cdc42T17N/PA-RacQ61L	PA-Cdc42T17N/PA-RacT17N
0 min *vs.* 22.5 min	0.5167	0.9265
Supplementary Figure 8. h		
Contl *vs.* PA-Cdc42Q79L	0.0021	
Contl *vs.* PA-Cdc42Q79L/PA-RacQ61L	0.0409	
Contl *vs.* PA-Cdc42Q79L/PA-RacT17N	< 0.0001	
Contl *vs.* PA-Cdc42T17N	< 0.0001	
Contl *vs.* PA-Cdc42T17N/PA-RacQ61L	< 0.0001	
Contl *vs.* PA-Cdc42T17N/PA-RacT17N	< 0.0001	
PA-Cdc42Q79L *vs.* PA-Cdc42Q79L/PA-RacQ61L	0.3599	

Supplementary Figure 9. c	contacts	cables	protrusions

Contl *vs.* PVR-DN/EGFR-DN	0.6903	< 0.0001	0.4891
Supplementary Figure 9. e			
Contl *vs.* PVR-DN/EGFR-DN	0.0089		
Supplementary Figure 9. f	retrograde flow	anterograde flow	
Contl *vs.* PVR-DN/EGFR-DN	0.0039	0.0232	
Supplementary Figure 9. i	cable discontinuity	F-actin cable/periphery ratio	protrusion number
before PA *vs.* after PA	< 0.0001	< 0.0001	< 0.0001
after PA *vs.* PVR-DN	0.2584	0.6841	0.5001
Supplementary Figure 9. k	cable discontinuity	F-actin cable/periphery ratio	protrusion number
before PA *vs.* after PA	0.0007	0.0021	0.0015
after PA *vs.* EGFR-DN	0.9705	0.1655	0.5481

Supplementary Figure 10. b	contacts	cables	protrusions
Contl *vs.*Mbc RNAi	0.9941	< 0.0001	0.0003
Contl *vs.*ELMO RNAi	0.9357	< 0.0001	0.0063
Contl *vs.*Raf RNAi	0.9824	0.0076	0.0225
Supplementary Figure 10. c	cable discontinuity		
PVR-DN *vs.*Mbc RNAi	0.3954		
PVR-DN *vs.*ELMO RNAi	0.8583		
Mbc RNAi *vs.*ELMO RNAi	0.6027		
Supplementary Figure 10. d	cable discontinuity		
EGFR-DN *vs.*Raf RNAi	0.1257		
Supplementary Figure 10. e	protrusion number		
PVR-DN *vs.*Mbc RNAi	0.4501		
PVR-DN *vs.*ELMO RNAi	0.7406		
Mbc RNAi *vs.*ELMO RNAi	0.7091		
Supplementary Figure 10. f	protrusion number		
EGFR-DN *vs.*Raf RNAi	0.0756		
Supplementary Figure 10. h	protrusion number		
Contl *vs.*Abi RNAi	<0.0001		
Contl *vs.*Scar RNAi	<0.0001		
Contl *vs.*Arp3 RNAi	<0.0001		
Contl *vs.*PAK1 RNAi	0.0003		
Contl *vs.*PAK3 RNAi	<0.0001		

Chapter ***II:*** *Tissue physical property governing collective cell migration*

II.1. Abstract

In addition to the intrinsic signals in migrating cells, external signals from the surrounding environment are also important for collective cell migration behaviours. The external environmental signals include the biochemical signals such as chemokines for chemotaxis, as well as some physical properties. Indeed, Collective cell movement is strongly influenced by the physical properties of its surrounding, which includes not only extracellular matrix but also substrate cells. Compared with the matrix environment, substrate cell physical properties and their role on cell migration are quite unclear. Drosophila border cell migration also provides a convenient in vivo model for addressing these questions about substrate cell environment. Except of E-cadherin adhesion as an important control, we have limited information from substrate cell physical properties. Our group recently revealed the importance of front invasive gaps between substrate cells, enriched with cortical tension continuum (from actomyosin and E-cadherin), in supporting border cell migration efficacy. Thus, my second PhD proposal aimed at understanding the control of this physical property and its role on collective border cell migration.

II.2. Results

II.2.1 Rac1 activity highly correlates with cortical F-actin signals in the “hot spot” environment

According to some previous studies, an invasive gap between nurse cells is mainly distributed along the center of the egg chamber, and it is the major travel path for migrating border cells (Aranjuez et al., 2016; Dai et al., 2020). From our unpublished results, this invasive gap is gradually established from stage 6 to stage 8, before the detachment of border cells. And this

invasive gap is strongly enriched with cortical F-actin and myosin signals, which show a strong positive- correlation pattern (Figure 1C, D). Since cortical tension is positively regulated by the strength of actomyosin network, this invasive gap thus exhibits the property of high cortical tension, thus explaining the disassociation of E-cadherin adhesion between nurse cells to form an empty space between cells. Importantly, our unpublished studies revealed that this invasive gap supports border cell migration via an “anchorage and constriction” mode (not shown here). Regarding the characteristics of high tension and porosity as well as the supporting-migration role, here we defined this invasive gap region as a "hot spot" environment. Here, an important question is how nurse cells establish this property of high cortical tension.

Although Rho1 signaling has been reported to control the myosin accumulation in nurse cell cortical region (Aranjuez et al., 2016), cortical F-actin and myosin signals seem not to be completely co-localized. It thus indicates that another signalling pathway, rather than Rho1, might provide the upstream control of nurse cell cortical F-actin network. By assessing PAK3RBD-GFP reporter in nurse cells, we unexpectedly detected the strong PAK3RBD-GFP reporter activity in nurse cells. In particular, this reporter activity was greatly concentrated in the invasive gap region of egg chamber (Figure 1A, B). Intriguingly, in nurse cells, the correlation between PAK3RBD and F-actin signals is significantly stronger than the one between F-actin and myosin signals (Figure 1E). This signal correlation difference thus indicates that high Rac1 activity may exist in nurse cells to control the formation of cortical F-actin network to support strong actomyosin contractility, thereby contributing to the high cortical tension distributed within the "hot spot" nurse cell environment, seemingly resembling the role of contractile Rac1 pool on supracellular cables in migrating border cells.

Since PAK3RBD-GFP reporter can monitor both Rac1 and Cdc42 activities, I next used genetic manipulation of Rac1 activity to confirm our hypothesis. We established either constitutively active (CA) or dominantly negative (DN) versions of Rac1 in the UASp expression vector for transgenic fly production, and then we used Nanos-Gal4 system to express either CA or DN form of Rac1 in germ cells of egg chambers. Compared with the control, The germline specific Rac1-CA expressing tissues were strongly degenerated (Supplementary Fig. 1A), which made it impossible to achieve egg chambers for the following experiments. In contrast, germline specific Rac1-DN expressing tissues were able to grow up normally. However, compared with the control tissue, the nurse cells with inhibitory Rac1 form exhibited the much less myosin intensity and smaller gap size, as well as the greater A-P/D-V ratio, which corresponds to a longer and narrower egg chamber (Supplementary Fig. 1B-F). These findings imply: 1) Rac1 signaling is the key upstream factor controlling the cortical tension of nurse cells; 2) nurse cell cortical tension = helps to preserve the structure of the "hot spot" environment and the shape of the egg chamber.

II.2.2 Rac1 activity controls cortical actomyosin network and thus invasive gap in nurse cell environment

Considering the genetic issue of disturbing tissue development or affecting tissue shape, we introduced transgenic flies expressing PA-Rac (either active or DN forms, PA-RacQ61L or PA-RacT17N, respectively)), tagged with mcherry, under the control of the nos-Gal4/UAS system, and photo-activated PA-Rac in the central nurse cells region to achieve the spatiotemporal control of Rac1 activity and then assess the effect on this invasive gap in nurse cell environment (see Methods).

First, we confirmed whether PAK3RBD-GFP reporter is actually influenced by optogenetic manipulation of Rac1 activity. Regarding the photo-bleaching effect, here we used moderate light illumination condition to photo-activate or -inhibit Rac1 in the central region of egg chambers. Photo-activation of Rac1 in nurse cells quickly enhanced the intensity of PAK3RBD-GFP reporter, while photo-inhibition of Rac1 in nurse cells reduced this reporter activity (Supplementary Fig. 2). This optogenetic experiment thus confirmed the specificity of this reporter to monitor the Rac1 activity in the cortical region of nurse cells, thus further supporting Rac1 as the key factor controlling the cortical F-actin network and cortical tension.

Second, we tested the effect of local photo-manipulation of Rac1 activity on the nurse cell invasive gap. Here, we monitored and quantified the accumulation of myosin signals as the indicator of nurse cell cortical tension property. Indeed, after the local inhibition of Rac1 activity in nurse cells, Myosin signal accumulation at nurse cell cortical regions at the central egg chamber was significantly reduced (Fig. 2E, H). Strikingly, we observed the gradual closing of the invasive gap between nurse cells at the central region of egg chambers (Fig. 2E-G). Oppositely, after a short time of local Rac1 activation in central nurse cell regions, nurse cell cortical tension drastically enriched myosin assembly at the cortical region, reflected by a large increase in myosin signals (Fig. 2A, D). Strikingly, With the gradual increase in cortical myosin assembly in nurse cells in the invasive gap region, a large number of bubble-like structures emerged from the nurse cell membrane at the invasive gap and gradually developed from the tiny to large structures, finally resulting in dramatic expansion of the invasive gaps between nurse cells (Fig. 2.A-C). Taken together, all these findings support our hypothesis that the light-induced Rac1 activity could modulate the tension property of nurse cell cortical region in "hot spot" environment, resulting in variations in the invasive gap formation (Fig.2 I, J).

II.2.3 The effects of Rac1 on the invasive gap are pressure dependent

Next, we characterized how the cortical tension property mediated by Rac1 activity guides the formation of different nurse cell environment. Here, we focused on the synergistic effect of nurse cell pressure property, considering the general principle of "pressure-tension balance" within cells. It has been known that cortical tension is equivalent to the membrane pressure to maintain the integrity of cells (Gilden and Krummel, 2010). For example, if cortical tension is disrupted at some local membrane region such as the blebbing process (Tinevez et al., 2009), the local pressure would allow the outward expansion of membrane at this reduced tension region till reaching the next local balance between cortical tension and membrane pressure.

To examine the role of osmotic pressure on these Rac1-mediated effects in the central region of egg chamber, we decreased or enhance the osmotic pressure in egg chamber by adding either sucrose or water to the culture medium. Reducing cytoplasmic pressure in egg chambers with the treatment of 220 mM sucrose drastically inhibited this Rac1-mediated effect (Fig. 3A, C). The local photo-activation of Rac1 activity by PA-Rac CA form was incapable of forming big bubble structures in the 'hot spot' environment, and for some pre-established bubbles, their dynamics and size remained minimal. In contrast, our observed effects of PA-Rac CA form in nurse cells were strongly amplified when cytoplasmic pressure in egg chambers was enhanced by the treatment of 25% water in the culture medium. The big bubble structures moved rapidly and exhibited remarkable dynamics after the local photo-activation of Rac1 (Fig. 3B, D).

II.2.4 Bubble structures correlate with segregation of cortical regions with distinct actomyosin networks

how do cytoplasmic pressure and cortical tension cooperate to modulate various nurse cell environment in the central region of egg chambers? Consistent with the principle of the "pressure-tension balance" model, gradual changes in cortical actomyosin network/tension from low to moderate naturally create invasive gaps between nurse cells from closed to some open. Here, it is difficult to understand how high cortical actomyosin network/tension synergize with high pressure to induce large and dynamic bubble structures between nurse cells in tissue central region. Interestingly and importantly, we observed that upon localized photoactivation of Rac1 in nurse cells, the enhanced actomyosin network gradually shifted from continuous to discontinuous distribution along cortical regions of nurse cells (Fig. 4A). It thus indicates that the emergence of a robust cortical actomyosin network and contractility is able to redistribute actomyosin networks across cortical regions, thereby leading to a separation of high actomyosin regions from the ones lacking actomyosin signals. This redistribution of high actomyosin network in nurse cell cortical regions is consistent with a previous report (Hannezo et al., 2015), and it thus provides a key answer for the formation of large bubble structures between nurse cells. Compared with the control condition, the enhanced or inhibited cytoplasmic pressure in egg chamber exhibited the similar re-distribution of high cortical regions from low cortical regions in nurse cells; differently, the intensity and the length of high actomyosin cortical regions were either increased or reduced between the egg chambers with the enhanced or inhibited cytoplasmic pressure (Fig. 3).

Next, we tested the role of this cortical segregation on large bubble formation between nurse cells. By performing the signal correlation analysis, we noticed that large bubbles mainly initiate and grow up from the membrane regions with weak cortical actomyosin signals (Fig. 4A). It thus

supports one hypothesis that cytoplasmic pressure can push out the cell membrane at the weak cortical regions, thereby enabling the emergence and gradual increase of large bubble structures between nurse cells. This hypothesis supports the synergistic role between high cytoplasmic pressure and low cortical tension, which is similar to that of bleb formation; and it thus explains the role of weak cortical regions on the bubble formation in nurse cells. However, nurse cells are tightly packed with the egg chamber, so the space between them is limited, compared to bleb-forming cells that do not have this spatial restriction. Given this spatial limitation, nurse cells thus need to use another mechanism to allow the formation and gradual changes of large bubble structures. Interestingly, we observed that as bubble emerged and grew, the base of the bubble shrunk significantly, mainly on the side where cortical actomyosin accumulation was high (Fig. 4B). Nurse cells appear to employ two distinct mechanisms to control the emergence and gradual increase of large bubble structures: inward constriction of nurse cells in high cortical regions to create new spaces, and outward membrane growth in low cortical regions to release local pressure effects.

To confirm these two distinct mechanisms, we next focused on the egg chambers with the mosaic-level expression of PA-Rac CA forms in nurse cells. After the concurrent light illumination of nurse cells with strong and weak expression of PA-Rac, large bubble structures mainly appeared from nurse cells with strong PA-Rac expression level, but not from those with weak PA-Rac expression (Supplementary Fig. 3A, B, D). In accordance with this bubble formation pattern, we observed the strong enhancement of actomyosin network as well as prominent cortical region separation in these high PA-Rac expressing nurse cells, compared with the low PA-Rac expressing cells (Supplementary Fig. 3A, C, F). More importantly, we observed the inward constriction of nurse cells concurrent with the outward membrane growth in the nurse cells with high PA-Rac

expression, while the nurse cells with low PA-Rac expression seem to maintain their original size (Supplementary Fig. 3A, E). Thus, the results from this mosaic system support our hypothesis of two distinct controlling mechanisms for large bubble structures.

Altogether, our results support a systematic cascade supporting bubble structures: 1) Robust actomyosin accumulation in nurse cell cortical regions results in strong segregation of cortical regions with distinct cortical actomyosin networks and contractility; 2) High pressure induces external membrane growth in low cortical regions of the nurse cells; 3) Simultaneously inward constriction of the nurse cells to create a new space for the emerging large bubble (Supplementary Fig. 3G).

II.2.5 The "hot spot" formation is decisive for border cell migration

Finally, we assessed how modification of various environmental formation affects the border cell migration. To do that we combined PA-Rac with SlboLifeAct-GFP to observe the migration behaviour of border cells after the photo-activation or photo-inhibition of Rac1 in front nurse cell environment. The local photo-inhibition of Rac1 activity in the "hot spot" environment gradually closed the invasive gaps between front nurse cells, and corresponding the leading protrusions of border cells gradually reduced to a tiny size (Fig. 5C, D). In contrast, strong local photo-activation of Rac1 activity in the "hot spot" environment quickly induced the bubble structures (similar to the above-shown effects during earlier stages), and strikingly, the leading protrusions of border cells initially grew longer and larger and then immediately collapsed (Fig. 5A, B). This could be due to the fact that a strong increase in Rac1 activity led to an enhancement of cortex actomyosin tension in this front nurse cell region, which thus enlarges the invasive gap of front nurse cells

thereby promoting protrusion growth; however, after a threshold, too strong cortical actomyosin tension in nurse cells mediated the formation of large bubble structures in the “hot spot” environment, which seriously damaged protrusion growth as well as migrating ability of border cells. Considering the inhibitory effect of bubble structures on border cell migration, we attempted to moderately increase Rac1 activity without inducing bubble structures in the “hot spot” environment” to determine its effect on border cell migration. Fascinatingly, if we modestly increased the activity of Rac1 via optogenetics, it appears to continuously widen the migration path in front nurse cell environment in favour of border cell migratory capacity, compared with the control condition (Fig. 5E, F). Taken together, these results support that too strong or weak cortical tension in front nurse cell environment prevents border cell migration by either closing invasive gap or inducing “damaged” bubble structures, whereas moderate cortical tension in front nurse cell environment favors border cell migration by continuously creating a “hot spot” environment (Fig. 5G, H).

II.3. Conclusions

Compared with the matrix environment, the physical property of environment substrate cells and its role on collective cell migration within tissue is little explored. Different from the matrix stiffness, cortical tension and its supporting E-cadherin adhesion are critical for collective border cell migration. Here, I revealed Rac1 as a key factor controlling the cortical F-actin network to support myosin assembly in nurse cells. Low cortical tension in nurse cells results in the closure of invasive gap, while too high tension in nurse cells leads to the formation of large bubble structures in this gap region. Mechanistically, robust tension in nurse cells causes the segregation of high-tension regions from low-tension regions, which initiates the pressure-mediated outward membrane growth and the tension-mediated inward cell constriction, thereby creating large bubble structures. Importantly, various modulations of invasive gaps in front nurse cells differently affect border cell migration ability. Thus, our studies reveal a critical factor controlling substrate cell tension property and its role in governing collective migration within cell-rich tissue.

II.4. Figures

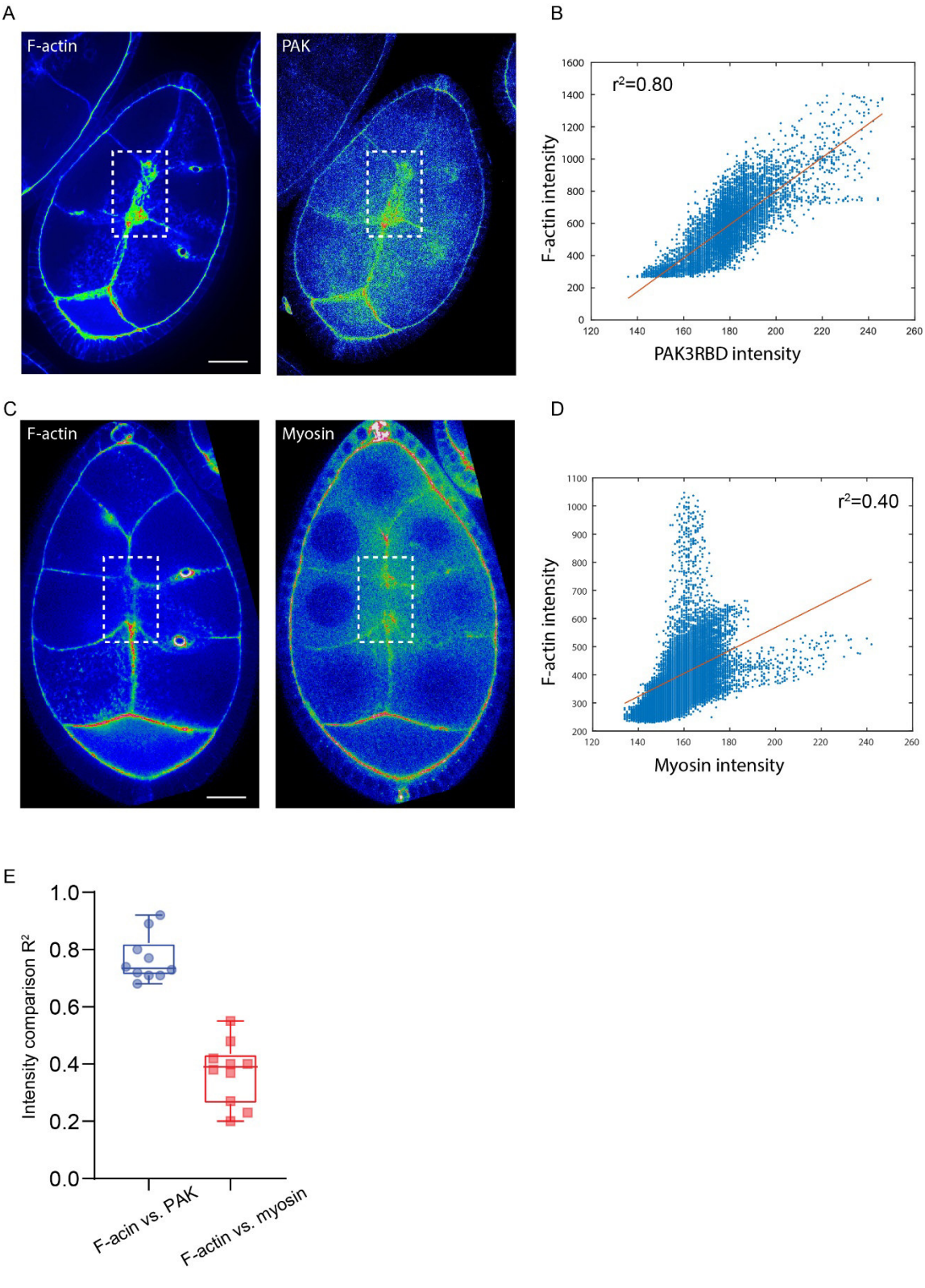
A
F-actin
PAK
B
r²=0.80
F-actin intensity
PAK3RBD intensity
C
F-actin
Myosin
D
r²=0.40
F-actin intensity
Myosin intensity
E
Intensity comparison R²
F-acin vs. PAK
F-actin vs. myosin

Figure 1. Comparison of subcellular F-actin signals, myosin signals and Rac1 activity in nurse cell "hot spot" environment.

A, C. Representative UtrABD-RFP and PAK3RBD-GFP images (**A**) and UtrABD-GFP and Sqh-RFP images (**B**) in WT *Drosophila* egg chambers. UtrABD-GFP and Sqh-RFP signals are used to monitor the F-actin and Rac1 distribution in nurse cells. White dot rectangles mark the "hot spot" region of nurse cells at the central region of egg chambers.

B, D. Scatter plot comparing a random sample of points in the "hot spot" regions for F-actin intensity and PAK intensity (**B**) and for F-actin and Myosin intensity (**D**). It is obvious that the colocalization value of F-actin signals and Rac1 activity is significantly higher than the one of F-actin and myosin signals in nurse cells.

E. Quantification of the intensity comparison R^2 between F-actin and PAK reporters, and between F-actin and Myosin reporters.

Scale bars are 20 mm in **A** and **C**. 25th and 75th percentiles as box limits, minimum and maximum values as whiskers; each datapoint is displayed as a dot (from 10 biologically independent samples for each border cell group) in **E**.

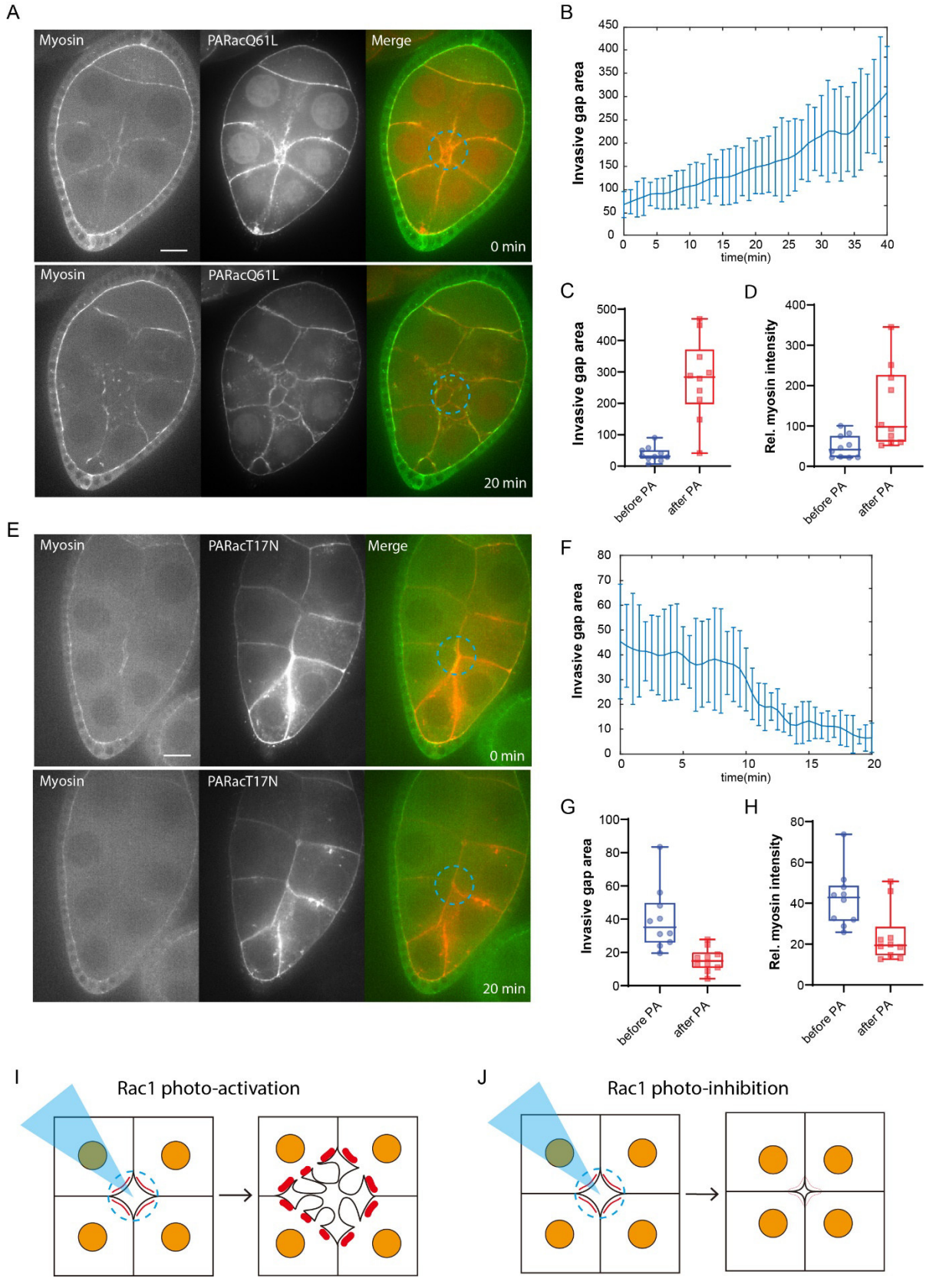
A
Myosin
PARacQ61L
Merge
0 min
Myosin
PARacQ61L
20 min
B
Invasive gap area
time(min)
C
Invasive gap area
before PA
after PA
D
Rel. myosin intensity
before PA
after PA
E
Myosin
PARacT17N
Merge
0 min
Myosin
PARacT17N
20 min
F
Invasive gap area
time(min)
G
Invasive gap area
before PA
after PA
H
Rel. myosin intensity
before PA
after PA
I
Rac1 photo-activation
J
Rac1 photo-inhibition

Figure 2. Focal Rac1 modifications by optogenetics regulate the invasive formations along with myosin signal assembly in cortical regions of nurse cells.

A, E. Representative time-lapse images of nurse cells expressing PA-RacQ61L-mCherry (**A**) or PA-RacT17N-mCherry (**E**), together with Sqh-GFP to monitor subcellular myosin signals, before and after photo activation of Rac1 activity at the "hot spot" environment. Dotted blue circle labelling the PA regions with blue light illumination. PA means photo-activation.

B, F. Time-lapse quantifications of relative invasive gap at the photo-treated "hot spot" environment after photo-activation of PA-RacQ61L-mCherry (**B**) or PA-RacT17N-mCherry (**F**) in nurse cells at the central region of egg chambers.

C, D, G, H. Quantification of relative invasive gap area (**C, G**) and relative Myosin intensity (**D, H**) before and after 20-minute photo-activation of PA-RacQ61L-mCherry (**C, D**) or PA-RacT17N-mCherry (**G, H**) in nurse cells at the central region of egg chambers.

I, J. Representative cartoons to show the effect of Rac1 photo-activation (**I**) and Rac1 photo-inhibition (**J**) at the invasive gap of nurse cells at the tissue center. Orange colors marks nurse cell nucleus. Dotted blue circle labelling the PA regions with blue light illumination. Dotted red lines mark the myosin assembly at nurse cell cortical regions. Blue triangles mark the blue light illuminations.

Scale bars are 20 μm in **A** and **E**. Data are presented as mean values ± SD in **B** and **F**. 25th and 75th percentiles as box limits, minimum and maximum values as whiskers; each datapoint is displayed as a dot (from 10 biologically independent samples for each border cell group) in **C, D, G, H**.

A +220mM sucrose

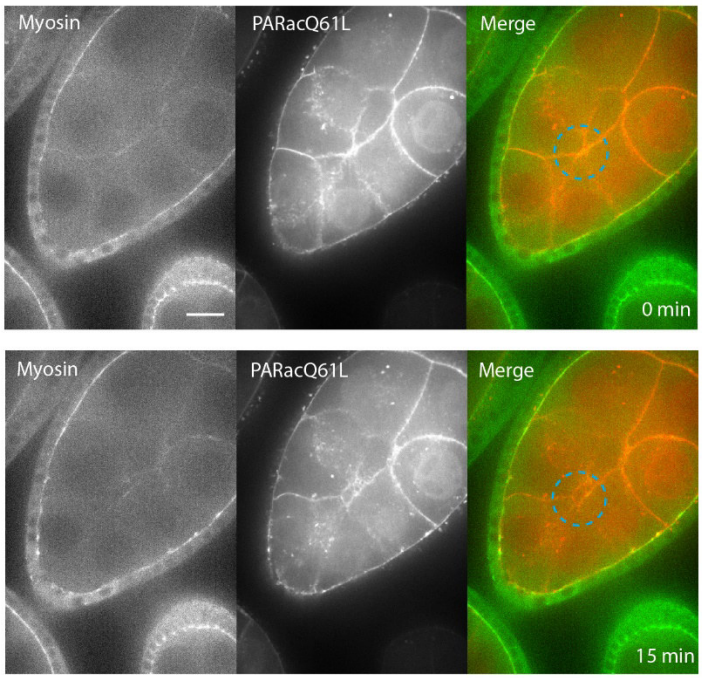

B +25% water

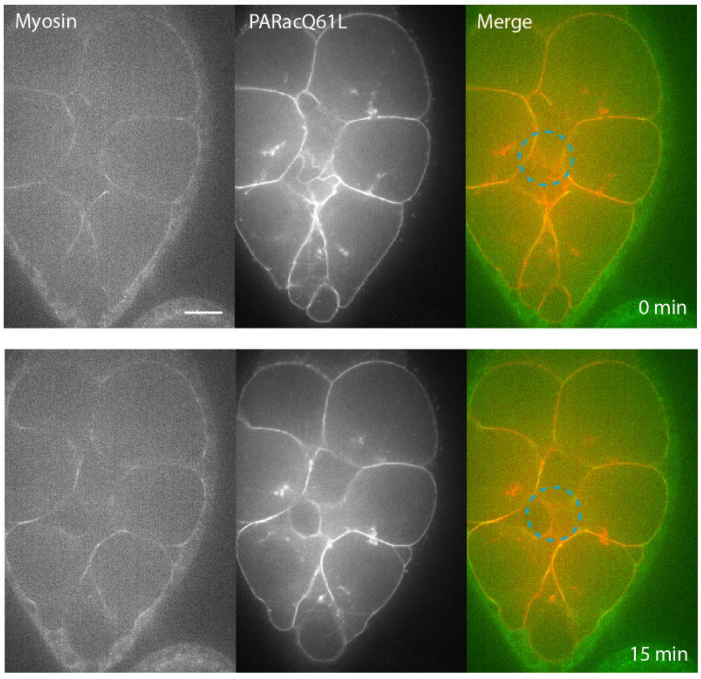

C

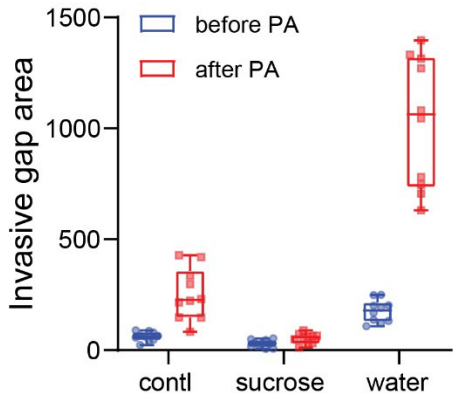

D

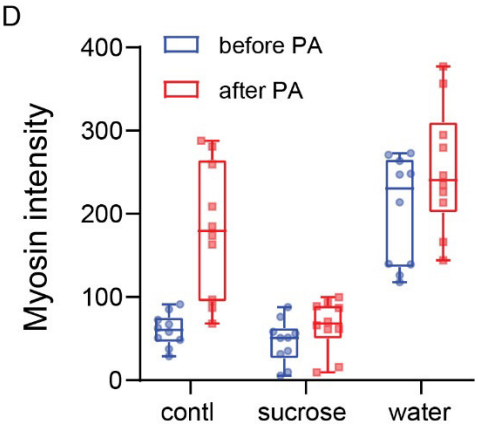

Figure 3. Effects of Focal Rac1 modifications by optogenetics are pressure dependent.

A, B. Representative time-lapse images of nurse cells expressing PA-RacQ61L-mCherry, together with Sqh-GFP to monitor subcellular myosin signals, treated with 220 mM sucrose (**A**) or with 25% water (**B**), before and after photo activating Rac1 activity at the "hot spot" environment.

C, D. Quantification of relative invasive gap area (**C**) and relative myosin intensity at the photo-treated "hot spot" environment (**D**) before and after 20-minute photo-activation of PA-RacQ61L-mCherry in nurse cells treated with 220 mM sucrose or with 25% water, compared with control.

Scale bars are 20 μm in **A** and **B**. Boxplot shows medians, 25th and 75th percentiles as box limits, minimum and maximum values as whiskers; each datapoint is displayed as a dot (from 10 biologically independent samples for each border cell group) in **C** and **D**.

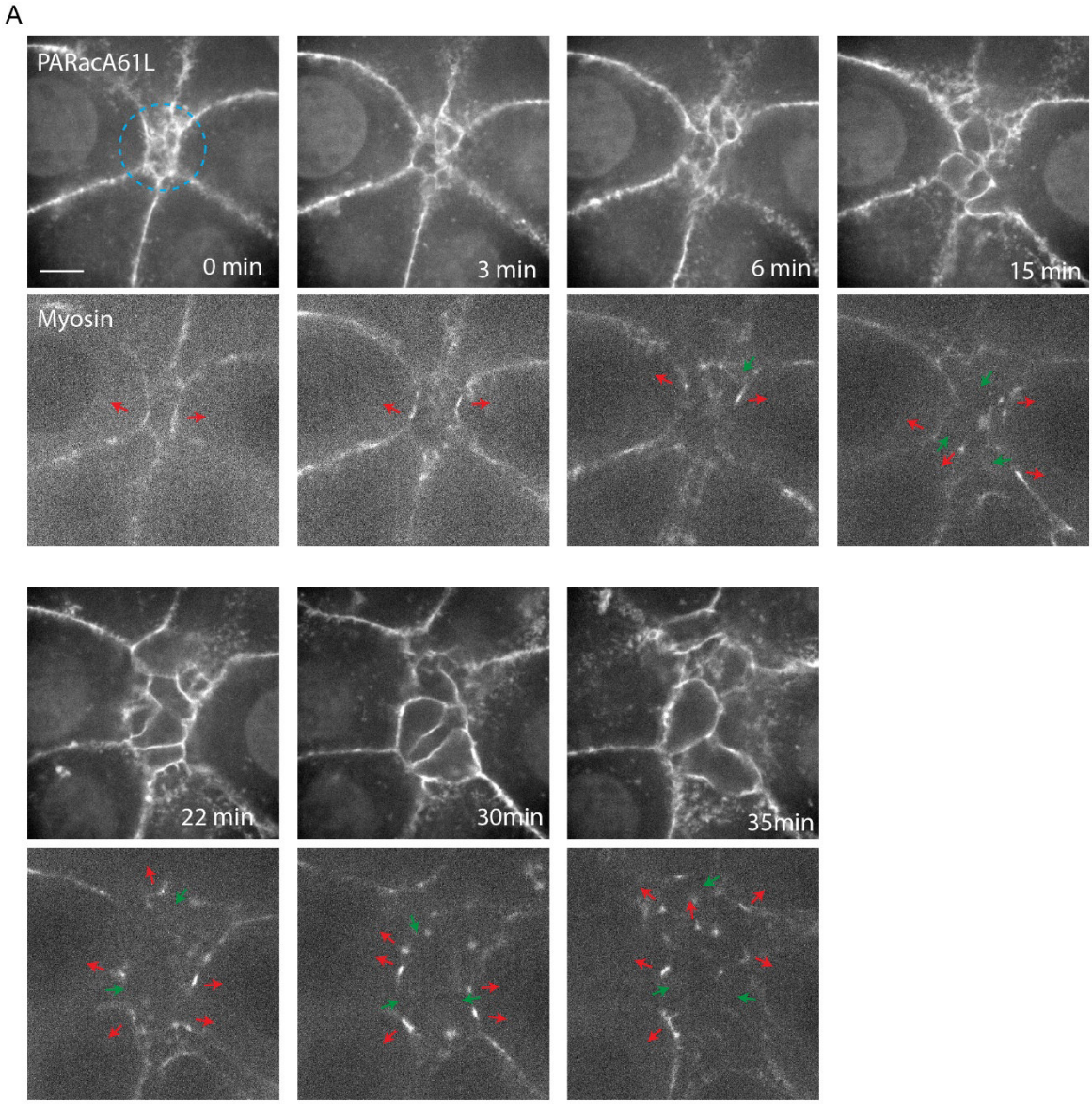
A
PARacA61L
0 min
3 min
6 min
15 min
Myosin
22 min
30min
35min

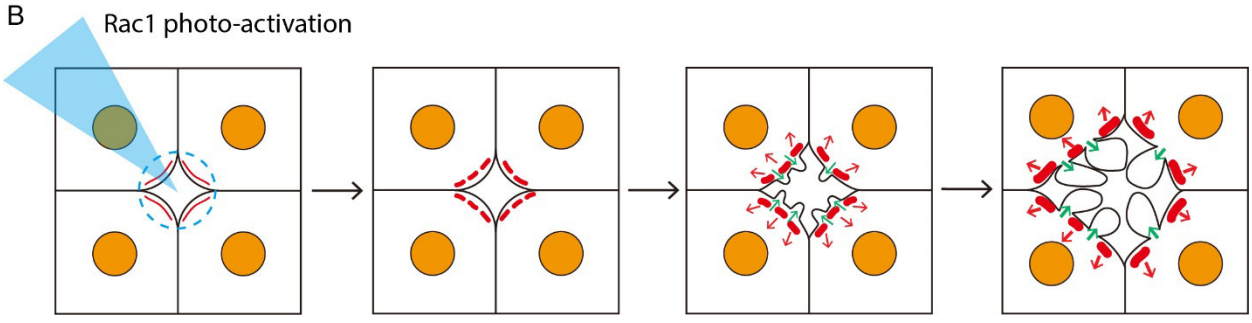
B
Rac1 photo-activation

Figure 4. Dynamics of the invasive formation in detail by Rac1 photo-activation.

A. Representative time-lapse images of nurse cells expressing PA-RacQ61L-mCherry, together with Sqh-GFP to monitor subcellular myosin signals, before and after photo activating Rac1 activity at the "hot spot" environment. Red arrows mark the contraction effect, and green arrows mark the pressure effect.

B. Representative cartoons to show the effect of Rac1 photo-activation at the invasive gap of nurse cells at the tissue center. Orange colors marks nurse cell nucleus. Dotted red lines mark the myosin assembly at nurse cell cortical regions, red arrows mark the contraction effect, and green arrows mark the pressure effect. Blue triangles mark the blue light illuminations.

Scar bar is 10 μm in **A**.

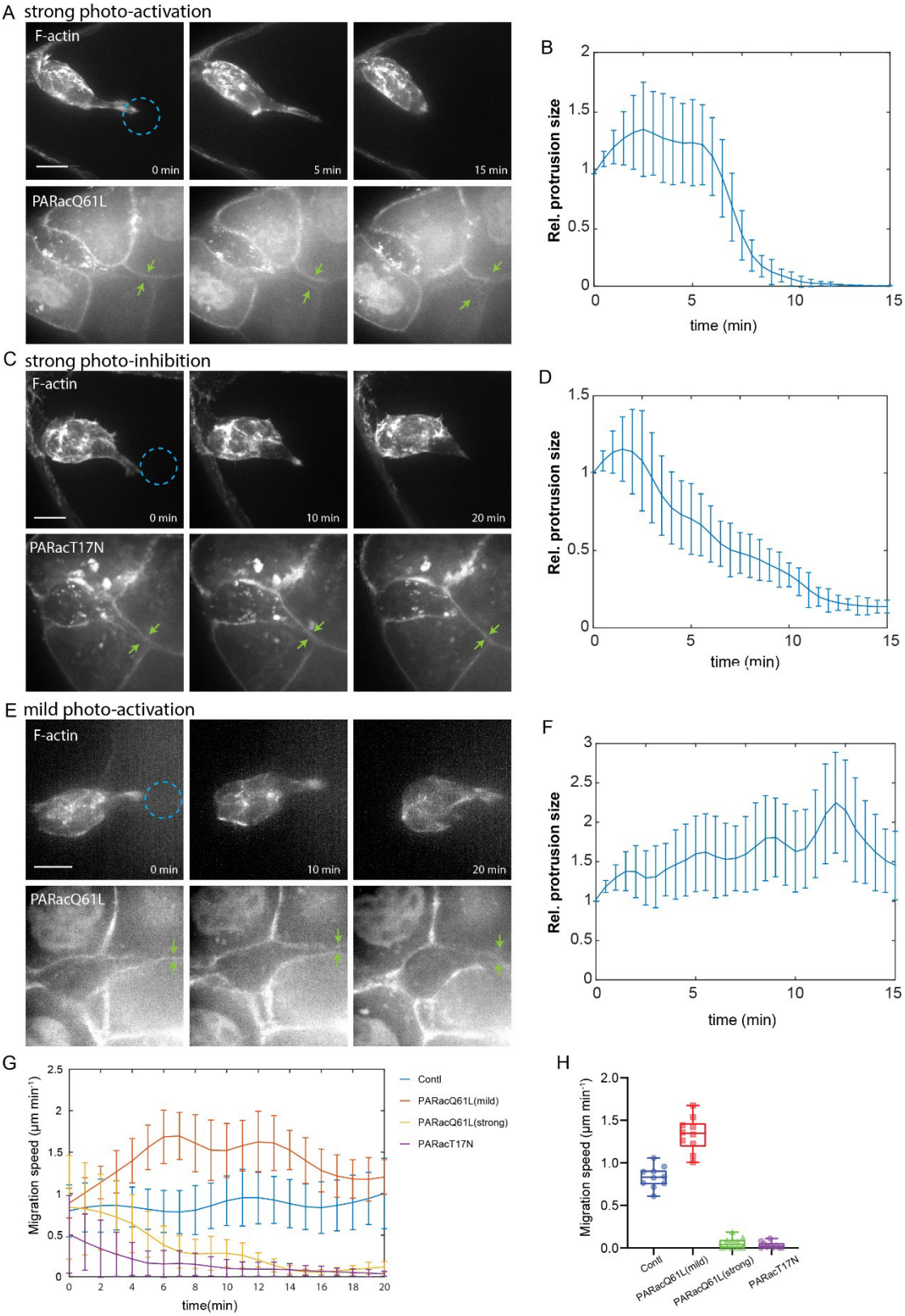
A strong photo-activation
F-actin
0 min
5 min
15 min
PARacQ61L
B
Rel. protrusion size
time (min)
C strong photo-inhibition
F-actin
0 min
10 min
20 min
PARacT17N
D
Rel. protrusion size
time (min)
E mild photo-activation
F-actin
0 min
10 min
20 min
PARacQ61L
F
Rel. protrusion size
time (min)
G
Migration speed (μm min⁻¹)
time(min)
Contl
PARacQ61L(mild)
PARacQ61L(strong)
PARacT17N
H
Migration speed (μm min⁻¹)
Contl
PARacQ61L(mild)
PARacQ61L(strong)
PARacT17N

Figure 5. Various Modulations of the invasive gap differently control border cell migration.

A, C, E. Representative time-lapse images of border cell groups expressing slbo::LifeAct-GFP to monitor protrusion dynamics, together with nurse cells expressing PA-RacQ61L-mCherry, before and after acute Rac1 photo-activation (**A**), acute Rac1 photo-inhibition (**C**), and moderate Rac1 photo-activation (**E**) at the "hot spot" environment. Dotted blue circle labelling the PA regions with blue light illumination. PA means photo-activation. Green arrows mark the invasive gap region in front nurse cell environment.

B, D, F. Time-lapse quantifications of one representative example of relative border cell protrusion size with acute Rac1 photo-activation (**B**), acute Rac1 photo-inhibition (**D**), and moderate Rac1 photo-activation (**F**) at the "hot spot" environment, before and after photo-activation.

G. Time-lapse quantification of migrating speed of border cells with acute Rac1 photo-activation, acute Rac1 photo-inhibition, and mild Rac1 photo-activation at the "hot spot" environment, after photo-activation of PA-Rac in front nurse cells.

H. Quantification of average migration speed of border cells acute Rac1 photo-activation, acute Rac1 photo-inhibition, and mild Rac1 photo-activation at the "hot spot" environment, after photo-activation of PA-Rac in front nurse cells.

Scale bars are 10 μm in **A**, **C** and **E**. Data are presented as mean values ± SD in **B, D, F and G**. Boxplot shows medians, 25th and 75th percentiles as box limits, minimum and maximum values as whiskers; each datapoint is displayed as a dot (from 10 biologically independent samples for each border cell group) in **H**.

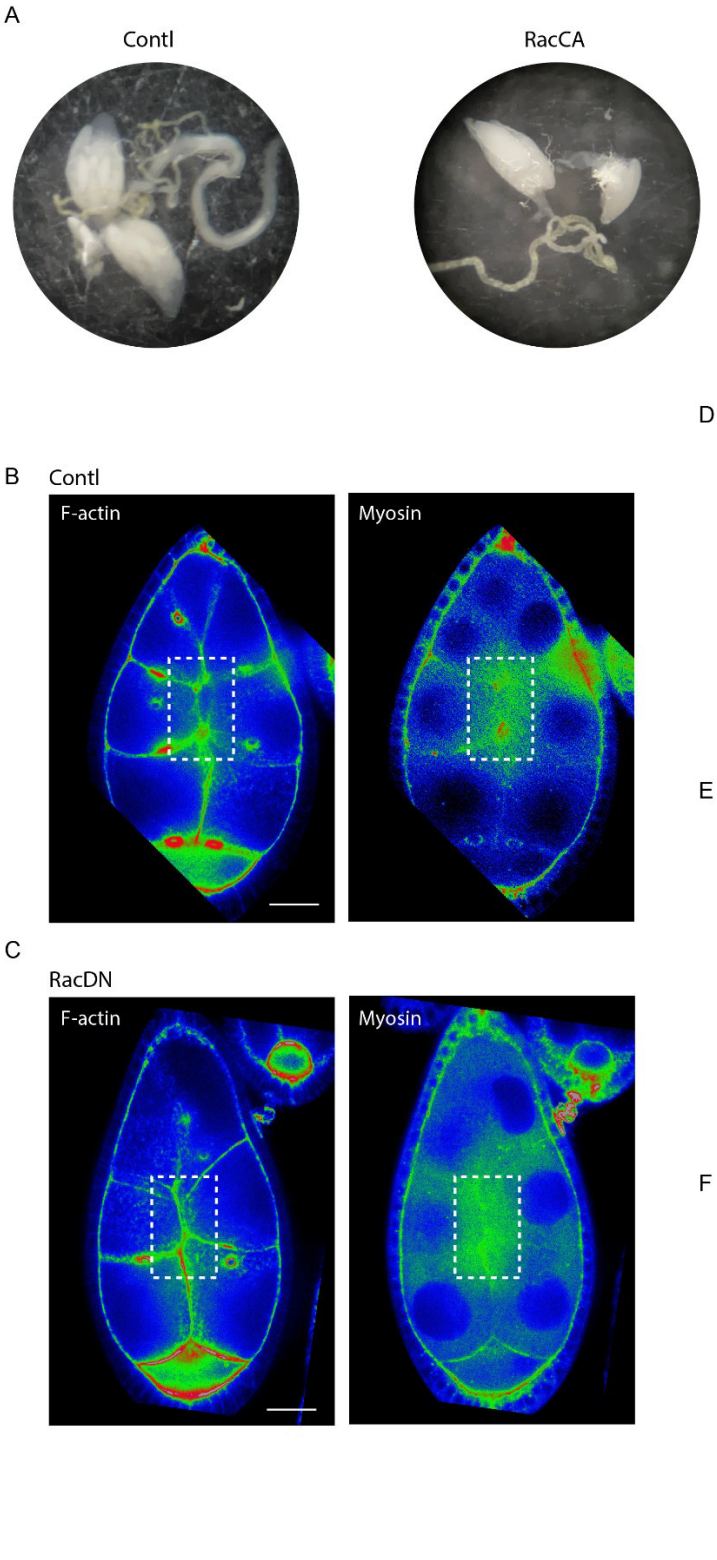
A
Contl
RacCA
B
Contl
F-actin
Myosin
C
RacDN
F-actin
Myosin
D
Invasive gap area
150
100
50
0
Contl
RacDN
E
Myosin intensity
100
80
60
40
20
0
Contl
RacDN
F
A-P/D-V ratio
2.5
2.0
1.5
1.0
0.5
0.0
Contl
RacDN

Supplementary Figure 1. Genetic tools are insufficient to modify the "hot spot" environment.

A. Representative image of fly ovaries with nurse cells expressing RacCA, compared with WT.

B. Representative UtrABD-RFP and Sqh-GFP images in nurse cells expressing either control (upper figures) or Rac1DN form (lower figures) to monitor the F-actin and myosin distribution in nurse cells. White dot rectangle marking the "hot spot" environment.

C-E. Quantifications of relative invasive gap size (**C**), relative Myosin intensity (**D**), the A-P/D-V ration of egg chamber (**F**) in nurse cells expressing either control or Rac1DN form.

Scale bars are 20 μm in **B** and **C**. Boxplot shows medians, 25th and 75th percentiles as box limits, minimum and maximum values as whiskers; each datapoint is displayed as a dot (from 10 biologically independent samples for each border cell group) in **D-F**.

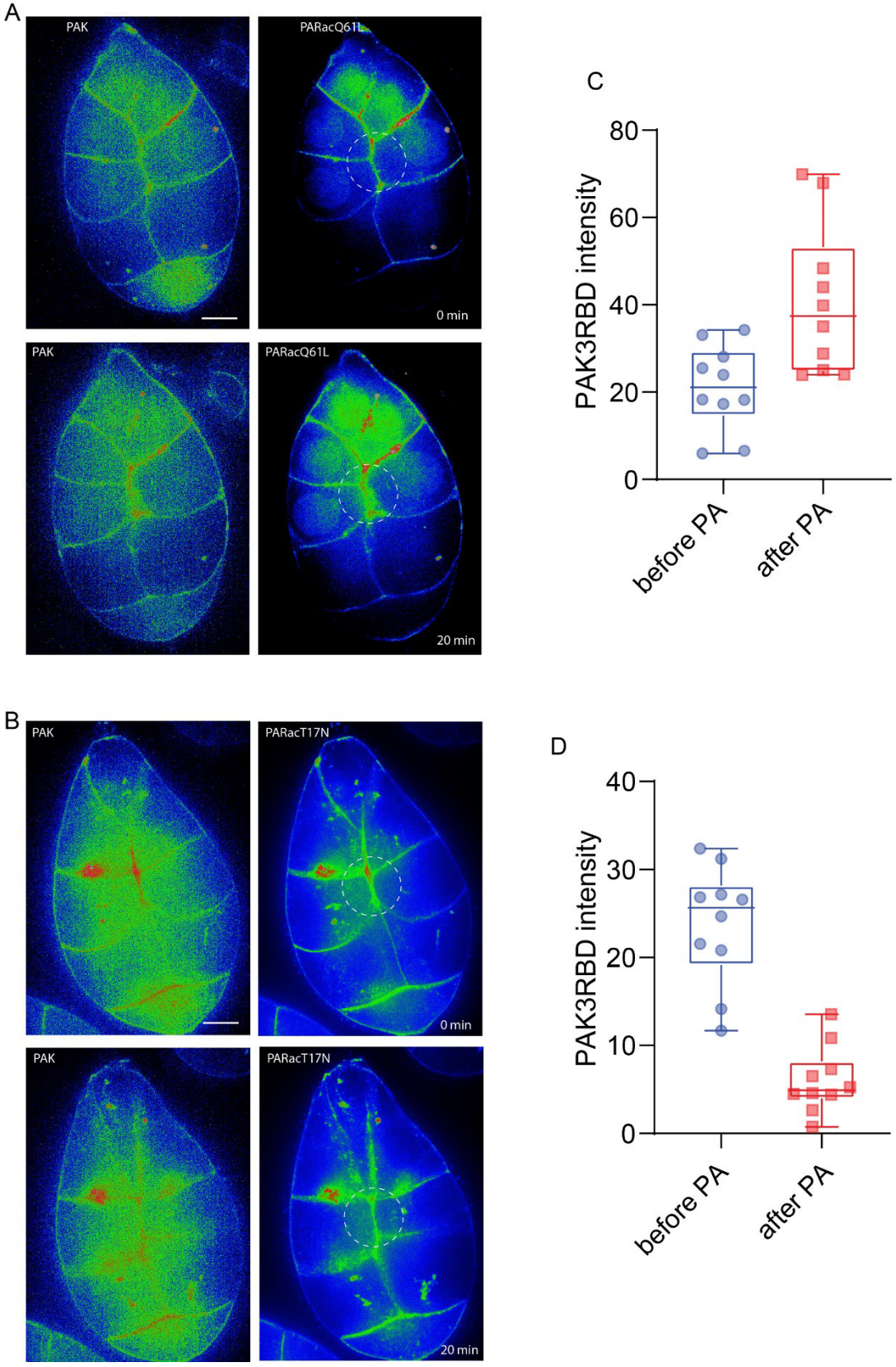
A
PAK
PARacQ61L
0 min
PAK
PARacQ61L
20 min
B
PAK
PARacT17N
0 min
PAK
PARacT17N
20 min
C
PAK3RBD intensity
80
60
40
20
0
before PA
after PA
D
PAK3RBD intensity
40
30
20
10
0
before PA
after PA

Supplementary Figure 2. Confirmation of Rac1 activity modified by PA-Rac in nurse cells.

A, B. Representative time-lapse images of nurse cells expressing PA-RacQ61L-mCherry (**A**) or PA-RacT17N-mCherry (**B**), together with PAK3RBD-GFP to monitor subcellular Rac1 activity, before and after photo activating Rac1 activity at the "hot spot" environment. Dotted white circle labelling the PA regions with blue light illumination.

C, D. Quantifications of relative PAK3RBD-GFP intensity in nurse cells expressing PA-RacQ61L-mCherry (**C**) or PA-RacT17N-mCherry (**D**), together with PAK3RBD-GFP to monitor subcellular Rac1 activity, before and after photo activating Rac1 activity at the "hot spot" environment.

Scale bars are 20 μm in **A** and **B**. Boxplot shows medians, 25th and 75th percentiles as box limits, minimum and maximum values as whiskers; each datapoint is displayed as a dot (from 10 biologically independent samples for each border cell group) in **C** and **D**.

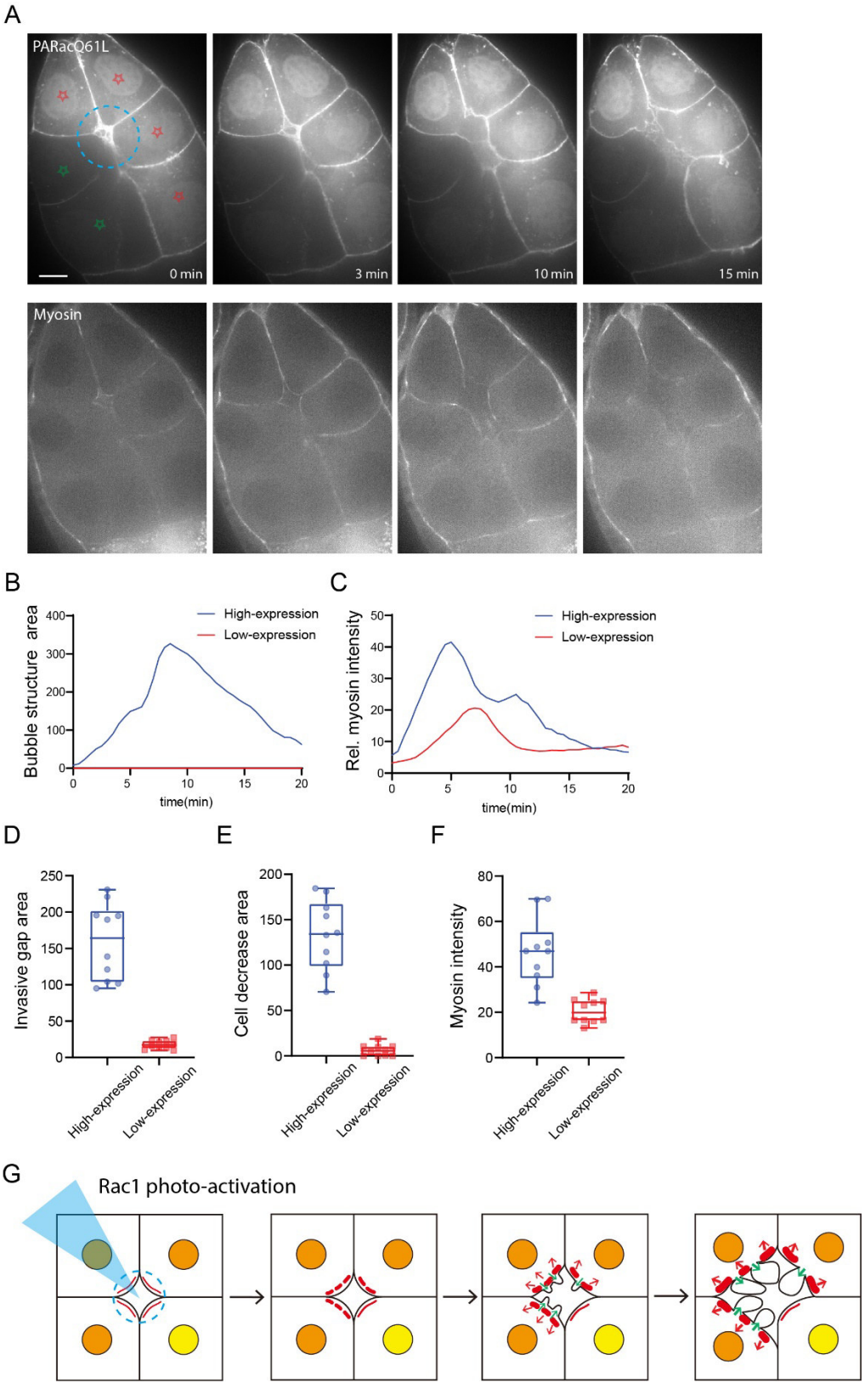
A
PARacQ61L
0 min
3 min
10 min
15 min
Myosin
B
Bubble structure area
High-expression
Low-expression
time(min)
C
Rel. myosin intensity
High-expression
Low-expression
time(min)
D
Invasive gap area
High-expression
Low-expression
E
Cell decrease area
High-expression
Low-expression
F
Myosin intensity
High-expression
Low-expression
G
Rac1 photo-activation

Supplementary Figure 3. The bubble structures in the "hot spot" environment are the Rac1 level dependent.

A. Time-lapse images of nurse cells with various expression levels of PA-RacQ61L-mCherry, together with sqh-GFP to monitor subcellular myosin activity. Here, 4 nurse cells express the high PA-Rac level marked with red stars, while 2 nurse cells express the low PA-Rac level that marked with green stars. Dotted blue circle labelling the PA regions with blue light illumination. PA means photo-activation.

B. Time-lapse quantification of bubble structure area with the one nurse cell expressing the high level of PA-RacQ61L-mCherry, compared with that expressing the low-level PA-RacQ61L-mCherry, before and after photo-activation.

C. Time-lapse quantification of relative myosin intensity of with the one nurse cell expressing the high level of PA-RacQ61L-mCherry, compared with that expressing the low-level PA-RacQ61L-mCherry, before and after photo-activation.

D-F. Quantifications of relative invasive gap area (**D**), relative cell decreased area (**E**) and relative Myosin intensity (**F**) in nurse cells with the high and low expression of PA-RacQ61L-mCherry, before and after photo-activation.

G. Representative cartoon to show the different effects of PA-Rac photo-activation in nurse cells with the high (orange labelled nucleus) and low (yellow labelled nucleus) expression of PA-RacQ61L-mCherry. Dotted blue circle labelling the PA regions with blue light illumination. Dotted red lines mark the myosin assembly at nurse cell cortical regions, red arrows mark the contraction effect, and green arrows mark the pressure effect. Blue triangles mark the blue light illuminations.

Scale bar is 20 μm in **A**. Boxplot shows medians, 25th and 75th percentiles as box limits, minimum and maximum values as whiskers; each datapoint is displayed as a dot (from 10 biologically independent samples for each border cell group) in **D-F**.

METHODS

Drosophila stocks and genetics

The following fly stocks were used: *Sqh::RLCmyosinII–mCherry* (from Eric E. Wieschaus)(Martin et al., 2009), *Slbo-Gal4* (from Pernille Rorth)(Duchek et al., 2001a), *UAS-Abi-GFP* (from Sven Bogdan)(Fricke et al., 2009), *slbo::LifeAct–GFP* (from this study), *slbo::LifeAct–RFP* (from this study), *UASt-PA-RacQ61L* (from this study), *UASt-PA-RacT17N* (from this study), *UASt-PA-RacQ61L-LovC450M* (from this study), *UASt-PA-RacT17N-LovC450M* (from this study), *UASt-PA-Cdc42Q61L* (from this study), *UASt-PA-Cdc42T17N* (from this study), *UASp-CIBN-CAAX/UASp-Cry2-RhoGEF2* (Opto-RhoGEF tool from Stefano De Renzis)(Izquierdo et al., 2018), *UASp-CIBN-CAAX/UASp-Cry2-Rho1DN* (Opto-Rho1DN tool from Bing He)(Eritano et al., 2020), and all these following stocks are from Bloomington *Drosophila* stock center: *UAS-Rac1DN* (BL6292), *UAS-Cdc42DN* (BL6288), *UAS-Rho1CA* (BL7330), *UAS-Rho1DN* (BL7327), *UAS-ROCKCA* (BL6668), *UAS-ROCK^{RNAi}* (BL34324), *UAS-SqhRNA* (BL34939), *UAS-Rac1^{RNAi}* (BL34910), *Rac2Δ ry506* (BL6675), *UAS-Rac3^{RNAi}* (BL51932), *UAS-Cdc42^{RNAi}* (BL35756), *UAS-Shg^{RNAi}* (BL32904), *UAS-Mbc^{RNAi}* (BL51460), *UAS-ELMO^{RNAi}* (BL28556), *UAS-Raf^{RNAi}* (BL55863), *UAS-Scar^{RNAi}* (BL51803), *UAS-Abi^{RNAi}* (BL51455), *UAS-Arp3^{RNAi}* (BL32921), *UAS-PAK1^{RNAi}* (BL28945), *UAS-PAK3^{RNAi}* (BL42664), *Rac1-GFP* (BL52284), *Rac2-GFP* (BL52286), *Rac3-GFP* (BL37970), *Cdc42-RFP* (BL42236) and *Sqh::PAK3-RBD-GFP* (BL 52303 and BL52304 combined together). *Slbo-Gal4* was used to drive different *UASt* or *UASp* transgenes including optogenetic tools. All stocks and crosses were maintained at room temperature.

For the optogenetic PA-Rac and PA-Cdc42 experiments, the progeny flies from the cross between *Slbo-Gal4* and *UASt-PA-Rac* or *UASt-PA-Cdc42* or both were kept at 18 °C for 2 days and then

fattened at 25 °C overnight before dissection. All steps were carried on in dark conditions, including cross, maintenance, and heat shock. *Drosophila* ovaries were dissected in weak light conditions, and egg chambers were mounted under red light condition before blue light illumination.

For the optogenetic Opto-RhoGEF or Opto-Rho1DN experiments, *tubP-GAL80^{ts}* flies are combined with *Slbo-Gal4* and then crossed with *UASp-CIBN-CAAX/UASp-Cry2-RhoGEF* (Opto-RhoGEF tool) or *UASp-CIBN-CAAX/UASp-Cry2-Rho1DN* (Opto-Rho1DN tool) to prevent the leaking expression of either optogenetic tool. The progeny flies from the cross were kept at 18 °C for 2 day and then fattened at 29 °C for 2 hours before dissection. All steps were carried on in dark conditions, including cross, maintenance, and heat shock, as for PA-Cdc42DN experiments. *Drosophila* ovaries were dissected in weak light conditions, and egg chambers were mounted under red light condition before blue light illumination.

DNA constructs and transgenic fly generation

PA-RacCA (Q61L/E91H/N92H), PA-RacDN (T17N), PA PA-Cdc42CA (Q61L/E91H/N92H), PA-Cdc42DN (T17N), the light insensitive controls PA-RacCA-C450M and PA-RacDN-C450M, all of which have no mCherry tag, were inserted into the pUASt *Drosophila* expression vector by the in-fusion cloning strategy (Invitrogen). The respective primers for PA-Rac and PA-Cdc42 are as follow:

Primers for PA-RacCA, PA-RacDN, PA-RacCA-C450M and PA-RacDN-C450M:

Sense: 5’-CGGCCGCGCTCGAGGGTACCATGGGTTCTGGATCCTTGGC-3’

Antisense:

5’- AAAGATCCTCTAGAGGTACCTCACAACAGCAGGCATTTTCTCTTCC-3’

Primers for PA-Cdc42CA and PA-Cdc42DN:

Sense: 5’-CGGCCGCGCTCGAGGGTACCATGGGATCCGAAATTTCTGCTCC-3’

Antisense:

5’-AAAGATCCTCTAGAGGTACCTTATTCATAGCAGCACACACCTGCG-3’

The primers for the introduction of C450M are the same primers described previously (Wang et al., 2010).

PA-RacCA (Q61L/E91H/N92H) and PA-RacDN (T17N), both of which have mCherry tag at the N-terminal, were inserted into the pUASp Drosophila expression vector by the in-fusion cloning strategy (Invitrogen). The respective primers for PA-Rac are as follow:

Sense: 5′- AGGTCCTGTTCATTGGTACCATGGCACACCATCACCAC-3′

Antisense:

5′- TCTGATCCCGGGCGGGTACCTCACAACAGCAGGCATTTTCTCTTCC-3′

RacCA (GV12) and PA-RacDN (T17N) were inserted into the pUASp Drosophila expression vector by the in-fusion cloning strategy (Invitrogen). The respective primers for PA-Rac are as follow:

Sense: 5’-AGGTCCTGTTCATTGGTACCATGCAGGCGATCAAGTGCG-3’

Antisense: 5'-TCTGATCCCGGGCGGGTACCTTAGAGCAGGGCGCACTTG-3’

To produce Slbo-LifeAct-GFP and Slbo-LifeAct-RFP, the cDNA sequences from LifeAct-GFP and LifeAct-RFP (Addgene) were inserted into our previously modified *Drosophila* expression

vector driven by Slbo promoter, by using gateway cloning strategy (Invitrogen). The respective primers for Slbo-LifeAct-GFP and Slbo-LifeAct-RFP are as follow:

Sense (For LifeAct):

5'-ATCCTCTAGGGTACGGTACCATGGGTGTCGCAGATTTGATC-3'

Antisense (for GFP):

5'-AAAGATCCTCTAGAGGTACCTCACTTGTACAGCTCGTCCATG-3'

Antisense (for RFP):

5'-AAAGATCCTCTAGAGGTACCTCAGCGCCTGTGCTATGTCTGCCC-3'

All transgenic flies (PA-RacCA, PA-RacDN, PA-RacCA-C450M, PA-RacDN-C450M, PA-Cdc42CA, PA-Cdc42DN, Slbo-LifeActGFP and Slbo-LifeActRFP) were generated by Centro de Biologia Molecular Severo Ochoa (CSIC/UAM) using the w1118 fly.

PAK3RBD-GFP cDNA was inserted into the pGEX-2TK expression vector by the in-fusion cloning strategy (Invitrogen). The respective primers for GST-PAK3RBD-GFP are as follow:

Sense: 5'-GGATCCCCGGGAATTCATATGAGCTTCACCAAGTGGTTCAAG-3'

Antisense: 5'-CAGTCACGATGAATTCTCACTTGTACAGCTCGTCCATGC-3'

Drosophila Rac1 (dRac1) cDNA was inserted into the pET-14b expression vector by the in-fusion cloning strategy (Invitrogen). The respective primers for His-dRac1 are as follow:

Sense: 5'-CGCGCGGCAGCCATATGATGCAGGCGATCAAGTGCG-3'

Antisense: 5'-GGATCCTCGAGCATATGTTAGAGCAGGGCGCACTTG-3'

Dissection and mounting of the *Drosophila* egg chamber

One- to three-day-old females were fattened on yeast with males for 1-2 days before dissection. *Drosophila* egg chambers were dissected and mounted in live imaging medium (Invitrogen Schneider's insect medium with 20% FBS and with a final PH adjusted to 6.9), using a similar version of the protocol described in ref (Prasad et al., 2015).

Imaging and photomanipulation

Time-lapse imaging was performed with a Leica spinningdisk confocal microscope with a 63×, numerical aperture 1.3 inverted oil lens, with a 488 nm laser and a 568 nm laser. For the acquisition of 3D images of various signals (including LifeAct-GFP, LifeAct-RFP and PAK3RBD-GFP), the Z-stack images with 13-17 slides and 1.5 μm interval covering the main regions of border cell groups have been captured, and the Z-stack images have been captured every 30 seconds; we confirmed that this Z-stack setting generates the 3D-reconstructed images with a resolution similar to those captured by the other Z-stack setting (with 55-73 slides and 0.33 μm interval), while producing little phototoxicity to affect border cell migration behaviours. For the 2D analyses of actin flow or Myosin-II signal accumulation, one layer of images at the central plane of border cell group have been captured every 10 seconds. To test the favorable time interval for the analysis of actin flows in border cells, we compared the actin flows captured every 2 seconds or 10 seconds, both of which produced the similar flow results for the flow speed (PIV strength), the flow direction (centripetal flows at cables, retrograde and anterograde flows at protrusions), negative divergence where Myosin-II signals were accumulated at cables. Thus, we only used the images captured per 10 seconds for all analyses of actin flows and Myosin-II signal accumulation in border cell migration, considering the variation of image focus which often occurs during the acquisition

of actin flows in border cells (dynamic imaging per 10 seconds can easily allow the re-adjustment of image focus during image acquisition). The same microscope setup was used when comparing intensity between different samples. Imaging data have been collected by Leica Metamorph software (version: Metamorph 7.8.13.0).

For photo-activationphoto-activation experiment, live-cell imaging was performed using a Leica spinningdisk confocal microscope with a 63× numerical aperture 1.3 inverted oil lens, with a 488 nm laser and a 568 nm laser. An external blue light laser (Roper system) has been integrated with this spinningdisk confocal microscope to do photo-activation experiments with either 3D or 2D mode. The external 450 nm laser was set at 35% power global control which was linked with Leica MetaMorph to allow the photo-activation by external blue light illumination. For the photo-activation of PA-Rac at the 3D mode for the acquisition of 3D time-lapse imaging, 16% power from this limited global laser power was used for 0.01 ms per pixel in a 5-μm circle and every photo-activation illumination took approximately 1-2 seconds, and photo-activation illumination was carried out every 30 seconds. Under this setting, blue light laser illumination can quickly photo-bleach the GFP signals, such as LifeAct-GFP or PAK3RBD-GFP, so that LifeAct-RFP was used in all PA-Rac experiments with the acquisition of 3D images in the previous study (Wang et al., 2020), Sqh-GFP has been used to monitor Myosin-II signals in border cells during the mCherry-tagged PA-Rac experiment, which might have used much weaker laser power that was difficult to affect cables at border cell groups for intercellular communication). For the photo-activation of PA-Rac at the 2D mode for the acquisition of 2D time-lapse imaging, 16% power from this limited global laser power was used for 0.003 ms per pixel in a 5-μm circle and every photo-activation illumination took approximately 0.33 seconds, and photo-activation illumination was carried out every 10 seconds. This setting allowed us to achieve the same effects on

intercellular communication and protrusion changes in border cell groups, and meanwhile avoiding the photobleaching effect on LifeAct-GFP or PAK3RBD-GFP signals, during the total 20 minutes of photo-activation experiments. Photo-activation of PA-Cdc42 at protrusions used the same setting as the PA-Rac experiments at either 3D or 2D modes. For the photo-activation of OptoRhoGEF or OptoRho1DN at the 2D mode for the acquisition of 2D time-lapse imaging, due to the much higher efficiency of membrane-anchored RhoGEF2 or Rho1DN to activate or inhibit Rho1, 8% power from this limited global laser power was used for 0.003 ms per pixel in a 5-μm circle and every photo-activation illumination took approximately 0.33 seconds, and photo-activation illumination was carried out every 10 seconds for 2D mode.

For photo-activation experiment in environment cells, live-cell imaging was performed using a Leica spinningdisk confocal microscope with a 63× numerical aperture 1.3 inverted oil lens, with a 488 nm laser and a 568 nm laser. An external blue light laser (Roper system) has been integrated with this spinningdisk confocal microscope to do photo-activation experiments with either 3D or 2D mode. The external 450 nm laser was set at 35% power global control which was linked with Leica MetaMorph to allow the photo-activation by external blue light illumination. For the photo-activation of PA-Rac at the 3D mode for the acquisition of 3D time-lapse imaging, 11-12% power from this limited global laser power was used for 0.01 ms per pixel in a 15-μm circle and every photo-activation illumination took approximately 1–2 s, and photo-activation illumination was carried out every 30 s. Under this setting, blue light laser illumination has no prominent photo-bleaching effect on various GFP signals, such as UtrABD-GFP and Sqh-GFP. For PAK3RBD-GFP, which is much weaker in fluorescence intensity, we reduced blue light laser power to 3-5% to avoid its photo-bleaching in our experiment. This moderate photo-activation setting has also

been applied to moderately photo-activate Rac1 to create constantly favorable environment for border cell migration.

Drug treatments

Egg chambers were dissected in live imaging medium, and then incubated with ROCK inhibitor Y27632 (Sigma) 250 μM for 20 min before being mounted for imaging. For the change in cytoplasmic pressure, egg chambers were dissected in live imaging medium, and then incubated with Sucrose (Sigma) 220 μM or 25% water-diluted medium for 20 min before being mounted for imaging.

Expression, purification of GST and his fusion proteins, and pull-down activation assay

Overnight cultures of *E. coli* transformed with pGEX-2TK or pET-14b plasmids were diluted 1:10 in L-broth medium with 100 μg/ml ampicillin and incubated at 37 °C with shaking to an A600 of 0.8. Isopropyl-β-d-thiogalactopyranoside was then added to a final concentration of 0.5 mM. After a further 3-6 h of growth at 37 °C (GST proteins) or 30 °C (His-dRac1 protein), cells were pelleted at 4500 × g for 10 min at 4 °C and resuspended in NETN Buffer (0.5% Nonidet P-40, 1 mM EDTA, 20 mM Tris pH 8, 100 mM NaCl) for GST-tagged proteins or in Purification Buffer (50 mM NaH_2PO4 pH 8, 0.5 M NaCl) for His-tagged proteins, containing proteases inhibitors cocktail (Roche) and lyzozyme (1 mg/ml). Cells were then sonicated and centrifuged at 10,000 ×g for 15 min at 4 °C. For the pull-down activation assay, 50 ng of His-dRac1 proteins, purified by nickel affinity chromatography (Ni-NTA Agarose, Invitrogen), were incubated for 15 mins at room temperature with GTPγS or GDP (Millipore) in Lysis Buffer (2% Nonidet P-40, 10 mM $MgCl_2$,

50 mM Tris pH 7.5, 0.5 M NaCl) complemented with 1/10th volume of Loading Buffer (150 mM EDTA). The reaction was stopped by adding 1/10th volume of Stop Buffer (600 mM $MgCl_2$) at 4°C. GST or GST-PAK3RBD-GFP fusion proteins, preloaded on Glutathione-Agarose beads (Sigma), were incubated for 30 mins at 4 °C with GTPγS- or GDP-loaded His-dRac1. After two washes with Wash Buffer (30 mM $MgCl_2$, 25 mM Tris pH 7.5, 40 mM NaCl), denatured samples were analyzed by western blot using His (Invitrogen, Clone name: HIS.H8; Catalogue number: MA1-21315; 1:1000 dilution) and GST (Invitrogen, Clone name: 8-326; Catalogue number: MA4-004; 1:1000 dilution) antibodies.

Definition of subcellular F-actin signal regions in border cells

We established a three-step semi-automatic method to discriminate subcellular actin network regions in border cells, including the inner cell-to-cell contacts, the peripheral cables and protrusions of border cells. This detailed information of this method based on Matlab software was as follows:

1. Defining the border cell edge feature by CellGeo analysis:

CellGeo method has been established for the identification of cell edge feature (Tsygankov et al., 2014). The detailed processing by CellGeo method has been described in ref (Tsygankov et al., 2014). Here, we used the 3D reconstructed images of border cell group expressing LifeAct-FP for the processing by CellGeo method, which thus allowed us to precisely define the protrusions and main body region of border cell group, as shown in Supplementary Fig. 1a.

2. Defining cables in border cell group:

We established a Matlab code to do semi-automatic labelling of cables and broken cable sections in border cell groups. We loaded the original cell picture and the processed image defined in the step-1 from CellGeo method, into our Matlab code platform. Then, we manually selected the first cell-to-cell boundary at one side of leader protrusion as the starting position, then clicked each boundary in a clockwise direction. Based on the processing by this Matlab code, the program allowed to connect the adjacent boundary, to determine F-actin cable arc according to the F-actin intensity, and to use different colours to mark the cables in different border cells. Then, the program generated a binary image containing only cables. Based on all these processing steps, the program finally calculated the mean intensity of F-actin signals at each cable but also area and length of each cable in border cell group.

3. Determining the cell-to-cell contacts in border cell group.

We adapted the Matlab code in step 2 to do the semi-automatic labelling of contacts between border cells. For the 3D reconstructed images of border cell groups, if we can easily see the contact regions of border cells, we marked the starting and ending point of each border cell contact before running the Matlab code. The program automatically labelled the whole contact region between two border cells. Considering that some 3D reconstructed images cannot show the inner contact regions well, we only did the 3D reconstruction of images at several Z-stack layers near the center of border cell groups, which allowed to get the clearer view of each border cell contact. And we used this reconstructed image for the Matlab analysis by the same processing setting. The program also calculated the mean intensity of F-actin signals at each contact and the area of contact between two border cells.

Image processing and data analysis

Images were processed with MATLAB (version: R2020b) and Image J (version: 1.53f51). For all images the background (intensity of area without sample) was subtracted.

Measurement of F-actin intensity and PAK3RBD-GFP intensity in different subcellular regions as follows: Our semi-automatic methods including CellGeo were used to discriminate and label the three different subcellular signal regions at contacts, cables or protrusions of border cell groups, by analyses of LifeAct signals. Then F-actin intensity was automatically collected from our semi-automatic methods by Matlab code. Based on this definition of three different subcellular regions in border cell groups, PAK3RBD-GFP intensity was automatically extracted from these three regions of border cells. Then, subcellular F-actin intensity or PAK3RBD-GFP intensity was used for various indicated quantification shown in figures and extended data figures. For the time-lapse photo-activation experiments, both LifeAct-RFP and PAK3RBD-GFP intensities were processed by Matlab to correct photo-bleaching automatically, before the imaging data processing.

Measurement of Myosin-II signal accumulation at cables as follows: Myosin-II signals were processed by Matlab to correct photo-bleaching automatically. Then the background noise signals were extracted from Myosin-II signals. These processed signals were used to quantify the intensity level at cables of either the whole border cell groups or the different border cells during the photo-activation experiments. Since the two polar cells at the center of border cell groups present strong mCherry tagged Myosin-II signals, those noisy signals in polar cells have been deleted from Fig. 4a, e, in order to get rid of noisy effect on the view of peripheral Myosin-II signal accumulation at supracellular cables.

Measurement of migration speed, protrusion number, cable discontinuity and border cell area:

The distance of the center of the border cell group between the first and 3 time points in a time lapse series was measured in Matlab software. This distance divided by the elapsed time gave the speed.

Cell protrusions were counted as follows: CellGeo software has been used to discriminate and label the protrusions and main body region of border cell groups. Based on this precise analysis of cell matrix for protrusion formation from main body regions, the protrusions of border cell groups were easily captured for the quantification of protrusion number. The area of border cell protrusions was also achieved for the following quantification of total area of border cell groups.

Cale discontinuity was calculated from the length ratio between the total broken cable sections and the total region (including all cables and broken cable sections) of border cell groups. Border cell cables and broken cable sections were labelled by our semi-automatic methods as mentioned above.

Border cell area was quantified from the calculation of the area from both protrusions and main body region of border cell group, both of which were automatically produced by our semi-automatic method as mentioned above.

Nurse cell size and bubble size were quantification from the calculation of nurse cell total area and one bubble total size (both from 3D reconstructed image). The boundary of nurse cells and bubbles were produced by our manual selection from the images, regarding the difficulty of automatically detecting the periphery of nurse cells and their bubble.

Box and whiskers plots (GraphPad Prism software [version: 8.0.2]) were used to represent the distribution of various signals including subcellular F-actin intensity, subcellular PAK3RBD-GFP intensity, Myosin-II intensity at cables, cable discontinuity, signal ratio at different subcellular regions, actin flow strength, actin flow speed, actin flow divergence: boxes extend from the 25th

to 75th percentiles, the midline represents the median and the whiskers indicate the maximum and the minimum values.

Analyses of actin flows in border cells

We used the Matlab code for Particle Image Velocimetry (PIV) analysis developed in the Stramer's team (Yolland et al., 2019). The detailed information for PIV, divergence and flow directions are as follows:

1. Cell segmentation:

Before the PIV analysis, we used Ilastik software to do the processing of cell segmentation. We used the function, project of pixel classification, in this Ilastik software.

2. PIV analysis of actin flows in border cells:

A 2D cross-correlation algorithm adapted from classical PIV was implemented. In brief, this method compares a region of interest in an image (source image) with a larger region of a subsequent image (search image). The sizes of the source and search regions are determined on the basis of the feature size to be tracked and the area of their expected displacement (i.e., actin bundles). For this analysis, source and search images encompassing areas of 1.4 μm^2 and 2.4 μm^2 were used. A cross-correlation map was computed by analysing the cross-correlation coefficient between the source image and the search image, by shifting the source across the search one pixel at a time. Network displacement was measured by finding the maximum coefficient within the resulting cross-correlation map. To filter anomalous tracking data, only displacements that had a cross-correlation coefficient above a certain threshold, c0, were kept. For the present work, the threshold was set at c0 = 0.5. Finally, a spatial convolution with a Gaussian kernel (size of 6 μm,

sigma of 1.2 μm), and temporal convolution with temporal kernel of 20 second (sigma 10 second) were used to interpolate the measured displacements to cover all the pixels within the cell outline. The complete algorithm for this analysis was implemented in Matlab.

3. Divergence analysis:

For quantification of divergence a central difference scheme was implemented to compute the spatial derivatives of the actin flow velocities ($\nabla \cdot V$).

4. Defining retrograde and anterograde flow regions:

Retrograde and anterograde flow were defined with respect to their respective alignment to cell motion. The direction of the actin flow at every point at protrusions was correlated with the instantaneous direction of cell motion using the cosine of the angle between these velocity vectors. Retrograde flow was defined as a negative correlation while anterograde flow was a positive correlation to cell motion.

Statistics and reproducibility

All data are presented as mean ± SEM. Statistical analysis to compare results among groups was carried out by the Mann–Whitney test (GraphPad Prism software). A value of $P > 0.05$ was considered to be not significant (ns); a value of $P < 0.05$ (*), $P < 0.01$ (**) or $P < 0.001$ (***) was considered to be differently statistically significant, while a value of $P < 0.0001$ (****) was considered to be remarkably statistically significant.

DISCUSSIONS

I. Two Rac1 pools integrate the direction and coordination of collective cell migration

While the exact factors and molecular mechanisms controlling either leading guidance or intercellular communication have been extensively studied, how these two important properties are well integrated to ensure collective guidance and thus efficient collective movement is not completely clear. Before our studies, a molecular mechanotransduction pathway had been reported to coordinate polarized Rac1 activation and lamellipodium formation at the multicellular length scale in Madin-darby canine kidney (MDCK) cell monolayers (Das et al., 2015; Farooqui and Fenteany, 2005). However, Rac1 involvement in the intercellular communication between MDCK cells is indirect and is mainly dependent on the pulling force of leading cells as well as actomyosin-based cell contractility (Das et al., 2015), also possibly linked to an ERK wave across the epithelial cell monolayer (Aoki et al., 2017; Hino et al., 2020). Different from this reported mechanotransduction system, here our studies highlight that Rac1 can directly participate into intercellular communication to maintain actomyosin mechanical properties at supracellular cables of collectively migrating border cells. Since Rac1 is also involved in the control of border cell protrusions for leading guidance, the dispatch and coordination of Rac1 activities at cables and protrusions are very critical for the respective roles in these two regions and the integration of leading guidance and intercellular communication. Different from the 2D collective movement of epithelial cells, the proper integration of both these properties in border cells is highly dependent on the equilibrium of Rac1 activity in cables and protrusions, with exacerbated Rac1 activity in either peripheral region resulting in border cells with tight or loose structures, respectively, strongly blocking efficiency of border cell migration. Therefore, the balance between these two

Rac1 pools coordinates front-rear group polarity and collective chemotaxis, which is completely absent in epithelial cell monolayers collectively migrating on a 2D extracellular matrix (Das et al., 2015; Farooqui and Fenteany, 2005).

The concept of “two Rac1 pools” will undoubtedly broaden the understanding of the different Rac1 roles in cell migration. Indeed, Rac1 activity is enriched in the leading edge, together with Cdc42, to govern the protrusive ability of migrating cells (Bolado-Carrancio et al., 2020; Lawson and Burridge, 2014; Ridley, 2011). The preference of Rac1 activity at lamellipodia and leading edge is completely opposite to that of RhoA activity which is mainly in more inside or rear regions of migrating cells (Bolado-Carrancio et al., 2020; Lawson and Burridge, 2014; Ridley, 2011). Mutual antagonism between Rac1 and Rho1 signalling in migrating cells thus governs either protrusive or tensile properties, respectively. Although Rac1 activity has been found within some stress fiber networks, it is not linked with RhoA signalling and its mediated actomyosin contractility (Guo et al., 2006; Kovac et al., 2013). Our studies reveal that Rac1 signalling has two opposite aspects tightly linked with either Rho1 or Cdc42 signalling to exert either tensile or protrusive properties respectively, within migrating border cells (Fig. 8b). The correlation and cooperation between Rac1 and Cdc42 or Rho1 signalling are very different between both border cell peripheral regions. 1) At border cell cables, Rac1 and Rho1 signalling appears to form a positive feedback loop: cable Rac1 activity provides pulsed actin flows for Myosin-II loading, maintaining both supracellular cable structures and mechanical force coupling between border cells; meanwhile, cable Rac1 activity is spatiotemporally and positively governed by Rho1–Myosin-II signalling, possibly via actomyosin mechanical properties, yet the detailed control mechanism is still unclear (Fig. 8c). Thus, this positive feedback loop would guarantee border cell tensile property for intercellular communication, coordinating individual cell

behaviour. Although previous studies reported that Rho1 signalling controls border cell group integrity and inner tensile property at border cell-cell contacts (Bastock and Strutt, 2007; Wang et al., 2020), we didn't detect that inhibition of Rho1−Myosin-II signalling in border cells prominently affected F-actin networks in the inner regions of border cell groups. This variation could be stemmed from the studies of different stages which might strongly affect the distribution and role of Rho1 signalling in border cells. 2) At border cell protrusions, Rac1 and Cdc42 signalling seem to participate to two different albeit synergistic protrusion controls: Rac1 activity governs global F-actin structures but also the initiation position of actin flows at protrusions, while Cdc42 activity controls flow speed and directionality, like the volume vs. faucet control of protrusion F-actin networks (Fig. 8d). Here, Cdc42 signalling has been identified, for the first time, as an important actin flow regulator at protrusions but also for flow exchange between protrusions and cables of migrating border cells. This role as a faucet control is critically important in the communication and maintenance of two Rac1 functional pools so that the respective balance of protrusive vs. tensile properties between cables and protrusions is achieved, thus creating the most efficient directed border cell migration behaviour. Thus, this novel function of Cdc42 signalling is very different from the reported roles of Cdc42 for leading edge polarization and migration of individually migrating or loosely connected astrocyte monolayers (Osmani et al., 2010; Osmani et al., 2006).

In addition, our newly established "two Rac1 pools" model contradicts the current mainstream "Rac1 activity gradient" model. In the "Rac1 activity gradient" model, PVR and EGFR have been thought to promote Rac1 activity and protrusion formation at leader border cells, while inhibiting Rac1 activity and protrusions in follower border cells (Cai et al., 2014; Wang et al., 2010) (Fig. 8a). Based on this hypothesis, guidance receptors have been considered to govern yet unknown

factors which are believed to repress the protrusive property of follower border cells. However, the phenotype due to concurrent inhibition of PVR and EGFR is quite different from that of either PVR or EGFR inhibition alone (Poukkula et al., 2011b; Prasad and Montell, 2007), thus pointing to unclear points arising from the "Rac1 activity gradient" model. By focusing on the analyses of subcellular Rac1 activity and dynamic actin flows, our studies seem to better interpret the different phenotypes between concurrent and individual inhibitions of guidance receptors. Our results support that PVR and EGFR signalling govern the correct distribution of Rac1 activity within the plasma membrane at protrusion tips and supracellular cables, respectively (Fig. 8e, f). Considering either Rac1 activity starting from the plasma membrane downstream of guidance receptors, the mis-localization of Rac1 activity, but not activity loss, through guidance receptor inhibition can largely explain both migratory behaviours as well as the respective rescue phenotypes by focal Rac1 activation. 1) When PVR signalling is inhibited in border cells, Rac1 activity would start within the cytosolic region of protrusions, thus changing the origin and directionality (from centripetal to centrifugal) of protrusion actin flows (Fig. 8f); meanwhile, enhanced actomyosin flows at cables would often pass through the protrusion bases quickly erasing dynamic protrusion growth, thus resulting in the frequent absence of large leading protrusions. 2) When EGFR signalling is inhibited in border cells, both Rac1 activity and F-actin signals would often be trapped within the cytosolic region near cables (Fig. 8e); normal retrograde actin flows at protrusions (looking centripetal) together with discontinued supracellular cables would thus limit the occurrence of cable actomyosin flows, creating prominent broken supracellular cables with much less flow dynamics. Thus, for either PVR or EGFR signalling inhibition, one would expect focal Rac1 activation at either protrusion tips or cables to gradually recover the correct origin and directionality of actin flows back to those observed in WT border cells, thus leading to defective

phenotype rescue. 3) When these two receptors are inhibited in border cells, Rac1 activity would be dropped within the cytosolic regions at protrusions and near cables, thus combining the disturbed effects on actin flows both at protrusions and cables (Fig. 8e, f): multiple-directed and often centrifugal actin flows at protrusions, together with weaker and limited actomyosin flows at discontinued cables, would thus synergize to dynamically generate random albeit larger protrusions in multiple border cells, meanwhile exacerbating the discontinued supracellular cable phenotype. This synergistic effect thus excludes the hypothesis of some unknown repressor in the follower border cells. Although cables are strongly damaged in border cells upon concurrent inhibition of both guidance receptors, these discontinued cables appear nonetheless to sense the local changes of cable or protrusion recovery in border cells by focal activation of Rac1 in either region. Thus, this further implies that communication and exchange of actin flows between protrusions and cables are always present, no matter whether Rac1 activity is mis-localized and F-actin flows are disturbed in either or both border cell peripheral regions.

The various modifications of both these Rac1 pools, as well as other important factors including Rho1, Cdc42 and two guidance receptors, thus emphasize the complexity in the border cell movement. In addition to border cell migration and epithelial cell monolayer, this complexity has been often observed in other collective cell movements (Haeger et al., 2015; Scarpa and Mayor, 2016). For example, subcellular and supracellular activities of RhoA and Rac1 require precise tuning in collective movement of neural crest cells to govern supracelluar cables, leader protrusions and contact inhibition of motion (Shellard et al., 2018; Theveneau et al., 2010); moreover, Rac2, Cdc42 and Rho1 have been found to be essential in the filopodia-based contact stimulation of myotube migration, while exhibiting differential control on protrusion dynamics and cell-matrix adhesion formation (Bischoff et al., 2021). Altogether, this complexity requires

spatiotemporal cooperation among all the controlling factors, so that the balance between protrusive and tensile properties is achieved to realise collective guidance, thus creating the efficiency of directed collective cell migration.

II. Tissue physical property governing collective cell migration

Collective cell migration during development and pathological processes often occurs in the cell-rich tissues which are composed of not only matrix but also other types of cells. Normally these other types of cells on which migrating cells move are named as stroma cells (also called substrate cells) (Ilina and Friedl, 2009). The characteristics and role of multicellular environment (substrate cell environment) in collective cell migration are poorly understood, compared with the ones of matrix environment. This lack of information about the cell-on-cell collective migration is due to the difficulty in establishing an in vitro cultured system to simulate and then study the cell-on-cell collective migration. Currently, there are a few in vivo models that provide an alternative system to study collective cell migration in multicellular environment, such as Drosophila border cell migration and neuron migration along glia (Allen and Lyons, 2018; Montell et al., 2012). The multicellular environment surrounding the migratory border cell cluster is composed of fifteen nurse cells that are coming from the 4-cycle division of a cyst-forming cell and then are gradually growing and are redistributed inside the egg chamber (McLaughlin and Bratu, 2015). Compared with the in vitro matrix environment, the complexity and evolution of in vivo multicellular environment, such as the growth and change of nurse cells, raises three important questions.

First of all, how does multicellular environment mechanically affect collective cell migration? Different from matrix, substrate multicellular environment supports collective cell migration via

the Cadherin-mediated adhesion and its-linked cortical actomyosin network (Allen and Lyons, 2018; Montell et al., 2012), thus with a quite different mechano-transduction system (Cadherin adhesion between migrating cells and substrate cells, vs. Integrin adhesion of migrating cells with matrix). As mentioned in introduction, the mechanical property of the matrix is able to modify the behavior of collectively migrating cells (Elosegui-Artola et al., 2018; Ladoux and Mège, 2017; Ladoux et al., 2016; Roca-Cusachs et al., 2013; van Helvert et al., 2018). However, what specific mechanical property is present in multicellular environment and how it plays a role in collective cell migration are missing.

Second, how does this mechanical property evolve in multicellular environment? A recent study unraveled that tissue morphogenesis stiffens matrix to trigger collective cell migration57. Interestingly, increased ECM stiffness has recently been shown to soften neural crest cells to initiate their migration. It seems that migrating cells and surrounding matrix environment form a tight-linked crosstalk to govern the initiation and progression of collective cell migration over the matrix environment. Although mechanical cell force and constraint are critically involved in tissue morphogenesis (Guillot and Lecuit, 2013; Heisenberg and Bellaïche, 2013; Petridou et al., 2017), it is unknown yet whether tissue morphogenesis can modify the substrate cell force or constraint to govern collective cell migration: especially how does a specific environment mechanical property spatio-temporally evolve? And how do these environmental changes respectively govern collective cell migration behavior?

Finally, how does this environment mechanical property control some additional extracellular signals to perturb collective cell migration? Normally cell-rich tissues contain a multitude of extracellular biochemical factors, often stored in extracellular vesicles (EVs), for cell-cell communication (Tkach and Théry, 2016; van Niel et al., 2018). Considering the active cell-cell

communication between migrating cells and substrate cells, it is tempting to speculate that extracellular biochemical factors, such as those stored in EVs, could be present in multicellular environment to modify collective chemotaxis. Unfortunately, these extracellular signals are little explored and their link with environment mechanical property has never been explored in collective cell migration within cell-rich tissues.

In the past 30 years, many important signaling pathways and factors (such as JAK-STAT, Ecdysone, chemoattractants…) have been identified by traditional genetic studies, almost completely from border cells, to differently control border cell migration: migratory cell fate, time window, direction etc (Bai et al., 2000; Beccari et al., 2002; Bianco et al., 2007b; Ghiglione et al., 2002; Jang et al., 2009; Llense and Martín-Blanco, 2008; Prasad and Montell, 2007; Silver and Montell, 2001; Wang et al., 2007). Although the nurse cell environment is also considered to be important in border cell migration, little is known about the important factors of nurse cells that control border cell migration. This lack of information is due to a genetic dilemma, potentially affecting other in vivo models of cell-on-cell collective migration, which prevents the studies of multicellular environment. Since the genetic inhibition of important factors in the nurse cell environment (such as the Rho1-myosin signaling pathway to control cortical tension in nurse cells, unpublished data) often blocks the ovarian germline development and progression to the stages when border cells form and migrate, it is impossible for genetic methods to study the role of nurse cells in the control of border cell migration. Thus, there is an urgent need to develop a technique with the more precise spatio-temporal control in order to overcome the genetic limitation.

In the past 5 years, our team started to apply optogenetic tools in *Drosophila in vivo* system to overcome the limitation of genetic manipulation, such as the degeneration of nurse cells by genetic modification of important genes. Thanks to the LARIAT-mediated photo-inhibition of GFP-

targets (Qin et al., 2018; Qin et al., 2017) in nurse cells (LARIAT expression is driven by Nanos-Gal4 specific for germline nurse cells), we found that myosin and E-cadherin signals in front nurse cells, but not in rear nurse cells, support dynamic protrusion growth and polarized border cell migration; importantly, strong myosin and E-cadherin signals are highly enriched in the invasive gaps between nurse cells, in which border cells migrate very quickly with an efficient protrusion growth; meanwhile, we also found that local myosin signals in front nurse cell gaps can be transiently affected by border cell protrusions via an some unclear mechanical communication between border cells and nurse cells. Thus, by using LARIAT, we were able to unravel a specific mechanical property in multicellular environment that strongly governs collective cell migration. This specific mechanical property is represented by the invasive gaps between nurse cells, which not only form a contact geometry and travel-path but also enrich the cortical tension continuum formed by E-cadherin and actomyosin network, both supporting the efficient migration of border cells. Normally matrix microenvironment (with a directed pattern, suitable pore size and adequately-stiff components to support transient adhesion) is considered as a favorable environment for efficient invasive cell migration (Ladoux and Mège, 2017). Considering the similarity to this favorable matrix microenvironment, we thus defined the invasive gaps between nurse cells as a “hot spot” environment.

My work of Rac1 role in nurse cell environment extended our understanding of “hot spot” environment, not only the formation of various nurse cell invasive gaps but also their distinct functions in controlling border cell migration. Firstly, my work evidenced that Rac1 activity in nurse cell cortical region is a key factor controlling cortical F-actin network to support actomyosin contractility in nurse cells. Secondly, I surprisingly found that robust Rac1 activation can induce an acute assembly of Myosin signals at cortical, which seems to result in the segregation of high

cortical regions from low cortical region thereby creating the formation of large bubble structures. Under normal condition, large bubble structures are seldom detected possibly due to not-too-strong actomyosin cortical tension in nurse cells; however, we can often detect the presence of some small bubble structures between nurse cells. It thus indicates that some local strong actomyosin cortical tension might exist to promote the formation of small bubble structures. Oppositely, if Rac1 activity is low, it might reduce actomyosin cortical tension in nurse cells, which thus results in the closure of invasive gap between nurse cells. Thirdly, my results demonstrate that too low and too high Rac1 activity in front nurse cell environment both repress border cell migration via the different controls on leading protrusion. Altogether, my studies support that moderate Rac1 activity, but not weak and acute Rac1 activity, is critical in the formation of invasive gaps in front nurse cells to facilitate border cell migration between nurse cells.

Finally, about the controlling mechanism of large bubble formation, we proposed a mechanism of the synergy between the pressure-mediated outward membrane growth and the tension-mediated inward cell constriction. Our hypothesis is based on the principle of "pressure-tension balance" model, which has been used to explain the bleb formation. However, our mechanism is different from the bleb formation, mainly due to the localization of cortical tension: in the bleb forming cells, cortical tension is considered to be generally equal at the other regions outside of blebs; while in the nurse cells, cortical tension will be segregated into the regions with either high to low tension, and this tension segregation might explain the much more robust constriction of cell main body and the much larger blebs structures, both of which are absent in the bleb-forming cells. Here, our observed large bubble structures are somehow similar to the formation of lumen during early development of mouse embryo (Dumortier et al., 2019). It has been recently reported that during the mouse pre-implantation development, enriched pressurized fluid is able to fractures cell-cell

contacts into hundreds of micrometer-size lumens, and then microlumens will be coarsened by actomyosin contractility into a basolateral lumen. Unlike the “hydraulic fracturing” mechanism that disrupt E-cadherin adhesions, the E-cadherin adhesions between nurse cells are unstable and often dissociated, and thus nurse cell pressure might be relatively stable during the formation of large bubble structures. However, the comparison between microlumen in mouse embryo and large bubble structures in nurse cells needs further investigation.

III. Upstream and downstream factors of protrusive vs. contractile Rac1 activity

Our study of migrating border cells revealed the differential control of protrusive vs. tensile Rac1 activity by chemokine receptors PVR and EGFR, respectively. Mechanistically, we identified two different downstream effector pathways, Mbc-ELMO and Raf signals, to control Rac1 activity at protrusions and cables. Our identification of Mbc-ELMO complex as the intermediator between PVR and protrusive Rac1 activity is consistent with several previous findings: (1) during elimination of oncogenic neighbours by JNK-mediated engulfment in Drosophila, upregulation of PVR in normal cells by JNK activation can induce the downstream Mbc-ELMO mediated phagocytic pathway (Ohsawa et al., 2011); (2) the Mbc-ELMO complex is known to act as a member of Rac GEFs to control Rac1 activity and lamellipodia formation in Drosophila dorsal closure, somatic muscle and dorsal vessel (Biersmith et al., 2015; Toret et al., 2018). Regarding EGFR-mediated control of tensile Rac1 activity, ERK/MAPK signalling has been implicated to drive the overexpression and activation of the Rac-GEF in BRAF- and NRAS-mutant melanoma, as well as in KRAS- and EGFR- mutant lung cancer (Cooke et al., 2020; Ryan et al., 2016). However, how ERK/MAPK signalling governs Rac-GEF and Rac1 activity, especially tensile Rac1 activity controlled by Raf in border cells, is little explored. This control might either go

through the direct activation of some Rac-GEFs, or be dependent on or associated with the Rho1-myosin mediated mechanical forces that might govern some GEFs or GTPase-activating (GAP) proteins. All these possibilities need further investigation.

Interestingly and importantly, our study of environmental nurse cells unraveled a novel role of Rac1 activity in supporting cortical actomyosin network, thereby governing nurse cell cortical tension to favor the formation of invasive gaps. The role of Rac1 in nurse cells seems to be similar to that of contractile Rac1 activity in migrating border cells. Considering the similarity of contractile effects and the occurrence period/tissue, it is highly possible that border cells and nurse cells might share the similar upstream controlling signals and factors for this contractile Rac1 pool in both migrating cells and environmental cells. Due to the limited time, it is unclear whether Rac1 activity at nurse cell cortical regions is interdependent on the Rho1-myosin signaling and actomyosin contractility, as observed in border cell supracellular cables, or it might be independent from the Rho1 signaling and actomyosin contractility while forming another type of synergy with Rho1 signaling. If it is similar to the contractile Rac1 pools, Rac1 signaling in nurse cells might also depend on the ERK/MAPK signalling as an intermediate between the Rho1-myosin signalling and some GEF or GAP controlling Rac1 activity. All these possibilities also need further investigation.

Compared with protrusive Rac1 pools, the downstream effectors of contractile Rac1 pools are much less understood. Thus, many questions remain to be address. Firstly, what are the effectors mediating polymerization of F-actin network? These effectors might be Wave/Scar complex and their downstream Arp2/3 complex, the most often observed factors for F-actin nucleation. If Wave/Scar and Arp2/3 complexes are really involved in cortical actomyosin network, how does they cooperate with myosin assembly to achieve the formation of actomyosin network? Since Rac1

and Rho1 signalling often antagonize each other, branched F-actin network cannot form a synergy with myosin signals at protrusions. It is obvious that either some downstream factors of Rac1 are different between protrusions and cables, or cell cables and protrusions use another key factor to govern either the synergy or the antagonism for the distinct downstream F-actin networks at protrusions and cables. Secondly, does Cofilin participate in the control of the branched F-actin network at cables, or of the centripetal flows often observed at cable regions? As we know, Cofilin is critical in breaking F-actin network, thus initiating the formation of new branched F-actin networks or mediating the disassembly of F-actin network. The Cofilin role thus promote the dynamics of F-actin network at protrusion growing regions. Thus, whether and how Cofilin might promote F-actin dynamics at supracellular cables are completely unknown. The F-actin dynamics possibly mediated by Cofilin might govern F-actin flows to support the pulsatile occurrence of actomyosin network at supracellular cables of migrating cells. Thirdly, what are downstream effectors of Rac1 in nurse cell cortical regions? The answers for downstream effectors of contractile Rac1 pool in border cells will undoubtedly facilitate us to reveal the key downstream effectors of Rac1 activity in nurse cell cortical regions, thus critically important in addressing how F-actin network support myosin signals at these cortical regions of environment.

GENERAL CONCLUSIONS

My PhD studies demonstrate the two novel functions of smallGTPase Rac1 in collectively migrating border cells and their surrounding nurse cell environment.

Conclusion I: Two Rac1 pools integrate the direction and coordination of collective cell migration.

Integration of collective cell direction and coordination is believed to ensure collective guidance for efficient movement. Previous studies demonstrated that chemokine receptors PVR and EGFR govern a gradient of Rac1 activity essential for collective guidance of Drosophila border cells, whose mechanistic insight is unknown. By monitoring and manipulating subcellular Rac1 activity, here I reveal two switchable Rac1 pools at border cell protrusions and supracellular cables, two important structures responsible for direction and coordination. Rac1 and Rho1 form a positive feedback loop that guides mechanical coupling at cables to achieve migration coordination. Rac1 cooperates with Cdc42 to control protrusion growth for migration direction, as well as to regulate the protrusion-cable exchange, linking direction and coordination. PVR and EGFR guide correct Rac1 activity distribution at protrusions and cables. Therefore, our studies emphasize the existence of a balance between two Rac1 pools, rather than a Rac1 activity gradient, as an integrator for the direction and coordination of collective cell migration.

Conclusion II: Tissue physical property governing collective cell migration.

The physical properties of matrix environment are known to be important for collective cell migration. However, what are the physical properties in substrate cells within tissue, and how these

properties control collective cell migration within tissue remain unknown. By monitoring and manipulating subcellular Rac1 activity in nurse cells, here I demonstrate that Rac1 activity determine the cortical F-actin network and actomyosin contractility and tension in nurse cells. The nurse cell cortical tension cooperates with cytoplasmic pressure to guide the formation of various nurse cell invasive gap, from the gap closure to the gap opening, as well as the occurrence of large bubble structures within the gap. The distinct modulations of nurse cell environment by Rac1 activity differently govern border cell migration via the control of leading protrusion growth. Therefore, our studies highlight the importance of Rac1 activity in substrate cell tension property and its mediated control of collective cell migration within cell-rich tissue.

REFERENCES

Abercrombie, M., Heaysman, J.E., and Pegrum, S.M. (1970). The locomotion of fibroblasts in culture. 3. Movements of particles on the dorsal surface of the leading lamella. Experimental cell research *62*, 389-398.

Abreu-Blanco, M.T., Verboon, J.M., and Parkhurst, S.M. (2014). Coordination of Rho family GTPase activities to orchestrate cytoskeleton responses during cell wound repair. Current biology : CB *24*, 144-155.

Affolter, M., Zeller, R., and Caussinus, E. (2009). Tissue remodelling through branching morphogenesis. Nat Rev Mol Cell Biol *10*, 831-842.

Allen, N.J., and Lyons, D.A. (2018). Glia as architects of central nervous system formation and function. Science (New York, NY) *362*, 181-185.

Aman, A., and Piotrowski, T. (2008). Wnt/beta-catenin and Fgf signaling control collective cell migration by restricting chemokine receptor expression. Developmental cell *15*, 749-761.

Amelio, I., Lena, A.M., Viticchiè, G., Shalom-Feuerstein, R., Terrinoni, A., Dinsdale, D., Russo, G., Fortunato, C., Bonanno, E., Spagnoli, L.G.*, et al.* (2012). miR-24 triggers epidermal differentiation by controlling actin adhesion and cell migration. The Journal of cell biology *199*, 347-363.

Anon, E., Serra-Picamal, X., Hersen, P., Gauthier, N.C., Sheetz, M.P., Trepat, X., and Ladoux, B. (2012). Cell crawling mediates collective cell migration to close undamaged epithelial gaps. Proceedings of the National Academy of Sciences of the United States of America *109*, 10891-10896.

Aoki, K., Kondo, Y., Naoki, H., Hiratsuka, T., Itoh, R.E., and Matsuda, M. (2017). Propagating Wave of ERK Activation Orients Collective Cell Migration. Developmental cell *43*, 305-317.e305.

Aranjuez, G., Burtscher, A., Sawant, K., Majumder, P., and McDonald, J.A. (2016). Dynamic myosin activation promotes collective morphology and migration by locally balancing oppositional forces from surrounding tissue. Molecular biology of the cell *27*, 1898-1910.

Arias-Romero, L.E., and Chernoff, J. (2013). Targeting Cdc42 in cancer. Expert opinion on therapeutic targets *17*, 1263-1273.

Assaker, G., Ramel, D., Wculek, S.K., González-Gaitán, M., and Emery, G. (2010). Spatial restriction of receptor tyrosine kinase activity through a polarized endocytic cycle controls border cell migration. Proceedings of the National Academy of Sciences of the United States of America *107*, 22558-22563.

Bagorda, A., and Parent, C.A. (2008). Eukaryotic chemotaxis at a glance. Journal of cell science *121*, 2621-2624.

Bai, J., Uehara, Y., and Montell, D.J. (2000). Regulation of invasive cell behavior by taiman, a Drosophila protein related to AIB1, a steroid receptor coactivator amplified in breast cancer. Cell *103*, 1047-1058.

Bastock, R., and Strutt, D. (2007). The planar polarity pathway promotes coordinated cell migration during Drosophila oogenesis. Development (Cambridge, England) *134*, 3055-3064.

Bazellieres, E., Conte, V., Elosegui-Artola, A., Serra-Picamal, X., Bintanel-Morcillo, M., Roca-Cusachs, P., Munoz, J.J., Sales-Pardo, M., Guimera, R., and Trepat, X. (2015). Control of cell-cell forces and collective cell dynamics by the intercellular adhesome. Nature cell biology *17*, 409-420.

Beccari, S., Teixeira, L., and Rørth, P. (2002). The JAK/STAT pathway is required for border cell migration during Drosophila oogenesis. Mechanisms of development *111*, 115-123.

Bianco, A., Poukkula, M., Cliffe, A., Mathieu, J., Luque, C.M., Fulga, T.A., and Rorth, P. (2007). Two distinct modes of guidance signalling during collective migration of border cells. Nature *448*, 362-365.

Biersmith, B., Wang, Z.H., and Geisbrecht, E.R. (2015). Fine-Tuning of the Actin Cytoskeleton and Cell Adhesion During Drosophila Development by the Unconventional Guanine Nucleotide Exchange Factors Myoblast City and Sponge. Genetics *200*, 551-567.

Bischoff, M.C., Lieb, S., Renkawitz-Pohl, R., and Bogdan, S. (2021). Filopodia-based contact stimulation of cell migration drives tissue morphogenesis. Nature communications *12*, 791.

Bixby, J.L., and Jhabvala, P. (1990). Extracellular matrix molecules and cell adhesion molecules induce neurites through different mechanisms. The Journal of cell biology *111*, 2725-2732.

Boettiger, D. (2012). Mechanical control of integrin-mediated adhesion and signaling. Current opinion in cell biology *24*, 592-599.

Bolado-Carrancio, A., Rukhlenko, O.S., Nikonova, E., Tsyganov, M.A., Wheeler, A., Garcia-Munoz, A., Kolch, W., von Kriegsheim, A., and Kholodenko, B.N. (2020). Periodic propagating waves coordinate RhoGTPase network dynamics at the leading and trailing edges during cell migration. eLife *9*.

Borghese, L., Fletcher, G., Mathieu, J., Atzberger, A., Eades, W.C., Cagan, R.L., and Rørth, P. (2006). Systematic analysis of the transcriptional switch inducing migration of border cells. Developmental cell *10*, 497-508.

Boyden, E.S., Zhang, F., Bamberg, E., Nagel, G., and Deisseroth, K. (2005). Millisecond-timescale, genetically targeted optical control of neural activity. Nature neuroscience *8*, 1263-1268.

Bugaj, L.J., Choksi, A.T., Mesuda, C.K., Kane, R.S., and Schaffer, D.V. (2013). Optogenetic protein clustering and signaling activation in mammalian cells. Nature methods *10*, 249-252.

Burridge, K., and Wennerberg, K. (2004). Rho and Rac take center stage. Cell *116*, 167-179.

Cai, D., Chen, S.C., Prasad, M., He, L., Wang, X., Choesmel-Cadamuro, V., Sawyer, J.K., Danuser, G., and Montell, D.J. (2014). Mechanical feedback through E-cadherin promotes direction sensing during collective cell migration. Cell *157*, 1146-1159.

Cai, D., and Montell, D.J. (2014). Diverse and dynamic sources and sinks in gradient formation and directed migration. Current opinion in cell biology *30*, 91-98.

Campbell, I.D., and Humphries, M.J. (2011). Integrin structure, activation, and interactions. Cold Spring Harbor perspectives in biology *3*.

Čapek, D., Smutny, M., Tichy, A.M., Morri, M., Janovjak, H., and Heisenberg, C.P. (2019). Light-activated Frizzled7 reveals a permissive role of non-canonical wnt signaling in mesendoderm cell migration. eLife *8*.

Carmona-Fontaine, C., Theveneau, E., Tzekou, A., Tada, M., Woods, M., Page, K.M., Parsons, M., Lambris, J.D., and Mayor, R. (2011). Complement fragment C3a controls mutual cell attraction during collective cell migration. Developmental cell *21*, 1026-1037.

Chang, J., and Chaudhuri, O. (2019). Beyond proteases: Basement membrane mechanics and cancer invasion. The Journal of cell biology *218*, 2456-2469.

Chen, W.T. (1979). Induction of spreading during fibroblast movement. The Journal of cell biology *81*, 684-691.

Chen, Z., Li, Q., Xu, S., Ouyang, J., and Wei, H. (2021). Nanotopography-Modulated Epithelial Cell Collective Migration. Journal of biomedical nanotechnology *17*, 1079-1087.

Chitnis, A.B., Nogare, D.D., and Matsuda, M. (2012). Building the posterior lateral line system in zebrafish. Developmental neurobiology *72*, 234-255.

Choi, P.W., Yang, J., Ng, S.K., Feltmate, C., Muto, M.G., Hasselblatt, K., Lafferty-Whyte, K., JeBailey, L., MacConaill, L., Welch, W.R.*, et al.* (2016). Loss of E-cadherin disrupts ovarian epithelial inclusion cyst formation and collective cell movement in ovarian cancer cells. Oncotarget *7*, 4110-4121.

Clark, K., Langeslag, M., Figdor, C.G., and van Leeuwen, F.N. (2007). Myosin II and mechanotransduction: a balancing act. Trends in cell biology *17*, 178-186.

Cobreros-Reguera, L., Fernández-Miñán, A., Fernández-Espartero, C.H., López-Schier, H., González-Reyes, A., and Martín-Bermudo, M.D. (2010). The Ste20 kinase misshapen is essential for the invasive behaviour of ovarian epithelial cells in Drosophila. EMBO reports *11*, 943-949.

Cohen, D.J., Nelson, W.J., and Maharbiz, M.M. (2014). Galvanotactic control of collective cell migration in epithelial monolayers. Nat Mater *13*, 409-417.

Cooke, M., Baker, M.J., and Kazanietz, M.G. (2020). Rac-GEF/Rac Signaling and Metastatic Dissemination in Lung Cancer. Frontiers in cell and developmental biology *8*, 118.

Coravos, J.S., and Martin, A.C. (2016). Apical Sarcomere-like Actomyosin Contracts Nonmuscle Drosophila Epithelial Cells. Developmental cell *39*, 346-358.

Cortese, B., Palamà, I.E., D'Amone, S., and Gigli, G. (2014). Influence of electrotaxis on cell behaviour. Integrative biology : quantitative biosciences from nano to macro *6*, 817-830.

Czeisler, C., Short, A., Nelson, T., Gygli, P., Ortiz, C., Catacutan, F.P., Stocker, B., Cronin, J., Lannutti, J., Winter, J.*, et al.* (2016). Surface topography during neural stem cell differentiation regulates cell migration and cell morphology. The Journal of comparative neurology *524*, 3485-3502.

Czerniak, N.D., Dierkes, K., D'Angelo, A., Colombelli, J., and Solon, J. (2016). Patterned Contractile Forces Promote Epidermal Spreading and Regulate Segment Positioning during Drosophila Head Involution. Current biology : CB *26*, 1895-1901.

Dai, W., Guo, X., Cao, Y., Mondo, J.A., Campanale, J.P., Montell, B.J., Burrous, H., Streichan, S., Gov, N., Rappel, W.J.*, et al.* (2020). Tissue topography steers migrating Drosophila border cells. Science (New York, NY) *370*, 987-990.

Das, T., Safferling, K., Rausch, S., Grabe, N., Boehm, H., and Spatz, J.P. (2015). A molecular mechanotransduction pathway regulates collective migration of epithelial cells. Nature cell biology *17*, 276-287.

Daub, J.T., and Merks, R.M. (2013). A cell-based model of extracellular-matrix-guided endothelial cell migration during angiogenesis. Bulletin of mathematical biology *75*, 1377-1399.

De Graeve, F.M., Van de Bor, V., Ghiglione, C., Cerezo, D., Jouandin, P., Ueda, R., Shashidhara, L.S., and Noselli, S. (2012). Drosophila apc regulates delamination of invasive epithelial clusters. Developmental biology *368*, 76-85.

Deisseroth, K. (2011). Optogenetics. Nature methods *8*, 26-29.

Denef, N., and Schüpbach, T. (2003). Patterning: JAK-STAT signalling in the Drosophila follicular epithelium. Current biology : CB *13*, R388-390.

Donà, E., Barry, J.D., Valentin, G., Quirin, C., Khmelinskii, A., Kunze, A., Durdu, S., Newton, L.R., Fernandez-Minan, A., Huber, W.*, et al.* (2013). Directional tissue migration through a self-generated chemokine gradient. Nature *503*, 285-289.

Doyle, A.D., Kutys, M.L., Conti, M.A., Matsumoto, K., Adelstein, R.S., and Yamada, K.M. (2012). Micro-environmental control of cell migration--myosin IIA is required for efficient migration in fibrillar environments through control of cell adhesion dynamics. Journal of cell science *125*, 2244-2256.

Doyle, A.D., Wang, F.W., Matsumoto, K., and Yamada, K.M. (2009). One-dimensional topography underlies three-dimensional fibrillar cell migration. The Journal of cell biology *184*, 481-490.

Duchek, P., and Rorth, P. (2001). Guidance of cell migration by EGF receptor signaling during Drosophila oogenesis. Science (New York, NY) *291*, 131-133.

Duchek, P., Somogyi, K., Jékely, G., Beccari, S., and Rørth, P. (2001). Guidance of cell migration by the Drosophila PDGF/VEGF receptor. Cell *107*, 17-26.

Dumortier, J.G., Le Verge-Serandour, M., Tortorelli, A.F., Mielke, A., de Plater, L., Turlier, H., and Maître, J.L. (2019). Hydraulic fracturing and active coarsening position the lumen of the mouse blastocyst. Science (New York, NY) *365*, 465-468.

Edgar, B.A., and Orr-Weaver, T.L. (2001). Endoreplication cell cycles: more for less. Cell *105*, 297-306.

Elosegui-Artola, A., Bazellières, E., Allen, M.D., Andreu, I., Oria, R., Sunyer, R., Gomm, J.J., Marshall, J.F., Jones, J.L., and Trepat, X. (2014). Rigidity sensing and adaptation through regulation of integrin types. Nature materials *13*, 631-637.

Elosegui-Artola, A., Trepat, X., and Roca-Cusachs, P. (2018). Control of Mechanotransduction by Molecular Clutch Dynamics. Trends in cell biology *28*, 356-367.

Eritano, A.S., Bromley, C.L., Bolea Albero, A., Schutz, L., Wen, F.L., Takeda, M., Fukaya, T., Sami, M.M., Shibata, T., Lemke, S.*, et al.* (2020). Tissue-Scale Mechanical Coupling Reduces Morphogenetic Noise to Ensure Precision during Epithelial Folding. Developmental cell *53*, 212-228 e212.

Etienne-Manneville, S. (2014). Neighborly relations during collective migration. Current opinion in cell biology *30*, 51-59.

Ewald, A.J., Brenot, A., Duong, M., Chan, B.S., and Werb, Z. (2008). Collective epithelial migration and cell rearrangements drive mammary branching morphogenesis. Developmental cell *14*, 570-581.

Farooqui, R., and Fenteany, G. (2005). Multiple rows of cells behind an epithelial wound edge extend cryptic lamellipodia to collectively drive cell-sheet movement. Journal of cell science *118*, 51-63.

Feng, J.F., Liu, J., Zhang, L., Jiang, J.Y., Russell, M., Lyeth, B.G., Nolta, J.A., and Zhao, M. (2017). Electrical Guidance of Human Stem Cells in the Rat Brain. Stem cell reports *9*, 177-189.

Fernandez-Espartero, C.H., Ramel, D., Farago, M., Malartre, M., Luque, C.M., Limanovich, S., Katzav, S., Emery, G., and Martin-Bermudo, M.D. (2013). GTP exchange factor Vav regulates guided cell migration by coupling guidance receptor signalling to local Rac activation. Journal of cell science *126*, 2285-2293.

Fraley, S.I., Feng, Y., Krishnamurthy, R., Kim, D.H., Celedon, A., Longmore, G.D., and Wirtz, D. (2010). A distinctive role for focal adhesion proteins in three-dimensional cell motility. Nature cell biology *12*, 598-604.

Freitas, J.T., Jozic, I., and Bedogni, B. (2021). Wound Healing Assay for Melanoma Cell Migration. Methods in molecular biology (Clifton, NJ) *2265*, 65-71.

Fricke, R., Gohl, C., Dharmalingam, E., Grevelhorster, A., Zahedi, B., Harden, N., Kessels, M., Qualmann, B., and Bogdan, S. (2009). Drosophila Cip4/Toca-1 integrates membrane trafficking and actin dynamics through WASP and SCAR/WAVE. Current biology : CB *19*, 1429-1437.

Friedl, P., and Gilmour, D. (2009). Collective cell migration in morphogenesis, regeneration and cancer. Nat Rev Mol Cell Biol *10*, 445-457.

Friedl, P., and Wolf, K. (2003). Tumour-cell invasion and migration: diversity and escape mechanisms. Nature reviews Cancer *3*, 362-374.

Fuchs, A. (1984). Fifty years Antonie van Leeuwenhoek. Its history and its impact. Antonie van Leeuwenhoek *50*, 425-432.

Fulga, T.A., and Rørth, P. (2002). Invasive cell migration is initiated by guided growth of long cellular extensions. Nature cell biology *4*, 715-719.

Furriols, M., Ventura, G., and Casanova, J. (2007). Two distinct but convergent groups of cells trigger Torso receptor tyrosine kinase activation by independently expressing torso-like. Proceedings of the National Academy of Sciences of the United States of America *104*, 11660-11665.

Galic, M., Jeong, S., Tsai, F.C., Joubert, L.M., Wu, Y.I., Hahn, K.M., Cui, Y., and Meyer, T. (2012). External push and internal pull forces recruit curvature-sensing N-BAR domain proteins to the plasma membrane. Nature cell biology *14*, 874-881.

Gambetta, G.A., and Lagarias, J.C. (2001). Genetic engineering of phytochrome biosynthesis in bacteria. Proceedings of the National Academy of Sciences of the United States of America *98*, 10566-10571.

Garcia, G.L., Rericha, E.C., Heger, C.D., Goldsmith, P.K., and Parent, C.A. (2009). The group migration of Dictyostelium cells is regulated by extracellular chemoattractant degradation. Molecular biology of the cell *20*, 3295-3304.

Geisbrecht, E.R., and Montell, D.J. (2004). A role for Drosophila IAP1-mediated caspase inhibition in Rac-dependent cell migration. Cell *118*, 111-125.

Ghabrial, A., Luschnig, S., Metzstein, M.M., and Krasnow, M.A. (2003). Branching morphogenesis of the Drosophila tracheal system. Annual review of cell and developmental biology *19*, 623-647.

Ghassemi, S., Meacci, G., Liu, S., Gondarenko, A.A., Mathur, A., Roca-Cusachs, P., Sheetz, M.P., and Hone, J. (2012). Cells test substrate rigidity by local contractions on submicrometer pillars. Proceedings of the National Academy of Sciences of the United States of America *109*, 5328-5333.

Ghiglione, C., Devergne, O., Georgenthum, E., Carballès, F., Médioni, C., Cerezo, D., and Noselli, S. (2002). The Drosophila cytokine receptor Domeless controls border cell migration and epithelial polarization during oogenesis. Development (Cambridge, England) *129*, 5437-5447.

Ghosh, D., Dutta, A., Kashyap, A., Upmanyu, N., and Datta, S. (2021). PLP2 drives collective cell migration via ZO-1-mediated cytoskeletal remodeling at the leading edge in human colorectal cancer cells. Journal of cell science *134*.

Gilden, J., and Krummel, M.F. (2010). Control of cortical rigidity by the cytoskeleton: emerging roles for septins. Cytoskeleton (Hoboken, NJ) *67*, 477-486.

Gritsenko, P.G., Ilina, O., and Friedl, P. (2012). Interstitial guidance of cancer invasion. The Journal of pathology *226*, 185-199.

Gross, O., Beirowski, B., Harvey, S.J., McFadden, C., Chen, D., Tam, S., Thorner, P.S., Smyth, N., Addicks, K., Bloch, W.*, et al.* (2004). DDR1-deficient mice show localized subepithelial GBM thickening with focal loss of slit diaphragms and proteinuria. Kidney international *66*, 102-111.

Guillot, C., and Lecuit, T. (2013). Mechanics of epithelial tissue homeostasis and morphogenesis. Science (New York, NY) *340*, 1185-1189.

Guilluy, C., Swaminathan, V., Garcia-Mata, R., O'Brien, E.T., Superfine, R., and Burridge, K. (2011). The Rho GEFs LARG and GEF-H1 regulate the mechanical response to force on integrins. Nature cell biology *13*, 722-727.

Guo, F., Debidda, M., Yang, L., Williams, D.A., and Zheng, Y. (2006). Genetic deletion of Rac1 GTPase reveals its critical role in actin stress fiber formation and focal adhesion complex assembly. The Journal of biological chemistry *281*, 18652-18659.

Haeger, A., Wolf, K., Zegers, M.M., and Friedl, P. (2015). Collective cell migration: guidance principles and hierarchies. Trends in cell biology *25*, 556-566.

Haga, R.B., and Ridley, A.J. (2016). Rho GTPases: Regulation and roles in cancer cell biology. Small GTPases *7*, 207-221.

Hakeda-Suzuki, S., Ng, J., Tzu, J., Dietzl, G., Sun, Y., Harms, M., Nardine, T., Luo, L., and Dickson, B.J. (2002). Rac function and regulation during Drosophila development. Nature *416*, 438-442.

Hannezo, E., Dong, B., Recho, P., Joanny, J.F., and Hayashi, S. (2015). Cortical instability drives periodic supracellular actin pattern formation in epithelial tubes. Proceedings of the National Academy of Sciences of the United States of America *112*, 8620-8625.

Harada, T., Swift, J., Irianto, J., Shin, J.W., Spinler, K.R., Athirasala, A., Diegmiller, R., Dingal, P.C., Ivanovska, I.L., and Discher, D.E. (2014). Nuclear lamin stiffness is a barrier to 3D migration, but softness can limit survival. The Journal of cell biology *204*, 669-682.

Harden, N., Loh, H.Y., Chia, W., and Lim, L. (1995). A dominant inhibitory version of the small GTP-binding protein Rac disrupts cytoskeletal structures and inhibits developmental cell shape changes in Drosophila. Development (Cambridge, England) *121*, 903-914.

Haston, W.S. (1987). F-actin distribution in polymorphonuclear leucocytes. Journal of cell science *88 (Pt 4)*, 495-501.

He, L., Wang, X., Tang, H.L., and Montell, D.J. (2010). Tissue elongation requires oscillating contractions of a basal actomyosin network. Nature cell biology *12*, 1133-1142.

Heasman, S.J., and Ridley, A.J. (2008). Mammalian Rho GTPases: new insights into their functions from in vivo studies. Nat Rev Mol Cell Biol *9*, 690-701.

Heisenberg, C.P. (2009). Dorsal closure in Drosophila: cells cannot get out of the tight spot. BioEssays : news and reviews in molecular, cellular and developmental biology *31*, 1284-1287.

Heisenberg, C.P., and Bellaïche, Y. (2013). Forces in tissue morphogenesis and patterning. Cell *153*, 948-962.

Hidalgo-Carcedo, C., Hooper, S., Chaudhry, S.I., Williamson, P., Harrington, K., Leitinger, B., and Sahai, E. (2011). Collective cell migration requires suppression of actomyosin at cell-cell contacts mediated by DDR1 and the cell polarity regulators Par3 and Par6. Nature cell biology *13*, 49-58.

Hino, N., Rossetti, L., Marín-Llauradó, A., Aoki, K., Trepat, X., Matsuda, M., and Hirashima, T. (2020). ERK-Mediated Mechanochemical Waves Direct Collective Cell Polarization. Developmental cell *53*, 646-660.e648.

Ho, C.Y., Jaalouk, D.E., Vartiainen, M.K., and Lammerding, J. (2013). Lamin A/C and emerin regulate MKL1-SRF activity by modulating actin dynamics. Nature *497*, 507-511.

Hogg, N., Patzak, I., and Willenbrock, F. (2011). The insider's guide to leukocyte integrin signalling and function. Nature reviews Immunology *11*, 416-426.

Hung, W.C., Chen, S.H., Paul, C.D., Stroka, K.M., Lo, Y.C., Yang, J.T., and Konstantopoulos, K. (2013). Distinct signaling mechanisms regulate migration in unconfined versus confined spaces. The Journal of cell biology *202*, 807-824.

Huveneers, S., and Danen, E.H. (2009). Adhesion signaling - crosstalk between integrins, Src and Rho. Journal of cell science *122*, 1059-1069.

Hwang, I.Y., Park, C., and Kehrl, J.H. (2007). Impaired trafficking of Gnai2+/- and Gnai2-/- T lymphocytes: implications for T cell movement within lymph nodes. Journal of immunology (Baltimore, Md : 1950) *179*, 439-448.

Ilina, O., Bakker, G.J., Vasaturo, A., Hofmann, R.M., and Friedl, P. (2011). Two-photon laser-generated microtracks in 3D collagen lattices: principles of MMP-dependent and -independent collective cancer cell invasion. Physical biology *8*, 015010.

Ilina, O., and Friedl, P. (2009). Mechanisms of collective cell migration at a glance. Journal of cell science *122*, 3203-3208.

Insall, R.H. (2010). Understanding eukaryotic chemotaxis: a pseudopod-centred view. Nat Rev Mol Cell Biol *11*, 453-458.

Insall, R.H., and Machesky, L.M. (2009). Actin dynamics at the leading edge: from simple machinery to complex networks. Developmental cell *17*, 310-322.

Izquierdo, E., Quinkler, T., and De Renzis, S. (2018). Guided morphogenesis through optogenetic activation of Rho signalling during early Drosophila embryogenesis. Nature communications *9*, 2366.

Jang, A.C., Chang, Y.C., Bai, J., and Montell, D. (2009). Border-cell migration requires integration of spatial and temporal signals by the BTB protein Abrupt. Nature cell biology *11*, 569-579.

Janiszewska, M., Primi, M.C., and Izard, T. (2020). Cell adhesion in cancer: Beyond the migration of single cells. The Journal of biological chemistry *295*, 2495-2505.

Jékely, G., Sung, H.H., Luque, C.M., and Rørth, P. (2005). Regulators of endocytosis maintain localized receptor tyrosine kinase signaling in guided migration. Developmental cell *9*, 197-207.

Julian, L., and Olson, M.F. (2014). Rho-associated coiled-coil containing kinases (ROCK): structure, regulation, and functions. Small GTPases *5*, e29846.

Jung, G., Wu, X., and Hammer, J.A., 3rd (1996). Dictyostelium mutants lacking multiple classic myosin I isoforms reveal combinations of shared and distinct functions. The Journal of cell biology *133*, 305-323.

Katoh, M. (2005). WNT/PCP signaling pathway and human cancer (review). Oncology reports *14*, 1583-1588.

Khalil, A.A., and Friedl, P. (2010). Determinants of leader cells in collective cell migration. Integrative biology : quantitative biosciences from nano to macro *2*, 568-574.

Kiehart, D.P., Crawford, J.M., Aristotelous, A., Venakides, S., and Edwards, G.S. (2017). Cell Sheet Morphogenesis: Dorsal Closure in Drosophila melanogaster as a Model System. Annual review of cell and developmental biology *33*, 169-202.

Kim, J.H., Serra-Picamal, X., Tambe, D.T., Zhou, E.H., Park, C.Y., Sadati, M., Park, J.A., Krishnan, R., Gweon, B., Millet, E.*, et al.* (2013). Propulsion and navigation within the advancing monolayer sheet. Nat Mater *12*, 856-863.

Kimura, K., Kawamoto, K., Teranishi, S., and Nishida, T. (2006). Role of Rac1 in fibronectin-induced adhesion and motility of human corneal epithelial cells. Investigative ophthalmology & visual science *47*, 4323-4329.

King, R.C. (1970). Ovarian development in Drosophila melanogaster.

Kirfel, G., Rigort, A., Borm, B., and Herzog, V. (2004). Cell migration: mechanisms of rear detachment and the formation of migration tracks. European journal of cell biology *83*, 717-724.

Kovac, B., Teo, J.L., Mäkelä, T.P., and Vallenius, T. (2013). Assembly of non-contractile dorsal stress fibers requires α-actinin-1 and Rac1 in migrating and spreading cells. Journal of cell science *126*, 263-273.

Krendel, M., and Mooseker, M.S. (2005). Myosins: tails (and heads) of functional diversity. Physiology (Bethesda, Md) *20*, 239-251.

Kriebel, P.W., Barr, V.A., Rericha, E.C., Zhang, G., and Parent, C.A. (2008). Collective cell migration requires vesicular trafficking for chemoattractant delivery at the trailing edge. The Journal of cell biology *183*, 949-961.

Kubow, K.E., and Horwitz, A.R. (2011). Reducing background fluorescence reveals adhesions in 3D matrices. Nature cell biology *13*, 3-5; author reply 5-7.

Ladoux, B., and Mège, R.M. (2017). Mechanobiology of collective cell behaviours. Nat Rev Mol Cell Biol *18*, 743-757.

Ladoux, B., Mège, R.M., and Trepat, X. (2016). Front-Rear Polarization by Mechanical Cues: From Single Cells to Tissues. Trends in cell biology *26*, 420-433.

Lafuente, E.M., van Puijenbroek, A.A., Krause, M., Carman, C.V., Freeman, G.J., Berezovskaya, A., Constantine, E., Springer, T.A., Gertler, F.B., and Boussiotis, V.A. (2004). RIAM, an Ena/VASP and Profilin ligand, interacts with Rap1-GTP and mediates Rap1-induced adhesion. Developmental cell *7*, 585-595.

Lämmermann, T., Bader, B.L., Monkley, S.J., Worbs, T., Wedlich-Söldner, R., Hirsch, K., Keller, M., Förster, R., Critchley, D.R., Fässler, R.*, et al.* (2008). Rapid leukocyte migration by integrin-independent flowing and squeezing. Nature *453*, 51-55.

Lämmermann, T., and Sixt, M. (2009). Mechanical modes of 'amoeboid' cell migration. Current opinion in cell biology *21*, 636-644.

Langridge, P.D., and Kay, R.R. (2006). Blebbing of Dictyostelium cells in response to chemoattractant. Experimental cell research *312*, 2009-2017.

Lauffenburger, D.A., and Horwitz, A.F. (1996). Cell migration: a physically integrated molecular process. Cell *84*, 359-369.

Lawson, C.D., and Burridge, K. (2014). The on-off relationship of Rho and Rac during integrin-mediated adhesion and cell migration. Small GTPases *5*, e27958.

Lecaudey, V., Cakan-Akdogan, G., Norton, W.H., and Gilmour, D. (2008). Dynamic Fgf signaling couples morphogenesis and migration in the zebrafish lateral line primordium. Development (Cambridge, England) *135*, 2695-2705.

Lee, H.S., Lim, C.J., Puzon-McLaughlin, W., Shattil, S.J., and Ginsberg, M.H. (2009). RIAM activates integrins by linking talin to ras GTPase membrane-targeting sequences. The Journal of biological chemistry *284*, 5119-5127.

Lee, S., Park, H., Kyung, T., Kim, N.Y., Kim, S., Kim, J., and Heo, W.D. (2014). Reversible protein inactivation by optogenetic trapping in cells. Nature methods *11*, 633-636.

Lee, T., Hacohen, N., Krasnow, M., and Montell, D.J. (1996). Regulated Breathless receptor tyrosine kinase activity required to pattern cell migration and branching in the Drosophila tracheal system. Genes & development *10*, 2912-2921.

Li, M., Wang, X., Rajagopalan, P., Zhang, L., Zhan, S., Huang, S., Li, W., Zeng, X., Ye, Q., Liu, Y.*, et al.* (2020). Toward Controlled Electrical Stimulation for Wound Healing Based on a Precision Layered Skin Model. ACS applied bio materials *3*, 8901-8910.

Liu, H., Yu, X., Li, K., Klejnot, J., Yang, H., Lisiero, D., and Lin, C. (2008). Photoexcited CRY2 interacts with CIB1 to regulate transcription and floral initiation in Arabidopsis. Science (New York, NY) *322*, 1535-1539.

Liu, J., Zhang, X., Cheng, Y., and Cao, X. (2021). Dendritic cell migration in inflammation and immunity. Cellular & molecular immunology *18*, 2461-2471.

Liu, Q., and Song, B. (2014). Electric field regulated signaling pathways. The international journal of biochemistry & cell biology *55*, 264-268.

Llense, F., and Martin-Blanco, E. (2008). JNK signaling controls border cell cluster integrity and collective cell migration. Current biology : CB *18*, 538-544.

Lu, Y., and Settleman, J. (1999). The role of rho family GTPases in development: lessons from Drosophila melanogaster. Molecular cell biology research communications : MCBRC *1*, 87-94.

Lungu, O.I., Hallett, R.A., Choi, E.J., Aiken, M.J., Hahn, K.M., and Kuhlman, B. (2012). Designing photoswitchable peptides using the AsLOV2 domain. Chemistry & biology *19*, 507-517.

Luo, L., Liao, Y.J., Jan, L.Y., and Jan, Y.N. (1994). Distinct morphogenetic functions of similar small GTPases: Drosophila Drac1 is involved in axonal outgrowth and myoblast fusion. Genes & development *8*, 1787-1802.

Majidpoor, J., and Mortezaee, K. (2021). Steps in metastasis: an updated review. Medical oncology (Northwood, London, England) *38*, 3.

Majumdar, R., Sixt, M., and Parent, C.A. (2014). New paradigms in the establishment and maintenance of gradients during directed cell migration. Current opinion in cell biology *30*, 33-40.

Majumder, P., Aranjuez, G., Amick, J., and McDonald, J.A. (2012). Par-1 controls myosin-II activity through myosin phosphatase to regulate border cell migration. Current biology : CB *22*, 363-372.

Mak, M., Spill, F., Kamm, R.D., and Zaman, M.H. (2016). Single-Cell Migration in Complex Microenvironments: Mechanics and Signaling Dynamics. Journal of biomechanical engineering *138*, 021004.

Malartre, M., Ayaz, D., Amador, F.F., and Martín-Bermudo, M.D. (2010). The guanine exchange factor vav controls axon growth and guidance during Drosophila development. The Journal of neuroscience : the official journal of the Society for Neuroscience *30*, 2257-2267.

Malet-Engra, G., Yu, W., Oldani, A., Rey-Barroso, J., Gov, N.S., Scita, G., and Dupré, L. (2015). Collective cell motility promotes chemotactic prowess and resistance to chemorepulsion. Current biology : CB *25*, 242-250.

Mansfield, S.G., al-Shirawi, D.Y., Ketchum, A.S., Newbern, E.C., and Kiehart, D.P. (1996). Molecular organization and alternative splicing in zipper, the gene that encodes the Drosophila non-muscle myosin II heavy chain. Journal of molecular biology *255*, 98-109.

Martin, A.C., Kaschube, M., and Wieschaus, E.F. (2009). Pulsed contractions of an actin-myosin network drive apical constriction. Nature *457*, 495-499.

Martin, P. (1997). Wound healing--aiming for perfect skin regeneration. Science (New York, NY) *276*, 75-81.

Mason, B.N., Starchenko, A., Williams, R.M., Bonassar, L.J., and Reinhart-King, C.A. (2013a). Tuning three-dimensional collagen matrix stiffness independently of collagen concentration modulates endothelial cell behavior. Acta biomaterialia *9*, 4635-4644.

Mason, F.M., Tworoger, M., and Martin, A.C. (2013b). Apical domain polarization localizes actin-myosin activity to drive ratchet-like apical constriction. Nature cell biology *15*, 926-936.

Matsuno-Yagi, A., and Mukohata, Y. (1977). Two possible roles of bacteriorhodopsin; a comparative study of strains of Halobacterium halobium differing in pigmentation. Biochemical and biophysical research communications *78*, 237-243.

Mayor, R., and Etienne-Manneville, S. (2016). The front and rear of collective cell migration. Nat Rev Mol Cell Biol *17*, 97-109.

McDonald, J.A., and Tomoyasu, Y. (2020). Sculpting new structures. eLife *9*.

McGregor, J.R., Xi, R., and Harrison, D.A. (2002). JAK signaling is somatically required for follicle cell differentiation in Drosophila. Development (Cambridge, England) *129*, 705-717.

McLaughlin, J.M., and Bratu, D.P. (2015). Drosophila melanogaster Oogenesis: An Overview. Methods in molecular biology (Clifton, NJ) *1328*, 1-20.

McMahon, A., Supatto, W., Fraser, S.E., and Stathopoulos, A. (2008). Dynamic analyses of Drosophila gastrulation provide insights into collective cell migration. Science (New York, NY) *322*, 1546-1550.

Mei, J., Böhland, C., Geiger, A., Baur, I., Berner, K., Heuer, S., Liu, X., Mataite, L., Melo-Narváez, M.C., Özkaya, E*., et al.* (2021). Development of a model for fibroblast-led collective migration from breast cancer cell spheroids to study radiation effects on invasiveness. Radiation oncology (London, England) *16*, 159.

Melani, M., Simpson, K.J., Brugge, J.S., and Montell, D. (2008). Regulation of cell adhesion and collective cell migration by hindsight and its human homolog RREB1. Current biology : CB *18*, 532-537.

Mellad, J.A., Warren, D.T., and Shanahan, C.M. (2011). Nesprins LINC the nucleus and cytoskeleton. Current opinion in cell biology *23*, 47-54.

Miki, H., Suetsugu, S., and Takenawa, T. (1998). WAVE, a novel WASP-family protein involved in actin reorganization induced by Rac. The EMBO journal *17*, 6932-6941.

Montell, D.J. (2003). Border-cell migration: the race is on. Nat Rev Mol Cell Biol *4*, 13-24.

Montell, D.J. (2008). Morphogenetic cell movements: diversity from modular mechanical properties. Science (New York, NY) *322*, 1502-1505.

Montell, D.J., Rorth, P., and Spradling, A.C. (1992). slow border cells, a locus required for a developmentally regulated cell migration during oogenesis, encodes Drosophila C/EBP. Cell *71*, 51-62.

Montell, D.J., Yoon, W.H., and Starz-Gaiano, M. (2012). Group choreography: mechanisms orchestrating the collective movement of border cells. Nat Rev Mol Cell Biol *13*, 631-645.

Montgomery, J., Carton, G., Voigt, R., Baker, C., and Diebel, C. (2000). Sensory processing of water currents by fishes. Philosophical transactions of the Royal Society of London Series B, Biological sciences *355*, 1325-1327.

Moon, J.J., Matsumoto, M., Patel, S., Lee, L., Guan, J.L., and Li, S. (2005). Role of cell surface heparan sulfate proteoglycans in endothelial cell migration and mechanotransduction. Journal of cellular physiology *203*, 166-176.

Motta-Mena, L.B., Reade, A., Mallory, M.J., Glantz, S., Weiner, O.D., Lynch, K.W., and Gardner, K.H. (2014). An optogenetic gene expression system with rapid activation and deactivation kinetics. Nature chemical biology *10*, 196-202.

Müller, K., Engesser, R., Timmer, J., Nagy, F., Zurbriggen, M.D., and Weber, W. (2013). Synthesis of phycocyanobilin in mammalian cells. Chemical communications (Cambridge, England) *49*, 8970-8972.

Murphy, A.M., and Montell, D.J. (1996). Cell type-specific roles for Cdc42, Rac, and RhoL in Drosophila oogenesis. The Journal of cell biology *133*, 617-630.

Murphy, N.P., Binti Ahmad Mokhtar, A.M., Mott, H.R., and Owen, D. (2021). Molecular subversion of Cdc42 signalling in cancer. Biochemical Society transactions *49*, 1425-1442.

Nagel, G., Ollig, D., Fuhrmann, M., Kateriya, S., Musti, A.M., Bamberg, E., and Hegemann, P. (2002). Channelrhodopsin-1: a light-gated proton channel in green algae. Science (New York, NY) *296*, 2395-2398.

Nanba, D., Toki, F., Asakawa, K., Matsumura, H., Shiraishi, K., Sayama, K., Matsuzaki, K., Toki, H., and Nishimura, E.K. (2021). EGFR-mediated epidermal stem cell motility drives skin regeneration through COL17A1 proteolysis. The Journal of cell biology *220*.

Narumiya, S. (1996). The small GTPase Rho: cellular functions and signal transduction. Journal of biochemistry *120*, 215-228.

Neuhaus, E.M., Almers, W., and Soldati, T. (2002). Morphology and dynamics of the endocytic pathway in Dictyostelium discoideum. Molecular biology of the cell *13*, 1390-1407.

Ni, M., Tepperman, J.M., and Quail, P.H. (1999). Binding of phytochrome B to its nuclear signalling partner PIF3 is reversibly induced by light. Nature *400*, 781-784.

Niewiadomska, P., Godt, D., and Tepass, U. (1999). DE-Cadherin is required for intercellular motility during Drosophila oogenesis. The Journal of cell biology *144*, 533-547.

Nikolopoulou, E., Galea, G.L., Rolo, A., Greene, N.D., and Copp, A.J. (2017). Neural tube closure: cellular, molecular and biomechanical mechanisms. Development (Cambridge, England) *144*, 552-566.

Nobes, C.D., and Hall, A. (1999). Rho GTPases control polarity, protrusion, and adhesion during cell movement. The Journal of cell biology *144*, 1235-1244.

Nogare, D.D., Nikaido, M., Somers, K., Head, J., Piotrowski, T., and Chitnis, A.B. (2017). In toto imaging of the migrating Zebrafish lateral line primordium at single cell resolution. Developmental biology *422*, 14-23.

Oesterhelt, D., and Stoeckenius, W. (1971). Rhodopsin-like protein from the purple membrane of Halobacterium halobium. Nature: New biology *233*, 149-152.

Ohsawa, S., Sugimura, K., Takino, K., Xu, T., Miyawaki, A., and Igaki, T. (2011). Elimination of oncogenic neighbors by JNK-mediated engulfment in Drosophila. Developmental cell *20*, 315-328.

Osmani, N., Peglion, F., Chavrier, P., and Etienne-Manneville, S. (2010). Cdc42 localization and cell polarity depend on membrane traffic. The Journal of cell biology *191*, 1261-1269.

Osmani, N., Vitale, N., Borg, J.P., and Etienne-Manneville, S. (2006). Scrib controls Cdc42 localization and activity to promote cell polarization during astrocyte migration. Current biology : CB *16*, 2395-2405.

Pacquelet, A., and Rørth, P. (2005). Regulatory mechanisms required for DE-cadherin function in cell migration and other types of adhesion. The Journal of cell biology *170*, 803-812.

Pantaloni, D., Le Clainche, C., and Carlier, M.F. (2001). Mechanism of actin-based motility. Science (New York, NY) *292*, 1502-1506.

Park, J.A., Atia, L., Mitchel, J.A., Fredberg, J.J., and Butler, J.P. (2016). Collective migration and cell jamming in asthma, cancer and development. Journal of cell science *129*, 3375-3383.

Peglion, F., Llense, F., and Etienne-Manneville, S. (2014). Adherens junction treadmilling during collective migration. Nature cell biology *16*, 639-651.

Perlin, J.R., and Talbot, W.S. (2007). Signals on the move: chemokine receptors and organogenesis in zebrafish. Science's STKE : signal transduction knowledge environment *2007*, pe45.

Petridou, N.I., Spiró, Z., and Heisenberg, C.P. (2017). Multiscale force sensing in development. Nature cell biology *19*, 581-588.

Petrie, R.J., Gavara, N., Chadwick, R.S., and Yamada, K.M. (2012). Nonpolarized signaling reveals two distinct modes of 3D cell migration. The Journal of cell biology *197*, 439-455.

Petrie, R.J., Koo, H., and Yamada, K.M. (2014). Generation of compartmentalized pressure by a nuclear piston governs cell motility in a 3D matrix. Science (New York, NY) *345*, 1062-1065.

Pinheiro, E.M., and Montell, D.J. (2004). Requirement for Par-6 and Bazooka in Drosophila border cell migration. Development (Cambridge, England) *131*, 5243-5251.

Plotnikov, S.V., Pasapera, A.M., Sabass, B., and Waterman, C.M. (2012). Force fluctuations within focal adhesions mediate ECM-rigidity sensing to guide directed cell migration. Cell *151*, 1513-1527.

Pollard, T.D., and Borisy, G.G. (2003). Cellular motility driven by assembly and disassembly of actin filaments. Cell *112*, 453-465.

Poukkula, M., Cliffe, A., Changede, R., and Rørth, P. (2011). Cell behaviors regulated by guidance cues in collective migration of border cells. The Journal of cell biology *192*, 513-524.

Prasad, M., Jang, A.C., Starz-Gaiano, M., Melani, M., and Montell, D.J. (2007). A protocol for culturing Drosophila melanogaster stage 9 egg chambers for live imaging. Nature protocols *2*, 2467-2473.

Prasad, M., and Montell, D.J. (2007). Cellular and molecular mechanisms of border cell migration analyzed using time-lapse live-cell imaging. Developmental cell *12*, 997-1005.

Prasad, M., Wang, X., He, L., Cai, D., and Montell, D.J. (2015). Border Cell Migration: A Model System for Live Imaging and Genetic Analysis of Collective Cell Movement. Methods in molecular biology (Clifton, NJ) *1328*, 89-97.

Prasad, M., Wang, X., He, L., and Montell, D.J. (2011). Border cell migration: a model system for live imaging and genetic analysis of collective cell movement. Methods in molecular biology (Clifton, NJ) *769*, 277-286.

Puck, T.T., Cieciura, S.J., and Fisher, H.W. (1957). Clonal growth in vitro of human cells with fibroblastic morphology; comparison of growth and genetic characteristics of single epithelioid and fibroblast-like cells from a variety of human organs. The Journal of experimental medicine *106*, 145-158.

Qadir, M.I., Parveen, A., and Ali, M. (2015). Cdc42: Role in Cancer Management. Chemical biology & drug design *86*, 432-439.

Qin, X., Hannezo, E., Mangeat, T., Liu, C., Majumder, P., Liu, J., Choesmel-Cadamuro, V., McDonald, J.A., Liu, Y., Yi, B.*, et al.* (2018). A biochemical network controlling basal myosin oscillation. Nature communications *9*, 1210.

Qin, X., Park, B.O., Liu, J., Chen, B., Choesmel-Cadamuro, V., Belguise, K., Heo, W.D., and Wang, X. (2017). Cell-matrix adhesion and cell-cell adhesion differentially control basal myosin oscillation and Drosophila egg chamber elongation. Nature communications *8*, 14708.

Raftopoulou, M., and Hall, A. (2004). Cell migration: Rho GTPases lead the way. Developmental biology *265*, 23-32.

Ramel, D., Wang, X., Laflamme, C., Montell, D.J., and Emery, G. (2013). Rab11 regulates cell-cell communication during collective cell movements. Nature cell biology *15*, 317-324.

Rane, C.K., and Minden, A. (2014). P21 activated kinases: structure, regulation, and functions. Small GTPases *5*.

Rao, M.V., Chu, P.H., Hahn, K.M., and Zaidel-Bar, R. (2013). An optogenetic tool for the activation of endogenous diaphanous-related formins induces thickening of stress fibers without an increase in contractility. Cytoskeleton (Hoboken, NJ) *70*, 394-407.

Rauzi, M., Lenne, P.F., and Lecuit, T. (2010). Planar polarized actomyosin contractile flows control epithelial junction remodelling. Nature *468*, 1110-1114.

Reffay, M., Parrini, M.C., Cochet-Escartin, O., Ladoux, B., Buguin, A., Coscoy, S., Amblard, F., Camonis, J., and Silberzan, P. (2014). Interplay of RhoA and mechanical forces in collective cell migration driven by leader cells. Nature cell biology *16*, 217-223.

Reymann, A.C., Boujemaa-Paterski, R., Martiel, J.L., Guerin, C., Cao, W., Chin, H.F., De La Cruz, E.M., Thery, M., and Blanchoin, L. (2012). Actin network architecture can determine myosin motor activity. Science (New York, NY) *336*, 1310-1314.

Richardson, A.M., Havel, L.S., Koyen, A.E., Konen, J.M., Shupe, J., Wiles, W.G.t., Martin, W.D., Grossniklaus, H.E., Sica, G., Gilbert-Ross, M.*, et al.* (2018). Vimentin Is Required for Lung Adenocarcinoma Metastasis via Heterotypic Tumor Cell-Cancer-Associated Fibroblast Interactions during Collective Invasion. Clinical cancer research : an official journal of the American Association for Cancer Research *24*, 420-432.

Riddiford, L. (1993). The Development of Drosophila Melanogaster.

Ridley, A.J. (2011). Life at the leading edge. Cell *145*, 1012-1022.

Ridley, A.J., Schwartz, M.A., Burridge, K., Firtel, R.A., Ginsberg, M.H., Borisy, G., Parsons, J.T., and Horwitz, A.R. (2003). Cell migration: integrating signals from front to back. Science (New York, NY) *302*, 1704-1709.

Roca-Cusachs, P., Sunyer, R., and Trepat, X. (2013). Mechanical guidance of cell migration: lessons from chemotaxis. Current opinion in cell biology *25*, 543-549.

Rørth, P. (2009). Collective cell migration. Annual review of cell and developmental biology *25*, 407-429.

Rørth, P. (2002). Initiating and guiding migration: lessons from border cells. Trends in cell biology *12*, 325-331.

Rørth, P. (2011). Whence directionality: guidance mechanisms in solitary and collective cell migration. Developmental cell *20*, 9-18.

Rosenberg, O.S., Deindl, S., Sung, R.J., Nairn, A.C., and Kuriyan, J. (2005). Structure of the autoinhibited kinase domain of CaMKII and SAXS analysis of the holoenzyme. Cell *123*, 849-860.

Rowe, R.G., and Weiss, S.J. (2008). Breaching the basement membrane: who, when and how? Trends in cell biology *18*, 560-574.

Ruohola, H., Bremer, K.A., Baker, D., Swedlow, J.R., Jan, L.Y., and Jan, Y.N. (1991). Role of neurogenic genes in establishment of follicle cell fate and oocyte polarity during oogenesis in Drosophila. Cell *66*, 433-449.

Ryan, M.B., Finn, A.J., Pedone, K.H., Thomas, N.E., Der, C.J., and Cox, A.D. (2016). ERK/MAPK Signaling Drives Overexpression of the Rac-GEF, PREX1, in BRAF- and NRAS-Mutant Melanoma. Molecular cancer research : MCR *14*, 1009-1018.

Sahai, E., and Marshall, C.J. (2003). Differing modes of tumour cell invasion have distinct requirements for Rho/ROCK signalling and extracellular proteolysis. Nature cell biology *5*, 711-719.

Samlaska, C.P., and Winfield, E.A. (1994). Pentoxifylline. Journal of the American Academy of Dermatology *30*, 603-621.

Sawada, Y., Tamada, M., Dubin-Thaler, B.J., Cherniavskaya, O., Sakai, R., Tanaka, S., and Sheetz, M.P. (2006). Force sensing by mechanical extension of the Src family kinase substrate p130Cas. Cell *127*, 1015-1026.

Scarpa, E., and Mayor, R. (2016). Collective cell migration in development. The Journal of cell biology *212*, 143-155.

Schober, M., Rebay, I., and Perrimon, N. (2005). Function of the ETS transcription factor Yan in border cell migration. Development (Cambridge, England) *132*, 3493-3504.

Schreier, T., Degen, E., and Baschong, W. (1993). Fibroblast migration and proliferation during in vitro wound healing. A quantitative comparison between various growth factors and a low molecular weight blood dialysate used in the clinic to normalize impaired wound healing. Research in experimental medicine Zeitschrift fur die gesamte experimentelle Medizin einschliesslich experimenteller Chirurgie *193*, 195-205.

Schumacher, L. (2019). Collective Cell Migration in Development. Advances in experimental medicine and biology *1146*, 105-116.

Schwarz, U.S., and Gardel, M.L. (2012). United we stand: integrating the actin cytoskeleton and cell-matrix adhesions in cellular mechanotransduction. Journal of cell science *125*, 3051-3060.

Seetharaman, S., and Etienne-Manneville, S. (2020). Cytoskeletal Crosstalk in Cell Migration. Trends in cell biology *30*, 720-735.

Sellers, J.R. (1999). Unphosphorylated crossbridges and latch: smooth muscle regulation revisited. Journal of muscle research and cell motility *20*, 347-349.

Shamloo, A. (2014). Cell-cell interactions mediate cytoskeleton organization and collective endothelial cell chemotaxis. Cytoskeleton (Hoboken, NJ) *71*, 501-512.

Shellard, A., Szabó, A., Trepat, X., and Mayor, R. (2018). Supracellular contraction at the rear of neural crest cell groups drives collective chemotaxis. Science (New York, NY) *362*, 339-343.

Shimizu-Sato, S., Huq, E., Tepperman, J.M., and Quail, P.H. (2002). A light-switchable gene promoter system. Nature biotechnology *20*, 1041-1044.

Silver, D.L., and Montell, D.J. (2001). Paracrine signaling through the JAK/STAT pathway activates invasive behavior of ovarian epithelial cells in Drosophila. Cell *107*, 831-841.

Simmich, J., Staykov, E., and Scott, E. (2012). Zebrafish as an appealing model for optogenetic studies. Progress in brain research *196*, 145-162.

Small, J.V., Stradal, T., Vignal, E., and Rottner, K. (2002). The lamellipodium: where motility begins. Trends in cell biology *12*, 112-120.

Spiering, D., and Hodgson, L. (2011). Dynamics of the Rho-family small GTPases in actin regulation and motility. Cell adhesion & migration *5*, 170-180.

Spradling, A., and Bate, M. (1993). The Development of Drosophila Melanogaster.

Starz-Gaiano, M., Melani, M., Wang, X., Meinhardt, H., and Montell, D.J. (2008). Feedback inhibition of Jak/STAT signaling by apontic is required to limit an invasive cell population. Developmental cell *14*, 726-738.

Stock, J., and Pauli, A. (2021). Self-organized cell migration across scales - from single cell movement to tissue formation. Development (Cambridge, England) *148*.

Suetsugu, S., Yamazaki, D., Kurisu, S., and Takenawa, T. (2003). Differential roles of WAVE1 and WAVE2 in dorsal and peripheral ruffle formation for fibroblast cell migration. Developmental cell *5*, 595-609.

Sun, Z., Amourda, C., Shagirov, M., Hara, Y., Saunders, T.E., and Toyama, Y. (2017). Basolateral protrusion and apical contraction cooperatively drive Drosophila germ-band extension. Nature cell biology *19*, 375-383.

Svitkina, T.M., and Borisy, G.G. (1999). Arp2/3 complex and actin depolymerizing factor/cofilin in dendritic organization and treadmilling of actin filament array in lamellipodia. The Journal of cell biology *145*, 1009-1026.

Swift, J., Ivanovska, I.L., Buxboim, A., Harada, T., Dingal, P.C., Pinter, J., Pajerowski, J.D., Spinler, K.R., Shin, J.W., Tewari, M.*, et al.* (2013). Nuclear lamin-A scales with tissue stiffness and enhances matrix-directed differentiation. Science (New York, NY) *341*, 1240104.

Tahara, N., Brush, M., and Kawakami, Y. (2016). Cell migration during heart regeneration in zebrafish. Developmental dynamics : an official publication of the American Association of Anatomists *245*, 774-787.

Tambe, D.T., Hardin, C.C., Angelini, T.E., Rajendran, K., Park, C.Y., Serra-Picamal, X., Zhou, E.H., Zaman, M.H., Butler, J.P., Weitz, D.A.*, et al.* (2011). Collective cell guidance by cooperative intercellular forces. Nat Mater *10*, 469-475.

Tekotte, H., Tollervey, D., and Davis, I. (2007). Imaging the migrating border cell cluster in living Drosophila egg chambers. Developmental dynamics : an official publication of the American Association of Anatomists *236*, 2818-2824.

Theveneau, E., Marchant, L., Kuriyama, S., Gull, M., Moepps, B., Parsons, M., and Mayor, R. (2010). Collective chemotaxis requires contact-dependent cell polarity. Developmental cell *19*, 39-53.

Tinevez, J.Y., Schulze, U., Salbreux, G., Roensch, J., Joanny, J.F., and Paluch, E. (2009). Role of cortical tension in bleb growth. Proceedings of the National Academy of Sciences of the United States of America *106*, 18581-18586.

Tischer, D., and Weiner, O.D. (2014). Illuminating cell signalling with optogenetic tools. Nat Rev Mol Cell Biol *15*, 551-558.

Titus, M.A., Kuspa, A., and Loomis, W.F. (1994). Discovery of myosin genes by physical mapping in Dictyostelium. Proceedings of the National Academy of Sciences of the United States of America *91*, 9446-9450.

Tkach, M., and Théry, C. (2016). Communication by Extracellular Vesicles: Where We Are and Where We Need to Go. Cell *164*, 1226-1232.

Toret, C.P., Shivakumar, P.C., Lenne, P.F., and Le Bivic, A. (2018). The elmo-mbc complex and rhogap19d couple Rho family GTPases during mesenchymal-to-epithelial-like transitions. Development (Cambridge, England).

Torkaman, G. (2014). Electrical Stimulation of Wound Healing: A Review of Animal Experimental Evidence. Advances in wound care *3*, 202-218.

Tozluoğlu, M., Tournier, A.L., Jenkins, R.P., Hooper, S., Bates, P.A., and Sahai, E. (2013). Matrix geometry determines optimal cancer cell migration strategy and modulates response to interventions. Nature cell biology *15*, 751-762.

Trepat, X., and Fredberg, J.J. (2011). Plithotaxis and emergent dynamics in collective cellular migration. Trends in cell biology *21*, 638-646.

Trichet, L., Le Digabel, J., Hawkins, R.J., Vedula, S.R., Gupta, M., Ribrault, C., Hersen, P., Voituriez, R., and Ladoux, B. (2012). Evidence of a large-scale mechanosensing mechanism for cellular adaptation to substrate stiffness. Proceedings of the National Academy of Sciences of the United States of America *109*, 6933-6938.

Tsygankov, D., Bilancia, C.G., Vitriol, E.A., Hahn, K.M., Peifer, M., and Elston, T.C. (2014). CellGeo: a computational platform for the analysis of shape changes in cells with complex geometries. The Journal of cell biology *204*, 443-460.

van de Merbel, A.F., van der Horst, G., Buijs, J.T., and van der Pluijm, G. (2018). Protocols for Migration and Invasion Studies in Prostate Cancer. Methods in molecular biology (Clifton, NJ) *1786*, 67-79.

van Haastert, P.J., Keizer-Gunnink, I., and Kortholt, A. (2007). Essential role of PI3-kinase and phospholipase A2 in Dictyostelium discoideum chemotaxis. The Journal of cell biology *177*, 809-816.

van Helvert, S., Storm, C., and Friedl, P. (2018). Mechanoreciprocity in cell migration. Nature cell biology *20*, 8-20.

van Niel, G., D'Angelo, G., and Raposo, G. (2018). Shedding light on the cell biology of extracellular vesicles. Nat Rev Mol Cell Biol *19*, 213-228.

Veeman, M.T., and McDonald, J.A. (2016). Dynamics of cell polarity in tissue morphogenesis: a comparative view from Drosophila and Ciona. F1000Research *5*.

Veltman, D.M., and Van Haastert, P.J. (2006). Guanylyl cyclase protein and cGMP product independently control front and back of chemotaxing Dictyostelium cells. Molecular biology of the cell *17*, 3921-3929.

Vicente-Manzanares, M., Ma, X., Adelstein, R.S., and Horwitz, A.R. (2009). Non-muscle myosin II takes centre stage in cell adhesion and migration. Nat Rev Mol Cell Biol *10*, 778-790.

Waldeland, J.O., Polacheck, W.J., and Evje, S. (2020). Collective tumor cell migration in the presence of fibroblasts. Journal of biomechanics *100*, 109568.

Wan, P., Wang, D., Luo, J., Chu, D., Wang, H., Zhang, L., and Chen, J. (2013). Guidance receptor promotes the asymmetric distribution of exocyst and recycling endosome during collective cell migration. Development (Cambridge, England) *140*, 4797-4806.

Wang, H., Guo, X., Wang, X., Wang, X., and Chen, J. (2020). Supracellular Actomyosin Mediates Cell-Cell Communication and Shapes Collective Migratory Morphology. iScience *23*, 101204.

Wang, H., Qiu, Z., Xu, Z., Chen, S.J., Luo, J., Wang, X., and Chen, J. (2018). aPKC is a key polarity determinant in coordinating the function of three distinct cell polarities during collective migration. Development (Cambridge, England) *145*.

Wang, X., Adam, J.C., and Montell, D. (2007). Spatially localized Kuzbanian required for specific activation of Notch during border cell migration. Developmental biology *301*, 532-540.

Wang, X., Bo, J., Bridges, T., Dugan, K.D., Pan, T.C., Chodosh, L.A., and Montell, D.J. (2006). Analysis of cell migration using whole-genome expression profiling of migratory cells in the Drosophila ovary. Developmental cell *10*, 483-495.

Wang, X., He, L., Wu, Y.I., Hahn, K.M., and Montell, D.J. (2010). Light-mediated activation reveals a key role for Rac in collective guidance of cell movement in vivo. Nature cell biology *12*, 591-597.

Wang, Y., Steimle, P.A., Ren, Y., Ross, C.A., Robinson, D.N., Egelhoff, T.T., Sesaki, H., and Iijima, M. (2011). Dictyostelium huntingtin controls chemotaxis and cytokinesis through the regulation of myosin II phosphorylation. Molecular biology of the cell *22*, 2270-2281.

Warchol, J.B., Herbert, D.C., Williams, M.G., and Rennels, E.G. (1975). Distribution of microtubules in prolactin cells of lactating rats. Cell and tissue research *159*, 205-212.

Ware, M.F., Wells, A., and Lauffenburger, D.A. (1998). Epidermal growth factor alters fibroblast migration speed and directional persistence reciprocally and in a matrix-dependent manner. Journal of cell science *111 (Pt 16)*, 2423-2432.

Weigelin, B., Bakker, G.J., and Friedl, P. (2012). Intravital third harmonic generation microscopy of collective melanoma cell invasion: Principles of interface guidance and microvesicle dynamics. Intravital *1*, 32-43.

Wessels, D., Lusche, D.F., Kuhl, S., Heid, P., and Soll, D.R. (2007). PTEN plays a role in the suppression of lateral pseudopod formation during Dictyostelium motility and chemotaxis. Journal of cell science *120*, 2517-2531.

Wolf, K., Mazo, I., Leung, H., Engelke, K., von Andrian, U.H., Deryugina, E.I., Strongin, A.Y., Bröcker, E.B., and Friedl, P. (2003). Compensation mechanism in tumor cell migration: mesenchymal-amoeboid transition after blocking of pericellular proteolysis. The Journal of cell biology *160*, 267-277.

Wolf, K., Te Lindert, M., Krause, M., Alexander, S., Te Riet, J., Willis, A.L., Hoffman, R.M., Figdor, C.G., Weiss, S.J., and Friedl, P. (2013). Physical limits of cell migration: control by ECM space and nuclear deformation and tuning by proteolysis and traction force. The Journal of cell biology *201*, 1069-1084.

Wolf, K., Wu, Y.I., Liu, Y., Geiger, J., Tam, E., Overall, C., Stack, M.S., and Friedl, P. (2007). Multi-step pericellular proteolysis controls the transition from individual to collective cancer cell invasion. Nature cell biology *9*, 893-904.

Wu, Y.I., Frey, D., Lungu, O.I., Jaehrig, A., Schlichting, I., Kuhlman, B., and Hahn, K.M. (2009). A genetically encoded photoactivatable Rac controls the motility of living cells. Nature *461*, 104-108.

Wu, Y.I., Wang, X., He, L., Montell, D., and Hahn, K.M. (2011). Spatiotemporal control of small GTPases with light using the LOV domain. Methods Enzymol *497*, 393-407.

Xiao, Y., Riahi, R., Torab, P., Zhang, D.D., and Wong, P.K. (2019). Collective Cell Migration in 3D Epithelial Wound Healing. ACS nano *13*, 1204-1212.

Yamada, K.M., and Sixt, M. (2019). Mechanisms of 3D cell migration. Nat Rev Mol Cell Biol *20*, 738-752.

Yang, X., Jost, A.P., Weiner, O.D., and Tang, C. (2013). A light-inducible organelle-targeting system for dynamically activating and inactivating signaling in budding yeast. Molecular biology of the cell *24*, 2419-2430.

Yao, T.P., Forman, B.M., Jiang, Z., Cherbas, L., Chen, J.D., McKeown, M., Cherbas, P., and Evans, R.M. (1993). Functional ecdysone receptor is the product of EcR and Ultraspiracle genes. Nature *366*, 476-479.

Yevick, H.G., Duclos, G., Bonnet, I., and Silberzan, P. (2015). Architecture and migration of an epithelium on a cylindrical wire. Proceedings of the National Academy of Sciences of the United States of America *112*, 5944-5949.

Yolland, L., Burki, M., Marcotti, S., Luchici, A., Kenny, F.N., Davis, J.R., Serna-Morales, E., Muller, J., Sixt, M., Davidson, A.*, et al.* (2019). Persistent and polarized global actin flow is essential for directionality during cell migration. Nature cell biology *21*, 1370-1381.

Zanotelli, M.R., Zhang, J., and Reinhart-King, C.A. (2021). Mechanoresponsive metabolism in cancer cell migration and metastasis. Cell metabolism *33*, 1307-1321.

Zhao, M. (2009). Electrical fields in wound healing-An overriding signal that directs cell migration. Seminars in cell & developmental biology *20*, 674-682.

Zhao, M., Song, B., Pu, J., Wada, T., Reid, B., Tai, G., Wang, F., Guo, A., Walczysko, P., Gu, Y.*, et al.* (2006). Electrical signals control wound healing through phosphatidylinositol-3-OH kinase-gamma and PTEN. Nature *442*, 457-460.

Zhou, X.X., Chung, H.K., Lam, A.J., and Lin, M.Z. (2012). Optical control of protein activity by fluorescent protein domains. Science (New York, NY) *338*, 810-814.